

STRUCTURE-PROPERTY RELATIONSHIPS IN CONJUGATED
DONOR/ACCEPTOR-FUNCTIONALIZED ARYLACETYLENES
AND DEHYDROBENZOANNULENES

by

ERIC LEWIS SPITLER

A DISSERTATION

Presented to the Department of Chemistry
and the Graduate School of the University of Oregon
in partial fulfillment of the requirements
for the degree of
Doctor of Philosophy

March 2008

University of Oregon Graduate School

Confirmation of Approval and Acceptance of Dissertation prepared by:

Eric Spitler

Title:

"STRUCTURE-PROPERTY RELATIONSHIPS IN CONJUGATED DONOR/
ACCEPTOR-FUNCTIONALIZED ARYLACETYLENES AND
DEHYDROBENZOANNULENES"

This dissertation has been accepted and approved in partial fulfillment of the requirements for the degree in the Department of Chemistry by:

Darren Johnson, Chairperson, Chemistry
Michael Haley, Advisor, Chemistry
Kenneth Doxsee, Member, Chemistry
Victoria DeRose, Member, Chemistry
David Strom, Outside Member, Physics

and Richard Linton, Vice President for Research and Graduate Studies/Dean of the Graduate School for the University of Oregon.

March 22, 2008

Original approval signatures are on file with the Graduate School and the University of Oregon Libraries.

modifications of molecular architecture effects on the photophysics, intramolecular charge transfer (ICT), or complexation properties are of importance in the rational design of the next generation of organic electronics.

Chapter I provides a review of recent advances in the field of annulene chemistry. It is organized by cycle type, size, and application within each category. Chapter II describes syntheses and ion responses of an array of donor/acceptor-functionalized arylacetylenes. The independent manipulation of frontier molecular orbital (FMO) energy levels is discussed in relation to a fluorescent switching phenomenon. Chapter III expands this effect to include [15]DBAs. The consequences of incorporating protonatable donor/acceptor groups into a macrocycle, as well as placement of the acceptor nitrogen are examined, and comparison of calculations to experimental results imply generation of transient ICT species with induced FMO localizations. Chapter IV describes the syntheses of acyclic tetrakis(phenylethynyl)benzene (TPEB) and [14]- and [15]DBA systems utilizing fluorinated acceptor groups. Comparisons between these inductive acceptors and earlier resonance acceptors are made, and imply greater stability and processing potential for optoelectronic applications. Chapter V describes a series of bis[18]DBAs functionalized with dibutylamino groups as donors and nitro groups as acceptors. The effects of 2-donor/2-acceptor versus 4-donor/4-acceptor motifs are explored, and trends are identified in the systematic adjustment of the optical band gap that will have important implications for the design of two-photon absorbing materials.

This dissertation includes my previously published and co-authored material.

CURRICULUM VITAE

NAME OF AUTHOR: Eric L. Spitler

PLACE OF BIRTH: Columbus, Ohio

DATE OF BIRTH: October 31, 1980

GRADUATE AND UNDERGRADUATE SCHOOLS ATTENDED:

University of Oregon

Ohio State University

DEGREES AWARDED:

Doctor of Philosophy in Chemistry, 2008, University of Oregon

Master of Science in Chemistry, 2004, University of Oregon

Bachelor of Science in Chemistry, 2003, Ohio State University

AREAS OF SPECIAL INTEREST:

Organic Chemistry

Organic Materials

Carbon-rich Chromophores and Fluorophores

PROFESSIONAL EXPERIENCE:

Graduate Research Associate, Department of Chemistry, University of Oregon
Eugene, Oregon, 2003-2007

Research & Development Intern, Invitrogen Corp.
Eugene, Oregon, June-September 2007

Graduate Teaching Associate, Department of Chemistry, University of Oregon,
Eugene, Oregon, 2003-2005

Undergraduate Research Assistant, Department of Chemistry, Ohio State
University, Columbus, Ohio, 2001-2003

GRANTS, AWARDS AND HONORS:

National Science Foundation IGERT Fellowship, 2005-2008

Magna Cum Laude, 1999

PUBLICATIONS:

Spitler, E. L.; Haley, M. M. Charge Transfer Pathway Topology-Optical Band Gap Correlations in Donor/Acceptor-Functionalized Bis(dehydrobenzo[18]annuleno)benzenes. *Org. Biomol. Chem.*, accepted.

Spitler, E. L.; Monson, J. M.; Haley, M. M. Structure-Property Relationships of Fluorinated Donor/Acceptor Tetrakis(phenylethynyl)benzenes and Bis(dehydrobenzoannuleno)benzenes. *J. Org. Chem.*, in press.

Spitler, E. L.; McClintock, S. P.; Haley, M. M. Dynamic Proton-Induced Emission Switching in Donor-Functionalized Dehydrobenzopyrid[15]annulenes. *J. Org. Chem.* **2007**, *72*, 6692-6699.

Samori, S.; Tojo, S.; Fujitsuka, M.; Spitler, E. L.; Haley, M. M.; Majima, T. Donor-Acceptor Substituted Tetrakis(phenylethynyl)benzenes as Emissive Molecules during Pulse Radiolysis in Benzene. *J. Org. Chem.* **2007**, *72*, 2785-2793.

Spitler, E. L.; Shirtcliff, L. D.; Haley, M. M. Systematic Structure-Property Investigations and Ion Sensing Studies of Donor/Acceptor-Functionalized Tetra(arylethynyl)benzenes. *J. Org. Chem.* **2007**, *72*, 86-96.

Spitler, E. L.; Johnson, C. A.; Haley, M. M. Renaissance of Annulene Chemistry. *Chem. Rev.* **2006**, *106*, 5344-5386.

Slepkov, A.; Hegmann, F. A.; Tykwinski, R. R.; Kamada, K.; Ohta, K.; Marsden, J. A.; Spitler, E. L.; Miller, J. J.; Haley, M. M. Two-Photon Absorption in 2-D Conjugated Quadrupolar Chromophores. *Opt. Lett.* **2006**, *31*, 3315-3317.

ACKNOWLEDGMENTS

The unique interdisciplinary nature of both the Chemistry Department at the University of Oregon, as well as the research projects undertaken in the Haley lab, have necessarily resulted in a number of cooperative efforts that have contributed to this dissertation and deserve recognition. First and foremost of course I must express my appreciation to my research advisor Professor Michael Haley, whose proactive approach to the preparation of this manuscript and whose involvement and encouragement over these past four years have resulted in a phenomenally productive and rewarding graduate career. I also wish to thank my doctoral committee members, past and present, whose rigorous critical reviews and suggestions have contributed to the quality and completeness of this work. Our lab's collaborators at other institutions, chiefly the research groups of Professors Rik Tykwinski and Frank Hegmann at the University of Alberta and Professor Tetsuro Majima at the University of Osaka, have provided testing and results for our compounds that serve to establish their exciting applications potential. I also want to thank Professor Uwe Bunz at Georgia Tech for many helpful suggestions and enthusiastic support, Professor O. Hayes Griffith here at the U of O for use of his group's fluorimeter, Dr. Lev Zakharov for his expert crystallographic services, and Dr. Jeremiah Marsden and Professor Joshua Pak, who both worked on related annulene projects in the past and whose efforts have formed the basis for my own investigations. I must also recognize Ben Boal and John "Mac" Monson, the undergraduate researchers who have contributed their efforts, and Zack Mensinger who worked on this project

during his first year rotation. Financial support has been provided by the National Science Foundation through direct research grants (CHE-0414175 and 0718242) as well as through the Materials Science Institute's IGERT funding (DGE-0549503). Finally I want to thank all the members of the Haley lab for their friendly assistance in all aspects of graduate life over these past years, as well as my parents for their unwavering support and faith in my goals.

TABLE OF CONTENTS

Chapter	Page
I. RENAISSANCE OF ANNULENE CHEMISTRY	1
General Introduction	1
Nomenclature and Origin	2
Annulenes	4
Dehydroannulenes	42
Benzoannulenes	73
Dehydrobenzoannulenes	81
Other Arene-fused Annulenes	130
Conclusions	138
Bridge to Chapter II	138
II. SYSTEMATIC STRUCTURE-PROPERTY INVESTIGATIONS AND ION SENSING STUDIES OF PYRIDINE-DERIVATIZED DONOR/ ACCEPTOR TETRAKIS(ARYLETHYNYL)BENZENES.....	140
Introduction	140
Results and Discussion	144
Synthesis	144
Molecular Orbital Plots	146
Electronic Absorption and Emission Spectra	149
TFA Titrations	157
Metal Ion Complexations	161
Conclusions	169
Experimental	171
Bridge to Chapter III	184
III. DYNAMIC PROTON-INDUCED EMISSION SWITCHING IN DONOR- FUNCTIONALIZED DEHYDROBENZOPYRID[15]ANNULENES.	185
Introduction	185
Results and Discussion	188
Synthesis	188
Absorption and Emission Data	190

Chapter	Page
Molecular Orbital Plots	193
TFA Titrations	196
Conclusions.....	202
Experimental	203
Bridge to Chapter IV	215
IV. STRUCTURE-PROPERTY RELATIONSHIPS OF FLUORINATED DONOR/ACCEPTOR TETRAKIS(PHENYLETHYNYL)BENZENES AND BIS(DEHYDROBENZOANNULENO)BENZENES.	216
Introduction	216
Results and Discussion	219
Synthesis	219
Electronic Absorption Spectra	223
Film Spectra	237
Self-Association	240
Conclusions	242
Experimental	244
Bridge to Chapter V	265
V. CHARGE TRANSFER PATHWAY TOPOLOGY-OPTICAL BAND GAP CORRELATIONS IN DONOR/ACCEPTOR-FUNCTIONALIZED BIS(DEHYDROBENZO[18]ANNULENO)BENZENES	266
Introduction	266
Results and Discussion	269
Synthesis	269
Electronic Absorption Spectra	273
Electronic Emission Spectra	278
Self-Association	280
Conclusions.....	282
Experimental	282

Chapter	Page
VI. CONCLUDING SUMMARY	294
APPENDICES	296
A. DYNAMIC PROTON-INDUCED EMISSION SWITCHING IN DONOR- FUNCTIONALIZED BIS(DEHYDROBENZO[18]ANNULENO)BENZENE	296
B. COMPUTATIONAL DETAILS	310
BIBLIOGRAPHY	334

LIST OF FIGURES

Figure	Page
CHAPTER I	
1. Various types of annulenes	2
2. [8]Annulene	4
3. Various forms of substituted [8]annulene.	6
4. [8]Annulene cyclophane structures.	8
5. Conformers of [10]annulene	9
6. Fused [10]annulenes	10
7. Bridged [10]annulenes	11
8. Representations of bridged [10]annulene	12
9. Cations from bridged [10]annulene solvolysis	12
10. Donor/acceptor-functionalized bridged[10]annulenes	13
11. Substituted derivatives of bridged [10]annulene	14
12. Isomers of [12]annulene	15
13. Isomerization and cyclization of [12]annulene	15
14. Automerization and pericyclic reactions in [12]annulene	16
15. Anion radicals of [12]annulene	17
16. Bridged [12]annulenes	18
17. Isomers of [14]annulene	19
18. Isomeric precursor to planar <i>cis</i> -[14]annulene	19
19. Isomers of methylated [14]annulene	21
20. Various bridged [14]annulenes	21
21. Dimethyldihydropyrene	23
22. Dehydroannulene-fused DMDHP	23
23. Isomers and dianion of [16]annulene	25
24. Isomers of [18]annulene	29
25. Anion radical of [18]annulene	33
26. Isomerization of [18]annulene anion radical	34
27. Conformations of [18]annulene dianion	34
28. [30]Annulene	38
29. Multiply-methylene-bridged [30]annulene	41

Figure	Page
30. Conformations of [24]annulene	42
31. Dehydro[8]annulene and anion radical	43
32. Dimeric anion radical of <i>sym</i> -[8]annuldiyne	44
33. Dehydro[10]annulene isomers and potential cyclization products	45
34. Calculated geometries and cyclization of dehydro[10]annulene	50
35. Isomers of dehydro[12]annulene and derivatives	51
36. Perethynylated dehydro[12] and [18]annulenes	57
37. Isomers of dehydro[14]annulene	59
38. Dehydroannulenediones and cyclo[18]carbon	60
39. Propellatriene-fused dehydroannulenes	62
40. Dodecadehydro[18]annulene and derivatives	63
41. Isomers of cyclo[18]carbon	64
42. <i>D_{6h}</i> -symmetric dehydro[18]annulenes	67
43. Cyclo[18]carbon precursors	68
44. Homoaromatic analogues of dehydro[18]annulene	71
45. Various 1,6-methano-bridged tetradecahydroannulenes	73
46. Highly-fused systems from attempted benzo[14]annulene syntheses	75
47. Annelated DMDHP photochromic switches	79
48. Theoretical carbon allotropes graphyne and graphdiyne	82
49. Various forms of dehydrobenzo[8]annulene and fused derivatives	85
50. Various dehydrobenzo[12]annulenes	86
51. Octadehydridibenzo[12]annulenes	87
52. Various metal-coordinated dehydrobenzo[12]annulene derivatives	92
53. Multiply-fused tribenzodehydro[12]annulenes	98
54. Various coordinated dehydrotribenzo[12]annulenes	103
55. Dehydromonobenzo- and dibenzo[12]annulenes 234-236	105
56. Variously benzannelated octadehydro[14]annulene analogues	109
57. Various coordinated fused dehydrobenzo[14]annulenes	111
58. Unusual novel dehydrobenzo[14]annulene structures 259-261	113
59. Dehydrobenzo[16]annulenes and a cobalt complex	114
60. DBA substructures of graphdiyne	117
61. DMDHP-fused and iron and cobalt-coordinated [18]DBA derivatives	124
62. Dehydrobenzo[20]annulenes and a cobalt complex	126

Figure	Page
63. Various higher dehydrobenzoannulenes	128
64. Dehydronaphthoannulenes	131
65. Various dehydrothienoannulenes	134
 CHAPTER II	
1. Conjugated pathways in TPEBs and DBAs	141
2. TAEB targets 1-9	142
3. Previously reported TPEBs 10-14	143
4. Molecular orbital plots of structures 1'-9'	148
5. Electronic absorption spectra of 1-14	151
6. Emission spectra of 1-9 in CH ₂ Cl ₂ and toluene	153
7. Emission maxima of 1-9 in CH ₂ Cl ₂	155
8. Quantum yield trends for 1-9 and 12-14	157
9. Donor/acceptor systems 18 and 19	158
10. Emission spectra of TFA titration of 2 in MeOH	160
11. Absorption spectra of TFA titration of 9 in MeOH	161
12. Emission spectra of ZnCl ₂ complexation of 1 in CH ₂ Cl ₂	163
13. Tetrapyrrolyl ligand 20	165
14. Emission spectra of addition of AgOTf to 1 in CH ₂ Cl ₂	165
15. Emission spectra of addition of AlCl ₃ to in MeOH to 9	167
16. Effect of various metals on 1 , 5 , and 9 in CH ₂ Cl ₂	168
17. Emission spectra of the effects of ZnCl ₂ and AlCl ₃ on 1 , 5 , and 9	169
18. Emission spectra of TFA titration of 1-9 in MeOH.....	181
19. Emission spectra of ZnCl ₂ complexation to 1-9 in CH ₂ Cl ₂	182
20. Emission spectra of addition of AlCl ₃ in MeOH to 1-9	183
 CHAPTER III	
1. Conjugated Pathways in TPEBs, DBAs and TAEBs.....	186
2. 15-membered macrocycle DBAs 1-3	187
3. Absorption and emission spectra of 3a-b and 6a-b	191
4. Molecular orbital plots of 3a' and 3b'	195
5. Absorption and emission spectra of TFA titration of 3a	197

Figure	Page
6. Absorption and emission spectra of TFA Titration of 3b	198
7. ¹ H NMR spectra in CD ₂ Cl ₂	201
8. Absorption and emission spectra of 6a and 6b with excess TBAF	207
9. Emission spectra of TFA titration of 3a in MeOH	207
10. Emission spectra of TFA titration of 6a and 6b	207
11. X-Ray crystal structure and packing in 3a	209
12. Molecular structure and packing in 3b	211
13. Molecular orbitals and relative energies of 3a ' ⁺ and 3a ' ^{d+}	213
14. Molecular orbitals and relative energies of 3b ' ⁺ and 3b ' ^{d+}	214

CHAPTER IV

1. Target TPEBs 1-9 and known TPEBs 10-15	218
2. Target DBAs 16-21 and previously reported DBAs 22-26	219
3. Electronic absorption spectra of 1-15	225
4. Electronic absorption spectra of 16-21	229
5. Absorption spectra of 1 , 16 , and 19	230
6. Electronic emission spectra of 1-12 in CH ₂ Cl ₂ and benzene	232
7. Expanded emission spectra of 1-6 in CH ₂ Cl ₂	233
8. Electronic emission spectra of 16-21 in CH ₂ Cl ₂ and benzene	233
9. Quantum yield trends for 1-12 and 16-21	237
10. Absorption and emission spectra of drop-cast films of 1-9	239
11. Concentration-dependent chemical shifts of 19	242
12. Emission spectra of 16 and 18 in various solvents	264
13. Concentration-dependent chemical shifts of 16 and 18	264

CHAPTER V

1. Previously studied DBAs and various conjugated pathways	268
2. Target Bis[18]DBAs 1-7	269
3. Donor/acceptor alkyne segments 8-11	271
4. Electronic absorption spectra of 1-7	274
5. Electronic absorption spectra of 12 , 14 , 1 , and 7	274
6. Emission spectra of 1 in various solvents	279

Figure	Page
7. Emission spectra of 4 in hexanes and dichloromethane	279
8. Examples of previously reported DBAs that display self-association in solution	280
9. Concentration-dependent chemical shifts in 3	281

APPENDIX A

1. Cruciform and annulenic donor/pyridyl acetylene systems and donor-functionalized Bis[18]DBA	297
2. Absorption and emission spectra of 3 and 5	299
3. Spectra of TFA titration of 3 and 5	301
4. Donor-functionalized 6-8	306
5. Spectra of 3 and 6-8 in CH ₂ Cl ₂ at indicated [TFA]	307
6. Emission spectra of <i>i</i> -Pr ₂ NH addition to 3 and 6-8	308

LIST OF TABLES

Table	Page
CHAPTER I	
1. Effect of bridging substituents on bond lengths of 54 and 55	22
2. Bond alternation of [18]annulene in various symmetry point groups	31
3. Activation parameters for thermal rearrangement of 65 to 72	36
4. Calculated bond length alternations in various annulenes	38
5. Bridgehead NMR shifts and redox potentials of BCO-fused annulenes	56
6. Comparisons between benzene and carbomer 141	70
7. Internal methyl proton δ values for benzoannulenes 163-178	76
8. Synthetic routes to hexadehydrotribenzo[12]annulene (207)	95
9. Dehydrobenzo[12]annulenes 228a-n	102
10. Bis-[14]cyclyne electron donor-acceptor systems 239-242	107
11. Dehydrobenzo[18]annulenes 277a-h	119
12. Dehydrobenzo[18]annulene electron donor-acceptor systems 278a-w	121
CHAPTER II	
1. Yields for preparation of TAEBS 1-9	146
2. Absorption and emission data and calculated net dipoles for 1-9	152
3. Summary of TFA-Induced emission shifting in 1-9	160
CHAPTER III	
1. Absorption and emission Data for 2a-b , 3a-b , and 6a-b	191
2. Summary of TFA-Induced emission shifting in 3a and 3b	198
3. Crystal data for 3a	210
4. Crystal data for 3b	212
5. Calculated band gap energies of 3a'/3a' ⁺ and 3b'/3b' ⁺	214
CHAPTER IV	
1. Yields for preparation of TPEBs 1-9	220
2. Yields for preparation of DBAs 16-21	223
3. Absorption and emission data for TPEBs 1-15	226
4. Absorption and emission data for DBAs 16-21	229

Table	Page
5. Emission data for 1-12 and 16-21 in benzene	235
6. Absorption and emission data for films of 1-9	240
7. Calculated association constants of 19 protons in CDCl ₃ at 20 °C	242
CHAPTER V	
1. Yields for alkyne segment couplings and cyclization to DBAs 1-7	272
2. Lowest energy absorptions in 1-7	274
3. Lowest energy absorption and emission wavelengths of 1 in various solvents	279
APPENDIX A	
1. Summary of TFA-induced spectral shifting in 3	303
2. Summary of TFA-induced spectral shifting in 5	304

LIST OF SCHEMES

Scheme	Page
CHAPTER I	
1. Conversion of [8]annulene radical to [16]annulene radical	5
2. Cyclizations of [10]Annulene	9
3. Cyclization of anion radicals of [12]annulene	17
4. Generation of [14]annulene from octalene	20
5. Photochromic switching in a DMDHP derivative	24
6. Cyclization of [16]annulene.....	28
7. Thermal rearrangements of [18]annulene	36
8. Generation of dehydro[8]annulene anion radical.....	44
9. A dehydro[10]annulene intermediate in cyclization of 89	47
10. Diels-Alder cyclization of 94	48
11. A dehydro[10]annulene in the cyclization of 94	49
12. Generation of dehydro[12]annulene	52
13. Preparation of various BCO-fused dehydroannulenes	55
14. Cycloreversion of dehydroannulenes to cyclo[n]carbons	62
15. Cycloreversion products of fused dehydro[18]annulenes.....	65
16. Various benzannulenes with crown-like structure	81
17. Generation of dehydrobenzo[8]annulene.....	83
18. Preparation of alkyl-substituted octadehydridibenzo[12]annulenes	89
19. Cycloreversion to strained annulene 208	93
20. Synthesis of ethynylated dehydrotribenzo[12]annulenes.....	100
21. Preparation and polymerization of a dehydrobenzo[14]annulene.....	106
22. Dodecadehydrotribenzo[18]annulene synthesis.....	115
23. Benzoquinone-fused dehydro[18]annulenes.....	123
24. Tetrathiophene annulene topologies	136
CHAPTER II	
1. Synthesis of Pyridine-based Donor/Acceptor TAEBS	145

Scheme	Page
CHAPTER III	
1. Preparation of DBPAs 3a and 3b	189
CHAPTER IV	
1. Synthesis of 3 and 9	220
2. Synthesis of 31	221
3. Synthesis of 17 and 20	222
4. Synthesis of 16 and 19	258
5. Synthesis of 18 and 21	261
CHAPTER V	
1. Synthesis of 1	271
2. Synthesis of 7	272
APPENDIX A	
1. Synthesis of 3	298

CHAPTER I

RENAISSANCE OF ANNULENE CHEMISTRY

General Introduction

The unifying theme of this dissertation is the synthesis and structure-property relationship study of π -conjugated arylacetylene and dehydrobenzoannulene (DBA) compounds that have been functionalized with electron donating and electron withdrawing (accepting) groups. Arylacenyls are simple chromophores composed of arene rings connected by a network of triple bonds, while DBAs contain arylacetylene units fused into a planarized macrocycle. This introductory chapter provides a thorough review of recent advances in annulenes in general, as well as DBAs in particular. The chapter includes my contribution to an article published under invitation in the journal *Chemical Reviews* (2006, 106, 5344-5386, © 2006 American Chemical Society). The article was co-authored with Professor Michael M. Haley, who provided editorial assistance, and Charles A. Johnson II.

Nomenclature and Origin

Originally defined by Sondheimer in the early 1960s,¹ an $[n]$ annulene is a monocyclic hydrocarbon comprised of alternating single and double bonds, where the number in brackets denotes the number of contiguous sp^2 carbon centers. By this definition, cyclobutadiene is therefore considered as [4]annulene, benzene as [6]annulene (**1**, Figure 1), and so on. Replacement of one or more of the double bonds with an acetylene unit affords a dehydroannulene (e.g., **2**). An unfortunate side effect of installing triple bonds in the hydrocarbon skeleton often is compound instability. On the other hand, fusion of one or more benzene rings to furnish a benzoannulene (e.g., **3**) or dehydrobenzoannulene (e.g., **4**) heightens macrocycle stability in general.

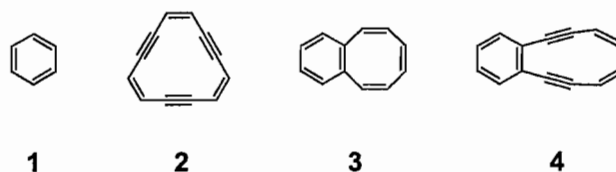


Figure 1. Various types of annulenes.

Throughout the 1960s and 1970s, these four classes of closely related molecules were targets of intensive study. The research groups of Nakagawa,² Staab,³ and Sondheimer,⁴ the principal protagonists of this era, prepared an impressive array of annulenic structures and showed that these hydrocarbons possess a fascinating wealth of chemistry, such as Bergman cyclization of **4** to give anthracene.⁵ The main factor driving annulene research was the dominating question of whether planar examples of such

macrocycles were able to sustain induced ring currents, and if so, what was the strength of those ring currents. From the myriad of compounds produced, the main conclusion was that ring currents in these systems became progressively weaker upon benzannulation, by inclusion of triple bonds, and/or with increasing ring size. While these studies validated theoretical conclusions based on the Hückel rule for annulenes, it became apparent that there needed to be additional impetus for annulene research; thus, interest waned and the area languished in the 1980s.

The last decade of the 20th century heralded a rebirth of annulene chemistry. A number of synthetic discoveries, most notably Pd-mediated cross-coupling reactions between sp and sp^2 carbon centers,⁶ were adopted from other areas of organic chemistry. These improvements made the previously laborious task of macrocycle assembly now a quick and efficient process. The ability to create new annulenes allowed chemists to functionalize easily the hydrocarbon backbone and thus tailor the chemical reactivity and physical properties of the macrocycles. Recognition of potential materials applications for these π -electron-rich systems has driven most of the annulene research conducted currently. Indeed, annulenes have been shown to exhibit nonlinear optical behavior, to polymerize yielding tubular polymers, and even to explode furnishing ordered carbon nanostructures (*vide infra*).

This chapter describes the numerous advances in the chemistry and reactivity of annulenes, dehydroannulenes, and their benzannelated analogues made over the last 20+ years.⁷ For work prior to 1985, the reader is referred to the outstanding three-volume book series by Balaban, Banciu, and Ciorba.⁸ To avoid creating an equally expansive

chapter, a number of benzoannulenes and annulene-like structures, such as the smallest annulenes, cyclobutadiene and benzene, have not been included. Other structures not included are the cyclic phenylenes, of which there are myriad derivatives; biphenylenes,⁹ triphenylenes,¹⁰ and tetraphenylenes¹¹ all have been recently reviewed. Systems which are homo-conjugated or meta- (1,3-) arene-fused have been excluded. Cross-conjugated annulenes,¹² Moebius annulenes,¹³ and annulenes with belt-shaped topologies¹⁴ (e.g., cyclocarbons, para- (1,4-) arene fusion) are covered by other authors in the special issue of *Chemical Reviews* in which this chapter appears.

Annulenes

[8]Annulenes. [8]Annulene (**5**, Figure 2), or cyclooctatetraene (COT), was first isolated in 1911,¹⁵ and caused a fair amount of confusion when it failed to display benzene-like properties. This was prior to publication of Hückel's now-famous rule that only conjugated systems with $(4n+2)$ π -electrons would exhibit what is now called aromaticity.¹⁶ The $(4n)$ π -electron [8]annulene, on the other hand, exhibits higher reactivity.¹⁷ [8]Annulene exists in a tub conformation, which undergoes rapid interconversion, and thus is considered nonaromatic.¹⁸

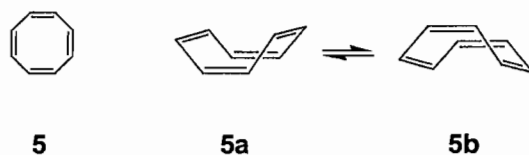
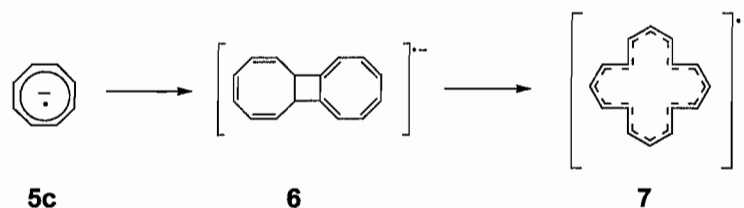


Figure 2. [8]Annulene.

Much of the recent work that has been done with [8]annulene involves the anion radical (**5c**) and dianion,^{18b,19a-h} both of which are planar and much more stable. The majority of work by Stevenson involves [8]annulene anion radical, which has been shown to dimerize to **6**, followed by ring opening to [16]annulene anion radical (**7**, Scheme 1).^{19a} Isotopic labeling experiments elucidated potential mechanisms for the dimerization. This reaction represents an improved route to the substituted [16]annulene anion radical, since direct synthesis is laborious and low-yielding.²⁰ Isotopic labeling and electron paramagnetic resonance (EPR) spectroscopy has also been used to explain sterically induced ring puckering as well as automerization of the anion.^{18b} Intramolecular π - π interaction results in transannular communication between the planar anion radicals of bis-COT systems (e.g., **8**, Figure 3),^{19e} which is not seen with the tub-shaped neutral COT. Stevenson has also recently prepared the highly-strained, high energy cycloprop[8]annulene (**9**),^{19h} the second known cyclopropannulene (cyclopropabenzene being the first¹⁹ⁱ).



Scheme 1. Conversion of [8]annulene anion radical to [16]annulene anion radical.

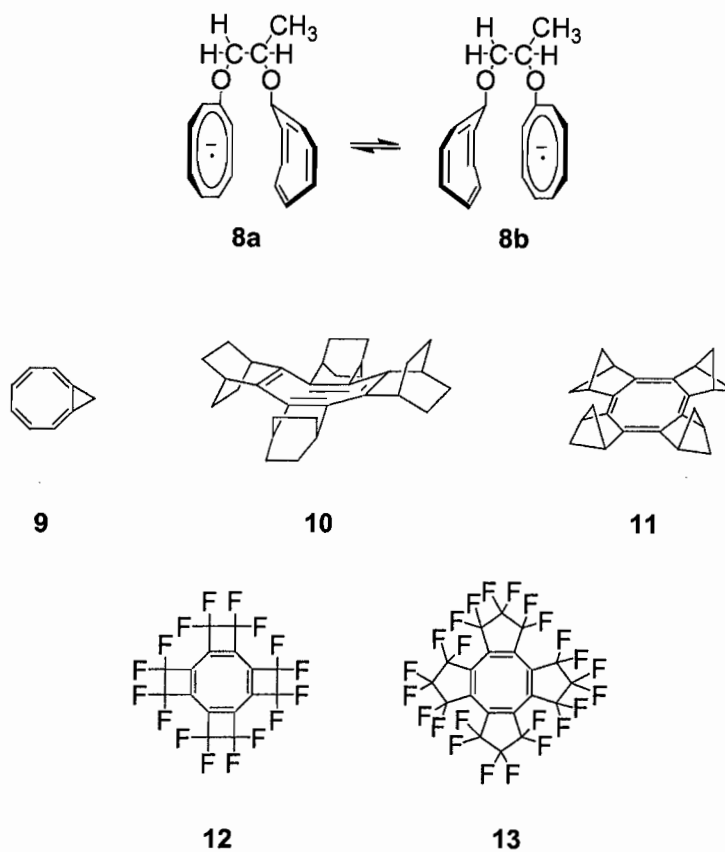


Figure 3. Various forms of substituted [8]annulene.

The cation radical of tetrakis(bicyclo[2.2.2]octene)-fused [8]annulene (**10**) was recently prepared by Komatsu et al.,^{19g} and was shown to adopt the tub shape, while the cation radical of tetrakis(bicyclo[2.1.1]hexene)-fused [8]annulene (**11**) was planar. The planarity of the latter is attributed to the highly strained bicyclohexene units. Similarly, perfluorinated tetrakis(cyclobuta)COT synthesized by Soulen et al. (**12**)^{21a} is planar, while perfluorinated tetrakis(cyclopenta)COT prepared by Gerson and Wirz^{21b} (**13**) is

tub-shaped. The former has shown powerful oxidizing properties, and its anion radical can be generated simply by contact with Hg metal.

Calculations by Baldrige and Siegel^{21c} on neutral, fused COT derivatives **10-13** showed that enforced planarization could lead to “directing” of the positions of the double bonds, i.e., *endo* or *exo* to the fused ring systems. For example, as depicted in Figure 3, **10**, **12**, and **13** show the double bonds in the *endo* positions, while in **11** they are *exo*. Theoretical calculations also suggest that correct choice of annelating group can afford the desired form. Preparation of neutral **11** by Komatsu confirmed both its planarity and preference for exocyclic double bonds crystallographically.^{21d} Effects of annelation on the antiaromaticity of COT and other phenomena have been well-examined,^{21e} and it was recently found that paratropic ring current persists well into the transition from the planar to the tub-shaped geometry, and that a minor distortion from the fully tub-shaped geometry is enough to restore it.^{21f}

Paquette and coworkers have synthesized doubly-stacked [8]annulene cyclophane **14**,²² which undergoes conformational equilibration involving bond-shift isomerization (Figure 4). The spectral data suggest that one isomer dominates, but no distinction between them is possible. The tetraanion **15** was prepared, requiring considerably strong reducing conditions at low temperatures. Interestingly, despite the strong Coulombic forces obviously present in the anion, homolytic cleavage of one of the ethano bridges does not occur. The authors observed bis-adducts from intramolecular cycloaddition upon heating, but the results were inconclusive.

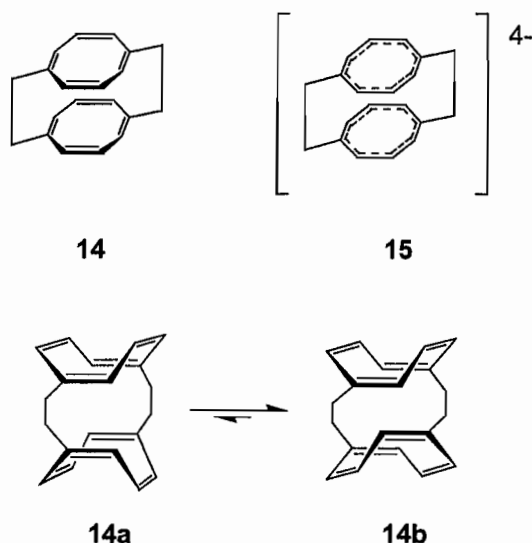


Figure 4. [8]Annulene cyclophane structures.

[10]Annulenes. [10]Annulene (**16**, Figure 5), by the $(4n+2)$ rule, would be expected to be aromatic. However, such aromaticity requires a planar all-*cis* conformation, introducing significant bond angle distortion to 144° . [10]Annulene was first synthesized definitively in 1969 by Masamune and Seidner,²³ who demonstrated that it existed in two distinct yet rapidly interconverting forms **16a** and **16b**, to which they assigned an all-*cis* “boat-like” conformation and a mono-*trans* “twist” conformation (Scheme 2). Both isomers were shown to undergo thermal cyclization to dihydronaphthalenes **17** and **18** while retaining their respective *cis* or *trans* character, as well as hydrogenation to cyclodecane. The lack of planarity and hence aromatic stability in either of these conformations explains the relatively high reactivity of [10]annulene, and implies significant bond localization rather than delocalization. The originally

reported structures have been refined through computations over the years,²⁴ using density functional theory and second-order perturbation theory. Comparison with experimental results has led to a re-evaluation of the reliability of density functional theory (DFT) in predicting aromatic structures. Indeed, several other structures have been calculated as only slightly higher or even lower in energy (16c-16e), revealing that further refinement of computational theories and methods involved may be required.^{24e,f} The most recent computational investigations into the mechanisms of bond shifting and automerization of 16 support the original assignments of the two major isomers as 16a and b.^{24g}

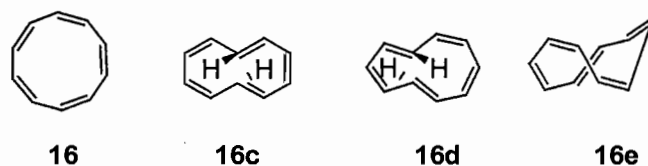
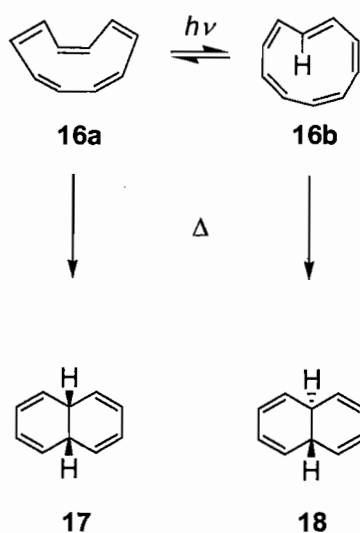


Figure 5. Conformers of [10]annulene.



Scheme 2. Cyclizations of [10]Annulene.

Typically, planarization of an annulenic backbone is induced via the introduction of linear triple bonds (a “dehydroannulene,” see Section 3). Schleyer and coworkers have pointed out, however, that planarization can be accomplished through fusion of one or more cyclopropyl, cyclobutyl or similar strained rings.^{24d} This is computed by DFT to reduce the ring strain in the molecules and cause the planar geometry to occupy minima with D_{5h} symmetry. The geometries of three [10]annulenes (Figure 6) with two (**19**) and five (**20**) fused cyclopropyl rings and five cyclobutyl rings (**21**) were calculated at B3LYP/DZd level of theory. All were found to satisfy various criteria for aromaticity, and are predicted to be more stable than the parent [10]annulene. The synthesis of perfluorotetracyclobutaCOT (**7**),²¹ mentioned in the previous section on [8]annulene, is pointed to as evidence for the synthetic accessibility of these cycloalkyl-fused annulene derivatives.

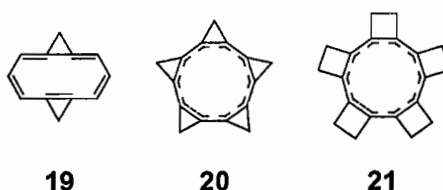


Figure 6. Fused [10]annulenes.

Bridged [10]Annulenes. The potential aromaticity of [10]annulene is more readily illustrated by locking the π -system into planarity, and thus, far more work has been done with 1,6-methano-bridged [10]annulenes²⁵ (**22**, first prepared by Vogel in

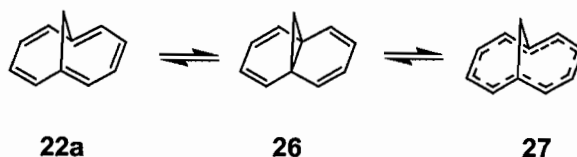


Figure 8. Representations of bridged [10]annulene.

In addition to the neutral bridged annulene systems, their anion, cation, or radical analogues can serve as effective probes of bond theory.²⁸ Spin density, paratropism, and conformational measurements of cation radicals and anions of bridged π -systems have proven especially useful in understanding the electronic effects of enforced planarity or nonplanarity. Studies of the ions of bridged [10]annulene as well as higher ring size ($4n+2$) systems display pronounced paratropic character that are particularly sensitive to electronic and geometric effects. Cations from solvolysis of 1- or 2-chloromethyl-1,6-methano[10]annulene (**28**, Figure 9) exhibit particular stability upon formation, much greater than that of corresponding naphthyl groups. On the other hand, the 11-(1,6-methano[10]annulenyl) cation **29** is destabilized relative to cycloheptatrienyl cation, with limited aromatic ring interaction.

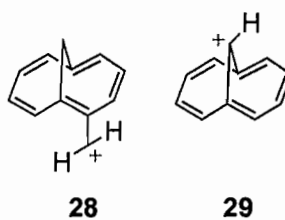


Figure 9. Cations from bridged [10]annulene solvolysis.

As well as serving as interesting aromaticity probes, bridged [10]annulene systems have demonstrated possible applications upon donor/acceptor functionalization. Pd-catalyzed coupling of phenylacetylene units to dihalo-1,6-methano[10]annulene, and similar coupling of ethynyl-1,6-methano[10]annulene to bromo-substituted azobenzene has yielded novel donor/acceptor structures (e.g., **30** and **31**, respectively, Figure 10).²⁹ Optical properties compare well with their benzene analogues, which have been shown to exhibit interesting nonlinear optical susceptibilities. The azobenzene derivatives also provide promising candidates for new azo dyes.

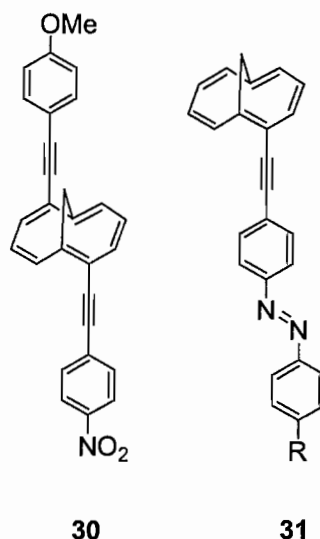


Figure 10. Donor/acceptor-functionalized bridged [10]annulenes.

The aromaticity and stability data on bridged annulenes gained by computation and experiment allows their more targeted application towards fused-ring syntheses. Gellman and coworkers^{26b} have developed a method using a semi-benzylic Favorskii

rearrangement to provide 1,6-methano[10]annulene derivatives **32** bearing substituents on both the bridge carbon and the aromatic ring, thus greatly increasing the availability of a wide variety of bridged annulenes. Another method affords enantiomerically pure 1,6-methano[10]annulene derivatives (**33**).^{26c} Both of these techniques have demonstrated generality and efficiency. A more convenient but less general procedure allows synthesis of 2,5-disubstituted 1,6-methano[10]annulene **34** from 1,6-diacetylcyclohepta-1,3,5-triene.^{26d} A reactive *o*-quinodimethane derivative, 1,6-methano[10]annulene-3,4-quinodimethane (**35**), has also been generated and trapped as various Diels-Alder adducts,^{26e} providing a practical method for the preparation of six-membered ring-fused [10]annulenes and a variety of theoretically and synthetically interesting compounds. It should be noted that these highlights represent only a few examples of the synthetic, computational, and spectroscopic work that has been undertaken in recent years.³⁰

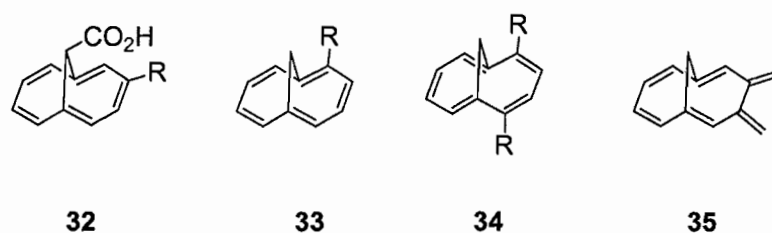


Figure 11. Substituted derivatives of bridged [10]annulene.

[12]Annulenes. Although there has been some controversy regarding the veracity of the preparation of the $(4n)$ π -electron [12]annulene (**36**, Figure 12),³¹ it was first reported in 1970 by Oth and coworkers.³² Low-temperature NMR spectroscopic analysis led the authors to conclude that **36** was significantly distorted from planarity due to steric

crowding by the internal protons (**36a**) and that it readily underwent *cis/trans* isomerization through intermediate **37** (Figure 13).

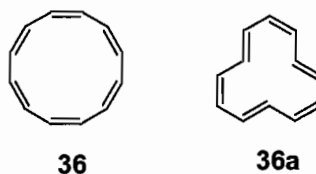


Figure 12. Isomers of [12]annulene

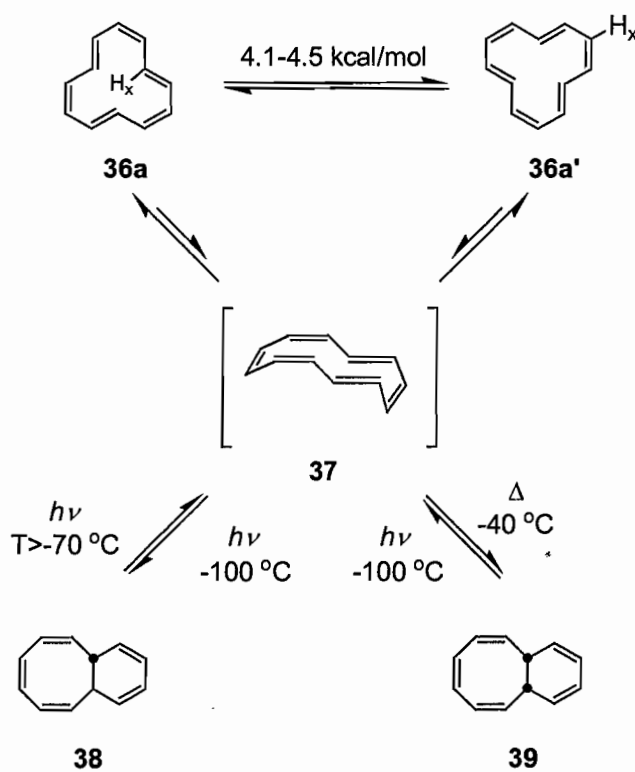


Figure 13. Isomerization and cyclization of [12]annulene.

The isolated electrocyclic ring closure products **38** and **39** led the authors to hypothesize a very low ($4.1\text{-}4.5\text{ kcal mol}^{-1}$) automerization energy barrier. Ever since, the

original experimental work, there have been numerous computational studies performed to determine what exactly is the most stable conformation of [12]annulene,^{31,33} some of which yielding starkly contradicting results. The automerization transition state has previously been calculated as a D_3 -symmetric structure (**40**, Figure 14), but very recent results support the original tri-*trans*-[12]annulene structure proposed by Oth,³⁴ with a delocalized (aromatic), C_2 -symmetric automerization transition state (**41**). This Möbius-like transition state occurs through a so-called “twist-coupled bond shifting”, wherein twisting of three adjacent carbon-carbon bonds is accompanied by bond length equalization. More complicated pericyclic reactions of [12]annulene (e.g., to **42**) have also been investigated computationally³⁵ and are believed to proceed through several transition states. For more on Möbius annulenes, the reader is referred to the contribution of Herges in the issue of *Chemical Reviews* in which this chapter appears.¹³

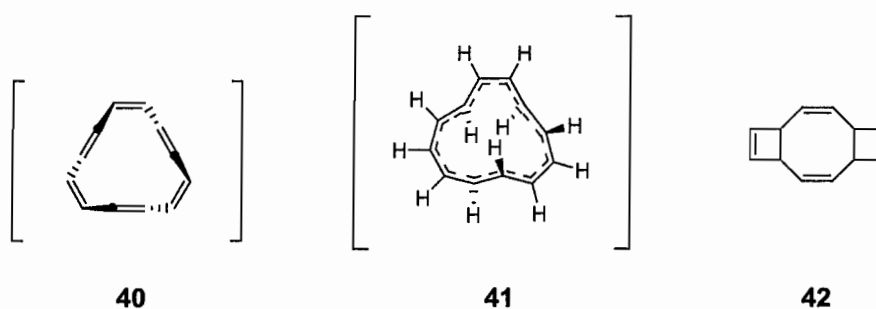


Figure 14. Automerization and pericyclic reactions in [12]annulene.

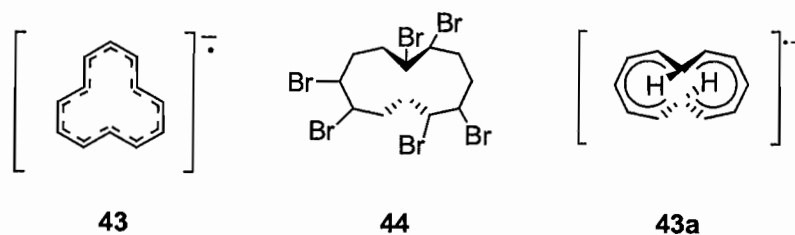
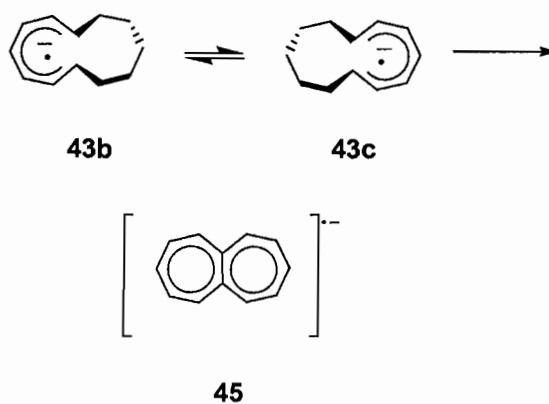


Figure 15. Anion radicals of [12]annulene.

The anion radical of [12]annulene (**43**, Figure 15) has been shown to be stable enough for spectroscopic characterization³⁶ and can be generated either from exposure of neutral [12]annulene to alkali metals or from dehydrohalogenation of 1,2,5,6,9,10-hexabromocyclododecane **44**, a fire retardant. The anion assumes a “half-planar” conformation (**43a**) wherein seven carbons lie in plane, and consequently contain most of the spin density, with the other five atoms twisted out of the plane, with rapid ($k = 10^6$ - 10^7 /sec) rearrangement between degenerate conformations (**43b** and **c**). Thermal dehydrogenation collapses the anion into the heptalene anion radical **45** (Scheme 3).



Scheme 3. Cyclization of anion radicals of [12]annulene.

Bridged [12]annulene **46** (Figure 16), like bridged [10]annulene, exhibits much greater stability than the parent annulene. 1,7-Methano[12]annulene was first prepared by Vogel in 1974,³⁷ and was found to be nonplanar with significant bond length alternation. Its relative stability, combined with a weakened (but still significant) cyclic conjugation makes it a good candidate for electron delocalization studies.³⁸ For example, fusion of a benzene ring onto the $4n$ π -electron system to make **47** results in a reduction of the paramagnetic ring current.³⁹

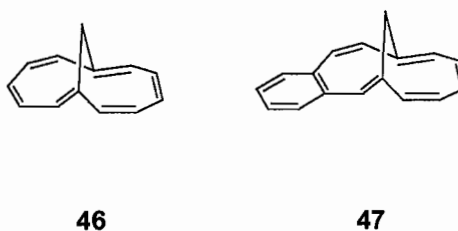


Figure 16. Bridged [12]annulenes.

[14]Annulenes. [14]Annulene (**48**, Figure 17) was first synthesized in 1960 by Sondheimer and Gaoni.⁴⁰ Computational and experimental studies performed since have consistently concluded that the molecule adopts a nonplanar conformation with a delocalized π -bond structure in the solid crystalline state.⁴¹ The nonplanarity is ascribed primarily to nonbonding interactions between the internal protons. Nearly equalized bond lengths (~ 1.40 Å) have been confirmed by calculation as well as X-ray analysis and low-temperature UV-Vis studies.^{41c} The photoelectron spectrum of [14]annulene^{41e} reveals a

vertical ionization energy consistent with an aromatic system. This study also concluded that of the three most-reported symmetry states for [14]annulene (C_{2h} , D_2 , and C_s), the C_{2h} -symmetric state **48a** with π -bond delocalization is the most favored. In solution, [14]annulene exists in equilibrium between the C_{2h} -symmetric state and a minor (8%) *trans* configuration **48b**,^{41a} though some have asserted that localized structures of [14]annulene may not even exist.^{41d}

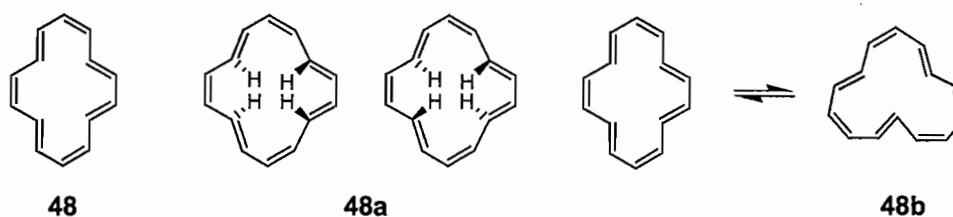
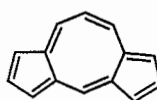


Figure 17. Isomers of [14]annulene.

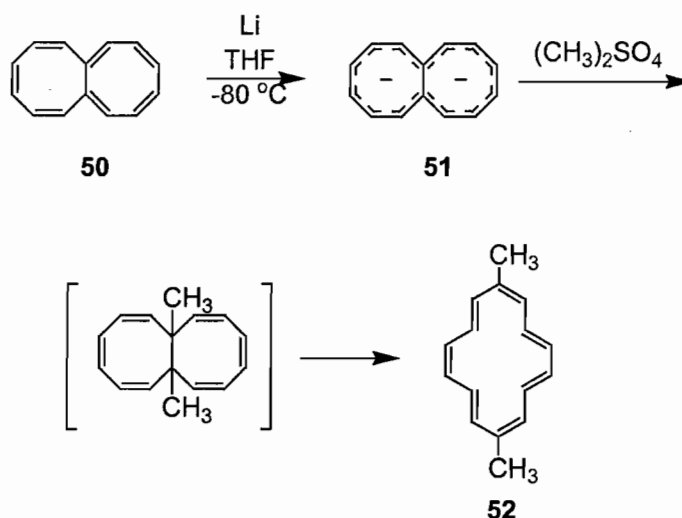
Although planar *cis*-[14]annulene is theoretical, isomeric precursors such as the little studied “nonalternant hydrocarbons” (e.g., **49**, Figure 18) have been synthesized and correlated to calculated frontier molecular orbitals of the as-yet unknown annulene.^{41f}



49

Figure 18. Isomeric precursor to planar *cis*-[14]annulene.

Octalene (**50**), another isomer, can be considered a perturbed [14]annulene with a zero-atom crosslink. That this structural variation does not preclude chemical similarity has been shown by reductive methylation of octalene (Scheme 4).^{41g} Treatment of octalene with Li metal results in the dianion **51**, which reacts with dimethyl sulfate to yield the disubstituted annulene **52**. NMR spectroscopy of **52** indicates a pyrene-like structure with four internal protons. Temperature dependence of the NMR signals also indicates equilibration between three configurations (**52a-c**, Figure 19) that allows inner and outer protons to be exchanged. The X-ray structure shows a centrosymmetric crystalline configuration that precludes bond alternation. The bond delocalization is retained even with significant (up to 20° torsional angles) deviation from planarity. A promising application arises with this substitution method, since direct treatment of the parent [14]annulene with electrophilic reagents results in polymerization rather than substitution.



Scheme 4. Generation of [14]annulene from octalene.

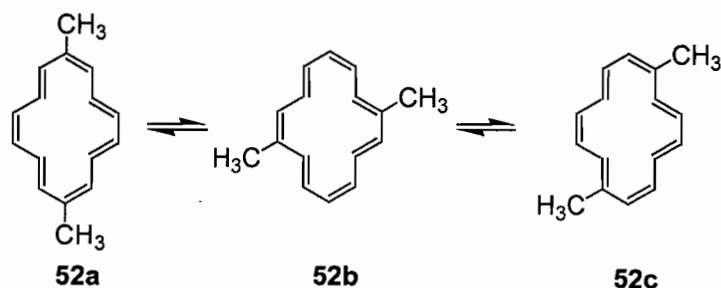


Figure 19. Isomers of methylated [14]annulene.

Bridged [14]Annulenes. As in the case of bridged [10]annulenes, bridged [14]annulenes (**53-55**, Figure 20) show sensitivity to the bridging group.⁴² Nonbonding interaction between bridging groups in multiply-bridged annulenes (both syn and anti) can cause severe distortions of the annulene ring.^{42a} Table 1 illustrates just two of the parameters that can be affected by several different substitutions in bridging pattern.

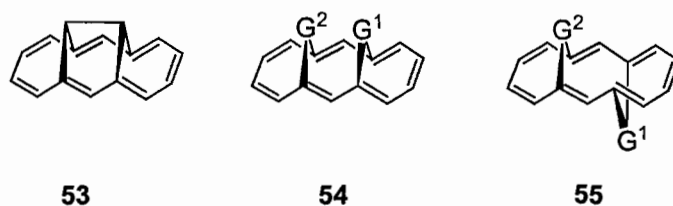


Figure 20. Various bridged [14]annulenes.

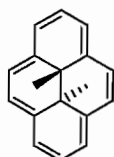
Table 1.^{42a} Effect of bridging substituents on carbon-carbon bond lengths of **54** and **55**.

	G ²	G ¹	G ² -bridged C-C distance, Å	G ¹ -bridged C-C distance, Å
a			2.294	2.294
b			2.290	2.274
c			2.279	2.274
d			2.325	2.356
e			2.259	2.249
f			2.470	2.472
g			2.359	2.360
h			2.340	2.326
i*			2.278	2.341
j*			2.502	2.440

*anti-bridged annulene **55**

Dimethyldihydropyrene (DMDHP **56**, Figure 21) and its numerous derivatives have been one of the most studied classes bridged[14]annulene systems known. The majority of work in this area over the last 20 years has been undertaken by Mitchell and coworkers.^{43a-k} It is only the second annulene to have its enthalpy of formation (ca. 339 kJ/mol) measured.^{43a} The planar, delocalized aromatic system^{43b} is complemented by the internal methyl units that reside above and below the plane, and thus present convenient handles for the probing of ring current effects from manipulation of the parent structure

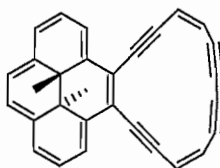
(most notably, from fusion of aromatic rings^{43c} or organometallic complexes^{43d} to the periphery, which can drastically and perhaps predictably attenuate the diatropicity of the annulene). Fusions of DMDHP units to each other^{43e} and into a cyclophane structure^{43f} have been accomplished.



56

Figure 21. Dimethyldihydropyrene.

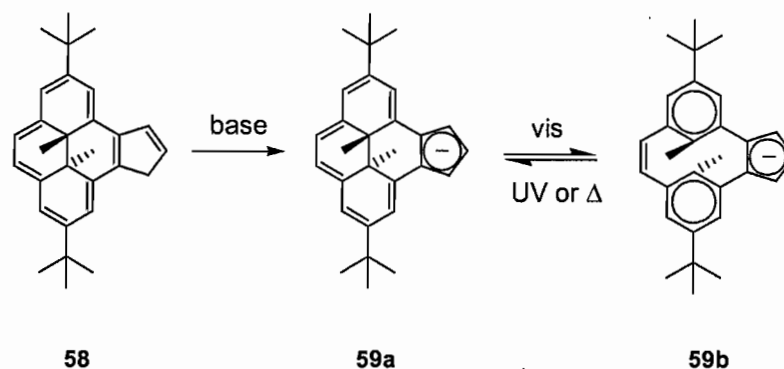
Fusion of a DMDHP to a dehydroannulene (e.g., **57**, Figure 22) has been shown to cause a reduction in diatropicity of both units.^{43g} The attenuation is used to infer a weak diatropic ring current associated with the dehydroannulene, but the degree of change is too small for the relative differences in aromaticity of the two units to be reliably measured. Dehydroannulenes are discussed in more detail in later sections.



57

Figure 22. Dehydroannulene-fused DMDHP.

A DMDHP derivative has also found application as a photomeric switch.^{43h} Exposure of the annulene-fused cyclopentadiene **58** to KH or $\text{LiCH}_2\text{SiMe}_3$ generates the [14]annulene-fused cyclopentadienide anion **59a** (Scheme 5), causing a reduction in diatropicity and significant deshielding of the internal methyl protons. The anion exhibits reversible photomeric opening of the bond between the methine bridges to generate **59b**, and it is concluded that the cyclopentadienide anion is acting in a manner chemically similar to benzene. Other derivatives of DMDHP have been prepared,^{43ij} and several photochemical studies have been performed.^{43k}



Scheme 5. Photochromic switching in a DMDHP derivative.

[16]Annulenes. The $(4n)$ π -system [16]annulene (**60**, Figure 23) was first synthesized in 1961 by Sondheimer and Gaoni.⁴⁴ Since then, a variety of conformations have been found to be stable, either through computation or X-ray crystallography.^{45,33d} The annulene exists predominantly in the alternating *cis/trans* configuration with four internal protons that contribute to the considerable distortion from planarity (**60a**). A minor (12%) isomer **60b** with five internal protons is believed to exist in equilibrium with

the major isomer (Figure 23).^{41a} Recently, several new conformations, some with Möbius topography, have been predicted computationally.^{33e} The geometry of the annulene shows significant temperature dependence in the NMR spectrum: as the temperature is decreased, the molecule becomes more planarized, and antiaromatic character increases.^{41a} Despite the classic hypothesis that $(4n)$ π -electron systems are inherently destabilized relative to their acyclic analogues, recent work has advanced the possibility that larger $(4n)$ systems like [16]annulene are only slightly destabilized by π -electron interactions.⁴⁶

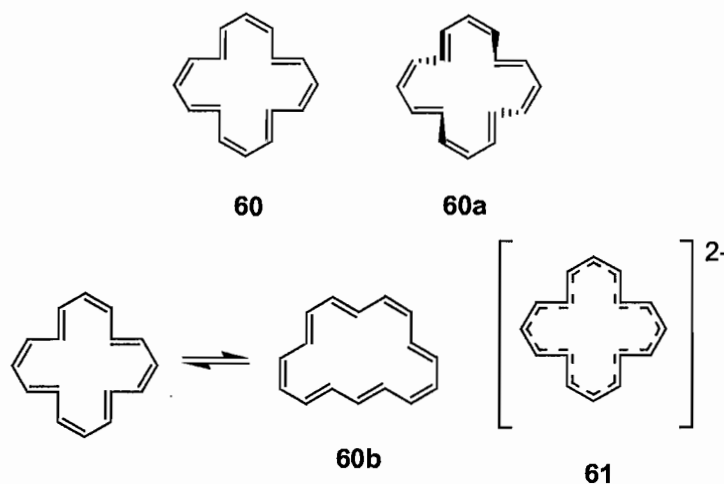


Figure 23. Isomers and dianion of [16]annulene.

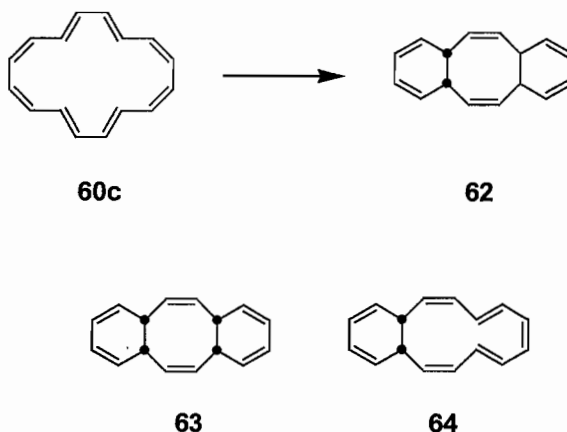
Stevenson and coworkers have performed several isotopic perturbation studies on 95% deuterated [16]annulene illustrating the dramatic effects of ring planarity on ring tropicity.⁴⁷ The shorter length of the C–D bond relative to the C–H bond results in decreased steric interactions on the interior of the ring, allowing the system to relax into a

more planarized state. This causes a marked increase in paratropicity, with the NMR resonance of the internal protons shifted downfield from 10.58 to 10.82 ppm upon deuteration.^{47a} The external protons experience a similar upfield shift. Calculations predict decreased dihedral angles along the C–C bonds of nearly half the annulene.

As in the case of [8]annulene (COT), the anion radical and dianion species (**7** and **61**, respectively) have been easily made by reduction of the neutral molecules with alkali metals.^{48a} Later, it was found that the anion can be generated by reduction of the [2 + 2] dimer of cyclooctatetraene (see Scheme 1) or by equimolar reaction of COT anion radical with neutral COT.^{48b} This last method shows the synthetic potential of anion radical-neutral molecule combination reactions. Formation of the dianion creates a $(4n + 2)$ π -electron system that displays even greater diatropicity than [18]annulene, and is believed to be significantly more stable than neutral [16]annulene. Isotopic perturbation studies of the dianion of [16]annulene^{47a} provide results directly opposite the neutral molecule: deuteration causes a pronounced increase in diatropicity, shifting the internal protons upfield from -8.03 to -8.11 ppm. The shifting of the external protons, however, are “not larger than experimental error”.

The cyclization reaction of [16]annulene (Scheme 6) was investigated experimentally in 1967,⁴⁹ and was reported to proceed from the C_s -symmetric conformation (even though it is 31.4 kJ/mol less stable than the lowest energy conformation) to the tricyclic product with two bridgehead hydrogens pointing in one direction (**62**) and the other two in another. It was not known whether the cyclization occurred in a stepwise or concerted manner. The cyclized product with all four

bridgehead hydrogens pointing in the same direction (**63**), however, was calculated to be thermodynamically more stable.^{33d} The electrocyclic reactions of [16]annulene have recently been investigated computationally using *ab initio* and density functional theory calculations.⁵⁰ Several intermediates and transition states were determined, and it was found that cyclization to the more stable product was likely to be stepwise, with first one ring closure followed by the other from a bicyclic intermediate **64**. The overall energy barrier was calculated as 131.0 kJ/mol, which is the relative energy of the first transition state. A viable concerted transition state for the cyclization could not be found. The four computed stepwise mechanisms for cyclization to the less thermodynamically stable product were much more complex: there were four transition states and three intermediates, with the lowest overall energy barrier of about 131.0 kJ/mol determined by the third transition state. This was exactly the same energy barrier as the cyclization to the more stable product. Based on these barriers, it was not possible to determine the dominant product of the reaction. A concerted transition state for this reaction also could not be determined.



Scheme 6. Cyclization of [16]annulene.

[18]Annulenes. [18]Annulene (**65**, Figure 24) represents a unique target of study, due not only to its status as a $(4n+2)$ annulene, but as a member of the aromatic subgroup $6(2p+1)$ in which the D_{6h} -symmetric point group is allowed without severe nonbonded interactions.^{51a} As annulene ring size increases, aromatic stabilization energies drop off and bond length alternation becomes more pronounced. An ongoing debate has centered around the ring size at which polyolefin-like, localized π -electron structures predominate over fully delocalized conjugation. Put simply, it is the question of the point at which drawing a closed circle inside the ring rather than alternating double and single bonds becomes inappropriate. Computational and theoretical estimates ranging from [30]annulene^{51b} all the way down to [10]annulene²³ have been put forward. More and more, the front lines of this debate take root at or near [18]annulene.

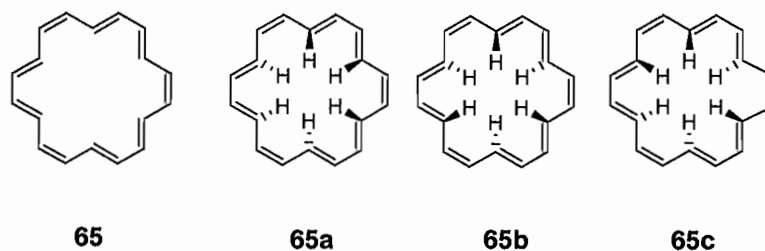


Figure 24. Isomers of [18]annulene.

Around the same time that Sondheimer and coworkers first synthesized **65**,^{52a} Longuet-Higgins and Salem predicted the diminishing aromatic stabilization of large $(4n+2)$ annulenes.^{52b} Even earlier, Mislow predicted the unlikelihood of planar D_{6h} [18]annulene due to steric interactions between the internal protons.^{52c} More recently, low-temperature NMR studies have yielded three conformations of nearly equal energy,⁵³ with three internal protons above the plane and three below, in three possible arrangements (**65a-c**). Furthermore, upon synthesis, chemical evidence revealed reactivity typical of localized π -bonds (addition rather than substitution), behavior drastically different than benzene. It may be a bit surprising then, that the X-ray crystal structure of **65**, first determined in 1965,^{54a} showed a nearly centrosymmetric molecule distorted from planarity by 0.085 Å and a C_{3i} symmetry only slightly distorted from D_{6h} symmetry. The nonplanarity was explained by intermolecular nonbonded repulsions and crystal packing forces. The crystal structure was re-evaluated in 1995,^{54b} and although an additional minor form with slightly different geometry was found, [18]annulene was confirmed by the authors as “having an essentially planar aromatic structure in the

crystal". The twelve 'inner' C–C bonds were determined to have lengths of 1.385 Å, and the six 'outer' bonds lengths of 1.405 Å, relatively close to the originally determined geometry. The authors also noted that the average C–C length in **65** is similar to benzene. The ring internal and reentrant angles are 124.0° and 127.9°, respectively.

Schleyer and coworkers have recently challenged the essential symmetry and planarity of [18]annulene,⁵⁵ calling the experimental data into question. It has been pointed out by Shaik, Hiberty et al.⁵⁶ that adjacent overlapping π -bonds prefer bond length alternation, but that in small cyclic conjugated systems, it is the σ framework that enforces a regular geometry. Cyclic conjugation is only weakened, not eliminated, by deviations from bond equalization. Thus, the bonds in benzene are equalized by the σ skeleton, *not* the conjugated π -system. Since this equalization tendency is a weaker force than the π preference for alternation, benzene is the exception to the norm, rather than the prototype for aromatic systems. Schleyer points out that this π -induced distortion is in no way inconsistent with aromatic character, but it is important to determine the point at which the competing forces of " σ resistance and π distortivity" balance completely.^{55a} To this end, Bühl and Schleyer used GIAO-B3LYP/6-311+G** methods to compute the ¹H NMR shifts of various boranes, carboranes, carbocations, and [*n*]annulenes, and demonstrated that computed values matched experimental values only when geometries were correct. They then used this method to show that the shifts were in good agreement only when **65** did not have D_{6h} symmetry (Table 2), and that the shifts computed using the geometry derived from the X-ray data were in disagreement with the experimental

shifts. Finally, they found that only a C_2 geometry gave acceptable results: at both the KMLYP and BHLYP levels, C_2 [18]annulene is lower in single-point energy.

Table 2. Bond alternation of [18]annulene in various symmetry point groups.

Point Group	Level of Theory	Δr (Å)	δH_{inner}	δH_{outer}
D_{6h}	B3LYP	0.017	-10.9 to -11.0	11.5 to 11.6
D_{6h}	KMLYP	0.015	-11.3 to -11.5	11.2 to 11.4
D_{3h}	KMLYP	0.095	-4.9 to -5.0	9.3 to 9.8
D_3	KMLYP	0.095	-4.2 to -5.1	9.4 to 9.5
C_2	KMLYP	0.099	-2.3 to -2.6	8.9 to 9.0
D_{6h}	BHLYP	0.015	-11.2 to -11.4	11.2 to 11.5
D_{3h}	BHLYP	0.094	-4.9 to -5.1	9.6 to 9.8
D_3	BHLYP	0.095	-4.3 to -4.6	9.5 to 9.7
C_2	BHLYP	0.100	-2.7 to -2.9	9.0 to 9.4
	Exp.	0.042	-2.99	9.3

6-31+G** basis set used for optimization of all structures; Δr is the distance between shortest and longest C–C bond lengths. δH_{inner} and δH_{outer} are the GIAO-B3LYP/6-311+G** ^1H NMR chemical shifts in ppm relative to TMS.

Schleyer explains the contradictory crystal data in part by static disorder, in which superposition of a lower symmetry structure leads to an apparent higher symmetry. Although the authors of the 1995 investigation ruled this possibility out, they were using earlier geometry models that overestimated ring diameters⁵⁷ well beyond the computed deviations between the C_2 , D_{3h} and D_{6h} structures. Another issue with the crystal data is dynamic disorder: the rapid interconversion between two C_2 structures passes through

D_{6h} as a transition state with a barrier of only $\sim 3 \text{ kcal mol}^{-1}$, which would produce a time-averaged structure.

Ermer has recently published a brief disputation of Schleyer and coworkers' assertions,⁵⁸ offering that it may in fact be possible to distinguish inversion disorder effects from true single structures at currently attainable resolutions. In addition, he noted that computation regards molecules as being in the gas phase, and that the small barrier to symmetrization could be overcome by π - π stacking and favorable crystal-packing forces, i.e., "driving the molecules in the crystal towards centrosymmetric forms with non-alternating character". If bond alternation does indeed exist in [18]annulene and then vanishes upon crystallization, it would be an extremely unusual phenomenon with important implications for solid state NMR. Clearly, further computational efforts are in order.

The same isotopic perturbation experiments undertaken by Stevenson and coworkers for [16]annulene were applied to [18]annulene.⁵³ Not surprisingly, the same effect, albeit opposite due to the aromaticity of **65** rather than antiaromaticity, is observed. Upon deuteration, the external proton NMR signals shift downfield from 9.17 to 9.20 ppm due to reduced steric crowding by the smaller deuterium and more effective π -orbital overlap, resulting in a more planarized structure with a larger ring current. Similarly, the internal protons experience an upfield shift from -2.96 to -3.08 ppm, again consistent with increased diatropicity.

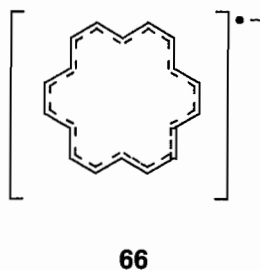


Figure 25. Anion radical of [18]annulene.

The anion radical of [18]annulene (**66**, Figure 25) is obtained via reduction by K metal and has been shown to undergo Jahn-Teller distortion to two different structures when the odd electron occupies the degenerate antibonding molecular orbitals (D_{2h} and C_{2h} symmetries).^{59a} The anion is not very stable, but persists for nearly an hour at room temperature. In contrast to the C_{2v} anion radical of benzene, rapid pseudorotation of the system is prevented by the nonplanarity of the radical, as evidenced by the complex EPR spectrum. The anion is proposed to equilibrate between two degenerate C_{2h} conformations (**66a** and **66c**, Figure 26), in which three internal protons are in the plane of the ring, two are below and one is above, through a D_{2h} transition state **66b** in which all internal protons are in the plane. These results imply that the disruptive effect of the odd electron amplifies the π -component to “overcome the symmetrizing force of the σ -framework”. It has been suggested that [18]annulene anion radical has the potential to represent a superconducting material.^{50,51}

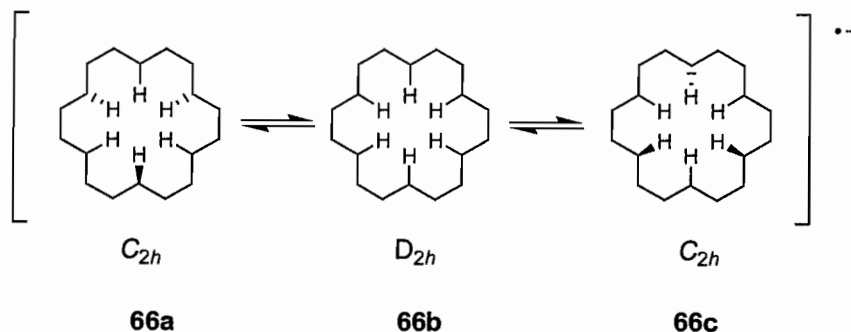


Figure 26. Isomerization of [18]annulene anion radical.

The dianion **67** also adopts one of two equilibrating nonplanar conformations (**a** and **b**, Figure 27, 2.3:1 ratio) with antiaromatic character and bond alternation. The dianion is also unstable relative to the neutral molecule.^{59b}

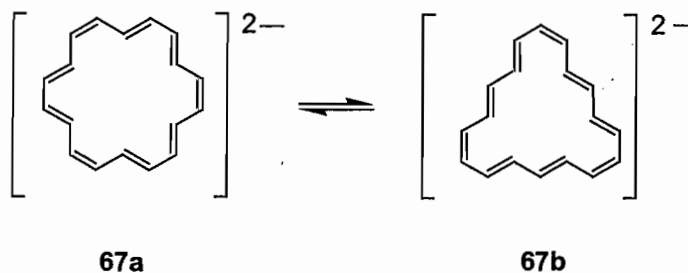
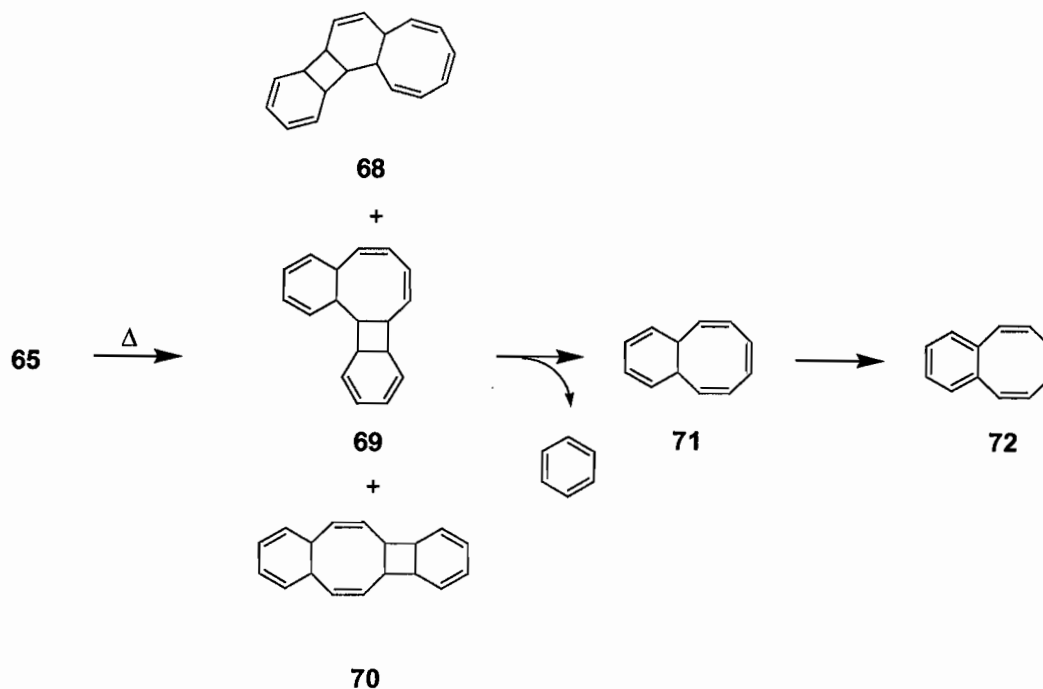


Figure 27. Conformations of [18]annulene dianion.

[18]Annulene has been shown to undergo thermal rearrangement (Scheme 7).⁶⁰ Although scanning calorimetry was able to determine the thermodynamic factors some years ago,^{60a} elucidation of the mechanism was achieved through reinvestigation of the thermograms using an iterative method of integration of the kinetic equations established.^{60b} The CALIT-3 program is able to simulate thermograms observed for

successive first-order reactions: the three first-order reactions [18]annulene \rightarrow **68-70** \rightarrow **71** + benzene and **71** \rightarrow **72**. Tetracyclic intermediates **68-70** believed to be generated in this reaction all play the same role in the mechanism and are therefore considered the same compounds from a kinetic standpoint. Using complex calorimetric methods in conjunction with the thermogram simulator program, a detailed mechanistic picture of the thermal rearrangement was deduced. The enthalpy of formation of [18]annulene ($123.4 \pm 3.7 \text{ kcal mol}^{-1}$ at 298.2 K), stabilization energy ($-37.6 \pm 4.6 \text{ kcal mol}^{-1}$) and π -bond delocalization energy ($\sim -120.5 \text{ kcal mol}^{-1}$) were determined. Activation enthalpy, entropy, and free energy for each step was also determined (summarized in Table 3). Interestingly, the last step in the mechanism is believed to include two suprafacial 1,5-hydrogen shifts. The kinetic parameters obtained are in good agreement with the thermograms, showing the utility of this method in analyzing complex reaction mechanisms.



Scheme 7. Thermal rearrangements of [18]annulene.

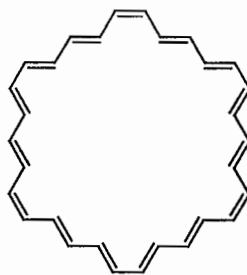
Table 3. Activation parameters for thermal rearrangement of **65** to **72**.

reaction	ΔH^\ddagger (kcal mol ⁻¹) ^a	ΔS^\ddagger (cal molK ⁻¹)	ΔG^\ddagger (kcal mol ⁻¹)
65 → 68-70	36.03 ± 0.01	13.88 ± 0.08	31.89 ± 0.01
68-70 → 71 + benzene	34.05 ± 0.2	14.20 ± 1.0	29.82 ± 0.2
71 → 72	32.90 ± 0.21	14.22 ± 0.13	28.56 ± 0.21

^aValues at 298.15K.

Higher Annulenes. The higher annulenes ($n > 18$) present less synthetic interest, mostly due to their significant bond alternation, asymmetry, and conformational flexibility. All annulenes up to $n = 30$ (**73**) have been synthesized except $n = 26$ and 28.

Most of the recent work has been computational in nature and aims at understanding the complex interplay between geometric, energetic, and magnetic properties. Aromatic stabilization energies are greatly reduced in the larger systems and it is believed that the mixing of low-lying excited states and ground states leads to pseudo-Jahn-Teller distortions.⁶¹ The search for a discrete transition point between delocalized and localized structures, mentioned in the previous section, prompted a computational study by Choi and Kertesz that investigated bond length alternation in large annulenes up to $n = 66$.^{62a} Various levels of theory and basis sets were sampled. While B3LYP/6-31G* acceptably predicted bond lengths of known ring sizes and oligoenes, Hartree-Fock methods consistently provided clearly incorrect (and at times impossible) values. Using experimental measurements as guides,^{62b} DFT calculations accurately quantified the bond length alternation ($\delta = R_{\text{single}} - R_{\text{double}}$) of the minimized structures of both $(4n)$ and $(4n + 2)$ annulenes as a function of ring size (Table 4). In the progression of $(4n + 2)$ annulenes, the data clearly show a sharp increase in δ for [30]annulene. Conversely, an enforced $\delta = 0$ produced a local maximum for [30]annulene – [66]annulene in the energy profiles. δ values for the lower $(4n + 2)$ annulenes ([14], [18], [22], and [26]) are essentially zero and thus are not reported.



73

Figure 28. [30]Annulene.**Table 4.** Calculated bond length alternations in various annulenes.^{62a}

	n	C-C (Å) ^a	C=C (Å) ^a	δ
(4n)	[20]	1.442	1.361	0.081
	[24]	1.432	1.363	0.069
(4n+2)	[14]	—	—	—
	[18]	—	—	—
	[22]	—	—	—
	[26]	—	—	—
	[30]	1.417	1.382	0.035
	[42]	1.425	1.374	0.051
	[54]	0.427	1.371	0.056
	[66]	1.427	1.371	0.056

^a Calculated at B3LYP/6-31+G** level of theory.

Another value investigated was the nucleus-independent chemical shift (NICS) parameter, which has proven an effective criterion for aromaticity.⁶³ NICS is the negative

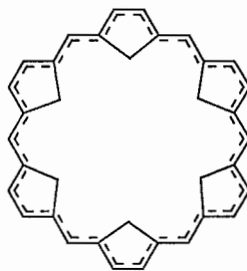
of the absolute magnetic shielding at the center of a ring current. A negative value denotes aromaticity and a positive value antiaromaticity (e.g., benzene = -11.5 ; cyclobutadiene = 28.8). A sharp decrease in magnitude of the NICS value for [30]annulene was predicted, going from -15.9 in the case of [26]annulene to -12.4 for [30]annulene, with a further, more gradual dropoff at larger sizes. It is noted that this is still a large and negative value, implying that bond alternation is not necessarily correlated to antiaromaticity. The reasonable conclusion is that [30]annulene is the most likely candidate for the “transition point” to a localized, yet still aromatic, structure. Surprisingly, using these methods, the calculated aromatic stabilization energies do not decrease with increasing ring size, but increase up to [18]annulene and then seem to converge to a limiting value of about 23 kcal mol^{-1} . This provides further evidence that total delocalization is not required for aromaticity.

In the same work for which a D_{6h} symmetry for [18]annulene was discounted,^{55a} Schleyer and coworkers also pointed to their computational comparison with experimental chemical shifts of [22]annulene, for which the crystal structure is not known. The large disagreement between the two sets of shifts led them to reject the reported D_{2h} symmetry and to assert bond alternation for [22]annulene which, by implication, “should be true of all the higher annulenes”. On the other hand, Yoshizawa and coworkers have performed vibrational analyses on both **65** and **73**^{51a} and have concluded that the B_{1u} and B_{2u} vibrational modes of [30]annulene lead to equivalent D_{3h} global minima, with a D_{6h} transition state and an energetic barrier of $2.3 \text{ kcal mol}^{-1}$ or less depending on the level of theory employed.

Yoshizawa and coworkers have also computed the electronic structure,⁶⁴ vibrational frequencies, and linear vibronic coupling constants of [30]annulene as well as its normal and deuterated mono- and trianions to analyze the vibronic interactions and their effects on Jahn-Teller distortions. They found that the lowest E_{2g} mode (38 cm^{-1}) affords unusually large vibronic coupling constants, and thus should play a significant role in Jahn-Teller distortions of **73**. This low-frequency mode is typical of nanosized molecular systems and is in stark contrast to the cases of benzene, in which only the highest E_{2g} vibrational modes (1656 and 3184 cm^{-1}) play a significant role in Jahn-Teller distortions, and of [18]annulene, where the lowest E_{2g} modes at 116 and 405 cm^{-1} and the highest stretching frequency of 3201 cm^{-1} are most important. This implies that the low-frequency modes become more important in carbon ring distortions as the annulene size increases. In both the mono- and trianion, the vibronic coupling constant of the 38 cm^{-1} mode is altered upon deuteration of the annulene and the vibronic coupling constant of the 1513 cm^{-1} mode is increased slightly.

Kiran and Nguyen⁶⁵ calculated an enforced delocalization for [30]- and [42]annulene using symmetrically placed methylene bridges connecting adjacent internal carbons to create multiple cyclopentadiene units in the interior of the structures (e.g., **74**, Figure 29). The induced ring strain is enough in these cases to cause stabilization of the delocalized (D_{6h}) structure in preference to the localized (D_{3h}) structure. However, the same strategy fails in the cases of [54]- and [66]annulene, which still prefer localized structures. The higher annulenes experience less ring strain from the methylene bridging. The lower symmetry structures all experience less ring strain, with the higher annulenes

experiencing much less. This shows that delocalization and aromaticity are adjustable in much the same way that, for example, the aromaticity of methano-bridged[10]annulene is enhanced (vide supra).



74

Figure 29. Multiply-methylene-bridged [30]annulene.

Oth and de Zélicourt performed a detailed low-temperature $^1\text{H-NMR}$ spectrum analysis of the $(4n)$ [24]annulene (**75**),⁶⁶ and deduced its conformations. As expected, the annulene shows significant bond alternation and a paramagnetic ring current with a $\Delta\delta$ of 7.72 between the inner and outer protons. In solution, a rapid equilibrium exists between the major and minor conformers **75a** and **75b** (Figure 30, $K \leq 0.05$), with the resonance energy of the antiaromatic system estimated to be -9 to -10 kcal mol⁻¹.

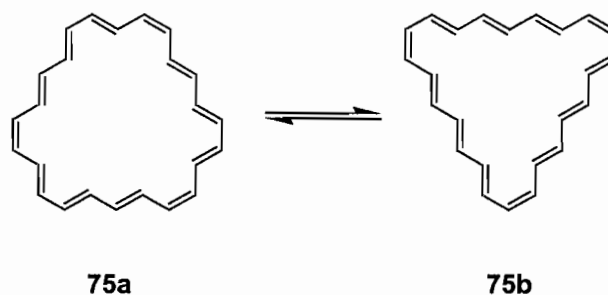


Figure 30. Conformations of [24]annulene.

Dehydroannulenes

From a synthetic standpoint, replacement of one or more of the double bonds of an annulene with triple bonds is a fairly straightforward process. The resultant dehydroannulene often though is considerably less stable than its annulene counterpart and thus prone to undergo deleterious side-reaction, decomposition, etc.; nonetheless, the heightened reactivity also leads to some unusual observations (*vide infra*).

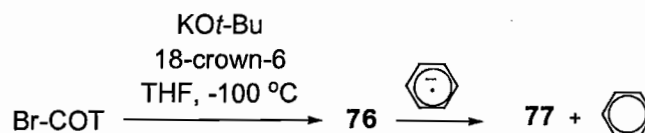
Dehydro[8]annulenes. Dehydro[8]annulene, or [8]annulyne (**76**, Figure 31), was first prepared by Krebs in 1965.^{67a,b} Huang and Sondheimer published a thorough review of work up to 1980,^{67c} and recent work has focused mostly on the anion radical.⁶⁸ Wenthold and Lineberger measured the photoelectron spectrum of $C_8H_6^{-68a,b}$ and reported that it very closely resembled that of the COT anion ($C_8H_8^-$) with similar structures. The anion radical is obtained by reaction of O^- with COT in a liquid N_2 -cooled flowing afterglow apparatus. There are two observed electronic states for [8]annulyne, the lowest described as a singlet 1,3,5-cyclooctatrien-7-yne (**76a**), and a higher triplet dehydrocyclooctatetraene state (**76b**). The electron affinity of neutral dehydro[8]annulene

is 1.044 ± 0.008 eV and the alkyne stretching frequency is 2185 cm^{-1} , which is expected for a strained triple bond in an eight-membered ring. Both the neutral molecule and ion are believed to be planar or pseudoplanar, unlike the tub-shaped COT.



Figure 31. Dehydro[8]annulene and anion radical.

Stevenson and coworkers have developed a one-step entrapment protocol for [8]annulyne anion radical 77^{68c} using dehydrohalogenation of Br-COT by *t*-BuOK in THF solution containing an equimolar amount of 18-crown-6 (Scheme 8). The resulting solutions are characterized by EPR spectroscopy. Neutral [8]annulyne is generated, and addition of benzene anion radical immediately forms the [8]annulyne anion radical which is stable for several hours. Observation of the uncomplexed anion radical is allowed by the presence of the crown ether, which prevents spin delocalization into the K cation. [8]Annulyne also undergoes [2 + 2] dimerization when kept below 173 K without exposure to an electron source. Subsequent exposure also generates the corresponding dimeric anion radical **78** (Figure 32). Several other similar experiments are carried out involving fusion of cyclobutadiene units to [8]annulyne. The authors believe these methods to be generally applicable to the synthesis and storage of various annulyne, bisannulyne, and annulenoannulene anion radicals.



Scheme 8. Generation of dehydro[8]annulene anion radical.

The *sym*-[8]annuldiyne **79** has also been prepared^{68d} using the same dehydrohalogenation method. Exposure to K metal in the presence of 18-crown-6 again leads to capture of its anion radical, inhibiting the rapid equilibration between alternating bond angle conformers induced by Jahn-Teller distortion. Fusion to a cyclobutadiene unit leads to the benzannelated anion radical **80**, but the EPR signal for this compound is weak. Under these conditions, the annuldiyne preferentially undergoes polymerization via extended [2 + 2] cycloaddition to form a solid (**81**) that is insoluble in THF. Characterization revealed extensive crosslinking, with the MALDI analysis showing periodic peaks separated by 100 mass units up through $m/z = 10000$. The crosslinking is believed to take place via suprafacial [2 + 2] cycloadditions of the cyclobutadiene units.

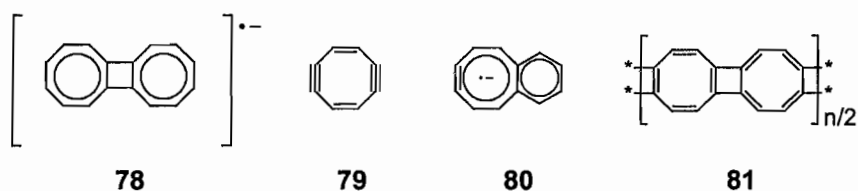


Figure 32. Dimeric anion radical of *sym*-[8]annuldiyne.

Dehydro[10]annulenes. Didehydro[10]annulene (**82**, Figure 33) has yet to be isolated and structurally studied, but recent computational results⁶⁹ suggest that, with its $(4n + 2)$ π -electrons, it should exhibit aromaticity in the planar geometry. The bond-localized configuration is expected to have C_2 symmetry with a tub shape similar to COT. This conformation is found to be more stable than the localized flat (C_{2v}) geometry, but the energetic differences between the two are smaller than for COT, apparently due to aromatic stabilization. The ease with which the bond angles are distorted reduces ring strain in the planar geometry.

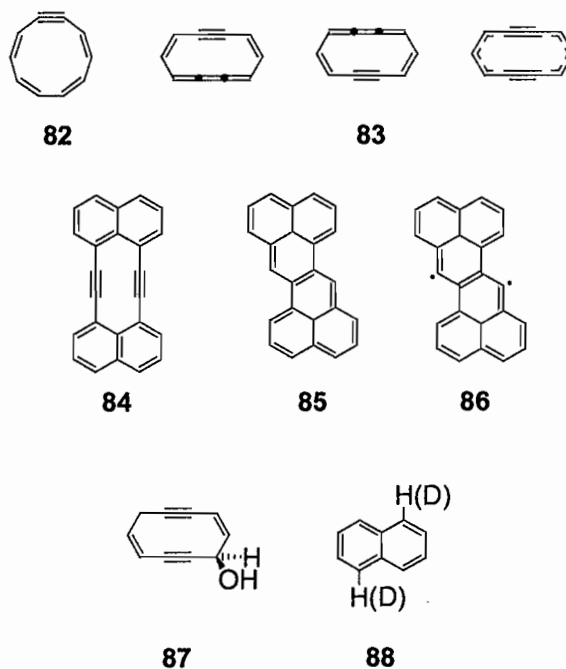
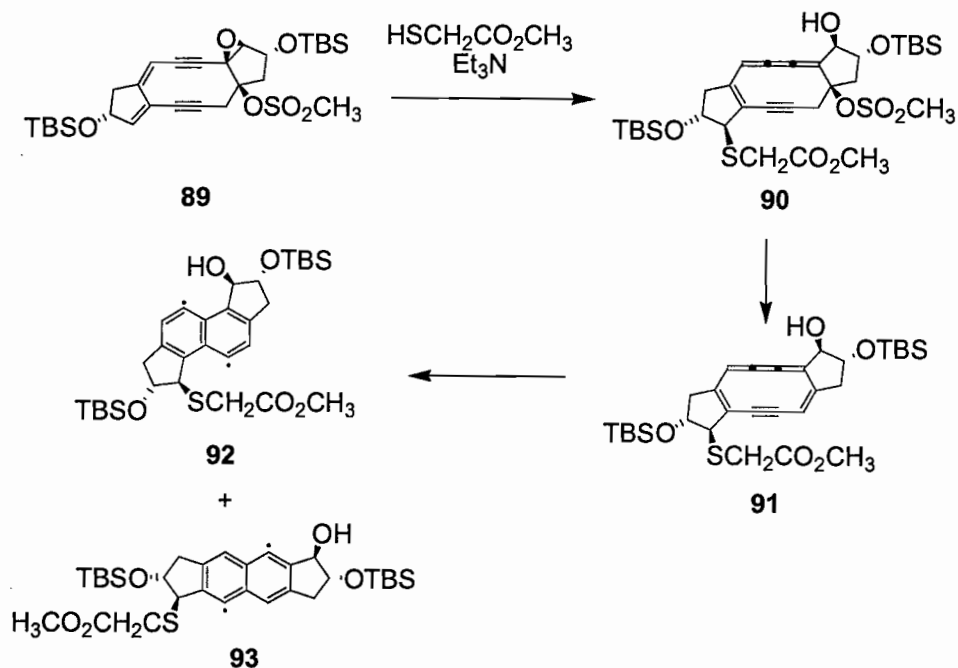


Figure 33. Dehydro[10]annulene isomers and potential cyclization products.

The first tetradehydro[10]annulene (**83**, Figure 33, various representations) was synthesized in 1992 by Myers and Finney.^{70a} The authors were interested in its potential

thermal rearrangement to the biradical 1,5-dehydronaphthalene and noted previous attempts by Sondheimer and Staab to prepare similar benzannelated hydrocarbon **84**, which instead lead to zethrene (**85**), presumably through a zethrene biradical **86**. Successful synthesis of tetrahydro[10]annulene proceeded from dehydration of the acetylenic alcohol **87**. The annulene had “no appreciable lifetime above $-40\text{ }^{\circ}\text{C}$ ”, and any attempts to prepare it above this temperature led immediately to the biradical. At $-90\text{ }^{\circ}\text{C}$, however, treatment of the alcohol with trifluoromethanesulfonic anhydride and triethylamine showed “clean and rapid conversion” to the desired product. Warming in deuterated solvents led to the corresponding 1,5-dideuteronaphthalene **88**. The kinetics for the cyclization were measured at $-51\text{ }^{\circ}\text{C}$ and were first order ($k = 4.6 \times 10^{-4}\text{ s}^{-1}$, $\Delta G^{\ddagger} = 16.3\text{ kcal mol}^{-1}$) with a cyclization half-life of $\sim 25\text{ min}$.

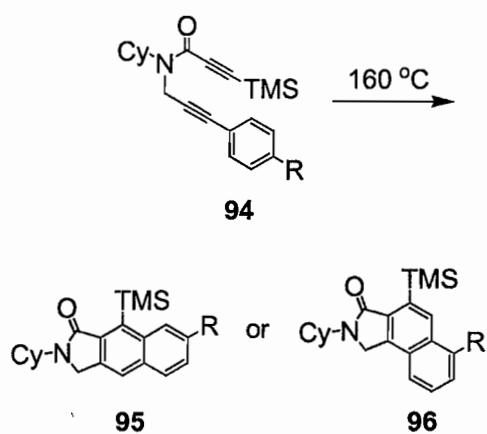
Indeed, soon after initial synthesis of the symmetric parent dehydroannulene, Myers and Dragovich reported the enantioselective synthesis of epoxy dienediyne structure **89**.^{70b} Ideally, **89** could undergo the same type of cyclization following attack by a thiol to make **90**, with subsequent elimination of the methanesulfonate to generate dehydroannulene **91** (Scheme 9). The reaction cascade is initiated by exposure to excess methyl thioglycolate and triethylamine in DMSO and THF at rt. The two expected isomeric naphthalene derivatives corresponding to biradicals **92** and **93** were isolated in 67% and 20% yield, respectively, showing the nondegeneracy of the cyclization pathways. These results represented the first step towards dehydronaphthalene biradical DNA cleavage agents.



Scheme 9. A dehydro[10]annulene intermediate in cyclization of **89**.

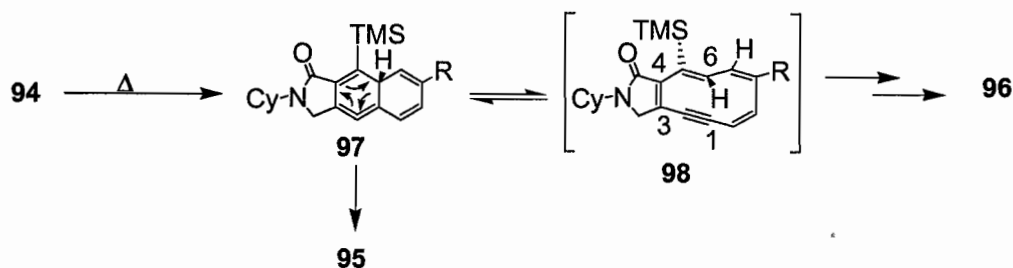
Rearrangements of cyclic allenes (isonaphthalenes) have recently been observed in the intramolecular Diels-Alder cyclizations of silyl-protected acetylenes **94a-c** with phenylacetylenes to selectively form either **95** or **96** (Scheme 10).^{71a-c} It is believed that cyclohexatriene intermediate **97** can either undergo isomerization to benzo[*f*]isoindol-1-one **95** (Scheme 11) or a six-electron electrocyclic ring-opening process through a more stable transition state, yielding the aromatic, bond-equalized dehydro[10]annulene **98**. Upon simultaneous rotation of two double bonds (between C5-C6 and C7-C8), the annulene can then further isomerize to a second cyclic allene, which affords benzo[*e*]isoindol-3-one product **96** upon rearomatization. The preference for each

pathway can be manipulated by varying solvent conditions. Carrying out the reaction in triethylamine leads almost exclusively to the “linear” cyclized product, while reaction in toluene affords the “angular” product only. It is theorized that the base catalyzes the rearomatization of the initial cyclic allene by proton abstraction. Echavarren and coworkers have proposed a similar dehydro[10]annulene intermediate^{71d} with an all-*cis* configuration as well as a possible carbene analog.



	R	solvent	product	%
a	H	Et ₃ N	95	89
b	OCH ₃	Et ₃ N	95	76
c	NO ₂	Et ₃ N	95	74
a	H	toluene	96	74
b	OCH ₃	toluene	96	54
c	NO ₂	toluene	96	70

Scheme 10. Diels-Alder cyclization of silyl-protected acetylene **94**.



Scheme 11. A dehydro[10]annulene intermediate in the cyclization of **94**.

A thorough computational study of dehydro[10]annulene and various cyclization transition states was recently reported by Navarro-Vazquez and Schreiner, in which the nearly planar C_1 “heart” geometry **99a** is calculated to be more stable than the potentially Möbius-like C_2 -symmetric “twist” configuration **99b** (Figure 34).⁷² This is ascribed to the release of strain energy caused by the introduction of the alkyne moiety. Degenerate interchange of this form proceeds through a C_2 transition state with a barrier of 13.5-17.4 kcal mol⁻¹ and conversion to its enantiomer through a planar C_s transition state with a barrier of only 4.3-4.8 kcal mol⁻¹. Cyclization of this form to a cyclic allene (**100**) takes place through a C_1 transition state (16.8 kcal mol⁻¹). [5,7]-Cyclization is possible, but not likely from the most stable “heart” form due to a barrier of 23.3 kcal mol⁻¹. [5,7]-Cyclization is favored, however, from the “twist” form by 2.4 kcal mol⁻¹. Rearomatization affords the final naphthalene (23.9 kcal mol⁻¹). The authors conclude that this “should be taken as the working mechanism for the reported isomerizations during dehydro Diels-Alder reactions of phenylacetylenes”.

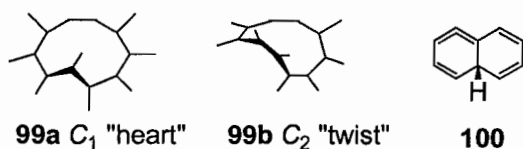


Figure 34. Calculated geometries and cyclization of dehydro[10]annulene.

Dehydro[12]annulenes. While the all-*cis* geometry of 1,2,5,6-tetrahydro[12]annulene **101a** has remained elusive, mono-*trans* structure **101b** has been known since the early 1960s (Figure 35).⁷³ 1,2,7,8-Tetrahydro-[12]annulene **102** is believed to adopt a D_2 -symmetric twist boat conformation **102b**, based on the NMR data. Compound **102** is calculated⁶⁹ to be $34.47 \text{ kcal mol}^{-1}$ more stable than **101**, and their antiaromatic character causes the energy of the planarized structures to be relatively high. Additional calculations suggest that fusion of cyclobutadiene units onto hexadehydro[12]annulene (**103**) effectively destroys the antiaromaticity of the 12-membered ring,⁷⁴ in contrast to hexadehydrohexaethynyl[12]annulene (**104**) which has only slightly attenuated antiaromaticity.

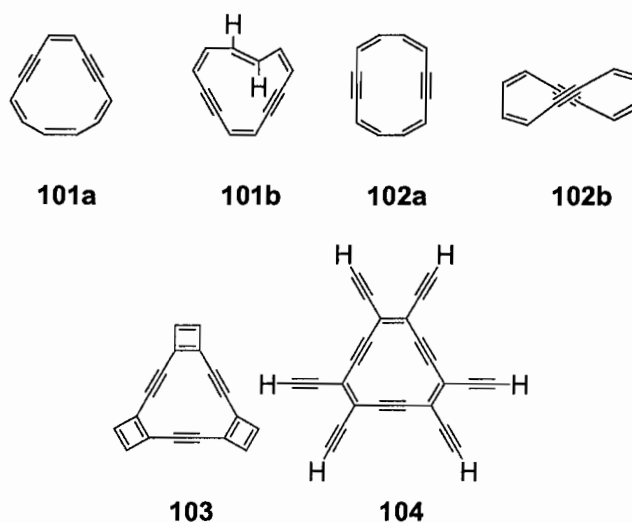
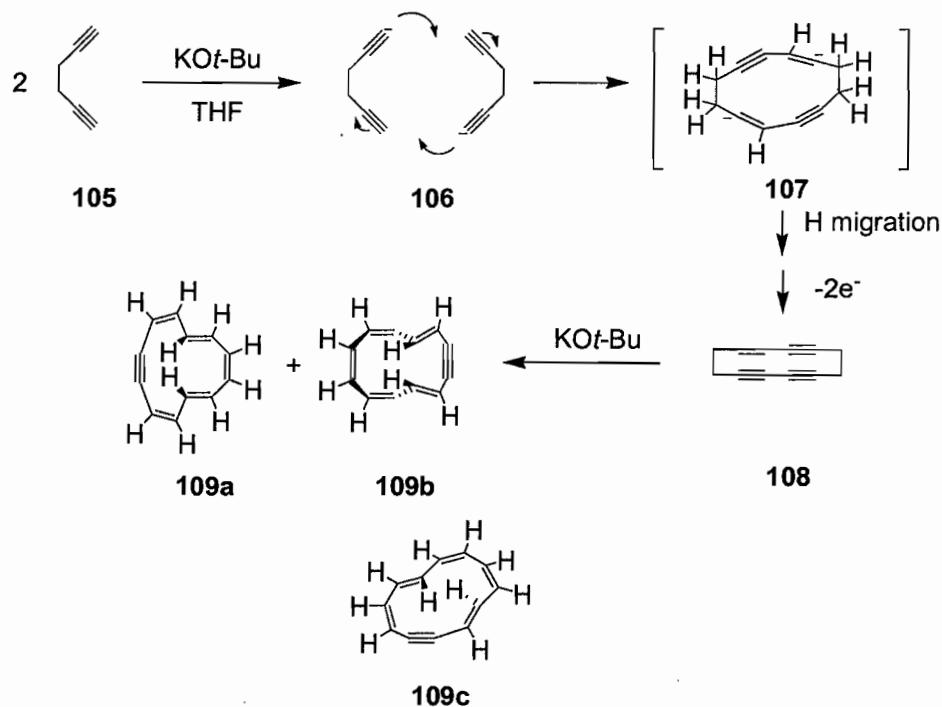


Figure 35. Isomers of dehydro[12]annulene and derivatives.

Stevenson and coworkers have adapted the original syntheses of **101-102** to prepare several isomers of didehydro[12]annulene (Scheme 12).⁷⁵ Exposure of commercially available 1,5-hexadiyne (**105**) to *t*-BuOK generates monoanion **106**, two of which cyclize to form dianion **107**. The dianion undergoes “transannular hydrogen migration and electron transfer” to cyclodecenyne **108**, which finally rearranges in the presence of *t*-BuOK to an isomer of didehydro[12]annulene **109a** or **b**. The conformations were assigned based on a detailed analysis of the NMR signals. Exposure of the annulenes to K metal in a THF/18-crown-6 solution generates the anion radicals, and eventually the dianions, which exhibit aromatic signatures in the ¹H NMR spectra: the internal protons resonate at -2.68 and -1.80 ppm, and the external protons appear as far downfield as 7.53 and 7.51 ppm. Interestingly, **109** does not appear to readily undergo

self-condensation, persisting for weeks in solution without any evidence for cycloaddition product formation.



Scheme 12. Generation of dehydro[12]annulene.

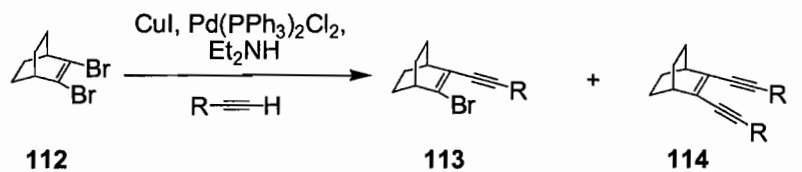
Annulene **109** was also prepared by serial dehydrohalogenation of hexabromocyclododecane **44**. The target molecule was not detected by NMR spectroscopy, but upon exposure of the solution to K metal, a strong, well-resolved EPR signal from the anion radical was observed. The signal was in good agreement with computation by DFT. Prolonged exposure led to the dianion, which was observed in the NMR spectrum. A new, less symmetric isomer **109c** was deduced, with internal protons appearing as a multiplet between -0.15 and -0.35 ppm, and a surprisingly far downfield

external proton at +13.54 ppm. This is believed to be due to the additive effect of the diatropicity and deshielding from the K cation. The other dianions of **109** do not experience this effect, but there is not as much ring strain in their alkyne units, which in **109c** may be causing π -orbital overlap with σ bonds on adjacent protonated carbons.

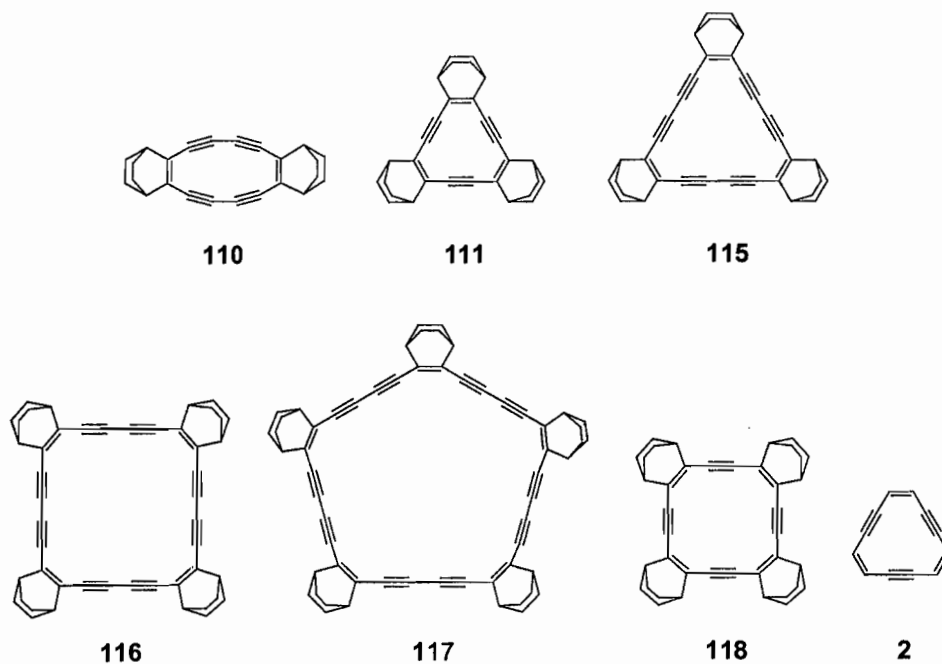
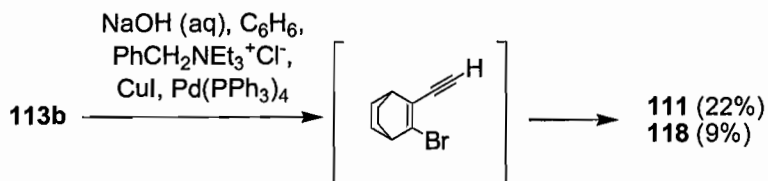
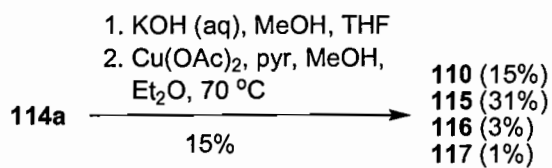
Komatsu and coworkers have prepared several dehydro[12]-, [18], [24], and [30]annulenes fused with bicyclo[2.2.2]octene (BCO) frameworks to stabilize the corresponding cations for investigation of the redox behaviors of these compounds.⁷⁶ Synthesis of dehydro[12]annulenes **110** and **111** (Scheme 13) proceeded from BCO dibromide **112** through stepwise assemblies of the acetylene linker units **113** and **114** using Pd- and Cu-catalyzed chemistry. Unfortunately, **110** is unstable and decomposes upon concentration without deaeration, while **111** decomposes even in deaerated solution over several days at rt. Dehydro[16]-, [18], [24], and [30]annulenes **115-118** were also synthesized in the same reactions. The ¹H and ¹³C NMR spectra were taken (Table 5), and the BCO protons are shown to be sensitive to the ring current effect. The signals for the bridgehead protons on the dehydro[12]annulenes are shifted significantly upfield from their aromatic-fused counterparts (e.g., ¹H NMR 1.76 and 1.72 ppm for **110** and **111**, respectively, vs 3.41 ppm for the 18-electron system **115**).

Cyclic voltammetry was also performed on the BCO-fused annulenes. For reduction, all showed reversible waves between -1.5 and -2.0 V (Table 5) with the antiaromatic systems at slightly less negative reduction potentials. Interestingly, during the oxidation process, reversible waves were observed only for annulenes with BCO units that were connected through just one acetylene spacer (such as **111**). Compound **111** is

more easily oxidized than **110**, which is more easily oxidized than the non-BCO-fused system **2**, prepared for comparison. The authors assert that this may indicate stabilization of the cationic π -systems by the BCO units, since such an effect might be attenuated by increasing the number of acetylenes per BCO unit. The authors also concluded that annelation with BCO units rigidly holds the σ -framework and donates electron density via induction and σ - π conjugation.⁷⁷ A plot of oxidation potential vs PM3-calculated HOMO energy shows a good linear correlation, but a plot of reduction potential vs calculated LUMO levels is scattered. This indicates that the rapid equilibration of conformers in solution may give rise to a variety of FMO levels, whereas the calculated LUMO levels are associated with the energy-minimized structure. This study effectively illustrates the electron-donating capability of the BCO group, and its ability to stabilize some cationic π -systems.



113a: R = TMS, 23% **114a:** R = TMS, 25%
113b: R = C(CH₃)₂OH, 31% **114b:** R = C(CH₃)₂OH, 38%



Scheme 13. Preparation of various sizes of BCO-fused dehydroannulenes.

Table 5. Bridgehead NMR shifts and redox potentials of BCO-fused annulenes.⁷⁶

compound	electron count	δ^a (ppm)	E_{red} , V ^b	E_{ox} , V ^b
110	(12 π)	1.76	-1.67	+0.93
111	(12 π)	1.72	-1.93	+0.54
115	(18 π)	3.41	-1.96	+1.21
116	(24 π)	2.68	-1.53	–
117	(30 π)	2.75	-1.90	+1.07
118	(16 π)	2.47	-1.96	+0.62
2	(12 π)	–	-1.58	+1.17

^a¹H NMR shift of bridgehead proton. ^bvs Ag/Ag⁺.

Diederich and coworkers have synthesized and studied a variety of perethynylated dehydroannulenes (e.g., Figure 36) as precursors to extended carbon sheet networks.⁷⁸ Oxidative Hay coupling of key bisalkyne **119**^{78a} provided dimeric dehydro[12]annulene **120**, trimeric dehydro[18]annulene **121**, as well as higher oligomers (yields from precursor shown). The TIPS-protected annulenes **120b** and **121b** are soluble, stable, and form deep red crystals and a yellow greasy solid, respectively. A crystal structure of **120b** revealed a planar carbon backbone, with a mean deviation from the plane of 0.089 Å. There is considerable strain in the molecule, with the butadiyne moieties having bond angles as low as 164.5°, and the inner C—C=C angles compressed to ca. 118°. Although the crystal is stable, uncrystallized solutions of **120b** decomposed upon concentration. TMS-derivative **120a** is much less stable, with solutions turning from purple to brown, and to black insoluble material in the solid form, even under cold (-20 °C) and dark conditions. Attempted desilylation with mild borax caused rapid decomposition upon

concentration of the product. Annulene **121a** decomposed slowly, but nevertheless grew bright yellow crystals over a period of nine months suitable for diffraction. The aromatic dehydro[18]annulene is perfectly planar, with the largest deviation from the plane of 0.074 Å. The acetylene segments adopt bond angles comparable to acyclic, strain-free analogues. Deprotection of **121a** afforded unstable **121c** in quantitative yield, and thus provides a precursor to oxidative couplings for the preparation of extended carbon sheet networks. Not surprisingly, **120** undergoes stepwise one-electron reductions to the aromatic dianion more readily than **121** to the antiaromatic dianion. The electronic absorption spectra exhibit significant vibrational fine structure, due to their rigid planarity. Annulene **120b** exhibits a UV cutoff around 480 nm, while the larger conjugated macrocycle **121b** has absorptions that extend out to 660 nm. The indicated HOMO-LUMO band gaps confirmed the essentially paratropic and diatropic natures of **120** and **121**, respectively.

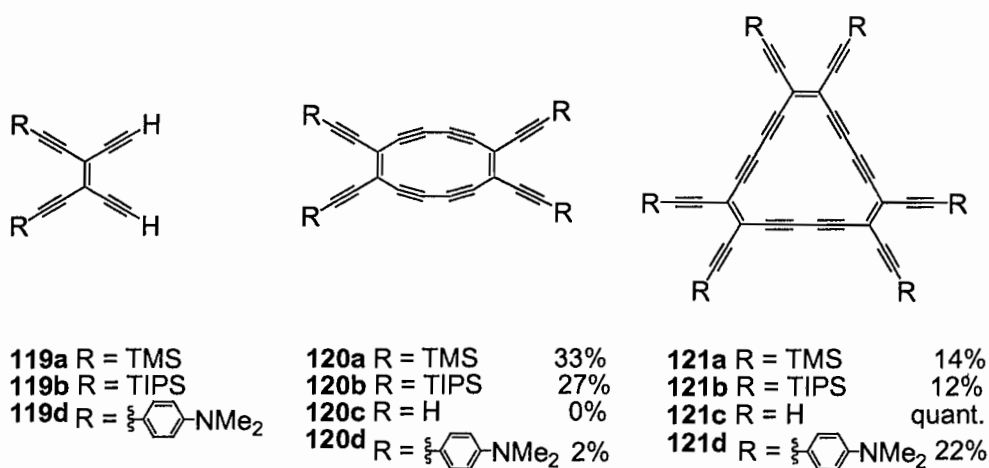


Figure 36. Perethynylated dehydro[12] and [18]annulenes.

Recently, donor-functionalized analogues **120d** and **121d** were reported.^{78b,c} Donor functionalization causes a bathochromic shift in the electronic absorption spectrum, with strong, broad bands appearing in comparison to **120b** and **121b**, indicating intramolecular charge transfer from the electron-rich aniline moieties to the annulenic cores. The bands disappear upon acidification, and are regenerated completely with addition of base. The λ_{max} of both charge transfer bands is the same (518 nm), but surprisingly the extinction coefficient is much higher in the aromatic system (105,200 vs 35,100 $\text{M}^{-1}\text{cm}^{-1}$). While it could be expected that charge transfer in **120d** would be more efficient, since antiaromaticity is reduced upon electron absorption, the UV-Vis results seem to suggest that this is not the case. Recently, the electronic excitations in **120d** and **121d** have been calculated using density functional theory.^{78d} In both cases the lowest excited states were found to correspond to a π - π^* transition involving intense intramolecular charge transfer from the donor groups to the cores. In the aromatic **121d**, however, the transition proceeds from the ground state to a degenerate excited state of E' symmetry. Since both of these E' states contribute to the oscillator strength, the charge transfer band is theorized to be more intense in the UV spectrum, which matches well with the experimental spectra for both annulenes.

Dehydro[14]annulenes. Although mono-*trans*-hexadehydro[14]annulene **122a** (Figure 37) was prepared in the mid 1960s,⁷⁹ the all-*cis* isomer **122b** is as yet unknown. Calculations suggest it adopts a tub-shaped conformation similar to didehydro[10]annulene **82**.⁶⁹ Haley and Boydston have synthesized the all-*cis*

octadehydro[14]annulene **123**, and have used ^1H NMR shifts to infer its diatropicity.^{80a} This parent compound was compared to various benzannelated analogues (see Section 5.3.3) and it was found that fusion of benzene rings to the systems causes upfield shifts, implying a gradual reduction in diatropicity. This lends support to the computational results described in the previous section concerning fusion of cyclobutadiene units to dehydro[12]annulene reducing its antiaromaticity.⁷⁴

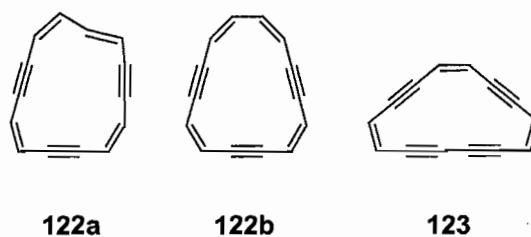


Figure 37. Isomers of dehydro[14]annulene.

Dehydro[6]annulenes. There has been surprisingly little new work involving dehydro[16]annulene, perhaps because dehydro[12]annulene has been much more extensively studied, and there is not believed to be a great deal of variation in structure and reactivity between these two ($4n$) annulenes. Furthermore, the macrocycle geometry required to provide the correct electron count does not lend itself well to the oxidative coupling reactions typically employed in synthesis (e.g., the low yield of tetramer **118** in Scheme 13). In most cases, synthesis of a dehydro[16]annulene represents one of a series of annulenes prepared either systematically,⁸⁷ or as one component of many in a one-pot intermolecular reaction.⁷⁶

Ojima, Yamamoto, and coworkers⁸¹ prepared several unique methanodehydro[16]-, [20], and [24]annulenedione structures (**124-126**, Figure 38) with an unusual 1,4-dichlorobutatriene moiety. A crystal structure of **124** revealed significant distortion from the expected C_s geometry, believed to be due to ring strain and transannular repulsion. The system is “fairly planar,” but the dihedral angle between the two ring systems separated by the methano bridge deviates from planarity by ca. 30° . The ^1H NMR spectrum shows that the inner protons of the annulenediones are shifted upfield relative to their respective acyclic precursors, while the outer protons are shifted downfield. The methylene protons are equivalent in the precursors, but separate into upfield and downfield components upon cyclization. Interestingly, these compounds actually exhibit diatropicity in CDCl_3 , due to the polarization of the carbonyl groups. The indications of **124-126** show enhanced diatropicity and delocalization (formal 14, 18, and 22 π -electron systems, respectively) in D_2SO_4 , which increases with ring size. This effect is so far unprecedented in true annulenes.

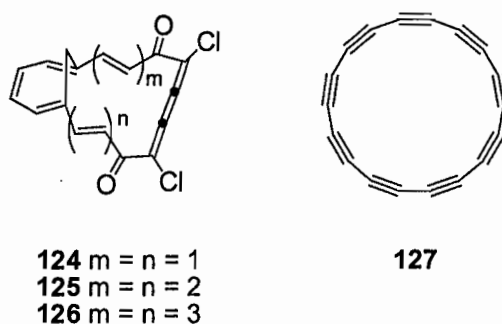


Figure 38. Dehydroannulenediones and cyclo[18]carbon.

Small carbon clusters have been extensively investigated systems,⁸² and there has been an impressive amount of work devoted to the smallest ($C_{n<10}$) clusters. With the ever-increasing interest in fullerene chemistry, this is also true of larger (C_{30-60}) carbon systems.⁸³ There has been comparatively little study involved with the intermediate size range, C_{10-24} , which are believed to exist as monocyclic rings. These monocyclic clusters, known as cyclo[n]carbons (e.g., **127**), exhibit a unique structure, composed of two sets of p-orbitals which are orthogonal to each other, raising the intriguing question of whether they obey the $(4n + 2)$ rule. Since cyclocarbons are belt-shaped compounds, the reader is referred to the contribution of Tobe and Tahara in the issue of *Chemical Reviews* in which this chapter also appears, which addresses this topic in detail. Our focus here is primarily on the dehydroannulene precursors. Only salient cyclocarbon results will be discussed.¹⁴

A very successful synthetic strategy towards accessing cyclo[n]carbons has been cycloreversion of ring-fused dehydroannulene precursors.⁸⁴ For example, Tobe and coworkers^{84a,b} have used laser ablation to induce $[2 + 2]$ cycloreversion of [4.3.2]propella-1,3,11-triene-fused dehydroannulenes to generate various sizes of cyclocarbon structures. Dehydroannulenes **128-132** were synthesized (Figure 39, yields shown) and subjected to laser ablation^{84a} and laser desorption-time of flight mass spectral analysis.^{84b} Peaks corresponding to the C_{16}^- anion of the target cyclocarbon were detected. Alternatively, irradiation with a low-pressure Hg lamp was used to induce photochemical $[2 + 2]$ cycloreversion (e.g., of **133** to **134** and **135**, Scheme 14),^{84b} but yielded only indane and polymeric materials that could not be characterized. Attempted

trapping of intermediates from the reaction using a furan matrix failed to afford the various [4 + 2] cycloaddition products.

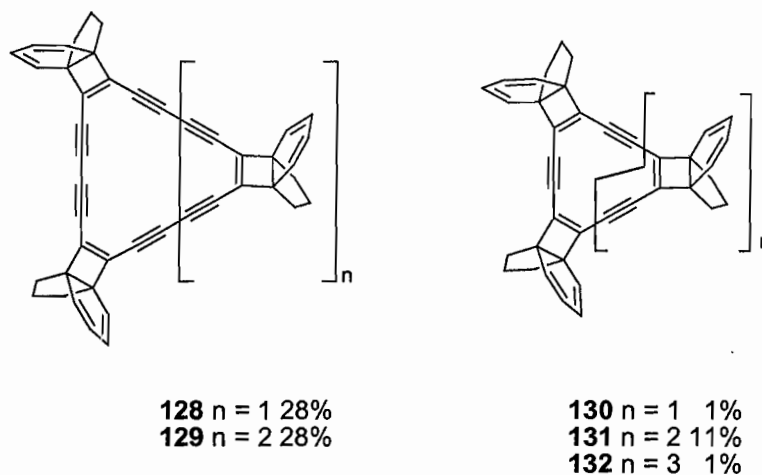
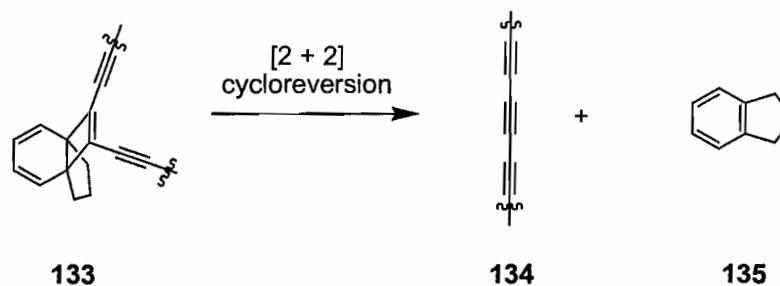


Figure 39. Propellatriene-fused dehydroannulenes.



Scheme 14. Cycloreversion of propellatriene-fused dehydroannulenes to cyclo[n]carbons.

Dehydro[18]annulenes. Although decidedly aromatic, unsubstituted dodecahydro[18]annulene **136**⁸⁵ is unstable and potentially explosive. As in the case of hexadehydro[12]annulene **103**, fusion of cyclobutadiene rings (**137**) is calculated to interrupt the ring current, which destroys the aromaticity,⁷⁴ while fusion of ethynyl units

(121c) only slightly reduces it. In the case of 137, however, it was calculated that the bond lengths of the formal single bonds are significantly shortened to 1.34 Å, as opposed to 1.39-1.43 Å in the other molecules studied, suggesting that the cyclobutadiene rings are “connected by cumulative double bonds yielding an allene structure”. Since synthesis of these higher annulenes typically involves oxidative alkyne cyclooligomerization, several ring sizes are generated in one pot, and so many studies concerning dehydro[18]annulenes are also applied to those of lower macrocycles, some of which are described previously (see Sections 3.3-3.5).

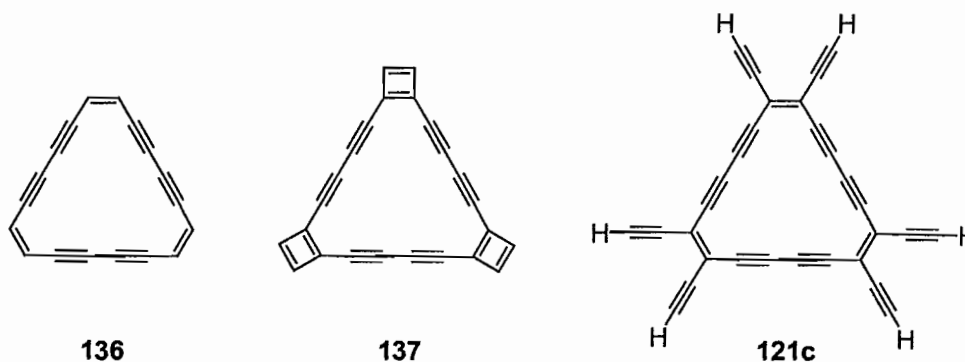


Figure 40. Dodecadehydro[18]annulene and derivatives.

The single crystal of the BCO-fused dodecadehydro[18]annulene **115** synthesized (Scheme 13) by Komatsu and coworkers⁷⁶ for their redox study was found to have an almost planar structure, with a butadiyne bond angle of 177.4°. Spectroscopic data for **115** was the same in solution and in the solid state. Comparison of the ¹H NMR data among the annulenes synthesized (Table 5) shows the diatropicity of the macrocycle; the

protons on the BCO units are the most downfield in each case. Similarly, the stability of **115** is shown by its resistance to both oxidation and reduction.

Indanyl-fused dehydro[18]annulene **128** was subjected to the same laser ablation conditions as dehydro[16]annulene **131** in an attempt to detect cyclo[18]carbon (**127**, Figure 41).^{84a} Mass spectral analysis shows a peak corresponding to C_{18}^- as the highest peak. The vibrational frequency deduced from the data collected is much lower for neutral C_{18} than for other clusters. This is explained by a possibly cumulenic structure for the $(4n + 2)$ clusters, rather than the localized single and triple bonds deduced for the $(4n)$ molecules (Figure 41).

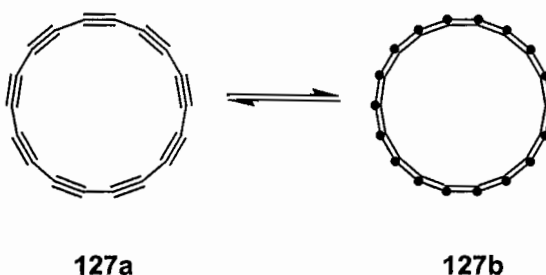
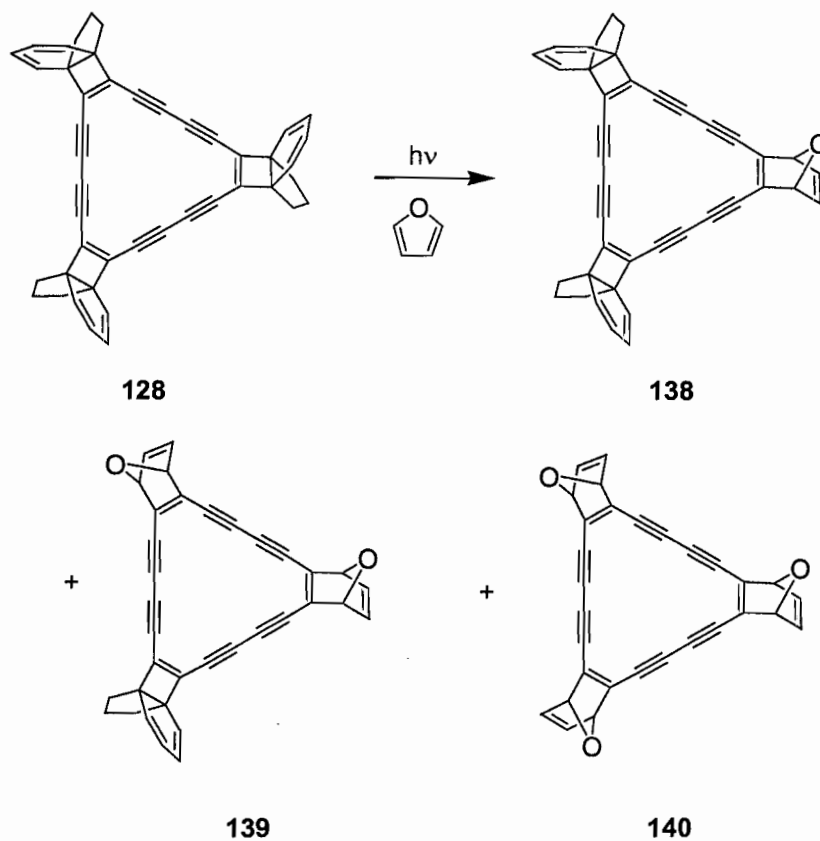


Figure 41. Isomers of cyclo[18]carbon.

Unlike the case of **131**, [2 + 2]cycloreversion of [18]annulene **128** in the presence of furan succeeded in furnishing trapped species (**138-140**, Scheme 15). In the absence of furan only indane and uncharacterizable polymeric material were obtained. While these results do not prove conclusively the formation of cyclo[*n*]carbons via this route, it does show that elimination of an indene unit does take place by cycloreversion to produce reactive dehydroannulene intermediates.



Scheme 15. Cycloreversion products of fused dehydro[18]annulenes.

Diederich et al. have similarly reported generation of ions of C_{18} from flash vacuum pyrolysis-induced cycloreversion of anthracene-fused dehydro[18]annulenes.^{84c} Ultraviolet irradiation under strong heating conditions followed immediately by time-of-flight mass spectrometry revealed a C_{18} fragment, while gentler heating conditions showed only anthracene fragments or the parent annulene, indicating that the retro-Diels-Alder reaction is the dominant fragmentation pathway. Bond-alternating acetylenic

cyclo[18]carbon **127a** is also calculated to be more stable than the non-alternating allenic form **127b**.

Ueda and coworkers have accomplished the synthesis of several dehydro[18]annulenes of the unusual type **141** (Figure 42) having D_{6h} symmetry.⁸⁶ This architecture is based on the Sworski concept of insertion of an unsaturated C_2 unit into each bond in benzene⁸⁷ and is expected to increase the size of the system, while not affecting the conjugation, aromaticity, or symmetry. An interesting question is what effect this expansion might have on the physical and chemical properties. Thus, various permutations of hexasubstituted derivative of **142** were assembled. All compounds are described as “quite stable”, with neither melting nor decomposition until 150-175 °C, at which point **142a** carbonizes, or 220-250 °C, around which **142b-d** decompose. In the crystal structure of **142b**, each “side” of the central ring has two “long” bonds, averaging 1.390 Å, and one “short” bond in between, averaging only 1.217 Å. This bonding pattern is not properly described by either the acetylenic or cumulenic model. The molecule does possess a planar π -system with D_{6h} symmetry in the solid state. The electronic absorption spectra of **142** show a pattern typical of $(4n + 2)$ annulenes, with two principal absorptions between 400 and 550 nm, each separated by about 50 nm, with hexaaryl-substituted **142b** and **c** possessing slight bathochromic shifts for these peaks.

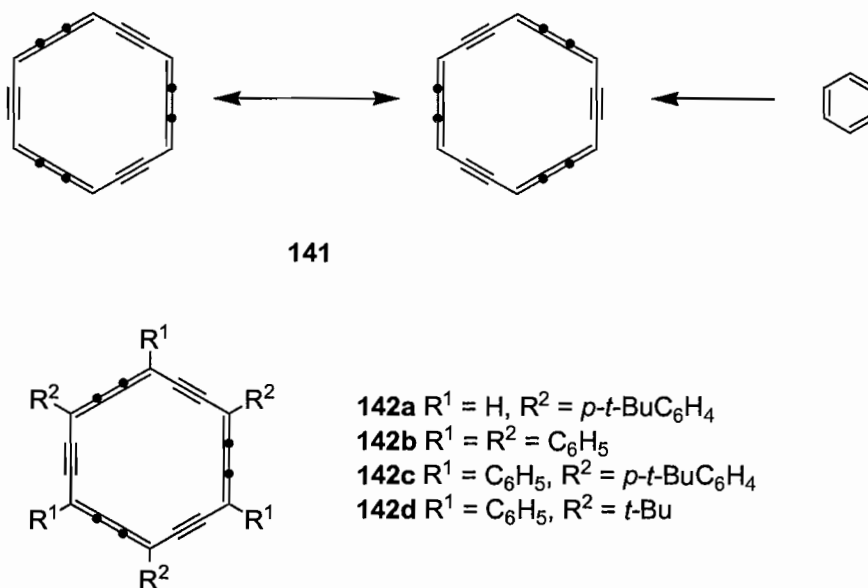
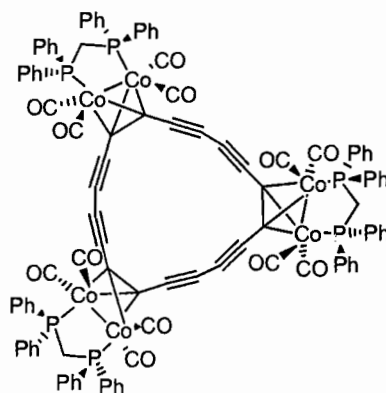
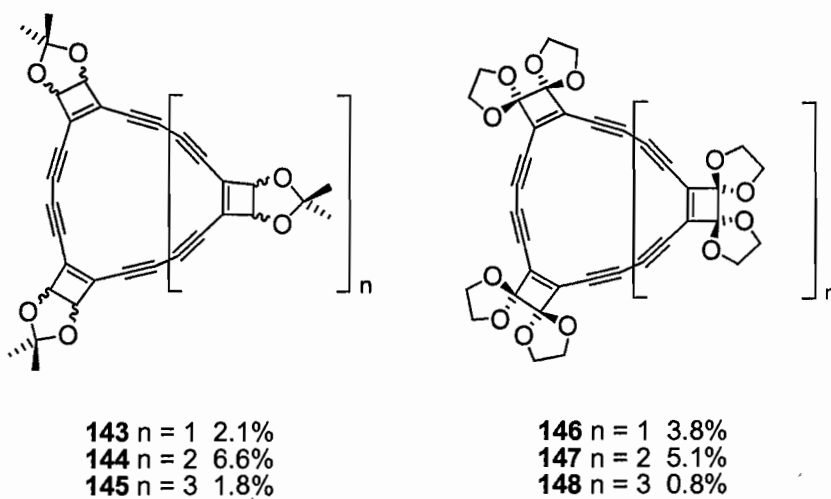


Figure 42. D_{6h} -symmetric dehydro[18]annulenes.

Diederich and coworkers have prepared several cyclobuteno-fused dehydro[18]annulenes, as well as higher oligomers, as potential precursors to cyclo[n]carbons.^{88a} The target molecules were the cyclobutenedione-fused dehydroannulenes as they could potentially undergo elimination of CO via radiation or flash vacuum pyrolysis to the corresponding cyclo[n]carbons. Since the cyclobutenediones were found to be unstable, the molecules were initially prepared as ketals **143-145** and bisketals **146-148** by cyclooligomerization of the corresponding diynes (Figure 43, yields from diynes shown). The protected dehydroannulenes were then subjected to acid hydrolysis, and the dione products were observed *in situ*, but not isolated. Low-temperature matrix isolation/laser desorption experiments provided circumstantial, but not direct, evidence of CO loss from the cyclobutenedione-fused

annulenes upon irradiation, via loss of the characteristic carbonyl peak at 1792 cm^{-1} and the appearance of a new band at 2115 cm^{-1} . Cyclocarbon **127** should have only weak IR absorptions, due to the symmetry of the alkyne groups. The electronic absorption spectra showed only disappearance of the long-wavelength bands upon irradiation, with no new bands generated. To date all attempts to isolate **127** have been unsuccessful.



149

Figure 43. Cyclobuteno-fused dehydro[18]annulene cyclo[18]carbon precursors and a stable hexacobalt complex.

Diederich has also synthesized a stable hexacobalt complex of cyclo[18]carbon (**149**, Figure 43).^{88b} The crystal structure confirms that it is indeed a complex of **127**, with a nearly planar C₁₈ ring, with the largest deviation from the plane of 0.19 Å. The corner bond angles are 131° and 134°, and the smallest diyne bond angle is 166°. While the next step to **127** would be demetallation under mild oxidation conditions, such attempts^{88c} using ceric ammonium nitrate, 4-methylmorpholine-*N*-oxide, and I₂ have all proven unsuccessful, yielding only polymeric material. It is likely that the stability of the complex, as well as steric hindrance from the ligands, prevents decomplexation. Although unambiguous evidence for the transient generation of cyclocarbons and their ions have been collected by various groups over the last fifteen years, it is clear that isolation and characterization of these synthetically intriguing structures from stable precursors is far from trivial, and may yet require the development of new techniques not currently available.

Dehydro[18]annulenes **121** prepared by Diederich and coworkers are described along with related structures **120** in the section concerning dehydro[12]annulenes, since they are synthesized at the same time. These systems are also discussed within the broader context of general acetylene chemistry in recent articles.⁸⁹

Chauvin and coworkers⁹⁰ have computationally investigated a variety of ring-expansion processes involving the unsaturated C₂ unit insertion mentioned above (Figure 42). These so-called “carbomers” have not been widely synthesized, but the non-derivatized **141** has been the subject of calculations aimed at finding out whether the physicochemical properties of benzene, of which **141** is the carbomer, are indeed

preserved in the larger structure, as would be predicted. An important question is whether the orthogonal set of p orbitals has an effect on the total aromaticity of the system (in-plane homoaromaticity). Geometric parameters, magnetic shielding (including NICS values), and MO calculations have been employed in order to deduce these effects. Bond distances in the carbomer (Table 6) are calculated to be slightly shorter than in benzene, due to the presence of the sp centers. The linear segments are slightly bowed outward, with corner bond angles of 122.6° vs 120° , and acetylenic (or allenic) bond angles of 178.7° . In comparison to the geometries of the dehydro[18]annulenes described above, the preservation of benzene-like character is remarkable. Calculation of the NICS at B3LYP/6-31+G* predicts values of -8.0 and -17.9 ppm for benzene and **141**, respectively, indicating that diatropicity is not only preserved, but enhanced.

Table 6. Geometric and spectroscopic comparisons between benzene and carbomer **141**.⁹⁰

parameter	benzene	141
$C_{sp2}-C_{sp2} / \text{\AA}$	1.394	
$C_{sp}-C_{sp} / \text{\AA}$		1.239
$C_{sp}-C_{sp2} / \text{\AA}$		1.369
$C_{sp(2)}-C_{sp2}-C_{sp(2)} / ^\circ$	120	122.6
$C_{sp2}-C_{sp}-C_{sp} / ^\circ$		178.7
NICS (B3LYP) / ppm	-8.0	-17.9
δ ^1H (B3LYP) / ppm	7.3	11.4
δ ^1H (expt) / ppm	7.27	9.87 ^a

^aValue for **142a** taken in CDCl_3 .

Predicted chemical shifts for the protons of each show a similar effect. The best experimental comparison comes from the triaryl derivative of **141**, **142a**, which shows a more moderate effect. The calculated resonance energy values of [n]annulenes vary with their carbomers in agreement with the Hückel rule, indicating that the π_{xy} system in the carbomer ring has little effect on the π_z system. Comparison of certain carbomers with only weakly homoaromatic analogues (e.g., **150** and [5]pericyclyne **151**,⁹¹ Figure 44) reveals that in-plane homoaromaticity exerts a weak influence at best and is “qualitatively bystanding”. Thus, it is concluded that carbomerization of an annulenic structure does indeed preserve aromatic character. For more on homoaromaticity, the reader is referred to the recent review by Williams.⁹²

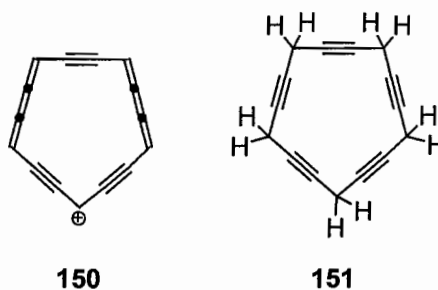


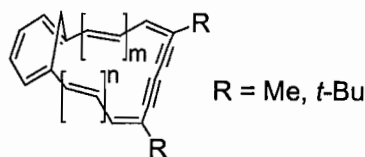
Figure 44. Homoaromatic analogues of dehydro[18]annulene.

Higher Dehydroannulenes. With each increase in ring size, the structural diversity attainable in the dehydro[n]annulenes grows exponentially. The oxidative cyclooligomerization route currently employed typically limits the isolability of higher annulenes from this route, however, where yields of higher macrocycles drop off quickly.^{78,88,89} On the other hand, the geometry of the monomer unit can sometimes favor

higher oligomers, as in the case of compounds **143-148**. The bond angles of the cyclobutene units cause ring strain upon formation of dehydro[18]annulene trimers **143** and **146** (the structures as drawn), which is alleviated in the dehydro[24]annulene tetramers **144** and **147**, thus affording a higher yield. The pentamers, however, are generated in smaller amounts. The opposite case is seen in the organometallic complex **149**, the tetramer of which is formed in very small amounts. It is worth noting that larger macrocycles also suffer from greater conformational freedom which hinders planar, delocalized structures. The diatropicity of dehydro[30]annulene **148**, for example, is highly reduced relative to **147**. Fusion of sterically restrictive units, such as cyclobutenes, can help enforce planarity and increase stabilization to a great degree.

A very systematic effort was undertaken by Ojima and coworkers⁹³ to synthesize a series of 1,6-methanotetradehydro[*n*]annulenes (**152**, Figure 45) where *n* = 18, 20, 22, 24, 26, 28, 30, 32, 34, 36, and 38. Each system was studied in order to determine the upper limit of ring current as a function of size. As noted earlier, the cutoff point for diatropicity in annulenes has been postulated in one study to occur around [30]annulene. In the case of dehydroannulenes, the rigid acetylenic linkages, and in this case, 1,6-methano bridging, will serve to draw out that boundary still further. Indeed, hexadehydro[24]annulene had been one of the largest (*4n*) annulenes known to be paratropic.⁹⁴ Ojima and coworkers synthesized each annulene in the same manner, and used the ¹H NMR shifts, as well as comparisons to their respective acyclic analogues, to assign the annulene's character as diatropic, paratropic, or atropic. It was found that diatropicity persists up until *n* = 34, but paratropicity only up to *n* = 28. The *n* = 32, 36,

and 38 annulenes are found to be atropic, with the conformational freedom that comes with their size overcoming any aromatic stabilization or antiaromatic destabilization.



152	$m = n = 1$	[18]
153	$m = 2, n = 1$	[20]
154	$m = n = 2$	[22]
155	$m = 3, n = 2$	[24]
156	$m = n = 3$	[26]
157	$m = 4, n = 3$	[28]
158	$m = n = 4$	[30]
159	$m = 5, n = 4$	[32]
160	$m = n = 5$	[34]
161	$m = 6, n = 5$	[36]
162	$m = n = 6$	[38]

Figure 45. Various 1,6-methano-bridged tetrahydroannulenes.

Benzoannulenes

Interest in benzoannulenes originated in the latter half of the 20th century as a means to simplify syntheses and stabilize annulene cores; however, incorporation of arene moieties into the cyclic structure enhanced bond localization and decreased annulene ring tropicity.^{4,7,8} Key pioneering contributors Staab, Sondheimer, Nakagawa, and Wittig produced a multitude of large benzannelated systems culminating in the late 1970s and early 1980s. Since then, *ortho*-fused benzoannulene production has been limited primarily to Mitchell's group with recent additions from Iyoda and Kuwatani.

Benzo[14]annulenes. Over the past 25 years, Mitchell and coworkers have prepared a large library of benzannelated dimethyldihydropyrenes (DMDHP) and

investigated their use as aromaticity probes.⁹⁵ Initial syntheses of the cycles focused on construction of a bis(bromomethyl)arene, conversion to a dithiacyclophane, and final elimination of Me₂S.⁹⁶ Although this method proved successful for isolating a multitude of new systems, the lengthy route required a different bromo-arene starting material for each benzoannulene. Examples of the more highly fused systems produced via this method include **163-165** (Figure 46).⁹⁶ In 1990, a new multipurpose route using Diels-Alder addition of dihydropyrene cores containing a reactive aryne functionality (**166**) with furan-substituted arenes followed by deoxygenation with Fe₂(CO)₉ was introduced.⁹⁷ The alternate route enabled the rapid production of several extensively annelated cycles (**167-171**) via common aryne **166**.^{97,98} The Mitchell group's most recent work in this area has focused on synthesis and comparison of benzo-, naphtho-, and anthraceno-annelated systems (**172-174**), where judicious use of bulky alkyl substituents permitted preferential annelation in the [*e*]-position.⁹⁹

The internal methyl protons of the benzoannulenes were found to be especially sensitive to ring current shielding but almost invariant to external substitution of the annulene core due to distance (> 5 Å). Dramatic chemical shift changes (up to 5 ppm) from DMDHP ($\delta = -4.25$), the direct result of bond fixation and aromaticity of the annelating species, have been observed for the group's benzoannulene derivatives. While higher annelation resulted in upfield shifts (less bond fixation) for [*a*]-fused cycles, downfield shifts (increased bond fixation) were observed for higher [*e*]-annelated systems (Table 7). The collected data has allowed the group to develop an empirical method to describe aromaticity of the new cycles as well as annelating species.

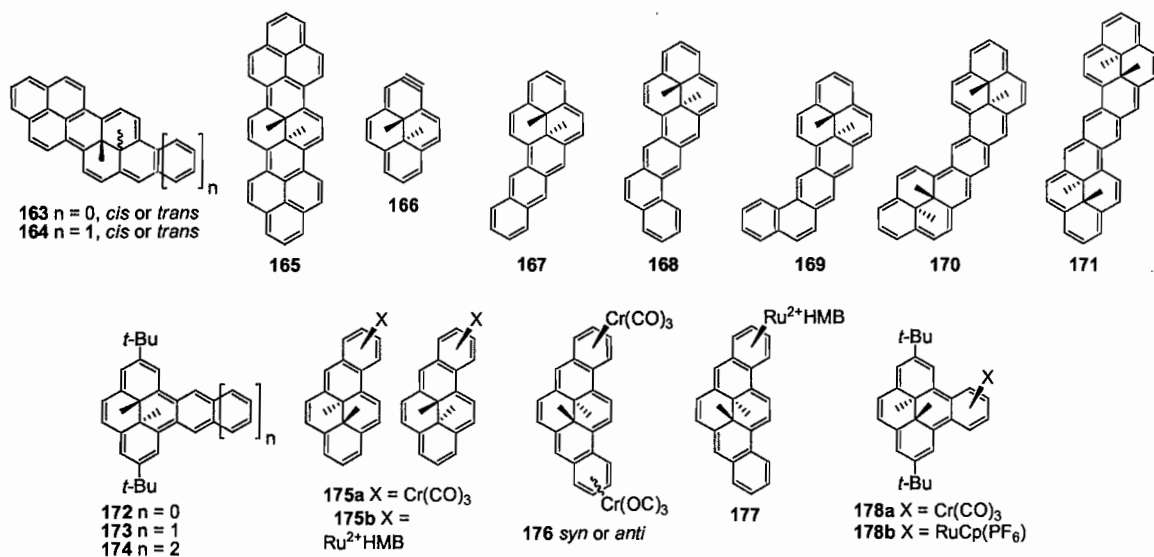


Figure 46. Highly-fused systems from attempted benzo[14]annulene syntheses.

Table 7. Internal methyl proton δ values for benzoannulenes **163-178**.

Benzoannulene Fusion Site	δ (Me)	Parent Benzoannulene δ (Me)
163-trans	—	N/A
164-trans	—	N/A
165	—	N/A
167	[a]	N/A
168	[a]	N/A
169	[a]	N/A
170	[a]	N/A
171	[a]	N/A
172	[e]	N/A
173	[e]	N/A
174	[e]	N/A
175a^a	[a]	-1.62
175b^b	[a]	-1.62
176 anti	[a]	0.02
176 syn	[a]	0.02
177^b	[a]	0.02
178a	[e]	-1.58
178b^c	[e]	-1.58

^a Major isomer^b Representative isomer^c Acetone-d₆

Mitchell's group reported the first mono- (**175a**) and dinuclear benzoannulene complexes (**176**) in 1990¹⁰⁰ and 1996,¹⁰¹ respectively, and has since prepared several additional Cr- and Ru-complexed organometallic analogs (**175b**, **177**, **178**) of previously reported benzannelated-DMDHPs (Figure 46).^{43d,102} Organometallic complexes **175-178** were obtained from the parent annulene by THF-catalyzed ligand exchange reaction with (η^6 -naphthalene)Cr(CO)₃, reflux with CpRu(CH₃CN)₃PF₆, or treatment with [RuCl₂(HMB)]₂ and AgBF₄. Isolation of the organometallic complexes occurred in moderate to good yields (50-80% for both isomers) but separation of isomeric analogs proved difficult in some cases (e.g., **175b**). Downfield shifts in δ values for the exotopic methyl groups upon metal complexation indicated more significant bond localization in the organometallic complexes than the parent benzo[14]annulenes (Table 7). Ru-complexes also possessed a slightly greater (< 1 ppm) bond-fixing ability than analogous Cr(CO)₃ systems.

In addition to service as an effective aromaticity probe, DMDHP is a photochrome that converts to a metacyclophanediene photoisomer upon irradiation with visible light and thermally reverts back to the bridged annulene by UV or heat (see **179**, Figure 47 for a representative benzannelated example).¹⁰³ The complete conjugation and orbital overlap of the annulene, which is disrupted by the stepped conformation of the metacyclophanediene, makes the annulene an ideal photochromic switch. Inability of the photoisomer to isomerize as well as lack of internal hydrogens, which can be abstracted to promote aromatization, are key advantages of the DMDHP systems over stilbene and dihydrophenanthrene photochromes. Experimental analysis has shown the DMDHP

switches to be extraordinarily robust with no detectable decomposition after repeated conversion by flashing light. Comparison of cycles produced in the early 1980s showed that site-specific annelation of the DMDHP core at the [a] and [e] positions respectively increased and decreased the thermal return reaction to the benzoannulene, the latter being the favored shift in rate for a photochromic switch.

The Mitchell group's recent efforts in this area include production of highly annelated DMDHP switches (**172-174**, Figure 46; **179**, **180**, Figure 47)¹⁰⁴ as well as exploration of multi-state π switches (**181-186**, Figure 47).^{104b,105} Compound **183**, the group's first 3-way photochromic switch, selectively differentiated the bis-pyrene (355 nm) and colorless bis-cyclophane (> 598 nm) from the thermodynamically preferred monopyrene-monocyclophane isomer. Bispyrene **184** showed that two DMDHPs linked by a conjugated diethynyl spacer did not affect the photochromism, in contrast to previously reported dithienylethene photochrome systems. Trispyrene systems **185a** and **185b**, shown in the most thermodynamically favored closed-open-closed orientation, are the group's newest multi-state π switches. Three of the five possible isomeric states of switch **185a** exhibited sufficient lifetimes to be observed by NMR spectroscopy and laser flash photolysis. Previously discussed organometallic analogs have also been examined for photochromic properties. Although the Cr-based systems did not exhibit photochromism, Ru-based **178b** exhibited electrochemic reversion to the pyrene in addition to photochromic and thermochromic methods.^{102c} Mitchell and coworkers have expanded their investigations of the DMDHP photochrome by incorporating it into larger porphyrin molecular triad systems (**186**) with either dihydroindolizine or fullerene

photochromes to create molecular AND (produces an output of one when both inputs are one) and INHIBIT (an AND gate with an additional event) gates.¹⁰⁶

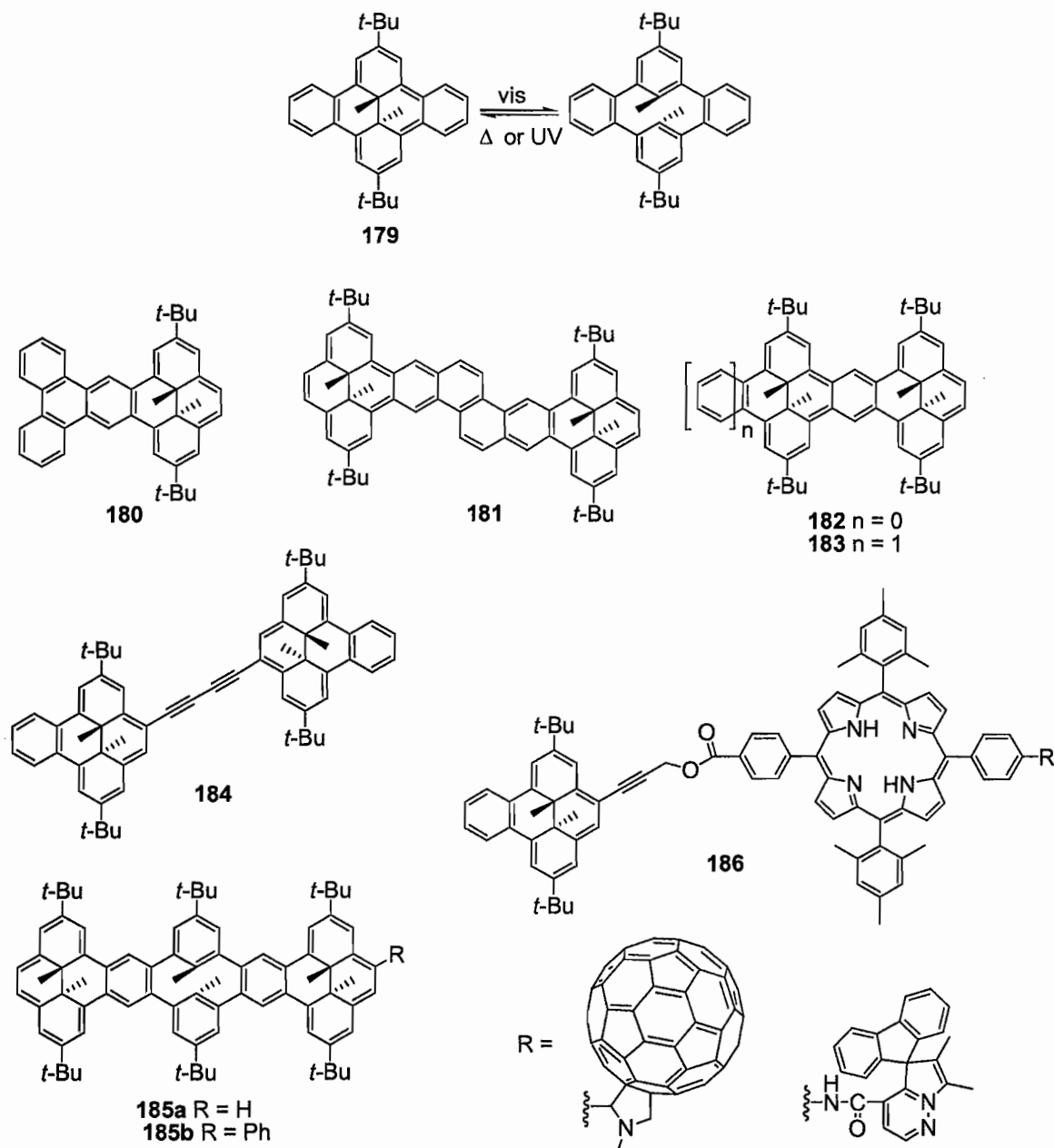
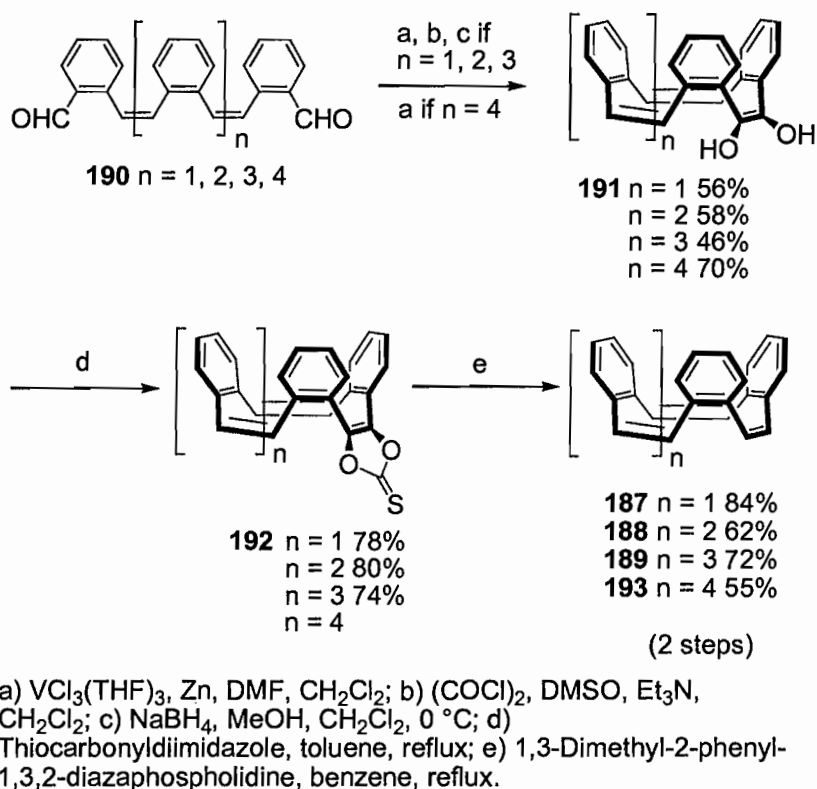


Figure 47. Annelated DMDHP photochromic switches.

Benzo[*n*]annulenes (*n* = 12, 16, 20, 24). Iyoda, Kuwatani, and coworkers have reported the production of several concave benzoannulene systems with alternating arene and alkene functionalities, of interest as precursors or mimics of larger conjugated systems (C₆₀ and C₇₀) and cyclic belts (see review of aromatic belts by Tobe et al.¹⁴). The simplest system beyond dibenzocyclooctatetraene, benzo[12]annulene **187**, was obtained in 1988 from Ni-catalyzed trimerization of 1,2-dibromo-1,2-dihydrobenzocyclobutene followed by thermal ring-opening.¹⁰⁷ The crown-like structure of cycle **187**, which results in an orthogonal relationship between benzene and ethylene linkages, prevents conjugation between arene rings. Due to interest in larger benzo[*n*]annulene systems (*n* > 12), the group explored alternate routes and developed a new versatile strategy that additionally afforded 16- (**188**) and 20-membered annulenes (**189**) in 2000.¹⁰⁸ V/Zn-mediated intramolecular pinacol coupling of bis-aldehyde **190** resulted in a combination of *threo* and *erythro* diol isomers, of which the former was converted to the *erythro* conformer (**191**) via Swern oxidation and NaBH₄ reduction (Scheme 16). Treatment with thiocarbonyldiimidazole afforded the penultimate thiocarbonate **192**, which was subsequently placed under Corey-Winter reductive dehydroxylation conditions to afford cycles **187-189** in 62-84% yields. Most recently the group produced the benzo[24]annulene analog (**193**) which displayed a unique benzene trimer substructure compared to the concave features of **187-189**.¹⁰⁹ Cycles **188** and **193** both displayed temperature dependence by NMR spectroscopy while the frameworks of **187** and **189**, concluded to be respectively too rigid and too flexible, did not display significant structural change with temperature variance. Although organometallic complexes of **187-**

189 and **193** have been observed, only cycles **188** and **189** formed complexes with the transition metal cavitated inside the annulene cage.



Scheme 16. Various benzannulenes with crown-like structure.

Dehydrobenzoannulenes

Dehydrobenzoannulenes (DBAs), also referred to as benzocyclynes, first appeared in the chemical record in the 1960s from the laboratories of Eglinton and Staab. Both groups continued their work into the late 1970s in conjunction with several other prominent chemists such as Nakagawa. Production of new cyclyne topologies in the early 1990s by Youngs and Vollhardt marked a resurgence in DBA synthesis that continues to this day. A key reason for this renaissance was isolation of the fullerenes^{83b} as well as

several theoretical studies that proposed unique thermal, optical, and electronic properties for highly unsaturated, non-natural carbon allotropes such as graphyne (**194**, Figure 48) and graphdiyne (**195**), for which benzocyclynes could be envisaged as model substructures.¹¹⁰

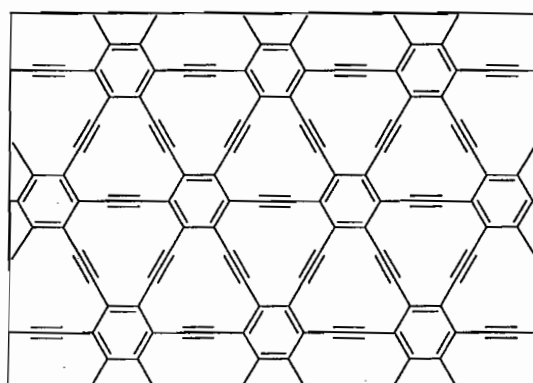
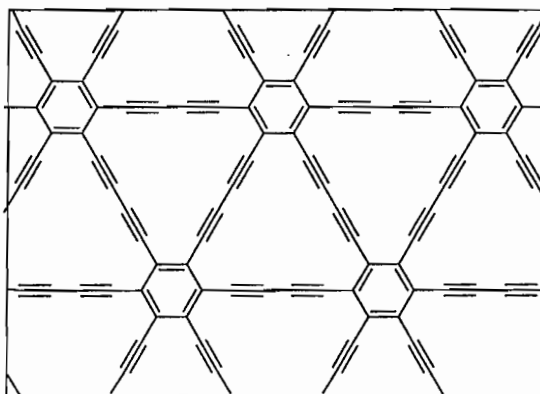
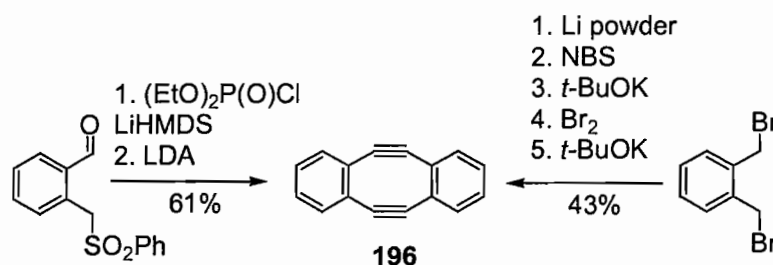
**194****195**

Figure 48. Theoretical carbon allotropes graphyne and graphdiyne.

Dehydrobenzo[8]annulenes. Cyclyne **196**, the simplest member of the DBA family, was first synthesized in 1974 by Sondheimer and coworkers in 27-36% yield via bromination of dibenzocyclooctatetraene and subsequent dehalogenation with *t*-BuOK.¹¹¹

Interest in this strained, anti-aromatic system continues due to the significant angle distortion of the alkyne moieties ($\sim 155^\circ$)¹¹² and possibility as a precursor for extended carbon-rich systems.¹¹³ Two different groups published superior alternate methods to the strained annulene in 2002 (Scheme 17). Otera and coworkers obtained the cycle in 61% yield via oxidative dimerization of *o*-(phenylsulfonylmethyl)benzaldehyde¹¹⁴ whereas Wudl et al. utilized two distinct multi-step routes, the more efficient (43% overall yield) and cost effective starting with α,α' -dibromo-*o*-xylene.¹¹⁵



Scheme 17. Generation of dehydrobenzo[8]annulene.

Three organometallic complexes of **196** have been reported since the DBA renaissance (Figure 49). Bis-Pt complex **197**, isolated in 1997 by Tanaka et al. during investigation of silylation reactions of dehydro[8]annulenes, was obtained quantitatively by reaction of **196** with two equivalents of $\text{Pt(PPh}_3)_4$ or $\text{Pt(CH}_2\text{=CH}_2\text{)(PPh}_3)_2$.¹¹⁶ Complexation of both alkyne moieties with Pt resulted in enhanced air and thermal stability with a decomposition temperature $\sim 100^\circ\text{C}$ higher than that reported for **196** ($\sim 110^\circ\text{C}$ dec).¹¹¹ Both Otera and Vollhardt reported Co-complexes of **196** five years later. Otera's laboratory produced dinuclear complex **198** by treatment of **196** with

$\text{Co}_2(\text{CO})_8$.¹¹⁷ Although metal coordination to the single ethynyl group altered C–C bond length (0.16 Å) and angle ($\sim 8^\circ$), the remaining alkyne moiety in Co-complex **198** remained unchanged in angle and length. Alternatively, Vollhardt and coworkers obtained (cyclobutadieno)dibenzocyclooctatrienyne complex **199** from photochemical treatment of a mononuclear metallacyclopentadiene(alkyne) complex precursor designed for angular [4]phenylene.¹¹⁸ The inherent strain in **199** resulted in a trapezoidal distortion of the cyclobutene moiety.

Wong's group prepared several analogs (**200-202**, **203a**, **203b**, **204**, Figure 49) of **196** in the early to mid 1990s. Benzo-fused cyclynes **200-202**, isolated as intermediates and characterized by high-resolution MS and/or NMR spectroscopy, were reacted with furan or isobenzofuran to construct benzo-fused tetraphenylenes.^{113a} The group's interest in strained dehydroannulenes, such as cycloocta-1,5-diene-3,7-acetylene, led to production of annelated cycles **203a**, **203b**, and **204**.¹¹⁹ Introduction of fluorene units provided enhanced stability and coplanar structures for **203a** and **203b**^{119a,b} in contrast to the highly reactive, non-planar parent tribenzocyclooctene **203c**, which exhibited a half life of 30 min at -60°C in solution.¹²⁰ The longevity of the fluorene derivatives, both crystalline solids that exhibited mp values $>200^\circ\text{C}$, was attributed to removal of the four eclipsed arene hydrogen atoms found in **203c**. Conversely, the improved stability (mp 183°C) of **204**, obtained in two steps from benzo[*a*]phenanthro[9,10-*e*]cyclooctene, was based on kinetic protection of the alkyne groups from close proximity of phenanthrene hydrogen atoms as well as decreased ring strain of the central core from sp^2 -C bond elongation.^{119c} More recently, Youngs reported formation of tetrasilyloxy **205** from

intermolecular Pd-catalyzed cross-coupling in low yield (10%), the result of competitive formation of a more stable indenoindene byproduct (69% yield).¹²¹

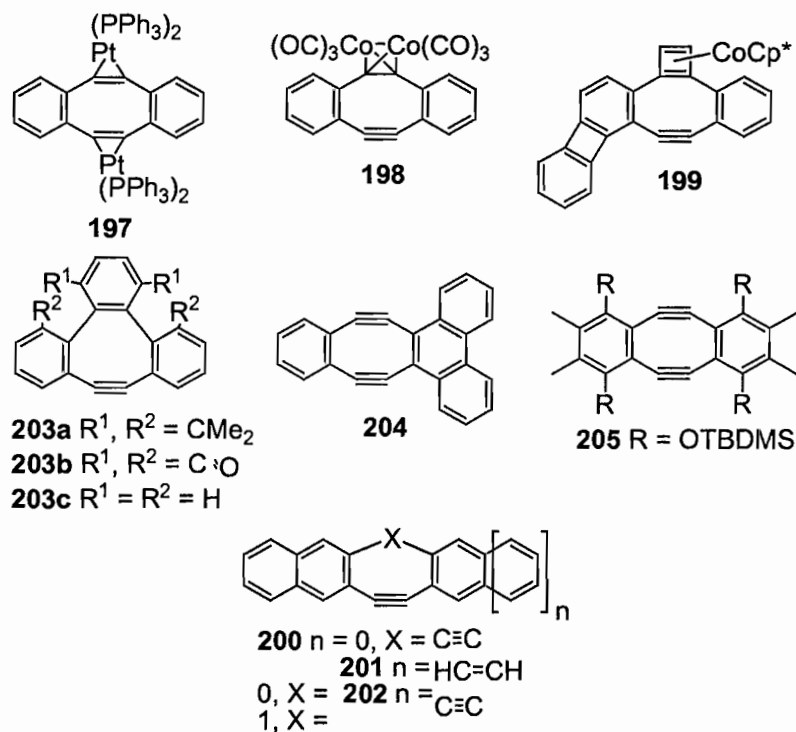


Figure 49. Various forms of dehydrobenzo[8]annulene and fused derivatives.

Dehydrobenzo[12]annulenes. Prior to 2005, only two topologies existed for dehydrobenzo[12]annulene: the highly colored, dimeric dibenzoannulene **206**, also known as the Eglinton-Galbraith dimer, and tribenzocyclyne **207** (Figure 50). Eglinton and coworkers first isolated cycle **206** in 1960 via high dilution oxidative coupling of *o*-diethynylbenzene.¹²² Production of tribenzocyclyne **207** was subsequently reported in 1966 by Eglinton via trimerization of the cuprous salt of *o*-iodophenylacetylene in pyridine.¹²³ Staab and Graf simultaneously reported **207** through a

halogenation/dehalogenation of a didehydrobenzoannulene obtained with Wittig chemistry.¹²⁴ Only with the Tobe group's report of highly strained dibenzocyclyne **208** almost forty years later did a new triyne topology enter the chemical record.¹²⁵

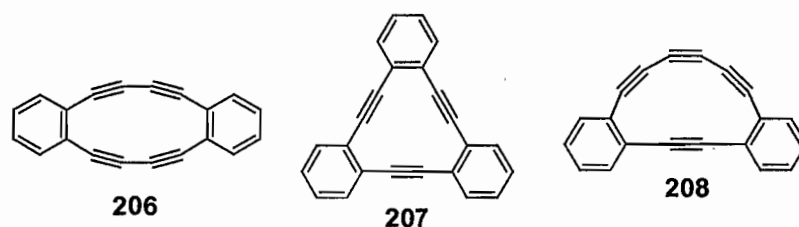


Figure 50. Various dehydrobenzo[12]annulenes.

Octadehydrodibenzo[12]annulenes. Utilizing their new route for differentially protected hexa-alkynylbenzenes via Diels-Alder cycloaddition of cyclopentadienones with alkynes, Rubin and coworkers investigated formation of larger graphyne substructures via Hay coupling in 1997.¹²⁶ The group successfully isolated **209a** in 20% yield from the final Cu-mediated homocoupling of 3,4,5,6-tetrakis(2-*t*-butylethynyl)-1,2-diethynylbenzene (Figure 51). Although produced in the same reaction, trimeric and tetrameric analogs could not be separated and further characterized. Octa-substituted **209a** showed notable stability over the parent cyclyne, likely due to steric effects of the bulky alkyl groups and interspersed solvent molecules observed in the crystalline state.

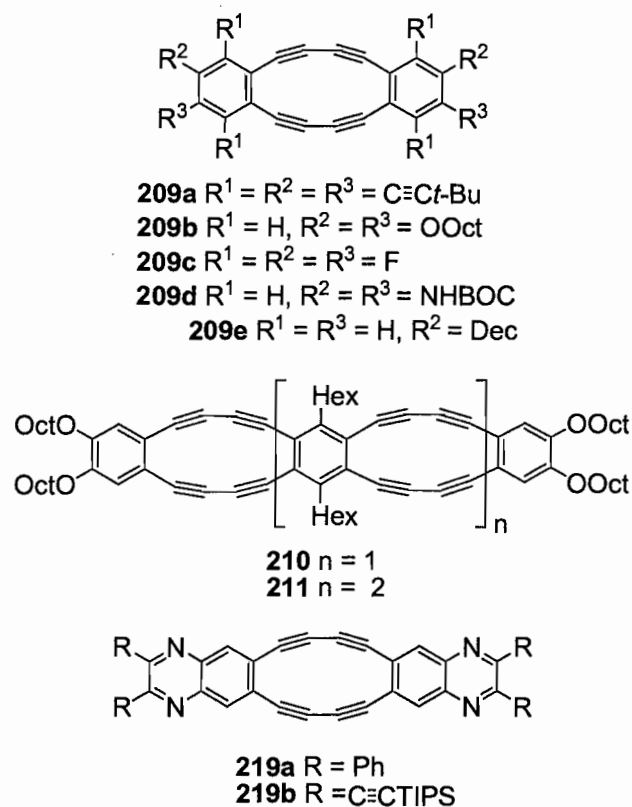
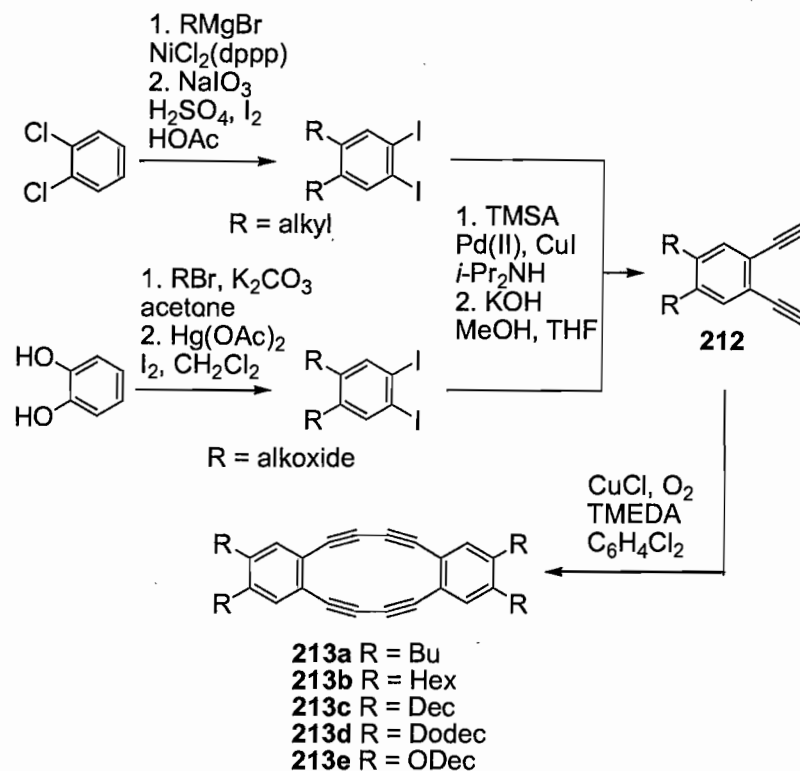


Figure 51. Octadehydrodibenzo[12]annulenes.

Gallagher and Anthony reported the production of linearly fused [12]annulene oligomers (**210**, **211**, Figure 51), referred to as acediynes, as well as tetraoctanoxy analog **209b** in 2001.¹²⁷ Contrary to traditional intermolecular Hay cyclization techniques, they constructed the extended structures stepwise via Pd-catalyzed homocoupling of alkoxy-substituted benzene rings to a central dialkyl core followed by intramolecular Hay coupling. The electronic absorption spectra of the acediynes, which displayed increased bathochromic absorption with oligomer length, allowed calculation of a saturation wavelength (625 nm) similar to linear acetylene-based polymers. While both **210** and

209b were found to be readily soluble and stable systems, oligomer **211** exhibited poor solubility in organic solvents and was found to decompose in non-deoxygenated solvents.

The Swager group's interest in precursors for novel conjugated organic polymers led to the study of dimerization reactions of *o*-diethynylbenzene analogs in 1994.¹²⁸ The penultimate diethynylbenzene derivatives (**212**) were prepared in good yield from either *o*-dichlorobenzene or catechol with Pd- and Ni-catalyzed cross-coupling reactions, respectively (Scheme 18). Intermolecular Hay coupling of the diethynyl monomers in *o*-dichlorobenzene afforded a mixture of the dimer (**213**) with larger macrocycles and oligomeric/polymeric components. Cycles **213b-e** were isolated in 17-74% yields while cycle **213a** and the larger macrocycles were analyzed as mixtures by ¹H NMR spectroscopy. Tetra-substitution of the strained core enhanced stability of the [12]cyclyne to several days at room temperature in contrast to the rapid and pronounced decomposition of concentrated samples of **206**. The solid-state structure of **213** displayed a staggered conformation with alternating in and out of plane orientation for substituents, a structural feature that prevented intermolecular interactions from adjacent butadiyne linkages. Investigation of thermal behavior by DSC showed polymerization between 100-125 °C with very narrow transitions ($\omega^{1/2} \sim 1.5$ °C). X-ray powder diffraction, cross polarization/magic angle spinning NMR spectroscopy, ESR, and the intractable nature of the resultant polymeric materials all indicated that tetrasubstituted [12]annulenes **213** did not exhibit a well-defined topochemical polymerization.



Scheme 18. Preparation of alkyl-substituted octadehydrodibenzo[12]annulenes.

Bunz and Enkelmann further investigated the Eglinton-Galbraith dimer (**206**) in 1999, specifically focusing on the solid-state behavior and crystal packing of the octadehydroannulene.¹²⁹ Co-crystallization with hexafluorobenzene and tetracyanoquinodimethane resulted in formation of 1:1 molecular complexes with guest molecules inserted between the stacked annulenic cores. Although concentrated samples would readily lose solvent and decompose, the solvent complexes were stable under ambient conditions if sealed in a capillary under partial pressure of solvent.

Komatsu and coworkers prepared octafluoro-analog **209c** in 2002 via Cu-mediated homocoupling of 1,2-diethynyl-3,4,5,6-tetrafluorobenzene (Figure 51).¹³⁰ The use of preparative GPC allowed facile isolation of **209c** in 48% yield as well as the trimer in lower yield. Although UV-Vis spectroscopy and DFT calculations indicated a comparable HOMO-LUMO with parent **206**, CV data indicated a more electron deficient cyclyne core and lower LUMO by a less negative reduction peak. Investigation into polymerization characteristics showed that despite suitable solid-state orientation of the diyne bridges, cycle **209c** was stable to topochemical polymerization. The cycle also exhibited explosive decomposition at higher temperatures (120-135 °C) than **206**, a deactivating effect attributed to the electron-withdrawing octafluoro-substitution.

A Ru-coordinated dehydrobenzo[12]annulene with exotopically fused diimine binding sites (**214**) was reported by Faust and Ott in 2004 (Figure 52).¹³¹ The metallacycle was obtained in 21% yield by four-fold Schiff-base condensation of BOC-protected tetra-amino[12]annulene **209d** with [(bpy)₂Ru(phenanthroline-5,6-dione)]²⁺(PF₆⁻)₂ in TFA and CH₃CN. The electron accepting nature of **214** was confirmed by CV experiments, which provided a similar reduction potential to that of the first reduction of the well-established electron acceptor C₆₀. Although responsible for a decreased excited state lifetime by intramolecular quenching, the dehydroannulene core did provide electronic benefits of bathochromic absorption and emission spectra for **214** compared to acyclic Ru-polypyridyl model complexes.

Cook and Heeney¹³² as well as Torres and coworkers¹³³ published reports in 2000 on phthalocyaninodehydroannulenes that differed only in arene substitution and transition

metal identity (Figure 52). Both groups used intermolecular Cu-mediated homocoupling reactions of diethynylphthalocyanino monomers with different results. Cook and Heeney obtained dimer **215a** in 24% yield as well as an additional 15% yield of dimer/trimer mixture with Eglinton conditions. Torres' group found that similar Eglinton coupling of the diethynyl precursor resulted only in an inseparable mixture of **215b** and trimer analog while increased temperature (70 °C) and higher concentration afforded cycle **215b** as the sole macrocyclic product in 51% yield. Although absorption spectra were run in different solvent systems, both macrocycles **215a** and **215b** exhibited λ_{cutoff} values >800 nm with a distinctive broadening and splitting of the Q-band, ascribed to intramolecular coupling of the phthalocyanine groups via the butadiyne linkages. Cook and Heeney further investigated the propensity for mesophase behavior, which showed that **215a** entered a mobile phase at 110 °C with an associated birefringence pattern. Heating of **215a** in toluene above 220 °C resulted in drastic changes in the absorption spectrum and the presence of higher molecular weight oligomers with interspaced molecular weights of **215a** by matrix assisted laser desorption ionization time-of-flight MS.

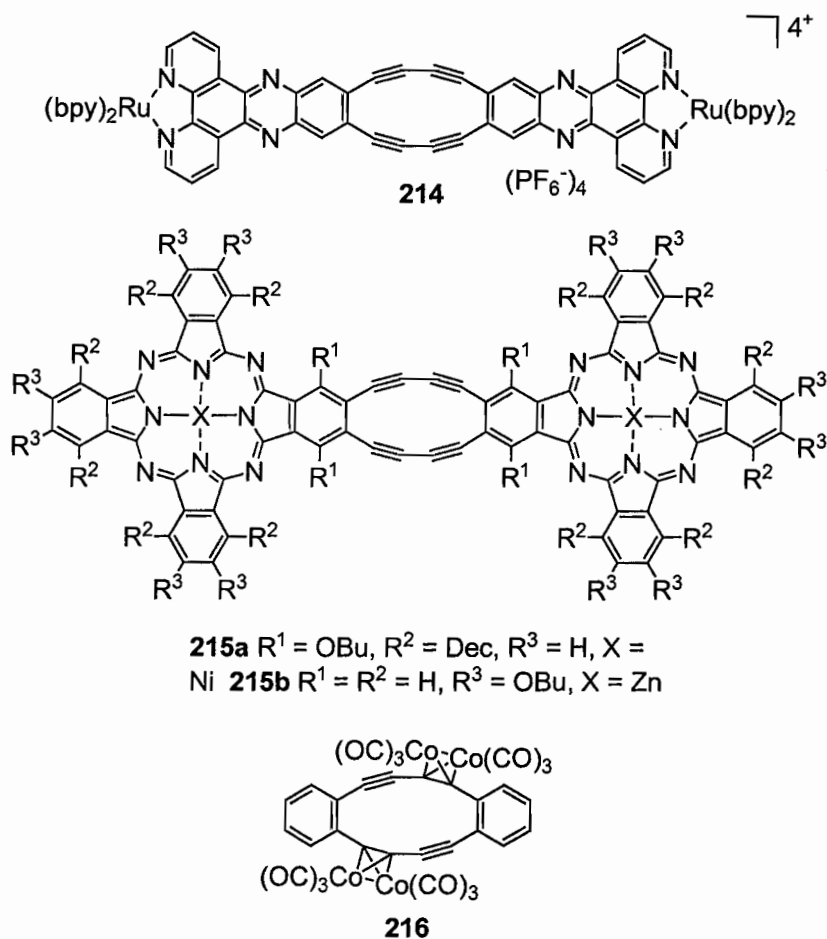
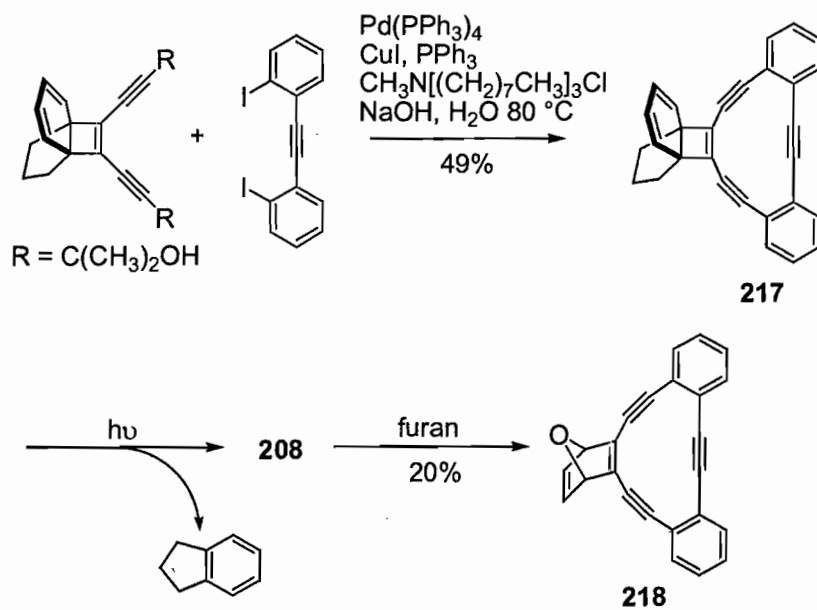


Figure 52. Various metal-coordinated dehydrobenzo[12]annulene derivatives.

The double addition organometallic product **216**, which displayed enhanced stability to several days in solution under ambient conditions, was obtained by Adams and Bunz in 36% yield via reaction of **206** with $Co_2(CO)_8$ at rt (Figure 52).¹³⁴ Co-complex incorporation was found to occur on opposite sides of the carbon-rich skeleton to minimize unfavorable steric interactions between metal complexes.

In 2005, the Tobe group reported production of triyne **208** by photochemical [2+2] cycloreversion of [4.3.2]propellatriene-annelated **217** (Scheme 19).¹²⁵ The highly strained cyclyne could only be isolated as a Diels-Alder adduct (**218**) with furan in 20% yield or as an anti- dimeric adduct in THF in 18% yield. Spectroscopic characterization (UV-Vis and FT-IR) of the new triyne occurred only at low temperature in either a 2-methyltetrahydrofuran glass or Ar matrix. DFT geometry optimization of **208** exhibited C_{2v} symmetry with the most significant distortion of the triyne moiety unevenly manifested in the central ethynyl group (147.1° , 150.8°).

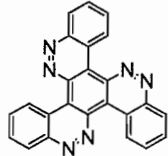
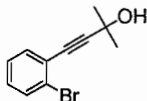
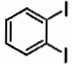
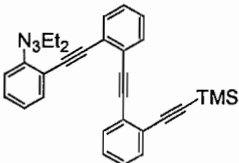
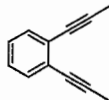
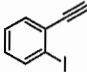
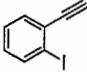


Scheme 19. Cycloreversion to strained annulene **208**.

Other novel substitutions of the benzo[12]cyclyne skeleton include a dialkyl analog (**209e**) prepared by Haley's group in 2004¹³⁵ and two new quinoxalinodehydroannulenes (**219a,b**) reported by Ott and Faust (Figure 51).¹³⁶ Cycles **219a** and **219b** were obtained in 53% and 86% yields from a one-pot deprotection/condensation reaction of **209d** with 1,2-diphenylethane-1,2-dione or 1,6-bis-(triisopropylsilyl)hexa-1,5-diyne-3,4-dione in TFA and HOAc, respectively. Cycle **219a**, which gradually decomposed under ambient conditions, was easily separated from other reaction components due to poor solubility whereas silyl-protected **219b** required GPC purification. Tetraethynyl-substituted **219b** exhibited bathochromic absorption and emission spectra (18 and 15 nm, respectively) compared to tetraphenyl **219a**, the result of limited π -delocalization from sterically-induced twisting of the phenyl substituents.

Hexadehydrotribenzo[12]annulenes. Several new routes, both inter- and intramolecular, have been reported for tribenzo[12]annulene **207** since the pioneering syntheses in 1966.^{123,124} Table 8 provides a chronological display of penultimate structure, reaction conditions, and cyclization yield for reports issued in the last 25 years. In addition to increased efficiency for the parent cyclyne, the new routes specifically allow straightforward access and tailored production of substituted analogs (Table 9), an important facet for use of these carbon-rich cycles in materials systems.

Table 8. Synthetic routes to hexadehydrotribenzo[12]annulene (**207**).

Entry	Cyclization Precursor	Conditions	Yield	Ref
1	 221	hydrazine hydrate, Raney Ni	20%	142
2	 220	Pd(PPh ₃) ₄ , CuI, NaOH, BTEACl, benzene, 85 °C	36%	137
3		acetylene, CuI, PdCl ₂ (PPh ₃) ₂ , DMF, piperidine, 60 °C	39%	138
4	 222	1. K ₂ CO ₃ , MeOH, THF 2. MeI, 120 °C 3. Pd(dba) ₂ , PPh ₃ CuI, Et ₃ N	69%	143
5		(<i>t</i> -Bu ₃ O)WC(<i>t</i> -Bu) ₃ toluene, 80 °C	54%	141
6		CuI, PPh ₃ , DMF 160-165 °C	55%	139
7		Pd(PPh ₃) ₄ , CuI BMIMBF ₄ , Et ₃ N	37%	140

The first significant intermolecular construction of **207** since Eglinton's initial Cu-mediated route was provided in 1988 by Linstrumelle and Huynh,¹³⁷ who obtained the benzocyclyne in 36% yield from an *in situ* alkyne deprotection/Pd-catalyzed cross-coupling of arene **220** (Table 8). Ten years later, Iyoda and coworkers reported an expedient route to cycle **207** via a one-step Pd-catalyzed reaction of *o*-diiodobenzene with acetylene (Entry 3, Table 8).¹³⁸ Two recent reports have presented new cyclization conditions with *o*-ethynyl iodobenzene as starting material (Entries 6, 7, Table 8): Iyoda and coworkers utilized a Pd-free, Cu-mediated route with PPh₃ and K₂CO₃ in DMF at high temperature¹³⁹ while Li et al. used a Sonogashira coupling in ionic liquid, which afforded use of reduced amounts of CuI to minimize homocoupling side reactions.¹⁴⁰ In 2003, Vollhardt and coworkers reinvestigated *o*-DBA production with Schrock's W-alkylidene catalyst and isolated **207** in 54% yield by three-fold intermolecular metathesis of 1,2-dipropynylbenzene (Entry 5, Table 8).¹⁴¹ Two intramolecular cyclization routes have also been reported for **207**. Barton and Shepherd isolated the cycle in 20% yield from vacuum thermolysis of benzotricinnoline **221** in 1984¹⁴² and Haley and coworkers produced the cycle in 69% from Pd-catalyzed cross-coupling of triyne **222** after triazene decomposition and iodination with MeI.¹⁴³

A key interest in cycle **207** arises from the theoretical and as yet unattainable carbon-rich network graphyne (**194**), of which **207** can be considered a subunit. Development of single molecule systems based on the structural motif of **207** has been explored for insight into properties of the extended network. Cyclyne **223a**, composed of two twelve-membered cycles fused to a central arene core, was first isolated by Haley

and coworkers in 2000 in low overall yield (4%) via a lengthy intramolecular sequence (12 steps) concluded by two-fold intramolecular Pd-catalyzed cross-coupling (Figure 53).¹⁴³ The electronic absorption spectra of **223a** displayed the characteristic three-peak pattern associated with the diphenylacetylene chromophore of **207** (280, 290, and 300 nm) with addition of a strong absorption at 325 nm and increase in λ_{cutoff} (>460 nm) by ~50 nm. The broad, exothermic decomposition of **223a** above 300 °C ($w^{1/2}$ ~30-40 °C) clearly indicated a marked difference in thermal properties associated with fusion of two tribenzo[12]cyclyne cores compared to **207**, which exhibited a distinct mp at 210 °C.

In 2003, Vollhardt's group reported an identical overall yield for bowtie **223a** in only three steps. Six-fold intermolecular metathesis of a 4:1 mixture of 1,2-dipropynylbenzene and 1,2,4,5-tetrapropynylbenzene provided **223a** in an amazing 6% yield.¹⁴¹ Although not reported due to solubility problems in 2000, Vollhardt obtained the ¹H NMR spectra of **223a** that confirmed a weak paratropic ring current of the anti-aromatic annulene core by a small upfield shift of the AA'BB' multiplet. Iyoda and coworkers more recently reported octabutyl-substituted analog **223b**, obtained from two-fold Cu-mediated coupling of 1,2,4,5-tetraiodobenzene with an alkyl-substituted 2,2'-diethynyldiphenylacetylene in 1% yield.¹³⁹ The group was first to report the fluorescence quantum yield ($\Phi = 0.21$) and an associated 190 nm Stokes shift for the graphyne bowtie.

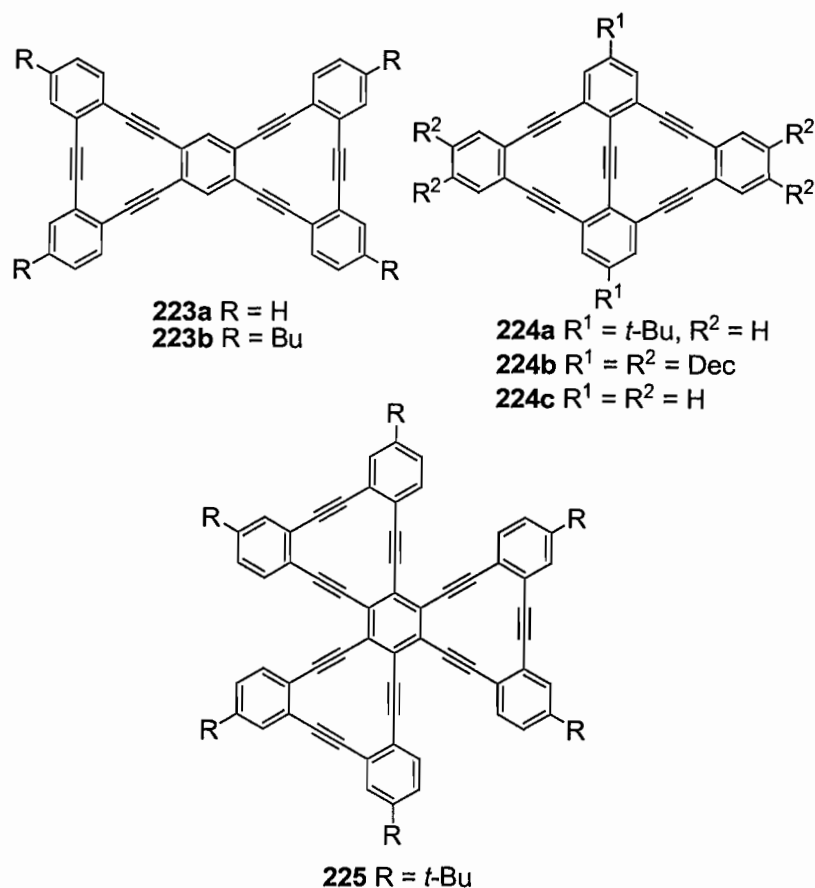


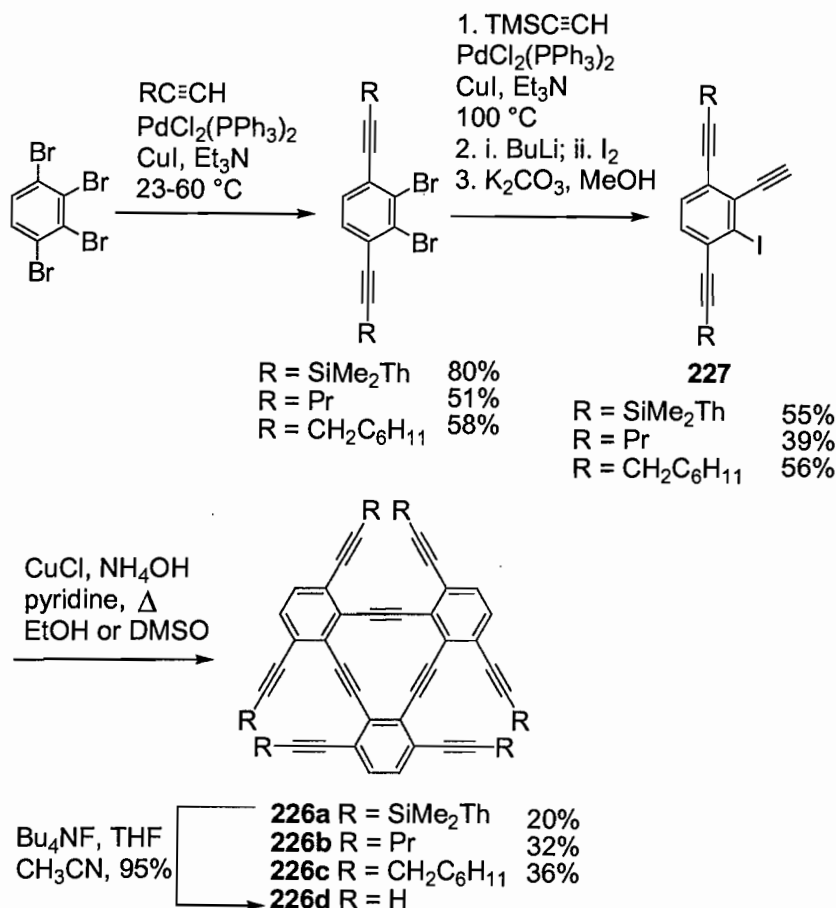
Figure 53. Multiply-fused tribenzodehydro[12]annulenes.

Additional single molecule systems based on the graphyne network include diamond-shaped cyclyne **224** and trefoil **225** (Figure 53). Concurrent with **223a**, Haley and coworkers first reported cyclyne **224a**, containing solubilizing *t*-butyl groups based on the poor solubility of **223a**, by an intramolecular stepwise route similar to that used for **207**.¹⁴³ In 2004, Tobe et al. reported **224b** by double cyclization of a didecyl-substituted 2,2',6,6'-tetrabromodiphenylacetylene precursor with 4,5-didecyl-1,2-diethynylbenzene in 9% yield and noted a significant improvement in solubility with addition of six decyl

groups.¹⁴⁴ Although the emission spectrum of **224b** exhibited resolved vibrational structure beyond **207**, the quantum yield ($\Phi = 0.06$) was inferior to **207** ($\Phi = 0.15$) and **223b**. Femtosecond Z-scans of **224b** in CHCl_3 resulted in second order hyperpolarizability values ($<4 \times 10^{-35}$ esu) lower than those predicted for the non-alkyl substituted parent of **224c** (5.49×10^{-35} esu).¹⁴⁵ The Tobe group most recently isolated the largest graphyne subunit, trefoil **225**, from three-fold pinacol coupling with $\text{Zn/VCl}_3(\text{THF})_3$ followed by chlorination/dehalogenation of the hexaethynyl precursor.¹⁴⁶

In 1997, Vollhardt's group prepared several substituted-hexaethynylbenzo[12]cyclyne systems (**226a-c**, Scheme 20) from Cu-mediated trimerization of triyne **227** in 20-36% yields.¹⁴⁷ Regioselective ethynylation of 1,2,3,4-tetrabromobenzene, which occurred at C1 and C4 with lower temperatures (30-60 °C) and C3 at increased temperature (100 °C), was used to construct the asymmetrically ethynylated skeleton of **227**. Lithium-halogen exchange followed by addition of I_2 afforded trialkynyliodobenzene **227** to facilitate a more successful three-fold cross-coupling. Reaction of **226a** with Bu_4NF afforded the relatively stable hexaethynylbenzene **226d** in near quantitative yield. The crystal structure of **226d**, which exhibited a slightly twisted deformation from planarity of the arene moiety, displayed a columnar supramolecular structure with alternating THF disks resultant from chelating C-H...O H-bonding between adjacent molecules. Distortion of the cyclyne core was more apparent in the substituted analogs (**226a-c**) due to steric congestion. Absorption spectra of the hexaethynylbenzo[12]cyclynes exhibited lower intensity for π - π^* transition than **207**, attributed to the decreased rigidity of the conjugated core. The group further

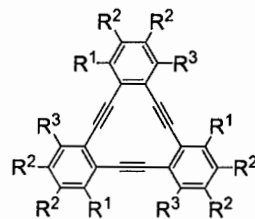
explored the use of **226a-d** as precursors for radial phenylenes, such as antikekulene, via Co-mediated cyclotrimerization.⁹



Scheme 20. Synthesis of ethynylated dehydrotribenzo[12]annulenes.

In collaboration with De Schryver and De Feyter, the Tobe laboratory has observed self-assembly of several polysubstituted benzo[12]cyclyne derivatives into ordered two-dimensional networks at the liquid-solid interface via scanning tunneling microscopy (STM).¹⁴⁸ In addition to **224b** and **228a**,¹⁴⁴ the group focused on several new

hexa-alkoxy analogs (**228b-d**, Table 9) of **207**, produced in 22-30% yield from three-fold coupling of 1,2-dialkoxy-4-ethynyl iodobenzene precursors by Iyoda's method,¹³⁹ as well as two hexa-alkoxy substituted cyclynes (**228e,f**) first reported by Youngs' group as potential liquid crystal precursors.¹⁴⁹ Analysis of cycle solutions in different solvents on HOPG showed that conjugated core shape, length of substituent chains, and solubility controlled identity, stability, and extent of monolayer formation. For example, in 1,2,4-trichlorobenzene, shorter chained **228a,b,e** predominately displayed a circular honeycomb pattern whereas longer alkoxy chained systems (**228c,d,f**) exhibited a linear arrangement of the triangular-shaped cyclyne cores. Increase in core size to diamond **224b** afforded kinetic formation of a linear monolayer that was replaced by a thermodynamically preferred Kagomé network.

Table 9. Dehydrobenzo[12]annulenes **228a-n**.

DBA	R ¹	R ²	R ³	Ref
228a	H	Dec	H	144
228b	H	ODodec	H	148
228c	H	OHexadec	H	148
228d	H	OOctadec	H	148
228e	H	ODec	H	149
228f	H	OTetradec	H	149
228g	OMe	H	OMe	155
228h	H	OHex	H	156
228i	H	F	H	138
228j	H	Br	H	141
228k	H	Me	H	138,139, 141
228l	H	Bu	H	139
228m	H	OMe	H	141
228n	H	OMe	OMe	140

Several different organometallic complexes of cyclyne **207** have been reported by Youngs and coworkers since 1985 (Figure 54). Combination of the respective parent cyclynes with Ni(COD)₂ in benzene afforded Ni-complexes **229a-c**, all exhibiting internal cavitation of the metal and coordination to all three ethynyl moieties.^{149,150}

Mononuclear and trinuclear cofacial Cu-complexes **230**¹⁵¹ and **231**¹⁵² were obtained from diffusion of saturated and stoichiometric benzene solutions of $\text{Cu}_2(\text{OTf})_2(\text{C}_6\text{H}_6)$ and **207**, respectively. Sandwich complex **232** was obtained from a mixture of **207** with AgSO_3CF_3 in a 3:1 ratio in THF followed by precipitation with hexanes¹⁵³ while 66-electron cluster **233** resulted from a mixture of the hexadecylcyclyne with $\text{Co}_2(\text{CO})_8$ in Et_2O .¹⁵⁴ All of the transition metal complexes were characterized by X-ray crystallography except **229c** and **233**, which were based on FD-MS, IR spectroscopy, and/or elemental analysis. Of note, complexes **229a** and **232** were respectively the first transition metal complex for the benzo[12]cyclyne and first observation of a macrocycle-metal sandwich complex. Iyoda et al. have also reported a 2:1 Ag-complex of octabutyl-substituted **223b**, which was characterized by time-of-flight MS and ^1H NMR spectroscopy.¹³⁹

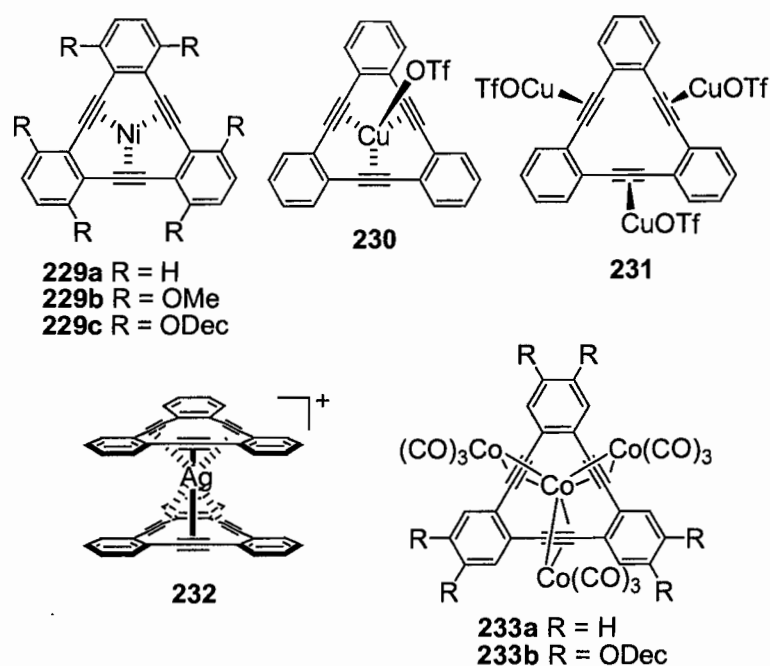


Figure 54. Various metal-coordinated dehydrotribenzo[12]annulenes.

Eight additional novel substitution patterns (**228g-n**, Table 9) have been reported for **207**. Youngs et al. produced *p*-dimethoxy substituted tribenzocyclyne **228g** in 1993 by three-fold Stephens-Castro coupling from a disubstituted *o*-ethynylidoarene in excellent yield as well as in low yield from Pd-catalyzed cyclotrimerization.¹⁵⁵ To explore the metal binding capability of **228g**, the group then treated the cycle with $(\text{NH}_4)_2\text{Ce}(\text{NO}_3)_6$ and converted a single dimethoxyarene substituent to a quinone moiety. Cycle **228h** was prepared recently by Moore's group with a precipitation driven Mo-amido metathesis catalyst in 86% yield.¹⁵⁶ The group confirmed reversible formation of **228h** by a scrambling experiment, which involved addition of a 1,3-dipropynylarene to the metathesis reaction and observation of two additional cycle products by MS. Polyalkyl- and polyalkoxycycles **228i-n** were prepared from substituted arene precursors by similar methods for **207** described in Section 5.2.2.1. and will not be discussed further (see Table 9 for correlation to references).

Linstrumelle and Huynh simultaneously reported production of monobenzo- and dibenzo[12]annulenes **234** and **235** with the new route to **207** in 1988 (Figure 55).¹³⁷ The novel monobenzannelated **234** was isolated in 21% cyclization yield while cycle **235** was obtained in comparable cyclization yield (11%) with the first reported Cu-mediated route used by Staab (10%).¹⁵⁷

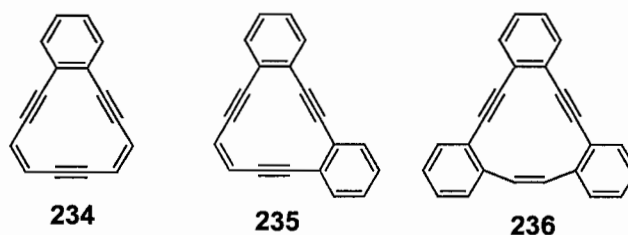
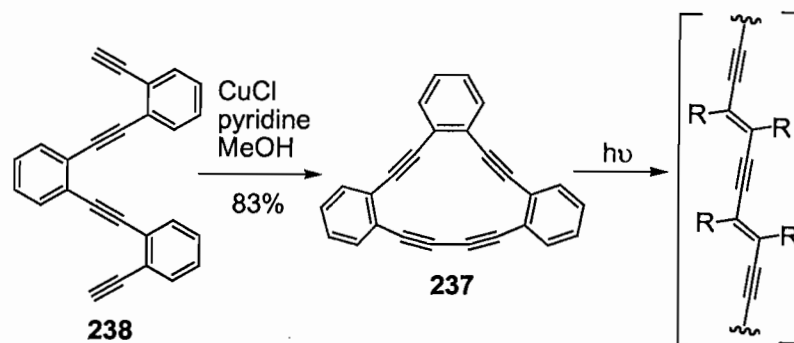


Figure 55. Dehydromonobenzo- and dibenzo[12]annulenes **234-236**.

Iyoda and coworkers produced tetrahydrobenzo[12]annulene **236** in 2000 from a precursor of **192** ($n = 1$).¹⁵⁸ The crystal structure of **236** exhibited a warped central core with the *Z*-alkene above the plane of the diphenylacetylene moieties. Investigation of Bergman chemistry of enediyne **236** afforded only the *E*-isomer upon irradiation but the desired annelated cyclooctatetraene product after thermal treatment at 250 °C for 4 d. Exploration of metal complexation of **236** resulted only in a mixture of several interesting polycyclic aromatic hydrocarbon products upon reaction with AuCl.

Dehydrobenzo[14]annulenes. Vollhardt and Youngs reported the first synthesis of octadehydrotribenzo[14]annulene **237** in 1995¹⁵⁹ from Glaser coupling of tetrayne **238**, previously prepared by Youngs' group (Scheme 21).¹⁶⁰ X-ray crystallography provided packing diagrams which supported proper orientation for topochemical polymerization of the butadiyne linkages to form an ene-yne polymer.¹⁶¹ The polymerization of the strained diphenyldiyne monomeric subunit was explored after observation that exposure of **237** to light rapidly changed the crystalline material to a surface with metallic, violet luster. The insoluble polymeric material, also available with application of direct pressure (20,000 psi) to crystals of **237**, was analyzed with high energy laser desorption time-of-flight MS,

which indicated the presence of oligomers up to $n = 9$, and DSC/TGA, which showed stability up to ~ 135 °C.

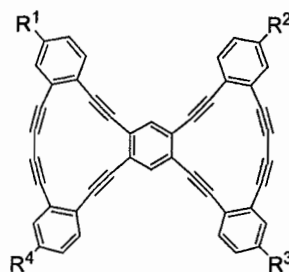


Scheme 21. Preparation and polymerization of a dehydrobenzo[14]annulene.

Haley's group investigated intramolecular charge-transfer in 2005 with a series of novel bis[14]cyclyne bowties (**239-242**, Table 10) consisting of electron donating (alkyl, NBu_2) and electron accepting (NO_2) substituents.¹⁶² During the macrocyclization of tetradonors **239** and **240**, the group discovered selective ring formation based on reactions conditions: Pd-catalyzed homocoupling favored formation of bis[14]annulenes **239-242** whereas Cu-mediated macrocyclization selectively favored isomeric bis[15]annulenes from common octayne precursors.^{162a} Analysis of the broad, low energy charge-transfer absorption bands of the new bowties indicated that linear charge-transfer pathways, planarity, and large net-dipoles were key factors for superior electronic properties. The new donor-acceptor systems displayed large Stokes shifts and exhibited a variety of emission colors, a direct result of a wide range of λ_{em} values (505-580 nm). Cycles **241** and **242** both displayed concentration dependence in ^1H NMR spectroscopy,

attributed to self-association as a result of face-to-face stacking in solution. Analogous bis[15]annulene systems were also constructed but will not be discussed due to cross-conjugation of the central arene ring.

Table 10. Bis-[14]cyclyne electron donor-acceptor systems **239-242**.



DBA	R ¹	R ²	R ³	R ⁴
239	Dec	Dec	Dec	Dec
240	NBu ₂	NBu ₂	NBu ₂	NBu ₂
241	NBu ₂	NBu ₂	NO ₂	NO ₂
242	NBu ₂	NO ₂	NO ₂	NBu ₂

Haley's laboratory reported several variably benzannelated octadehydro[14]annulene analogs (**243-246**, Figure 56) in 2000 and 2001 and investigated the bond-fixing ability of benzene on the parent annulene (**123**) with spectroscopy and NICS calculations.^{80,163} Incorporation of successive arene rings into **123** resulted in an upfield shift of alkene proton resonances by 0.67 and 0.38 ppm, respectively. Comparison of arene protons *ortho* to the diacetylene bridge between mono-, di- and tribenzo[14]cyclynes also displayed upfield shifts ($\Delta\delta$ 0.19-0.25) upon higher

benzannelation. The decreased aromaticity indicated by the continued upfield shift upon benzannelation was ascribed to competing ring currents. This consistent and rather sensitive effect on proton resonances for both alkene and arene protons of **243-246** provides further support for use of this methodology as a qualitative aromaticity probe.

The Haley group expanded on this aromaticity study by collaboration with Mitchell and Hopf in 2001 and 2005, respectively.^{43g,164} Both mono- (**247, 248**) and bis[14]cyclynes (**249**) fused to a DMDHP core were initially produced and subsequent investigation by ¹H NMR spectroscopy and NICS calculations confirmed the existence of weak diatropic ring currents for the *ortho*-fused systems. Cyclophane systems **250** and **251** were most recently prepared via cross-coupling of 4,5-diethynyl-[2.2]-paracyclophane with either 1-iodo-2-(trimethylsilylethynyl)benzene or (*Z*)-(4-chloro-3-buten-1-ynyl)trimethylsilane. The diatropic ring current of **250** and **251** was confirmed by changes in the chemical shift of cyclophane hydrogen atoms directly above the cycle core, with a larger effect observed for the more aromatic **251**.

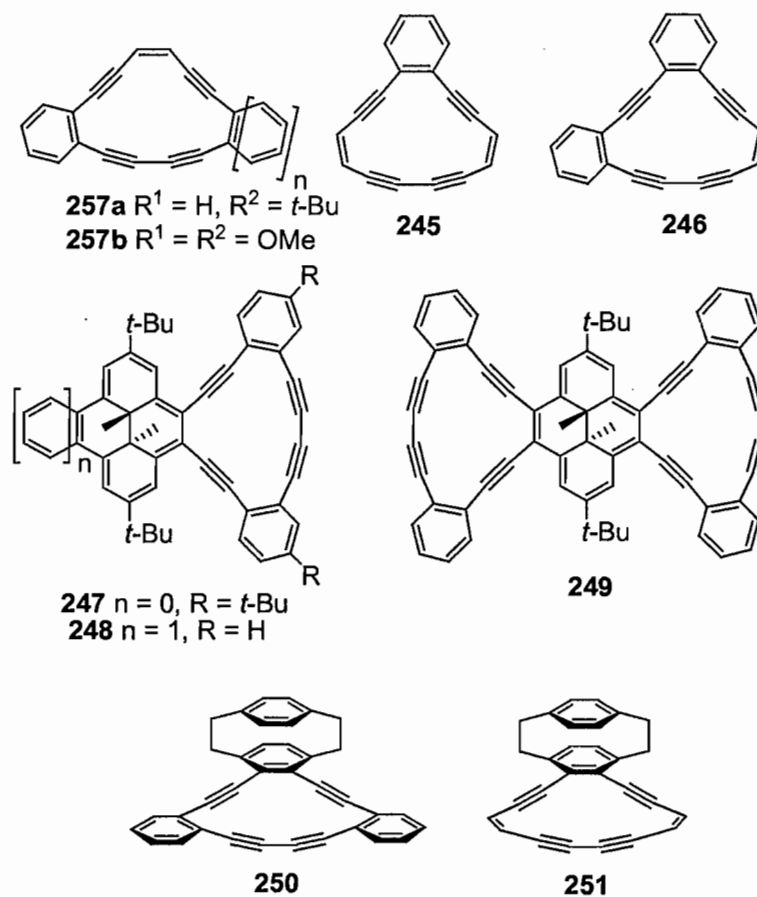


Figure 56. Variably benzannelated octadehydro[14]annulene analogues.

Through a series of articles initiated in 2001, Bunz reported a multitude of organometallic cycles with either a cyclobutadiene(cyclopentadienylcobalt) (**252-256**) or cyclopentadienyl-ferrocene complex (**257-258**) incorporated into the [14]annulene skeleton (Figure 57).¹⁶⁵ Pd-catalyzed cross-coupling of iodoarenes to diethynyl-metallated cores followed by alkylation and deprotection furnished the penultimate polyynes for monocycles **252** and **257**. Production of the larger asymmetric systems required a combination of acetal protecting groups and Ohira-Bestmann alkylation to

control substitution of the central organometallic cycle. Final macrocyclization by homocoupling under Vögtle conditions afforded the monocycles (19-93% yields) and fused systems (16-94% yields). The group conducted a detailed analysis of the solid-state structures of the new metallacyclines. Although the majority of the CpCo-monocycles crystallized in different space groups, all lacked close proximity of butadiynyl moieties, a possible reason for observed melting transitions instead of solid-state polymerizations for **252b-252f**. Seco-wheel **255** exhibited a distinct flattening of the hydrocarbon ligand beyond the non-linear distortion of the less constrained butterfly **253b**, which suggested a full wheel analog would be highly planar. Cycle **253b** also displayed an interesting grid-like supramolecular ordering that repeated the cyclobutadiene complex's tetragonal geometry, a phenomenon that suggested the potential for an extended network of covalently linked all-cyclobutadiene wheel substructures. A comparison of ^1H NMR spectroscopic δ values of the various substituted monocycle analogs indicated that both organometallic complexes were more aromatic than benzene by ring-current criteria, with cyclobutadiene(cyclopentadienylcobalt) superior to cyclopentadienyl-ferrocene.

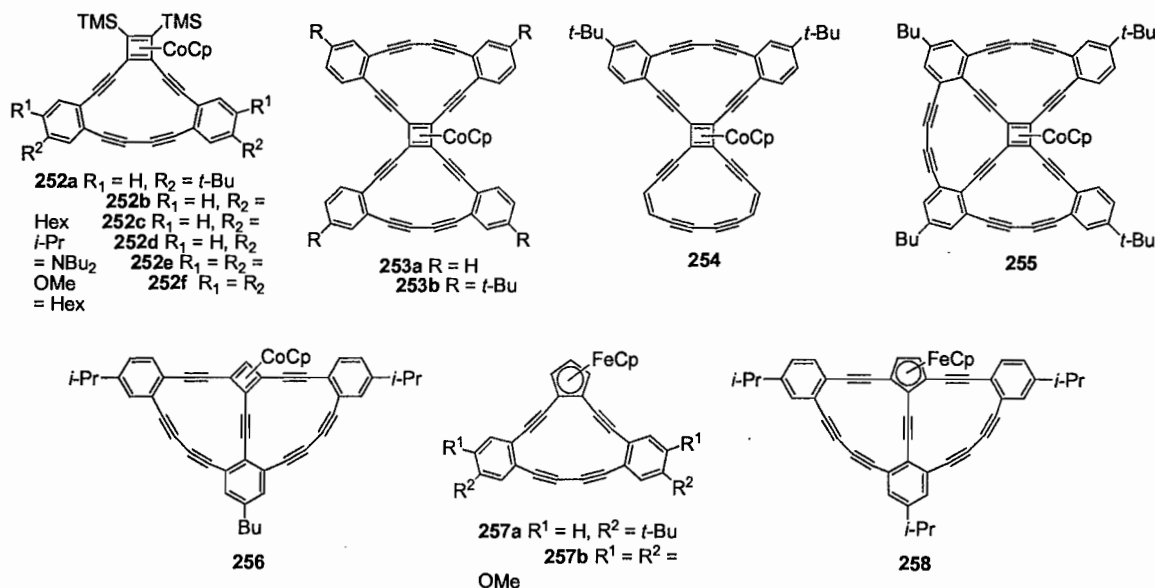


Figure 57. Various FeCp and CoCp-coordinated cyclobutadienyl- and cyclopentadienyl-fused dehydrobenzo[14]annulenes.

Two unique [14]annulene topologies, including either cumulene or triyne motifs, have been reported by Japanese research groups in the last 10 years (Figure 58). Kuwatani and Ueda produced a new Sworski-type octadehydro[14]annulene (**259a**) as well as derivatized analogs **259b-d** in 1995.¹⁶⁶ The 14-membered ring was constructed with methodology used for the benzo[*n*]annulenes (Section 4.2.1) prior to introduction of the cumulene functionalities by three different routes dependent on R group substitution. The aromatic enediynes showed limited stability, with only **259b** and **259c** stable upon concentration. The absence of ¹³C NMR spectroscopy resonances in the characteristic region of alkyne or cumulenic sp-hybridized carbons suggested the significance of the two non-equivalent resonance contributors of **259**.

Tobe et al. synthesized dibenzo[14]cyclyne **260** via elimination of indane from a pentayne analog of [4.3.2]propellatriene **217**.¹²⁵ In contrast to highly reactive **208**, triyne **260** was sufficiently stable in solution for spectroscopic characterization. The presence of two new resonances downfield from the propellatriene precursor were in agreement with calculated values as well as the diatropic current of [14]cyclynes. The lower yields of the intramolecular and furan [4 + 2] adducts of **260** suggested decreased reactivity of the central alkyne group, a factor confirmed by decreased angle distortion from DFT calculations (157-165°).

Wheel-shaped fenestrane **261**, consisting of complete fusion of two 14- and two 15-membered benzocyclynes to a central arene core, was produced in 2004 by Marsden, O'Connor, and Haley (Figure 58).¹³⁵ Cycle **261**, calculated to possess a slightly concave distortion, displayed enhanced solubility beyond its planar bisannulene substructure **239** as well as a bathochromic λ_{cutoff} and broadened absorption patterns due to more complex conjugated circuits.

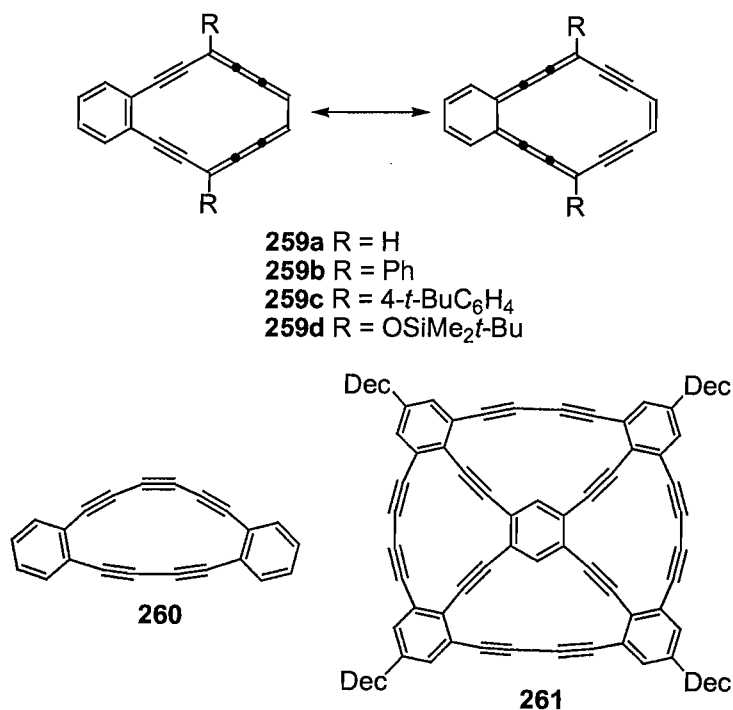


Figure 58. Unusual novel dehydrobenzo[14]annulene structures **259-261**.

Dehydrobenzo[16]annulenes. Tetracobalt complex **262** (Figure 59) was obtained in 70% yield¹⁶⁷ from reaction of the parent tetrabenzo[16]annulene (**263a**), first reported in 1966 by Eglinton and coworkers,¹²³ with two equivalents of Co₂(CO)₈ in THF at rt. Higher concentrations of Co₂(CO)₈ afforded only **262**, a steric factor due to close proximity of CO ligands to the uncomplexed alkyne groups. The tetranuclear-Co complex exhibited enhanced solubility beyond the bowl-shaped parent cyclyne.

Haley and coworkers introduced a new tribenzo[16]cyclyne topology in 1997 with the production of **264** via a multi-step intramolecular route (Figure 59).¹⁶⁸

Tetrakis(4,5-dialkoxyphenyl)tetraynes **263b** and **263c** were produced by Youngs et al. in

16% cyclization yield as coproducts during the Cu-mediated intermolecular synthesis of triynes **228e** and **228f**.¹⁴⁹

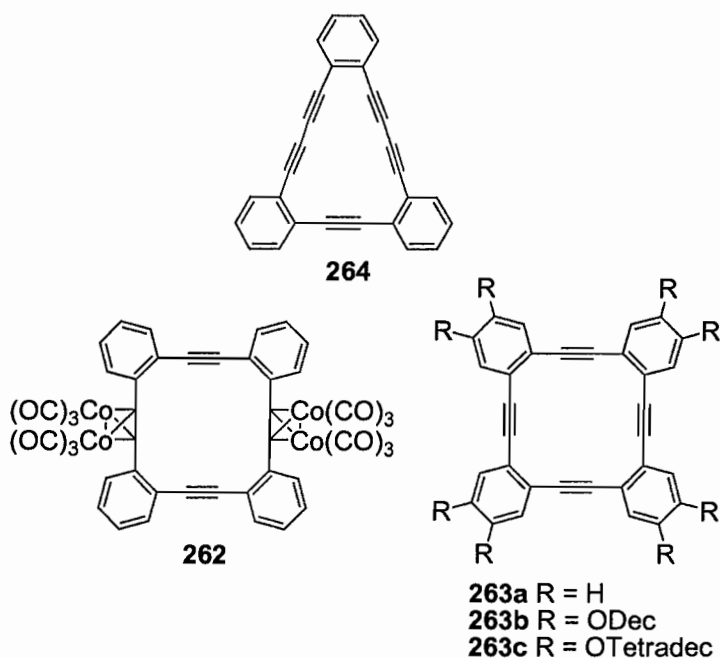
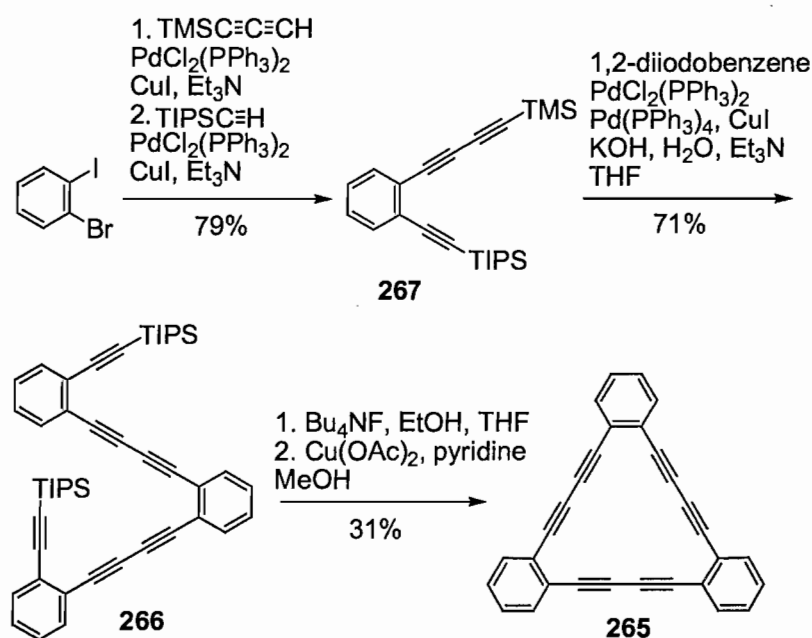


Figure 59. Dehydrobenzo[16]annulenes and a cobalt complex.

Dehydrobenzo[18]annulenes. Tribenzo[18]annulene **265**, first targeted by Eglinton and Galbraith in 1960 via intermolecular coupling of *o*-diethynylbenzene,¹²² was not isolated until 40 years later by Haley's laboratory.¹⁶⁹ Cycle **265** was obtained in 35% yield via Cu-mediated intramolecular homocoupling of hexayne **266** following desilylation (Scheme 22). The key triethynyl arene intermediate **267**, produced from selective, successive alkynylations of 2-bromoiodobenzene, was reacted with 1,2-diiodobenzene under *in situ* deprotection/alkynylation conditions, a procedure the group developed to overcome the inherent instability of terminal phenylbutadiyne

moieties.¹⁶⁸ Incorporation of two decyl groups into **265** was found to improve yield of the final step (56%) as well as cycle solubility. Diatropicity of the [18]cyclyne was confirmed by a small but distinct downfield shift ($\Delta\delta = 0.2-0.25$) of the arene protons upon cyclization. A slight hypsochromic shift in absorption (<19 nm) for the tribenzo derivative **265** compared to [18]annulene (**136**) indicated limited electronic effect from benzannellation.



Scheme 22. Dodecadehydrotribenzo[18]annulene synthesis.

Due to lack of feasible synthetic routes to graphdiyne, substructures based on cycle **265**, which could be considered a core structure for the extended network, have been produced to gain insight into materials properties of the bulk non-natural allotrope. The Haley group has expanded their initial synthesis of **265** to produce several

macrocyclic systems composed of two (**268-270**),¹⁶⁹ three (**271-273**),^{169,170,171} and four (**274-276**)¹⁷¹ fused dehydrobenzo[18]annulenes (Figure 60). Macrocyclization of the smaller systems (**268-272**, 6-88% yields) was accomplished with a combination of both Cu(I)- and Cu(II)-mediated homocoupling in pyridine and MeOH, while both Pd- and Cu-mediated homocoupling techniques were used for construction of **273-276** (1-49% yields). Comparison of the UV-Vis spectra of the allotropic substructures indicated that chromophore length instead of overall conjugation dominated electronic absorption. Specifically, bowtie **268** ($\lambda_{\max} = 413, 431$ nm), which contains two linear diphenylbutadiyne chromophoric pathways, exhibited bathochromic absorption beyond the constitutional isomer **270** ($\lambda_{\max} = 404, 420$ nm), which contains only one linear tetrayne pathway, and the more highly conjugated half-wheel **271** ($\lambda_{\max} = 411, 426$ nm). Substructure **276**, the largest carbon-rich single molecule (~5 nm) based on the graphdiyne network, exhibited electronic absorption ($\log \epsilon = 5.59$; $\lambda_{\text{cutoff}} = 462$ nm) that fell only 23 nm short of a calculated saturation wavelength for graphdiyne. The new substructures all exhibited exothermic decomposition above 200 °C with broader or more disordered transitions associated with the larger systems (**272-276**). Although several different solubilizing groups were explored, the largest substructures suffered from poor solubility predicted for the parent network; specifically, **275** and **276** could not be characterized by NMR spectroscopy.

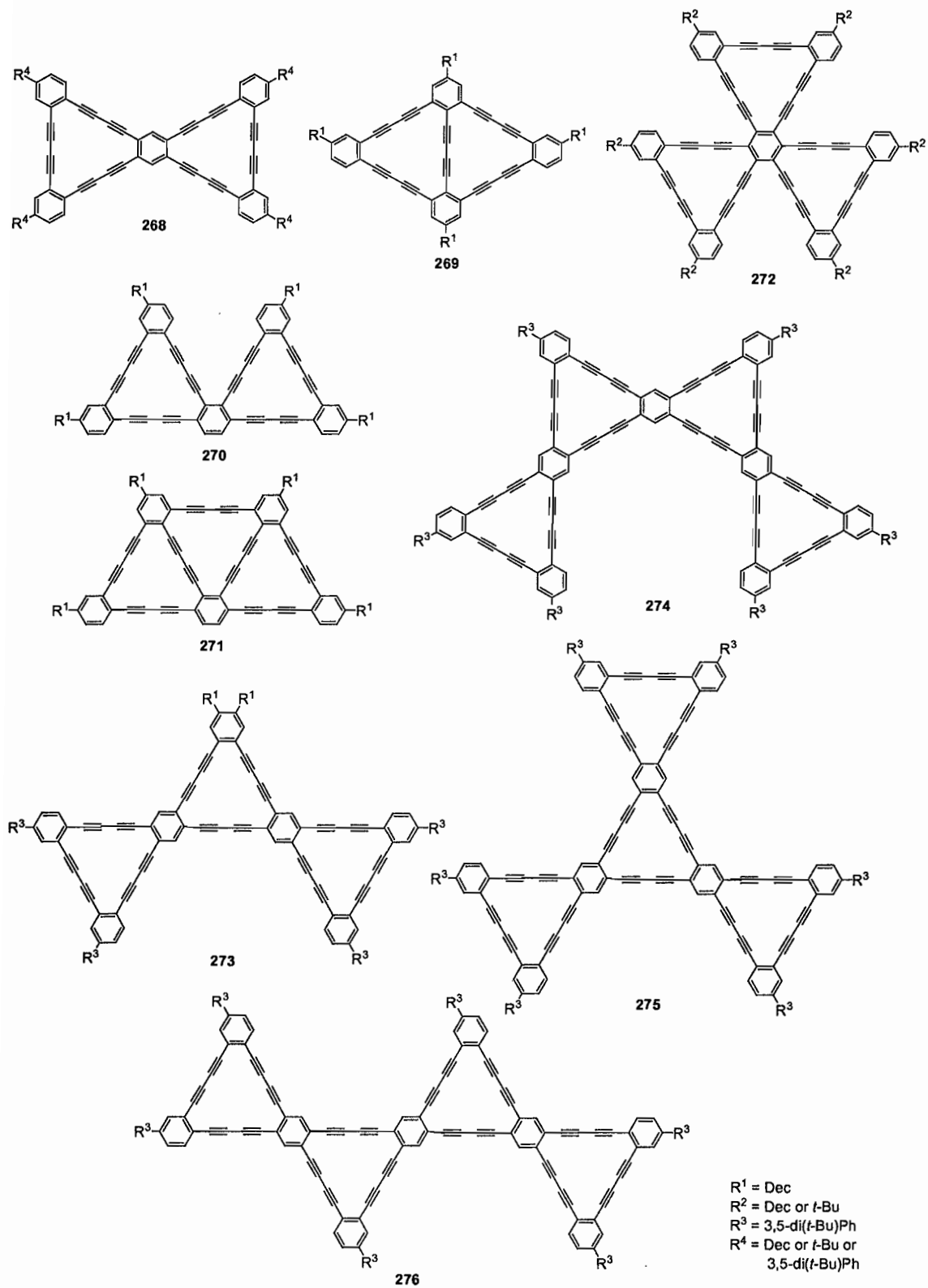
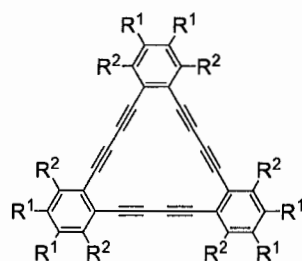


Figure 60. DBA substructures of graphdiyne.

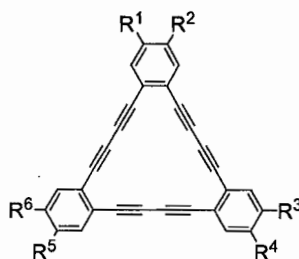
A recent collaboration between the Haley and Tobe laboratories resulted in isolation of tribenzo[18]cyclynes **277a-277e** (Table 11) and investigation of self-assembly of the derivatized molecules via STM.¹⁷² The cyclynes, obtained by Hay coupling in CH₂Cl₂ in 8-15% yield, required recycling GPC purification to remove homocoupling byproducts. Although Swager reported **277a** and **277b** in 1994, the cycles were analyzed only as a mixture with tetrameric and oligomeric components by ¹H NMR spectroscopy.¹²⁸ Use of Pd-catalyzed homocoupling in *i*-Pr₂NH and THF surprisingly produced trimeric and tetrameric analogs without dimeric octadehydrodibenzoannulene byproducts, likely due to decreased solubility of the dimer. Initial STM studies elucidated formation of quadratic monolayers for shorter chained systems (**277b**) but linear monolayers for cyclynes with R ≥ ODodec (**277c-e**), a factor attributed to less efficient substituent chain interdigitation resultant from the lengthened butadiyne spacer.

Table 11. Dehydrobenzo[18]annulenes **277a-h**.

DBA	R ¹	R ²	Ref
277a	Dec	H	128,172,178
277b	ODec	H	128,172
277c	ODodec	H	172
277d	OTetradec	H	172
277e	OHexadec	H	172
277f	F	F	130
277g	Hex	H	128
277h	Bu	H	178

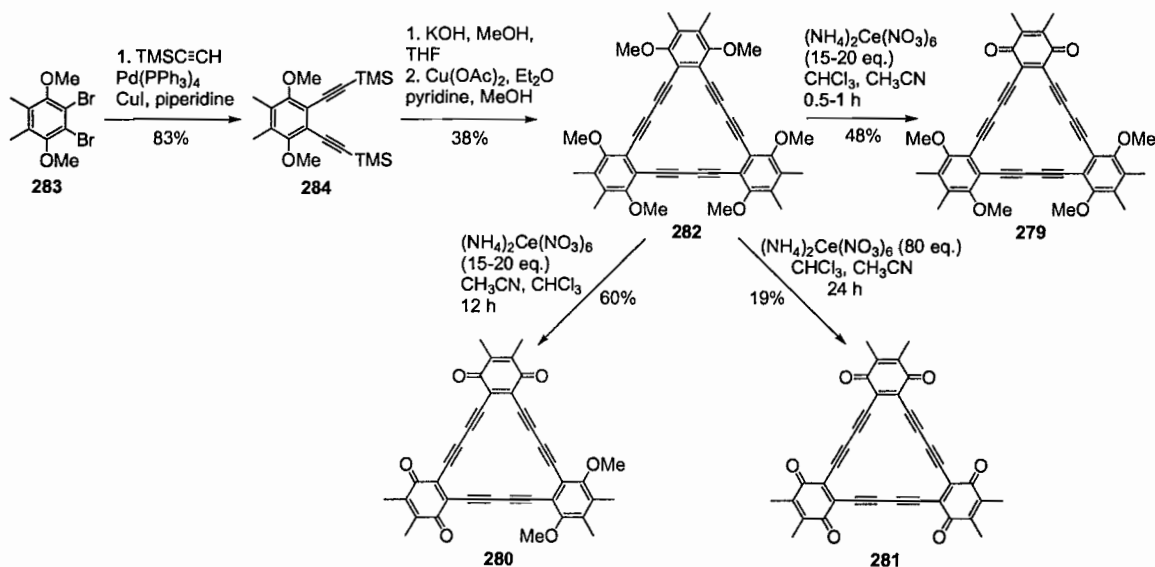
Based on the group's successful approach to **265**, Pak and Haley reported a series of novel site specific electron donor and/or acceptor functionalized [18]annulenes (**278a-p**, Table 12) in 1999.¹⁷³ A stepwise intramolecular synthesis starting with functionalized 1,2-dihaloarenes allowed access to previously inaccessible asymmetric C_{2v} and C_s topologies, a pronounced deficiency of intermolecular cyclotrimerization. UV-Vis spectroscopy, specifically the effects on the four characteristic π - π^* absorption bands of the [18]cyclyne core, were used to investigate the structure-property relationships of the new donor-acceptor systems. The alkoxy systems (**278b,c,p**) exhibited a bathochromic

shift and broadening of the low energy absorption but retained the annulenic core pattern, suggestive of electron localization in the cyclyne core. Incorporation of stronger donor or acceptor functionalities (e.g., NBu_2 , NO_2) resulted in broadened absorption pattern, increased molar absorbtivity, and bathochromic λ_{cutoff} values. The greatest low energy absorption ($\lambda_{\text{max}} = 422 \text{ nm}$, $\epsilon = 57300 \text{ M}^{-1} \text{ cm}^{-1}$) was observed in cycle **278m**, composed of both strong donors and acceptors as well as a linear conjugation pathway between the substituents. Further study of conjugation pathway between donor-acceptor substituents showed that linear relationships (**278m**) provided enhanced charge-transfer compared to cross-conjugated isomers. Four of the systems (**278j-m**) and a new hexa-substituted analog (**278q**) were further analyzed for second-order NLO susceptibility in 2001.¹⁷⁴ Cycle **278j**, which possessed a dipolar solid-state structure, exhibited the largest second-order NLO response as well as superior β values compared to 4-dimethylamino-4'-nitrostilbene. Systems **278r-w** were more recently produced to explore alternate donor (NHBu) and acceptor (CN , CO_2Me) groups.¹⁷⁵

Table 12. Dehydrobenzo[18]annulene electron donor-acceptor systems **278a-w**.

DBA	R ¹	R ²	R ³	R ⁴	R ⁵	R ⁶
278a	Dec	Dec	H	H	H	H
278b	OMe	OMe	H	H	H	H
278c	OOct	OOct	H	H	H	H
278d	H	H	H	NO ₂	NO ₂	H
278e	Dec	Dec	H	NO ₂	NO ₂	H
278f	OMe	OMe	H	NO ₂	NO ₂	H
278g	OOct	OOct	H	NO ₂	NO ₂	H
278h	NBu ₂	H	H	H	H	H
278i	H	H	H	NBu ₂	NBu ₂	H
278j	NO ₂	H	H	H	H	NBu ₂
278k	NO ₂	NBu ₂	H	H	H	H
278l	NO ₂	H	H	NBu ₂	H	H
278m	NO ₂	NBu ₂	H	NO ₂	NBu ₂	H
278n	NO ₂	NBu ₂	H	NBu ₂	NO ₂	H
278o	OH	NO ₂	H	NBu ₂	NBu ₂	H
278p	-O(CH ₂ CH ₂ O) ₄ -		H	H	H	H
278q	NO ₂	NBu ₂	NO ₂	NBu ₂	NO ₂	NBu ₂
278r	NO ₂	NBu ₂	NO ₂	NBu ₂	NBu ₂	NO ₂
278s	NHBu	NO ₂	H	NO ₂	NBu ₂	H
278t	NHBu	NO ₂	H	CN	NO ₂	H
278u	CN	CN	H	NBu ₂	NBu ₂	H
278v	Dec	Dec	H	CN	CN	H
278w	CO ₂ Me	H	CO ₂ Me	H	CO ₂ Me	H

In 2004, Komatsu's group published a series of *p*-benzoquinone-fused hexadehydro[18]annulenes (**279-281**) as well as hexadonor **282**.¹⁷⁶ Synthesis began with Pd-catalyzed cross-coupling of dihaloarene **283** and TMSA (Scheme 23). Desilylation of the resultant diyne (**284**) with KOH and use of oxidative Eglinton conditions afforded the [18]annulene **282** in 38% yield. Different electron-donor and/or acceptor systems were obtained by sequential oxidative replacement of dimethoxyarene rings with electron accepting *p*-benzoquinone moieties. Treatment of **282** with 15-20 equivalents of CAN over 1 h afforded **279** while increased reaction time (12 h) produced **280**. Trisquinone system **281** required 24 h with 80 equivalents of CAN. The intramolecular charge-transfer of **279** and **280**, which was confirmed with DFT calculations, exhibited superior absorption spectra ($\lambda_{\text{cutoff}} \sim 600$ nm) and broadened low-energy bands compared to tris-donor **282** and tris-acceptor **281**. The solvatochromism exhibited by **279** and **280** was very limited, a combination of poor solubility of the cyclynes and delocalization of the HOMO-LUMO over the entire cyclyne π -system. Incorporation of *p*-benzoquinone moieties was also found to increase diatropicity of the [18]cyclyne core due to the enhanced double bond character at the site of ring fusion.



Scheme 23. Benzoquinone-fused dehydro[18]annulenes.

Bowtie **285** represents the sole [18]annulene dimethyldihydropyrene probe produced in Haley and Mitchell's collaboration (Figure 61).¹⁶⁴ The downfield shift of arene proton resonances upon cyclization was attributed to through-space deshielding caused by an interior annulene ring current. The larger changes in chemical shift for hybrid **285** compared to benzocyclyne analog **268** agreed with previous assertions that DMDHP is less aromatic than benzene and hence less able to bond fix a fused arene.

Concurrent with isolation of the [14]annulenes described in Section 5.3.4, Bunz and coworkers prepared several organometallic [18]annulene analogs (**286-289**, Figure 61) as well as a hybrid bowtie system consisting of 14- and 18-membered cycles fused to a central cyclobutadiene-CoCp complex (**290**).^{165c,d,177} Transmission electron microscopy of the HCl-treated soot from explosive decomposition of **286a**, **286d**, and **288a** showed a variety of onion-shaped carbon nanostructures which became increasingly ordered upon

annealing up to 900 °C. Preorganization of the butadiyne moieties was concluded as a key factor for explosive decomposition, which occurred only with crystalline samples instead of precipitated powders. Additionally, cycle **288a** exhibited a unique difference in solid-state structure from the other organometallic systems that possibly accounted for the propensity to form ordered carbon-rich structures: the diyne units of adjacent systems possessed several close contacts, i.e., the bonds were within the sum of the van der Waals radii (3.6 Å) for sp-C atoms.

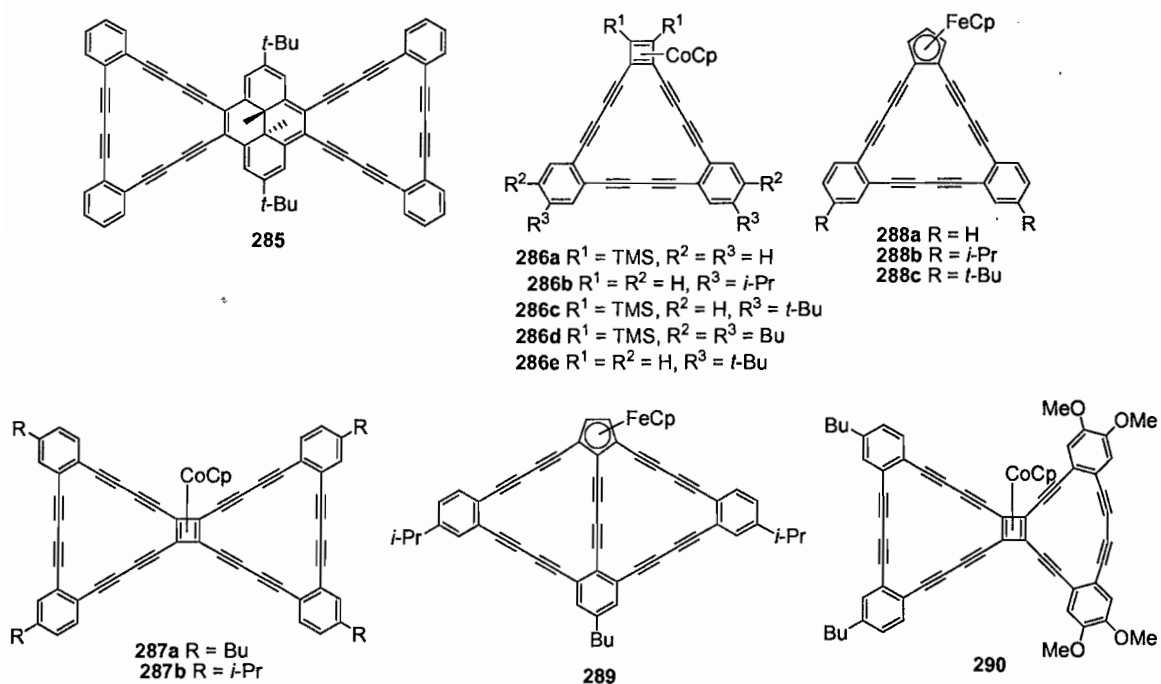


Figure 61. DMDHP-fused and various iron and cobalt-coordinated [18]DBA derivatives.

Komatsu's octafluoro-trimeric cyclyne **277f** and two hexa-alkyl [18]cyclynes (**277g,h**) obtained independently by Swager and Baranovic's groups have also been reported (Table 11). Polyfluorinated **277f**, obtained as a coproduct with dimeric **209c** from homocoupling of 1,2-diethynyl-3,4,5,6-tetrafluorobenzene, underwent exothermic decomposition at 221 °C, almost 11 °C lower than the parent [18]annulene.¹³⁰ Although several different alkyl (Bu, Dec, Dodec) and alkoxy-substituted (ODec) analogs were characterized as mixtures in NMR spectroscopy, cycle **277g** was effectively isolated from tetrameric and oligomeric components during Swager's investigation in 1994.¹²⁸ Baranovic and coworkers recently published a detailed vibrational spectroscopy study on **277a** and **277h** as well as several theoretical hexa-substituted analogs of **265**.¹⁷⁸

Dehydrobenzo[20]annulenes. Boese, Matzger, and Vollhardt produced the first tetrabenzo[20]annulene (**291a**) in 1997 by Eglinton coupling of bis(2-ethynylphenyl)ethyne in low yield (Figure 62).¹⁷⁹ The twisted D_2 -symmetric confirmation of cycle **291a** as shown by X-ray crystallography was not susceptible to UV-light induced topochemical polymerization like **237**; however, the system exploded violently under vacuum at 245 °C to afford ordered onion- and tube-type nanostructures. Cycle **291b** was subsequently produced to explore the possible enantiomerization of the chiral, twisted solid-state structure. Low temperature NMR spectroscopy of **291b** ($\Delta G^\ddagger = 9 \text{ kcal mol}^{-1}$) showed an enhanced interconversion rate not only beyond tetrabenzocyclooctatetraene ($\Delta G^\ddagger > 45 \text{ kcal mol}^{-1}$) but cyclooctatetraene as well. Haley and coworkers simultaneously reported an isomeric [20]cyclyne topology (**292**), which displayed a saddle-like distortion and generated 50 kJ mol^{-1} more energy upon

decomposition than **291a**, as well as an alternate synthesis of **291a** via their *in situ* deprotection/alkynylation route.¹⁶⁸ The enhanced energy of decomposition of **292** was attributed to a combination of greater alkyne distortion and difference in solid-state packing.

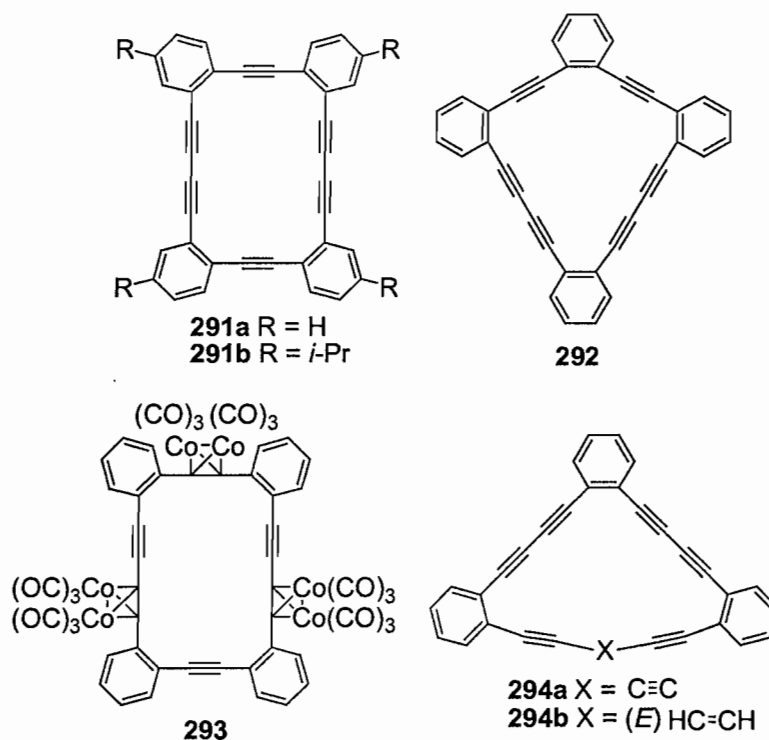


Figure 62. Dehydrobenzo[20]annulenes and a cobalt complex.

Production and thermal decomposition of hexanuclear Co-complex **293** (Figure 62) was published two years after the report of cycle **291a**.¹⁸⁰ In contrast to the carbon-rich system, the organometallic analog decomposed below 200 °C with the release of CO. Thermal treatment up to 800 °C resulted in formation of carbon onions and multi-walled

nanotubes with metal composition concentrated amorphously or coating the tubes and onions.

A single tribenzo[20]heptayne (**294a**) and partially reduced analog (**294b**) have also been prepared by Haley's group.^{168b,181} In agreement with an anti-aromatic π -system, the new [20]cyclynes exhibited either weakly paratropic or atropic behavior compared to *ortho*-diethynylbenzene in NMR spectroscopy. The unrestrained rotation of the isolated alkene bond was clearly demonstrated when the vinyl protons of **294b** did not resolve into discreet resonances in low temperature NMR spectroscopy at $-90\text{ }^{\circ}\text{C}$.

Higher Dehydrobenzo[*n*]annulene Systems ($n > 20$). Four dehydrobenzo[22]annulenes (**295**, **296**, Figure 63) have been reported to date, all produced in 1997 and 1998 by Haley's group.^{168,181} Cycle **296a**, of note as one the first two triacetylenic annulenes (see also **294a**, Section 5.6.3.), was obtained in a near identical fashion to **265** with a phenylhexatriyne synthon instead of butadiyne-substituted **267** (Scheme 22). Although cycles **296a-c** all exhibited diatropic shifts upon cyclization, the proximal ($\Delta\delta$ 0.05-0.08) and distal ($\Delta\delta$ 0.02-0.05) arene protons of the systems containing either one or two *E*-alkene bonds were paratropically shifted compared to benzocyclyne **296a**. The more constrained topologies of **296b** and **296c** resulted in larger interconversion rates ($\Delta G^{\ddagger} = 18.9\text{-}19.1\text{ kcal mol}^{-1}$) and temperatures ($T_c = 94\text{-}115\text{ }^{\circ}\text{C}$) for alkene moieties compared to **294b** as well as [18]annulene.

Hexadecadehydrotetrabenzo[24]annulene **297a** was first reported in 1994 by Youngs and coworkers (Figure 63).¹⁸² Similar to Sondheimer's route to [24]annulene in 1970,¹⁸³ intermolecular Glaser homocoupling of bis(2-diethynylphenyl)ethyne afforded

the parent cyclyne in 50% yield. The crystal structure of **297a** displayed a characteristic saddle-like distortion, suggestive of localized π -electron density, and limited ethynyl distortion (0.6 - 6°). In the same year, Youngs' group introduced an additional hexabenz[24]cyclyne topology (**298**), which exhibited more significant ethynyl distortion (1.2 - 8.1°) as well as a distorted boat conformation with D_2 symmetry instead of the expected boat conformation.¹⁶⁷ An alternate intramolecular route to **297a** using triyne **267** was published in 1997 by Haley.¹⁶⁸ Several substituted analogs of **297a** have also been reported by Swager (**297b**),¹²⁸ Haley (**297c**),¹³⁵ and Faust (**299a,b**).¹³⁶

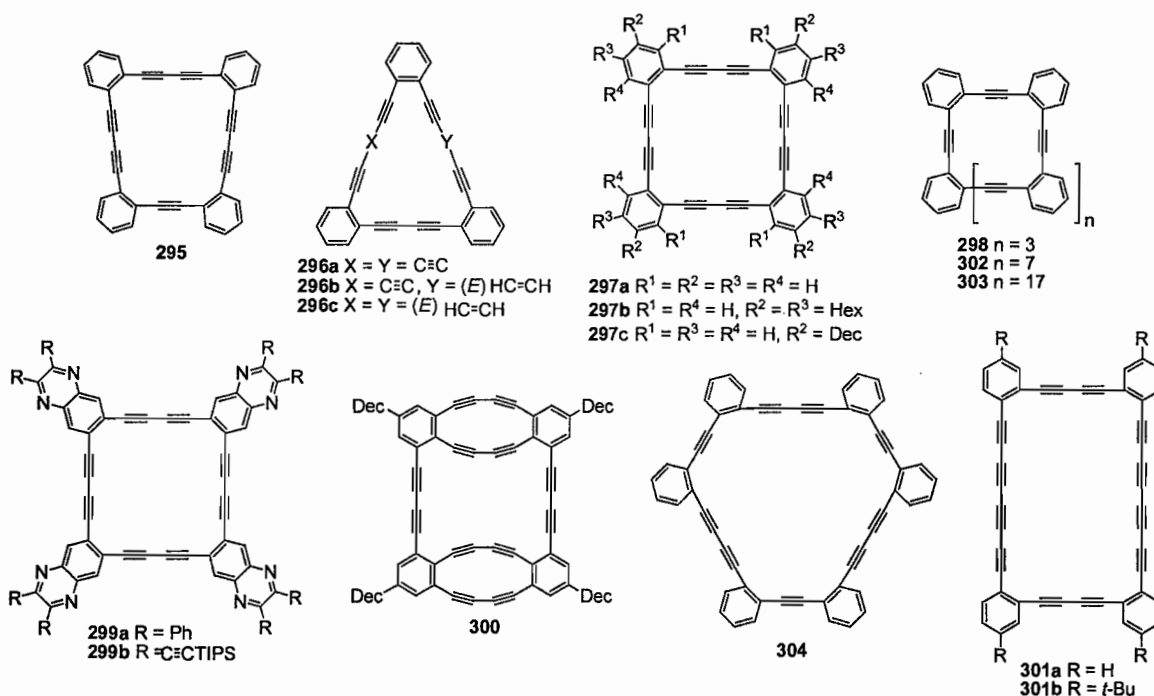


Figure 63. Various higher dehydrobenzoannulenes.

Macrocycle **300**, an unusual topology containing a [24]cyclyne and two [12]cyclyne cores, was isolated by Haley's group in 2004 from a key polyynes intermediate used for fenestrane **261** (Figure 63).¹³⁵ Treatment of (2,2',6'6'-tetraethynyl)diphenyl-2,4-butadiyne with Cu(OAc)₂ and CuCl in pyridine at 50 °C resulted in initial intramolecular homocoupling, which formed the [12]cyclyne core, followed by intermolecular cyclization to afford the [24]cyclyne ring. The electronic absorption spectra of **300** exhibited a 75 nm red-shifted λ_{cutoff} and 35 nm greater λ_{max} than **297c** and **209e**, respectively.

Tetrabenzo[32]cyclynes **301a** and **301b** (Figure 63), reported in 1997 by Haley et al. via Cu-catalyzed cyclization in 51-64% yield, were the first reported DBA containing tetrayne linkages.¹⁸⁴ The tetrayne moiety was constructed by *in situ* desilylation and dimerization of butadiynyltrimethylsilane groups via addition of K₂CO₃ to Eglinton homocoupling conditions. In contrast to smaller cycles, cyclization of **301a** and **301b** exhibited very minimal (< 2 nm) bathochromic absorption compared to the hexayne precursor, a factor attributed to the large size and non-planar structure. The electronic absorption spectra of the remarkably stable dodecayne system, which exhibited no decomposition over several weeks in solution or solid-state, was only slightly red-shifted (≤ 20 nm) beyond the characteristic pattern of 1,8-diphenyloctatetrayne.

Youngs and coworkers' interest in carbon-rich cycle precursors for rigid-rod polymers and fullerene tubules resulted in isolation of dehydrobenzo[40]annulene **302** in 1993.¹⁶⁰ The large DBA was produced by two-fold intermolecular cross-coupling of phenylacetylene oligomers. The crystal structure exhibited a highly distorted, compact

structure, the result of π - π interaction between two non-adjacent phenyl rings.¹⁸⁵ Further investigation of the cyclization reaction by time-of-flight secondary ion MS showed higher analogs ($n = 17, 27, 37,$ and 47) from the intermolecular coupling; however, only **303** was isolated as a discrete product from the higher homologues. Vollhardt's group was also able to isolate large macrocyclic byproducts during production of **237**, namely [30]annulene **304** in 5% yield as well as trace amounts of a pentameric [50]annulene characterized by NMR spectroscopy and MS.¹⁵⁹

Other Arene-fused Annulenes

Naphtho-fused Systems. Komatsu et al. reported a series of 2,3-annelated 1,4-dimethoxynaphthalene cycles (**305-310**) in 1998 (Figure 64).¹⁸⁶ Alkynylation of 2,3-dibromo-1,4-dimethoxynaphthalene followed by desilylation with KF and Eglinton homocoupling conditions afforded cycles **305-309** in low yield with [18]annulene **306** as the prevalent species (31% yield). Pd-catalyzed cross-coupling of 2-methyl-3-butyn-2-ol with 2,3-dibromo-1,4-dimethoxynaphthalene followed by *in situ* deprotection/three-fold cyclotrimerization produced trinaphtho[12]cyclyne **310** in 25% yield. Comparison of ¹H NMR spectra showed very little difference between the new cycles, attributed to rapid conformational changes for the non-planar systems (**307-309**) and lack of ring current in the central annulene core. The atropicity of the naphtho-annulenes was confirmed with the crystal structure of **310**, which indicated increased bond length (~ 0.03 Å) of the 2,3-naphtho fusion site. Minimal variance in redox potentials between anti-aromatic (**305**) and aromatic systems (**306**) provided further evidence that the systems were better

attributed as naphthalene moieties connected by alkyne bonds instead of DBAs. An additional trinaphthocyclyne (**311**) with fusion at the 1,2-positions was recently reported by She and Pan and coworkers.¹⁴⁰ While use of THF as solvent afforded only trace amounts of product, the group's previously discussed use of an ionic liquid as solvent afforded the cycle in 16-21% yield.

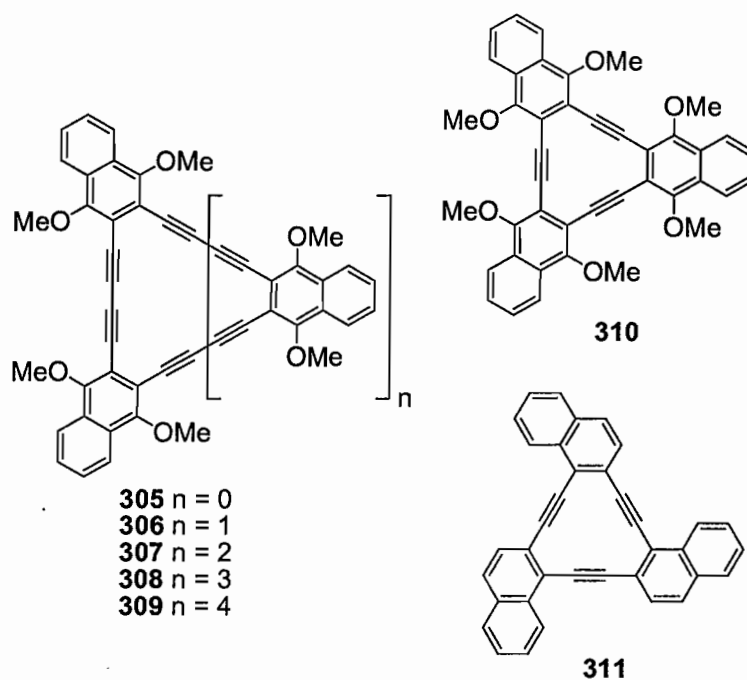
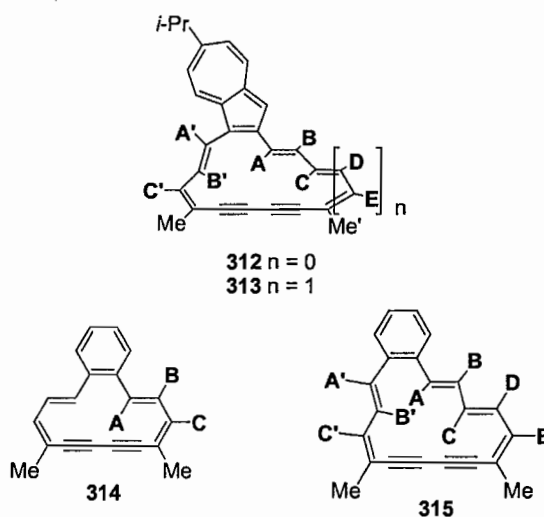


Figure 64. Dehydronaphthoannulenes.

Azuleno-fused Systems. Ojima, Yasunami, and coworkers have prepared both dehydro[14]- and [16]annulenes fused with azulene rings (**312** and **313**).¹⁸⁷ Their chemical shifts were then compared to benzo-fused annulenes **314** and **315** to determine effects on ring tropicity (Table 13).¹⁸⁸ The roughly analogous internal and external protons in **312** are consistently upfield and downfield from those in **314**, respectively.

Between **313** and **315**, the trend is the opposite. Taking these shifts as an evaluation of aromaticity, it is clear that fusion to an azulene system causes much less attenuation of diatropic/paratropic character. This gives rise to the possibility of using the “strength” of a particular system, fused to an annulene, in suppressing tropicity to quantify that system’s aromaticity itself.

Table 13. Azuleno-fused systems **312-315**.



	δ , ppm			
^1H	312	314	313	315
A	3.81	4.99	9.89	1.70
A'	6.83		6.55	5.94
B	8.10	7.44	6.35	5.73
B'	4.70		10.00	6.07
C	7.36	7.08	8.75	9.42
C'	7.74		6.11	6.07
D			7.11	5.73
E			5.90	5.94
Me	2.55	2.36	1.66	1.70
Me'	2.48		1.65	

Pyridannulenes. Baxter and Dali-Youcef recently synthesized the first all nitrogen heterocyclic *o*-fused dehydroannulenes (**316**, **317a**, Figure 65) as well as an additional hybrid cycle containing both pyridine and benzene rings (**317b**).¹⁸⁹ [20]Annulene systems **317a** and **317b** were constructed in a stepwise intramolecular fashion by selective alkynylation of 3-bromo-4-iodopyridine whereas tripyrid[12]cyclyne **316** was obtained via intermolecular three-fold coupling of 4-ethynyl-3-iodopyridine. Cycle **316** possessed a selective photoluminescent quenching sensory response for Pd(II) and also precipitated as a coordination polymer upon high Ag(I) concentrations.

Dehydrothieno[12]annulenes. Youngs reported the first thienocyclyne (**318**, Figure 65) in 1990 from cyclotrimerization of 3-ethynyl-2-iodothiophene via Stephens-Castro conditions in 20% yield.¹⁹⁰ The initial route for the 2,3-thieno-fused cycle from trimerization of isomeric 2-ethynyl-3-iodothiophene starting material produced only insoluble orange material. Interest in the cycle originated from successful metal complexation of **207** and a calculated larger internal cavity for **318**, anticipated to cavitate Pd or Pt atoms. An organometallic complex of **318** was isolated four years later; however, the tetranuclear Co-complex exhibited significant distortion of the cyclyne core with Co-complexation of only two alkyne groups.^{190b}

Several additional 3,4-thienofused cyclyne analogs (**319a-d**, Figure 65) were published by Youngs' group in 1999 while investigating liquid crystallinity of substituted cyclynes.¹⁴⁹ The new systems were prepared from sequential, selective alkynylation of tetraiodothiophene and cyclized with Pd(0) in 1-25% yields. The cyclotriynes gradually decomposed under ambient conditions and did not display liquid crystallinity. The crystal

structures showed that π - π interactions between cyclyne cores were prevented by intermolecular attractions of substituent chains and conjugated cores, thus precluding columnar or slipped stacked arrangements exhibited by other known liquid crystalline systems.

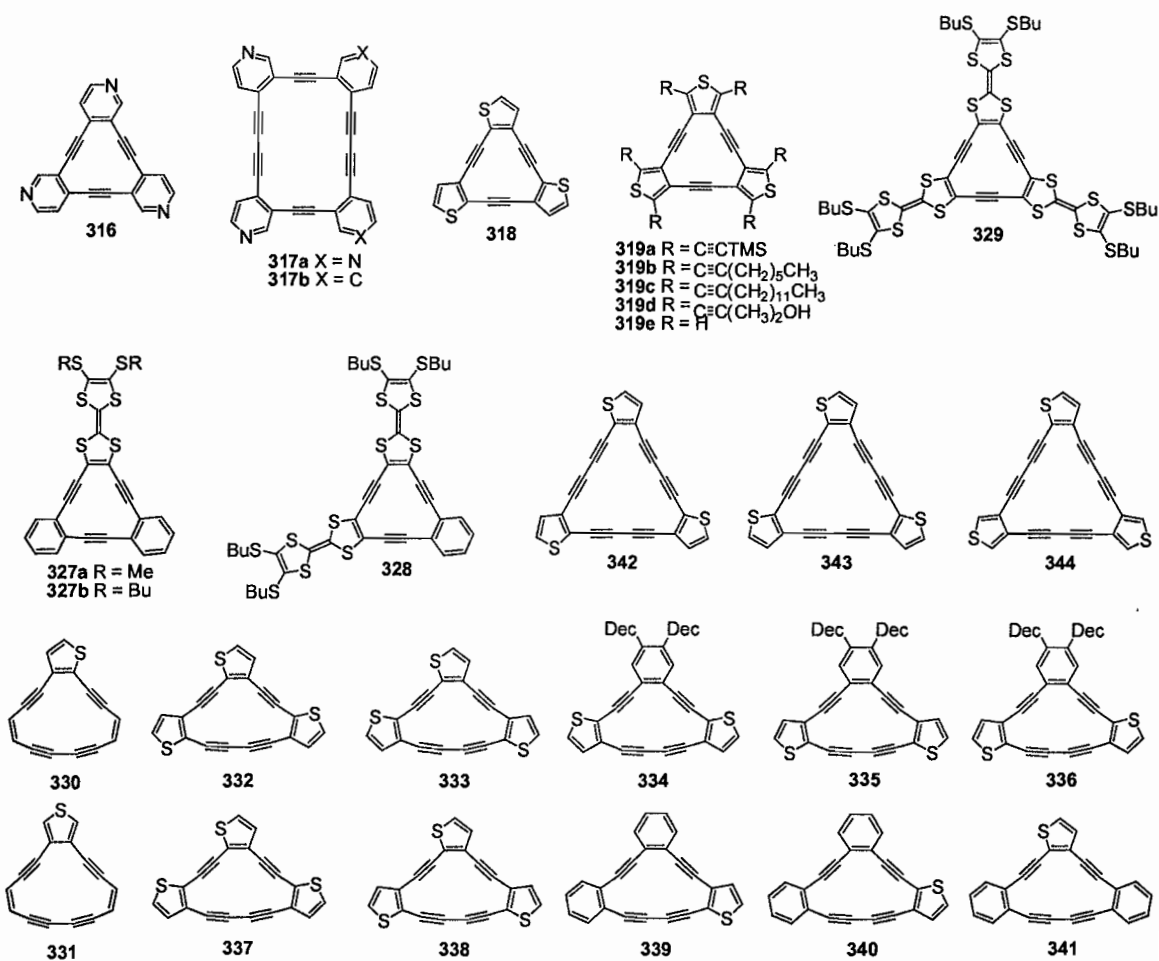


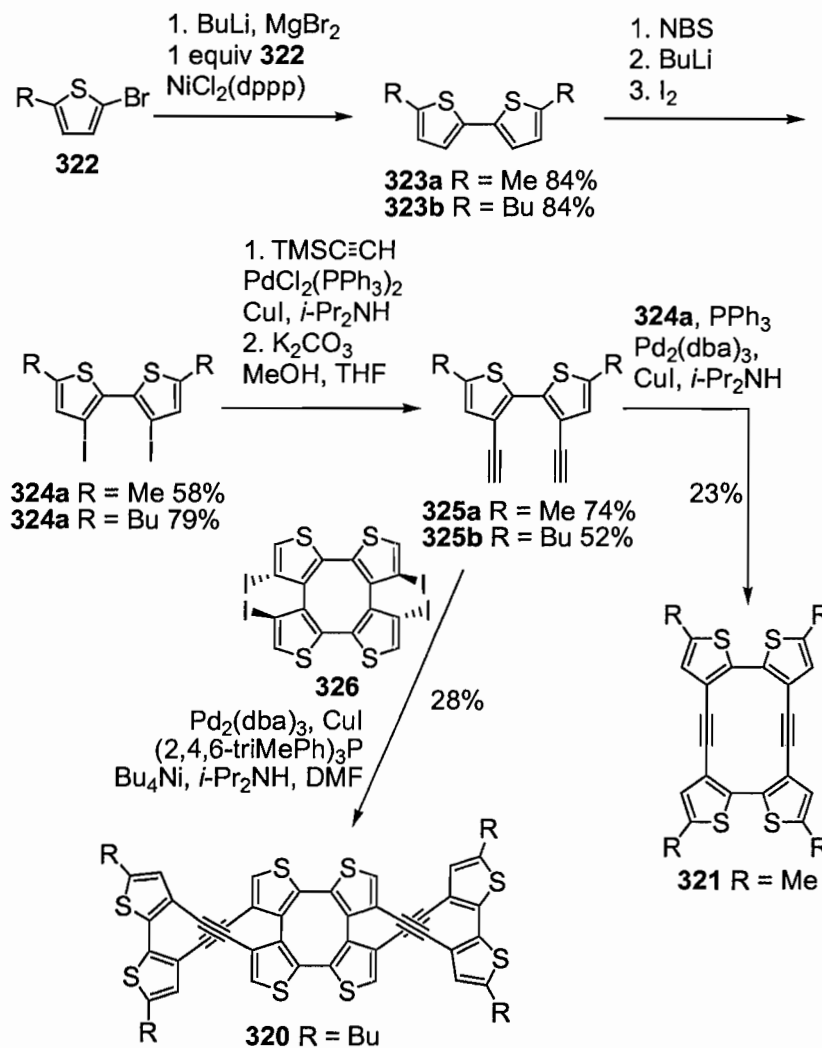
Figure 65. Various dehydrothienoannulenes.

Iyoda and coworkers produced the first parent thieno[12]annulene with fusion in the 3,4-positions (**319e**, Figure 65) in 2004 by Pd-catalyzed six-fold coupling of 3,4-

diiodothiophene with acetylene gas in 37%.¹³⁸ The group noted a significant increase in reaction rate for the diiodothiophene starting material compared to arene systems. A 2:1 sandwich complex of **319e** with Ag was proposed as a staggered conformation based on minimal changes in ¹H NMR spectra, a contrast with lack of shielding expected for an eclipsed conformation.

Investigation of single molecule electromechanical actuators and molecular muscles by Marsella's group afforded additional octa- and tetrathiophene topologies **320** and **321** in 2000 and 2002, respectively.¹⁹¹ Synthesis began with 5-alkyl-2-bromothiophene **322**, obtained from the corresponding alkylthiophene via bromination (Scheme 24). Conversion of **322** to a Grignard intermediate with BuLi and MgBr₂ and subsequent Ni-mediated homocoupling provided bithiophene **323** in 84% yield. Bromination of the 3,3'-positions followed by lithiation and iodination provided **324** in slightly lower yield. Cyclization precursor **325** was obtained in 52-74% yield by Pd-catalyzed cross-coupling of TMSA followed by desilylation with weak base. Four-fold Pd-catalyzed cross-coupling of **325b** with previously reported tetraiodotetrathienylene **326** afforded the octa-aryl double helix **320** in 28% yield. Key intermediate **325a** was more recently reacted with diiodobithiophene **324a** to produce the diyne macrocycle **321** in comparable cyclization yield. A large redox-induced conformational change between twisted and planar topologies, associated with an 18% change in distance, was predicted for the 2-electron oxidation of **321** based on DFT calculations. The associated inversion barrier (9.7 kcal mol⁻¹) was calculated to be less than the parent tetra(2,3-thienylene),

which bodes well for the group's target of actuating electromechanical stimuli through regiospecific homopolymers.



Scheme 24. Tetrathiothiophene annulene topologies.

Tetrathiafulvaleno[12]annulenes. Mono- (**327**), bis- (**328**), and tristetrafulvalenylacetylene (**329**) macrocycles were reported by Iyoda et al. in 2004 (Figure 65).¹⁹² The π -amphoteric systems, the result of tetrathiafulvalene (TTF) donor

and [12]cyclyne acceptor moieties, were constructed with stoichiometric Pd- and Cu-catalysts under Krause's conditions in moderate to low yields (17-53%). The solid-state structure of **327a** displayed a slipped-stack dimeric association with a staggered cofacial array in addition to boat conformations for the TTF moieties. CV studies indicated a four-step redox process for the hybrid cycles **327** and **328** with oxidation potentials suitable for service as conducting radical salts. The hybrid cycles also formed sandwich complexes with Ag salts, both assigned as staggered conformations from upfield shifts in ^1H NMR spectroscopy.

Dehydrothieno[14]annulenes. Over the past five years, the Haley group has prepared a large collection of novel thioannulated octadehydro[14]annulenes (**330-341**, Figure 65). Monothiophene systems **330** and **331**, which readily polymerized upon concentration to afford an insoluble material, were found to survive for several weeks in dilute solutions at $-20\text{ }^\circ\text{C}$, a sufficient time to characterize the systems with MS and NMR/UV-Vis spectroscopy.^{80b} Asymmetric cyclyne **330** was found to be more aromatic by ring current criterion than **331** due to an increased double bond character at the site of ring fusion. Cycles **332-341** have recently been prepared by the group and electronic absorption and CV studies are currently underway.¹⁹³

Dehydrothieno[18]annulenes. In an analogous route to **265**, Sarkar and Haley isolated regioisomeric dehydrothieno[18]annulenes **342-344** in 2000 via a thieno-analog of intermediate **267** (Figure 65).¹⁹⁴ Although longer than traditional 3-fold intermolecular trimerization routes for [18]cyclynes, the intramolecular route provide the only route to asymmetric C_{3h} and C_s isomers. Cycles **342** and **343** displayed enhanced electronic

absorption spectra ($\lambda_{\text{max}} = 428 \text{ nm}$) compared to the 3,4-fused trithienocyclyne **344**, a factor attributed to the enhanced double bond character of 2,3-fusion and more efficient overall conjugation. The three macrocycles were transformed to insoluble black material above 150 °C over a narrow temperature range in DSC measurements. Under TGA, a minimal weight loss (<5%) at the corresponding DSC exotherm suggested a solid-state polymerization reaction for cycle **342**.

Conclusions

This chapter illustrates the complex diversity of structures and wide variety uses of annulenic molecules. No longer are these aesthetically pleasing compounds purely the realm of physical organic chemists. Besides traditional application as probes for ring currents, annulenes now have demonstrated potential as DNA cleaving agents, optoelectronic materials, molecular actuators, and sources for novel carbon allotropes. Such new uses, coupled with modern techniques for their synthesis, have truly heralded a renaissance in annulene chemistry, a renaissance that should continue for some considerable time.

Bridge to Chapter II

Chapter II examines the effects of donor/acceptor substitution on the photophysical properties of acyclic tetrakis(arylethynyl)benzene (TAEB) chromophores which utilize di-*n*-butylmino groups as donors and pyridyl groups as acceptors. The consequences of small structural variations on an array of isomers are described, and the results of

selective ionization of either the donor or acceptor segments either through titrimetric protonation or metal complexation. These acyclic arylacetylenes represent an important aspect of dehydrobenzoannulene study, since it enables us to examine the effects of conjugation, donor/acceptor-functionalization, and carbon-carbon bond linearity independent of the enforced planarization caused by formation of a cycle. In Chapter II, an interesting two-stage emission switching phenomenon is discovered, whereby the spatial localization of the molecules' frontier molecular orbitals (FMOs) on donor and acceptor segments leads to independent manipulation of FMO energy levels manifested in the emission spectra. These structure-property relationship studies help elucidate factors important to targeted design of organic materials for customized applications such as fluorescent sensor arrays, optical devices and semiconductors.

CHAPTER II

SYSTEMATIC STRUCTURE-PROPERTY INVESTIGATIONS AND ION SENSING STUDIES OF PYRIDINE-DERIVATIZED DONOR/ ACCEPTOR TETRAKIS(ARYLETHYNYL)BENZENES

Introduction

This chapter was co-authored with Laura D. Shirtcliff, who performed the molecular orbital computations and Professor Michael M. Haley, who conceptualized the project and provided editorial assistance. This chapter includes work that was published in the *Journal of Organic Chemistry* (2007, 72, 86-96, © 2007 American Chemical Society).

Carbon-rich, highly conjugated organic molecules have been the subject of considerable study in recent years,¹ primarily because of their unique optoelectronic properties.^{2,3} These compounds are now recognized as ideal materials for advanced applications including organic light-emitting diodes, thin film organic transistors, solar cells, and optical storage devices.¹⁻³ We recently presented detailed structure-property relationship investigations into donor/acceptor-substituted tetrakis(phenylethynyl)benzenes and related bis(dehydrobenzoannuleno)benzenes (Figure

1).⁴ These carbon-rich chromophores exhibit a high degree of conjugation, and consequently possess multiple pathways for intramolecular electronic and photonic transfer. As a result, these molecules are excellent candidates for many of the optical materials applications mentioned above.^{3,5,6} Their electronic absorption and emission profiles exhibit sensitivity to functional group substitution pattern as well as solvent environment. These compounds also possess significant nonlinear optical susceptibilities arising from the highly polarized conjugation pathways between the electron donating and accepting groups.^{6a,g,h,7}

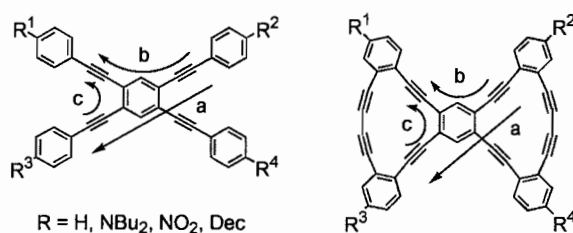


Figure 1. Conjugated pathways present in tetrakis(phenylethynyl)benzenes (TPEBs) and structurally related bis(dehydrobenzoannuleno)benzenes (DBAs).

One intriguing facet of these studies is the effect of the relative strengths of the donor and/or acceptor groups on the optical properties. Studies on similar systems show that the degree of donating and/or accepting ability can significantly influence the electronic spectra.^{6g,h,8} An expanded continuation of our studies therefore involves varying not only the substitution pattern on the central benzene ring, but also the identity of the functional groups on/in the peripheral arene rings. In particular, the effect of differing electron-accepting groups is of interest in determining structure-property

relationships. Arylacetylenes have shown themselves amenable to “tuning” of electronic and optical properties by fundamental variations in the charge transfer pathway as well as chemical environment.^{6a,g,h,8} In this paper we examine the effect of a pyridyl group as the (weaker) electron acceptor in place of the previously-reported nitrophenyl-functionalized systems.

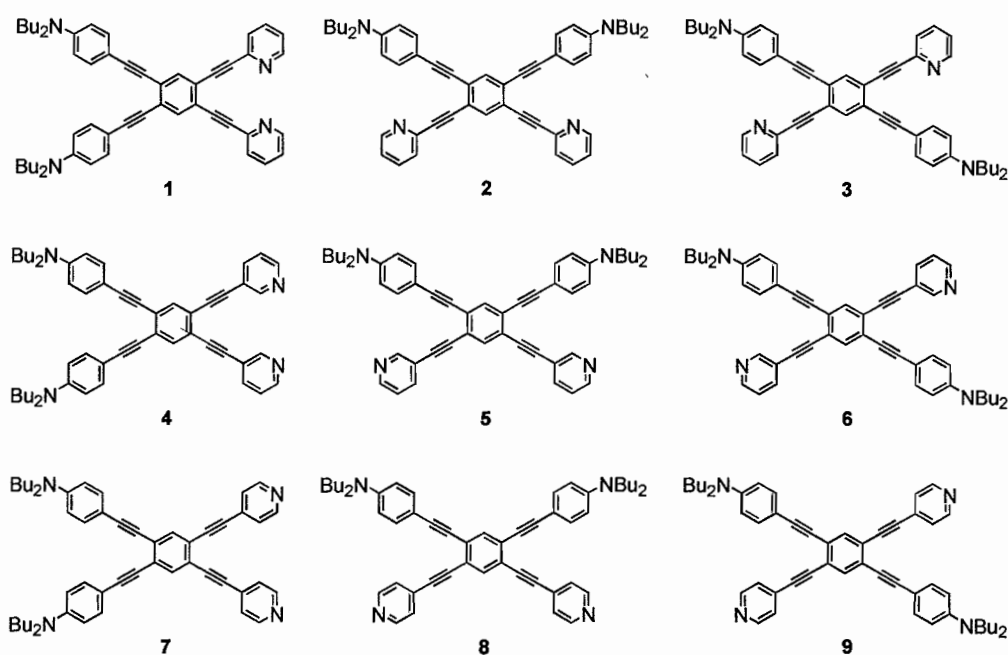


Figure 2. Isomeric donor/acceptor tetrakis(arylethynyl)benzene (TAEB) targets **1-9** with pyridine acceptors.

Donor/acceptor properties in related phenyleneethynylene/vinylene cruciforms, including one that incorporates 4-substituted pyridines, have been studied recently by Bunz et al.,⁹ and have been shown, in addition to possessing unique optical properties, to exhibit exciting potential for selective ion sensing via intramolecular charge transfer

switching.¹⁰ The range of possible compounds expands greatly with variation not only of the ethynylpyridine substitution pattern (three substitution isomers), but also the position of the nitrogen atom within the ring relative to the acetylenic linker (three possible positions). Preparation of all nine permutations of the donor/acceptor-functionalized tetrakis(arylethynyl)benzenes (TAEB) should permit a systematic study of the effects of small structural variations on the charge transfer pathways as well as the overall materials properties of each system, and could potentially lead to customization of optical band gaps for specialized materials applications. Herein we present the syntheses and spectrophotometric studies of a family of pyridine-based donor/acceptor TAEBs (**1-9**, Figure 2) and comparison with the known parent nonfunctionalized (**10**), tetradonor (**11**), and nitrophenyl acceptor analogues (**12-14**, Figure 3).⁴ We also report our initial investigations into proton-induced and metal ion complexation-induced electronic spectra shifts. In all cases we retain the *N,N*-dibutylaniline moiety as the electron donor unit.

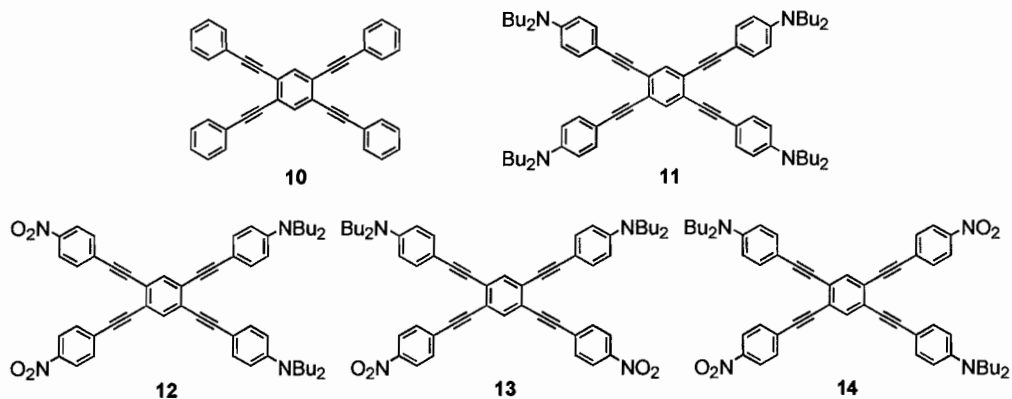
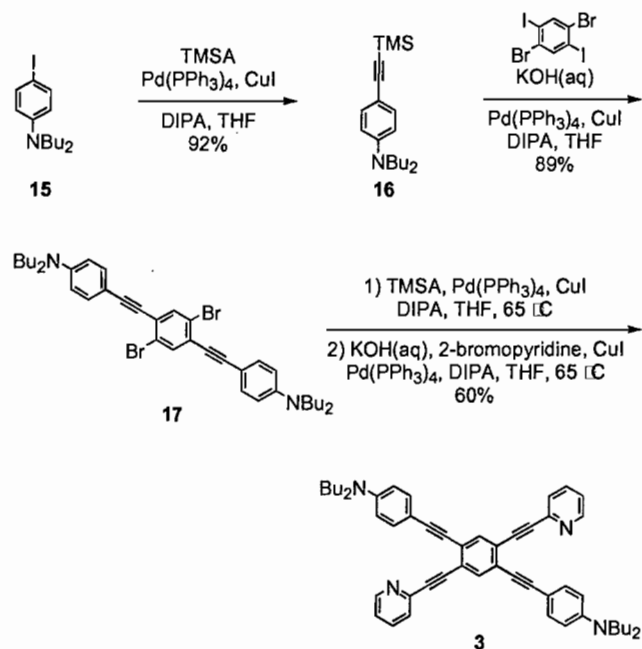


Figure 3. Previously reported TPEBs **10-14**.

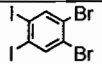
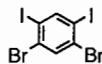
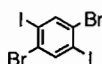
Results and Discussion

Synthesis. The general synthetic strategy for tetrakis(arylethynyl)benzenes **1-9**, as previously reported in our extensive work on annulenes¹¹ and benzenes **10-14**,^{4a,c} relies on successive Pd-catalyzed Sonogashira cross-coupling reactions (Scheme 1).¹² Donor and acceptor segments are attached to a central tetrahalobenzene ring in a stepwise fashion that takes advantage of the electronic preferences of the catalytic cycle, as well as the reactivity difference between aryl bromides and aryl iodides toward cross-coupling.¹² Specifically, Sonogashira reaction of *N,N*-dibutyl-4-iodoaniline **15** with trimethylsilylacetylene (TMSA) affords **16**.^{4a} *In situ* desilylation under basic conditions¹³ and two-fold cross-coupling of the “donor” alkyne to an isomer of dibromo-diiodobenzene furnishes one of three key intermediates (e.g., **17**). Reaction at room temperature allows selective coupling to the more reactive iodides to yield **17**. TMSA is then coupled to the bromine positions on the central ring at elevated temperatures to overcome the electronic unfavorability of an electron-rich arene towards the Sonogashira reaction. The product is an electron-rich alkyne, which is activated towards the final step, two-fold coupling of bromopyridine, an electron-poor arene, to yield **3**. All nine regioisomers are readily obtained in this manner.

Scheme 1. Representative synthesis of pyridine-based donor/acceptor TAEBs

Although the final cross-coupling should be electronically favored, yields of the products (Table 1) have proven variable. This can potentially be explained by complexation of the Pd or Cu catalysts to the pyridine nitrogens. In particular, compounds in which the pyridine rings are *ortho* to each other have the potential for bidentate chelation, which could complicate the workup. Also, $^1\text{H-NMR}$ spectra of insufficiently-purified samples of products invariably contained a prominent triphenylphosphine signature, necessitating multiple chromatographic purifications. In the cases of 4-bromopyridine, the hydrochloride salt was used because of stability issues, and was not totally soluble in the reaction solvents (THF and diisopropylamine [DIPA]), which could also have an adverse effect.

Table 1. Yields for preparation of TAEBS 1-9

haloarene	donor coupling	TMSA/2- bromopyridine coupling (pdt)	TMSA/3- bromopyridine coupling (pdt)	TMSA/4- bromopyridine coupling (pdt)
	70%	17% (1)	47% (4)	20% (7)
	89%	79% (2)	59% (5)	54% (8)
	89%	60% (3)	51% (6)	89% (9)

Molecular Orbital Plots. Molecular orbital plots of simplified structures of **1-9** (calculated with the Gaussian 98¹⁴ suite of programs at the B3LYP/6-31G*¹⁵ level of DFT) are shown in Figure 4, with NBU₂ groups replaced with NMe₂. Similar to those for **12-14**,^{4a} the FMO plots of **1'-9'** indicate that most of the highest occupied molecular orbital (HOMO) density lies on the “donor” end of each chromophore, and much of the lowest unoccupied molecular orbital (LUMO) density lies on the “acceptor” end, irrespective of the particular substitution isomer. As with their analogue **14**, the *para*-substituted **3'**, **6'**, and **9'** show the most complete localization of the isosurface between the donor and acceptor units of the molecule; only a small amount of the LUMO density lies within the donor segments. As is shown by the MO plots, the overlap of the HOMO and LUMO on each compound is relatively small, occurring primarily at the central benzene ring. There is little to no overlap at the peripheries, indicating significant separation of the S₀ and first S₁ states. These results give good evidence of the intramolecular charge transfer nature of the HOMO-LUMO transitions, and thus the

optical data should provide useful information about their potential as nonlinear optical materials. It is worth noting that more of the LUMO density lies on the central arene ring of **1'-9'** than in **12-14**, which may support the hypothesis that the charge transfer efficiency can in fact be “tuned” by adjusting the strength of the acceptor group. It is also somewhat surprising that **4'-6'** show nearly as much FMO separation as **1'-3'** and **7'-9'**, even though the acceptor nitrogens are not situated to accept electron density via resonance. The efficiency of these partially inductive systems expands the library of possible acceptors even further. One or more trifluoromethyl groups appended to the acceptor arene segments, for example, may display similar behavior, as well as prove more chemically stable.¹⁶

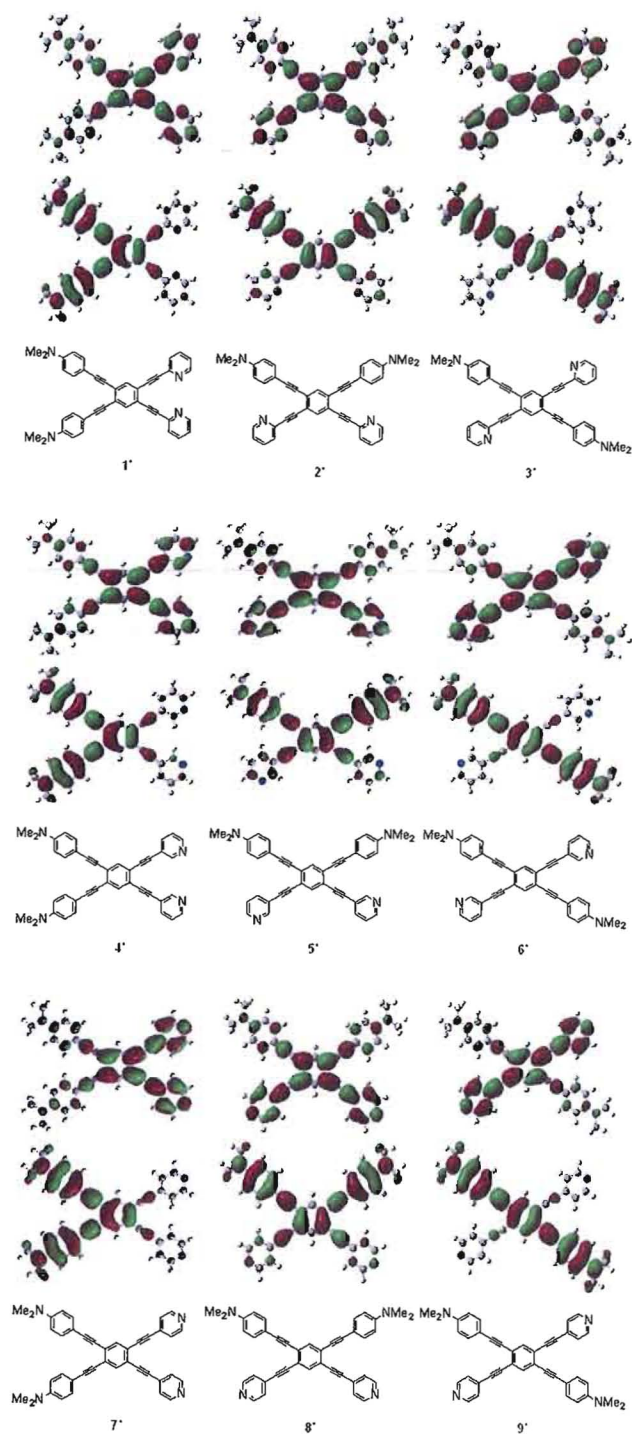


Figure 4. Molecular orbital plots (B3LYP/6-31G*) of simplified structures 1'-9'. The lower plots represent the HOMOs, and the upper plots represent the LUMOs.

Electronic Absorption and Emission Spectra. The absorption spectra of the TAEBs (Figure 5a-c and Table 2) provide some insight into the electronic structure of the systems. All display a characteristic pattern of two broad absorption bands between 350 and 500 nm. Lowest-energy bands are described in Table 2, and the next higher bands are given in the experimental section.¹⁷ Comparison with the parent non-functionalized compound reveals significant broadening and large (~75 nm) red shifts, and more moderate red shifts (~15 nm) relative to the tetradonor compound. Such bathochromic shifts upon donor/acceptor functionalization are indicative of intramolecular charge transfer.¹⁸ On the other hand, comparison with the nitro acceptor analogues **12-14** (Figure 5d) show sharper cutoffs (below 550 nm) for **1-8**, possibly due to the weaker pyridyl acceptor groups. This could indicate more π - π^* character in the excited state. Another striking difference is the similarity of the lowest energy absorption band shapes among different substitution isomers. For **12-14**, what we choose to call the *para* isomer (here **14**, in which like groups are *para* to each other with respect to the central benzene ring) exhibits a very low-intensity charge transfer band. This is explained by the lack of linear charge transfer pathways from the donors to the acceptors. The *ortho* and *meta* isomers, however, both have linear charge transfer pathways, and show strong charge transfer bands. In the weaker acceptor systems presented here, substitution pattern seems to have little effect on the strength of the charge transfer bands. This can be explained by the greater LUMO density on the central benzene ring for all compounds, leading to a less drastic separation of partial charges among isomers. Extinction coefficients average in the 30,000-50,000 M⁻¹ cm⁻¹ range, in good agreement with the nitro analogues. For all

compounds, the trend for longest wavelength λ_{\max} appears to be *ortho* < *meta* < *para*, with *para* isomers displaying the most red-shifted charge transfer bands. The only deviation from this trend is seen in **1**, where the charge transfer band overlaps the next highest wavelength band, and is thus only a shoulder, making exact determination of the λ_{\max} difficult. We have also calculated dipoles for **1-9** at B3LYP/6-31G*, which consistently show an inverse relationship with longest wavelength λ_{\max} : all *para* isomers are calculated as 0.00 D, and all *ortho* isomers are in the 8-13 D range. These trends agree with our previous data for **12-14**. A small solvatochromic effect was observed for all nine compounds: absorption spectra displayed charge transfer bands that experienced an average ~5 nm blue shift in toluene, compared to CH₂Cl₂. This in itself is not very interesting, but comparison between the absorption and emission spectra reveal some dramatic differences.

The electronic emission spectra of **1-9** in both CH₂Cl₂ and toluene are shown in Figure 6 and summarized in Table 2. The most striking feature of these spectra is the strong solvatochromism exhibited. While for a given solvent, the emission λ_{\max} does not vary much between compounds, changing the solvent leads to a shift of about 40-65 nm.

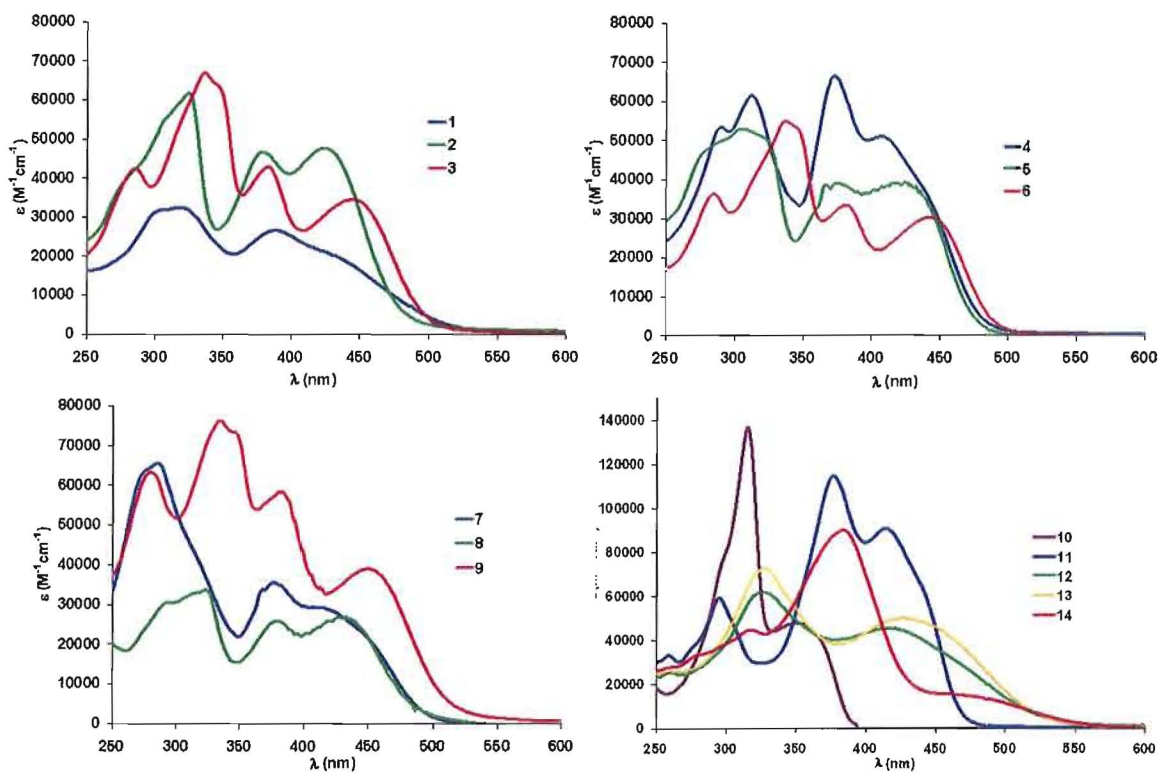


Figure 5. Electronic absorption spectra of (a) 1-3, (b) 4-6, (c) 7-9, and (d) 10-14. All spectra recorded in CH_2Cl_2 at analyte concentrations of 15-25 μM .

Table 2. Electronic absorption and emission data and calculated (B3LYP/6-31G*) net dipoles for TAEBs 1-9

compd	Solvent	Lowest Energy Abs λ_{\max} [nm] (ϵ [$M^{-1} \text{cm}^{-1}$])	Em λ_{\max} [nm]	Stokes Shift [nm]	Φ_F^b	Net Dipole [D]
1	CH ₂ Cl ₂	435 ^a (21,000)	547	112	0.31	7.90
	PhMe	402 ^a (17,660)	482	80	0.63	
2	CH ₂ Cl ₂	424 (47,540)	550	126	0.42	7.75
	PhMe	418 (35,680)	499	81	0.57	
3	CH ₂ Cl ₂	446 (34,490)	550	104	0.49	0.00
	PhMe	437 (37,760)	508	71	0.47	
4	CH ₂ Cl ₂	406 (50,920)	537	131	0.41	11.40
	PhMe	404 (52,030)	482	78	0.45	
5	CH ₂ Cl ₂	424 (39,010)	547	123	0.47	6.50
	PhMe	416 (40,610)	488	72	0.49	
6	CH ₂ Cl ₂	441(30,210)	538	97	0.49	0.00
	PhMe	436 (29,780)	494	58	0.41	
7	CH ₂ Cl ₂	407 (29,370)	558	151	0.20	13.10
	PhMe	407 (45,660)	499	92	0.20	
8	CH ₂ Cl ₂	432 (26,820)	553	121	0.29	9.25
	PhMe	427 (29,640)	503	76	0.30	
9	CH ₂ Cl ₂	449 (39,050)	558	109	0.27	0.00
	PhMe	440 (36,780)	512	72	0.38	

^a approximate value as band is only a shoulder.

^b calculated relative to fluorescein at pH = 8.

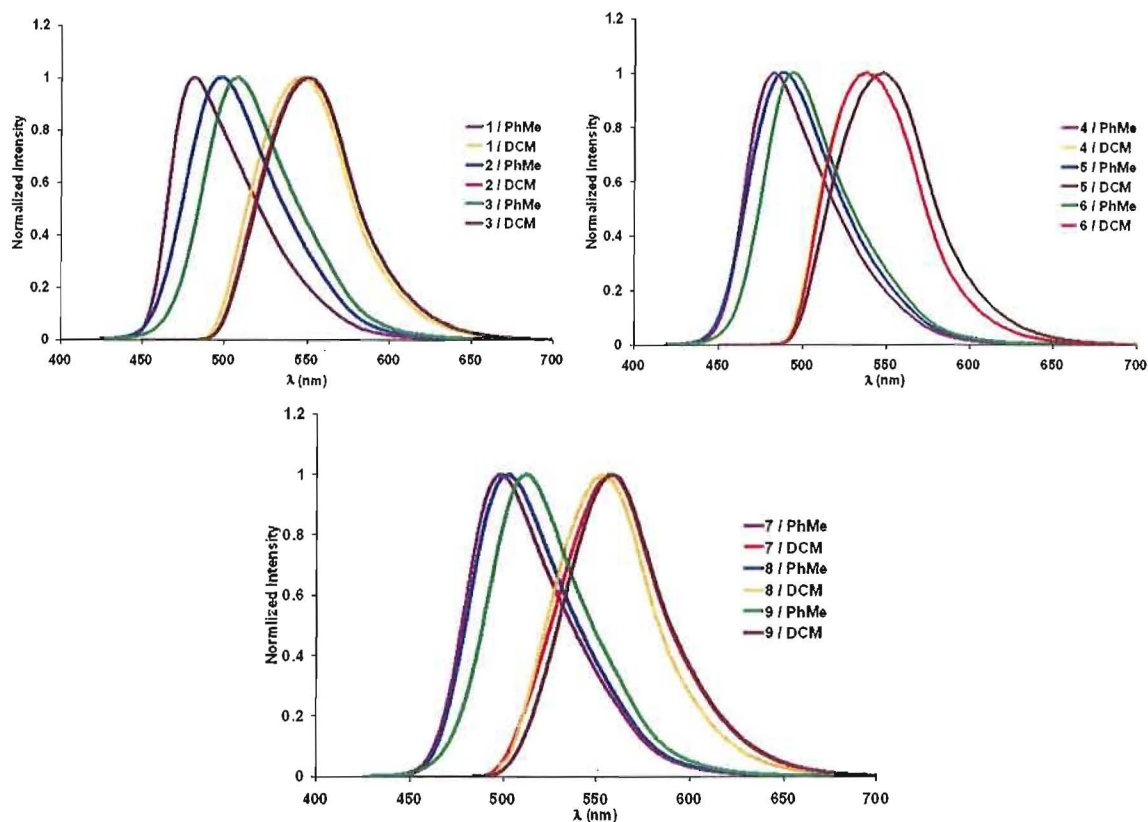


Figure 6. Emission spectra of (a) 1-3, (b) 4-6, and (c) 7-9 in CH_2Cl_2 (DCM) and toluene (PhMe). All spectra were recorded at analyte concentrations of 15-25 μM with excitation at the wavelengths of the lowest energy absorbance band of each (see Table 2).

This effect, which is not observed to such an extent in either **12-14** or analogous planarized donor/acceptor annulenes,^{4a} can be attributed in part to solvent stabilization of the charge transfer excited state. A polarized excited state is more stabilized by a polar solvent than a nonpolar solvent, while the nonpolar ground state is relatively unaffected, leading to a significant narrowing of the transition band gap, and hence a bathochromic

shift in the absorption and emission spectra.¹⁹ In this case, the emission spectra show the most dramatic shifts. Further red-shifting is observed in MeOH (Figure 10 and Table 3). A possible explanation may be that the ground states of **1-9** are predicted to be much less polar than **12-14** or the annulenes. A less polar ground state should lead to a greater decrease in the $S_0 \rightarrow S_1$ transition energy (red shift) upon switching to a more polar solvent. It is interesting to note that **1-9** visibly fluoresce in CH_2Cl_2 , whereas **12-14** do not. The visible fluorescence is clearly related to the acceptor strength. Stronger donors and/or acceptor groups lead to very charge transfer-like HOMO-LUMO transitions,^{8d,e,20} wherein fluorescence can be quenched in polar solvents. A weaker acceptor would exhibit a transition that is more $\pi-\pi^*$ -like in character, and resemble the parent **10** and tetradonor **11**, which *do* strongly fluoresce in polar solvents. This effect is not due to formation of dimers or higher aggregates in solution: experiments reveal no observable concentration dependence of ^1H NMR chemical shifts or emission wavelength over a 100-fold concentration gradient (e.g., 0.13-13 mM). This parallels our previously published data concerning nitrophenyl analogues **12-14**: significant aggregation requires enforced planarization to the corresponding (dehydrobenzoannuleno)benzene variants.^{4a} Overall, these results support the hypothesis that varying the acceptor strength allows us the ability to fine-tune the optical band gap.

Another structure-property question of interest was whether substitution isomer or nitrogen placement within the pyridine ring had the dominant effect on the optical properties of **1-9**. Figure 7 shows the emission spectra of all nine isomers in CH_2Cl_2 , expanded in the 520-580 nm region in order to examine each isomer's λ_{max} . It is clear that

nitrogen placement within the pyridine ring (and hence the efficiency of the charge transfer pathway at the termini) has a greater influence on fluorescence wavelength red-shifting: when the acetylene linker chromophore is in the 3-position relative to the nitrogen, the emission has the shortest wavelength, and when the acetylene linker is at the 4-position, it has the longest. This trend holds true within each triad of compounds, and makes intuitive sense: the 2- and 4-ethynylpyridyl isomers both possess proper resonance forms for electron transfer using arrow-pushing formalism, and the 4-ethynylpyridyl isomers in particular possess linear charge transfer conduits. The 3-ethynylpyridyl isomers satisfy neither condition, and thus are closer in emission wavelength to the π - π^* transitions of the parent **10** and tetradonor **11**.

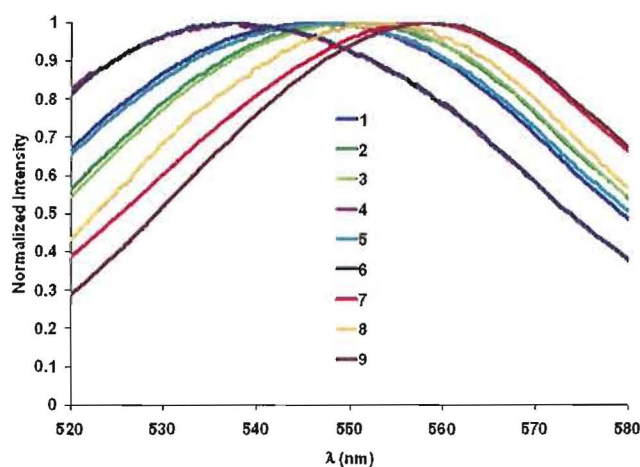


Figure 7. Emission spectra maxima of **1-9** in CH_2Cl_2 .

The fluorescence quantum yields for **1-9** in CH_2Cl_2 were calculated from the steady-state spectroscopic measurements using the techniques described by Drushel et

al.²¹ The values are given in Table 2, and are also illustrated graphically in Figure 8, arranged in order of increasing acceptor strength. A noteworthy trend is the increasing quantum efficiency going from *ortho* to *meta* to *para* substitution isomer. This follows the trend in the longest wavelength λ_{\max} in the absorption spectra, and Φ_f decreases as calculated ground state net dipole increases. Similarly, nitrogen placement within the ring has a significant effect: For a given substitution isomer, placing the nitrogen in the 3-position relative to the acetylene linker produced the largest Φ_f , and placement in the 4-position produced the smallest. The quantum yields of the all- π - π^* tetradonor system **11** and nitro acceptor analogues **12-14** were previously found to be 0.71 and >0.01 in CH_2Cl_2 , respectively.^{4a} This data leads to the conclusion that the more π - π^* -like the system, the higher the fluorescence quantum yield. This is a well-established phenomenon, wherein decreased band gaps increase the accessibility of nonradiative de-excitation pathways via vibronic coupling.²² This can also help explain the fact that **9** does not follow the general trend seen in Figure 8: it is significantly red-shifted with respect to **7** and **8**, and hence the decreased band gap is enough to lower the quantum yield more than the other isomers. Quantum yields in toluene were also determined, but there are no readily discernible trends. They are generally higher in toluene than CH_2Cl_2 , though in some cases they are equal or lower. These results further indicate that solvent stabilization of the charge transfer excited state has a dramatic effect on the optical properties.

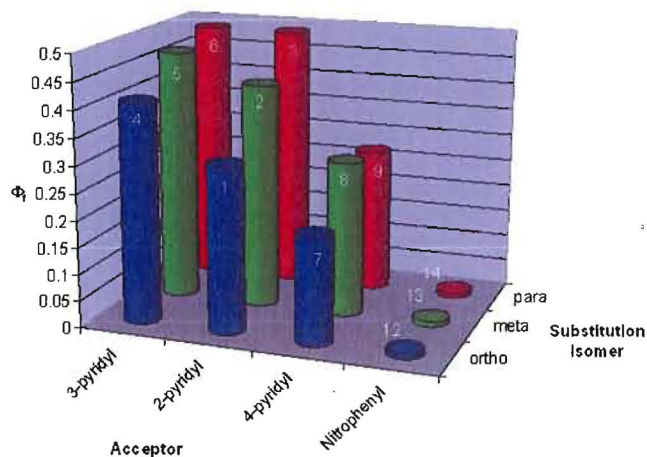


Figure 8. Graphical illustration of quantum yield trends for 1-9 and 12-14 in CH_2Cl_2 .

TFA Titrations. Recent work by Bunz and coworkers^{9,23} showed that donor/acceptor-functionalized aromatic cruciform structures (e.g., **18**, Figure 9) can serve as ion sensors via “switching” of intramolecular charge transfer band gaps. Disrupting either the electron donor or acceptor has marked effects on the HOMO and LUMO energies, and protonation or complexation to metal ions represents a facile method of investigating the consequent structure-property implications. In the Bunz studies, protonation of the donor group of **18** with trifluoroacetic acid (TFA) in MeOH to pH = 2.7 led to a 161 nm hypsochromic shift (due to stabilization of the HOMO, thus widening the band gap), followed by a 105 nm bathochromic shift with further acidification to pH = 0.34, i.e., protonation of an acceptor group (stabilizing the LUMO, which narrowed the band gap). This preferential protonation of the donor group first and then the acceptor group achieved a “switching” effect where shifting initially occurred in one direction, and then shifted back in the other direction with further addition of acid. Similarly, results by Fang and coworkers^{10a} indicate two-stage Hg ion sensing by **19**, which undergoes a 48

nm bathochromic shift in the absorption spectrum with exposure of up to ten equivalents of Hg^{2+} , followed thereafter by a 120 nm hypsochromic shift.

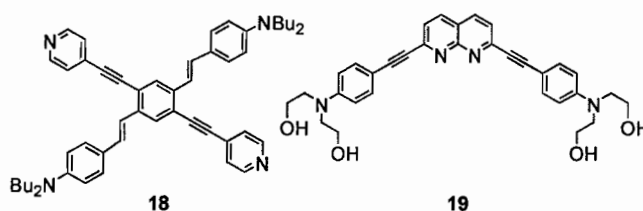


Figure 9. Donor/acceptor systems **18** prepared by Bunz et al.⁹ and **19** by Fang et al.^{10a}

The structural similarity between **1-9** and **18** suggested that our systems might respond in an analogous manner. Each compound was titrated with TFA in MeOH, and the emission spectra recorded (e.g., Figure 10 for **2**. See Figure 18 for spectra of **1-9**). In every case, a large (avg. 172 nm) hypsochromic shift was displayed (Table 3), from the visible red region to borderline UV (Figure 11 inset). A significant increase in fluorescent intensity at each new λ_{max} was also exhibited. In general, the most hypsochromic state was achieved in each case at or around a TFA concentration of 10^{-2} M. TAEBs **4-6** required a slightly more acidic environment, reaching their shortest wavelength maxima near $10^{-1.3}$ M TFA. This shifting was accompanied in the absorption spectra by a gradual loss of the intramolecular charge transfer band (e.g., Figure 11). Further addition of TFA caused a bathochromic shift into the visible blue-green region. In examining the three-by-three array, several striking trends are obvious. TAEBs **4-6** experience the least secondary shifting (ca. 31 nm), and **7-9** experience the most (avg. 85 nm). This makes

intuitive sense, as **4-6** experience the least communication through the conjugated pathways, leading to a less sensitive charge transfer switching mechanism manifested in the fluorescence emission. The opposite is true for **7-9**. Another increase in relative fluorescent intensity is seen during the second shift for **7-9**, as well as for **1, 4** and **6**. This is in stark contrast to **18**, in which the quantum yield is ultimately cut in half upon full protonation.^{9b} An interesting trend is noticeable for **1-3**, where the final relative fluorescent intensity decreases going from the *ortho* to the *meta* to the *para* isomer. This trend has yet to be explained satisfactorily, but within each triad the *ortho* isomer seems to be the most “sensitive” to protonation, and so may be related to the net dipole. Overall, these results support Bunz’ findings that the donor nitrogens are protonated first, followed by the acceptor nitrogens. This is a surprising result, based on the expected relative pK_as of related compounds. Although diethylaniline has a pK_a of 6.7 and pyridine a pK_a of 5.3, our systems should more resemble expanded analogues of 4-(*N,N*-dimethylamino)pyridine (DMAP), in which the pyridine nitrogen is protonated first with a pK_a of 9.2. The properties displayed both here and with **18**, therefore, represent rare if not unique behavior.

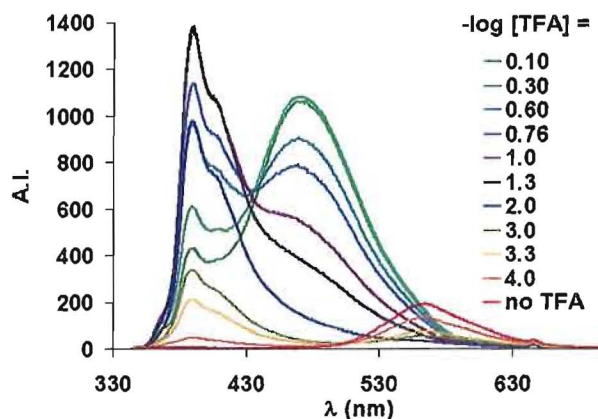


Figure 10. Example emission spectra of TFA titration of **2** in MeOH. The small peaks appearing in the spectra past 600 nm arise from interference by doubling of the excitation wavelength. Peaks from the excitation wavelength have been subtracted from each spectrum when necessary for clarity. All spectra were recorded at approx. 4 μ M concentration. Excitation at most intense absorption peak (300-350 nm, present under all conditions).

Table 3. Summary of TFA-induced Fluorescence Emission Shifting of TAEBs **1-9**

compd	Initial λ_{em} (nm)	Blue-shifted λ_{em} (nm)	Red-shifted λ_{em} (nm)
1	566	388	468
2	564	390	472
3	561	393	464
4	561	390	422
5	557	388	418
6	560	388	419
7	569	391	488
8	567	391	476
9	572	413	485

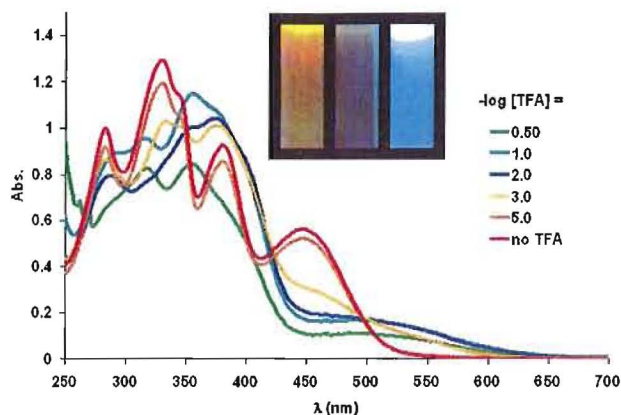


Figure 11. Absorption spectrum of TFA titration of **9** in MeOH at approx. $15 \mu\text{M}$ concentration. Inset: solutions of **9** in MeOH with no TFA (left), and at 10^{-2} M (middle) and $10^{-0.3}$ M TFA (right); illumination by high-intensity 365 nm lamp.

Metal Ion Complexations. Bunz et al. also observed “switching” behavior upon complexation of Zn ion.^{9a,b} These authors used the similar response to protons and metal ions to discount the possibility of ion binding to the electron-rich aromatic π -face, in favor of binding directly to the nitrogens. Several efforts were made to reproduce this behavior in **1-9** using $\text{Zn}(\text{OTf})_2$ in CH_2Cl_2 ; however, the dramatic effect of protonation on our systems remained elusive when $\text{Zn}(\text{OTf})_2$ was used. No significant shifting activity was observed for any of the compounds under these conditions. It is possible that the Zn^{2+} ion may simply be too “soft” for efficient binding to the acetylene-based chromophores. Indeed, alkynes are often believed to confer less conjugation than olefins,²⁴ and it may be this fundamental structural difference between our compounds and **18** that causes the striking disparity in behavior. Using fluorescence quantum yield as

a qualitative indicator of charge transfer efficiency and conjugation supports this hypothesis: **1-9** exhibit quantum yields of ca. 0.20-0.50 in CH₂Cl₂, whereas **18** has a quantum yield of 0.11 in the same solvent.

Efficient metal binding could potentially be promoted through the use of coordinating solvents such as THF. To help determine the effect of Zn²⁺ on **1-9** (e.g., Figure 12 for **1**. See Figure 19 for spectra of **1-9**), we exposed dilute (~0.4 mM) CH₂Cl₂ solutions of each compound to between 0.1 and 100 equivalents of ZnCl₂ in CH₂Cl₂ diluted from a commercially available solution in THF and observed the change in the electronic emission spectra.²⁵ In each case, complexation produced an immediate bathochromic shift, as well as a quenching of fluorescent intensity. Red-shifting continued until approximately 1 equivalent by up to 60 nm, but quenching continued until approximately 5-10 equivalents of ZnCl₂. During this period, the solutions of **4-6** fade from between green and yellow to cloudy and colorless. Although no particulates are visible, this may imply that non-fluorescent micro-aggregates of a high Zn:ligand complex are desolublized. Upon addition of up to at least 100 equivalents, fluorescent intensity returns at the new red-shifted wavelength, typically as a bright orange-red to deep red solution (note the contrast to the modest effect of ZnCl₂ in 100% CH₂Cl₂, Figures 16 and 17). It is believed that as more Zn-containing solvent is added, the complex becomes re-solublized. This behavior is puzzling and may reflect complex equilibria involving metal chelation mechanism(s). TAEBS **1-3** and **7-9** do not display this behavior, and experience only red-shifting and quenching, with no increase in fluorescence at the new wavelength with addition of up to 100 equivalents of Zn²⁺. The

more efficient charge transfer pathways in these compounds may cause more efficient binding to the Zn ions, precluding the more dynamic equilibria seen with **4-6**. Deep red solutions are formed in the cases of **7-9**, possibly due to enhanced complexation through the more effectively conjugated 4-pyridyl ligands. It is also possible that these systems, potentially less-conjugated than **18**, experience ion binding through the aromatic π -faces, rather than the nitrogens directly. This sensitivity to specially-solublized Zn ion may have potential for further development as fluorescent probes, especially given their additional pH-sensing properties. It should be stressed, however, that these results are necessarily qualitative in nature, and their greatest value is perhaps in illustrating the contrast in fundamental behavior upon minor structural alteration between our and Bunz' cruciform architectures.

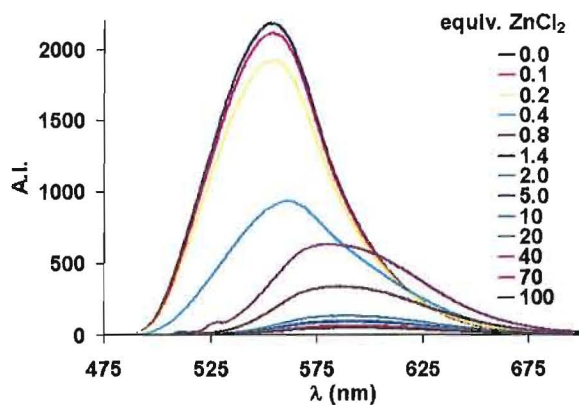


Figure 12. Example emission spectra of ZnCl_2 complexation to **1**. All spectra were recorded in CH_2Cl_2 at approx. 0.4 mM concentration. Small peaks appearing before 530 nm result from interference from the excitation wavelength. Excitation at wavelength of lowest energy absorption peak (450-525 nm, present under all conditions).

It has been shown that tetrakis(2-pyridylethynyl)benzene (**20**, Figure 13) acts as efficient bidentate ligands for Ag ions.²⁶ Crystal data revealed that AgOTf complexation to **20** enforces a conformation in which the nitrogens all point inward towards the Ag ions, with additional weak interactions between the triflate oxygen and the aromatic hydrogens at the 3-positions. With this in mind, we investigated the potential Ag(I) binding ability of **1**. It possesses the same structure as **20** at the acceptor end, with the donor electrons providing fluorescence. TAEB **1** was exposed to dilute AgOTf solutions in CH₂Cl₂, and the emission spectra recorded (Figure 14). An immediate bathochromic shift from 550 to 611 nm was observed, along with a precipitous drop off of fluorescent intensity. At one equivalent of Ag ion, the analyte solution achieved a dark red color (Figure 14 inset). Additional AgOTf had much less effect as up to 50 equivalents was required to cause the second, hypsochromic shift to a pale indigo color. As the (already low) peak at 611 nm disappears, the peak at 406 nm simultaneously grows more intense. In light of Bunz's findings, these results lead to the extrapolative hypothesis that in this case, initial binding of Ag ion is to the pyridine nitrogens in a bidentate fashion, followed by the much less efficient subsequent binding to the donor nitrogens. This would have the effect of first stabilizing the LUMO, causing the red shift, and then stabilizing the HOMO, causing the blue shift. If the switching hypotheses are correct, it would seem that **1** represents a reverse-type sensor relative to **18**. Unfortunately, attempts at growing crystals of **1-9** either alone or in the presence of metal ions have been unsuccessful to date.

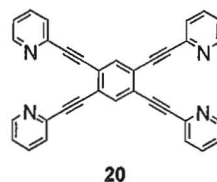


Figure 13. Tetrapyrridyl ligand **20** prepared by Bosch et al.²⁶

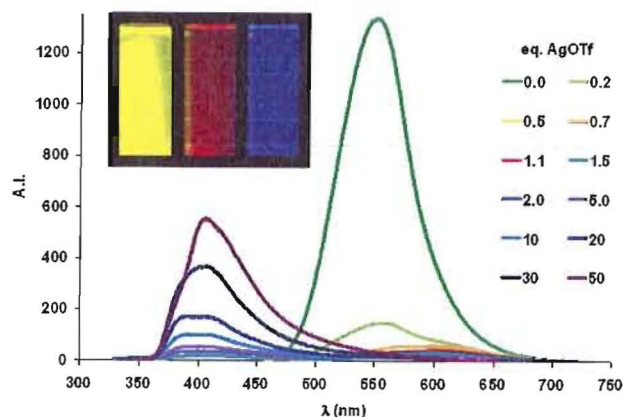


Figure 14. Emission spectra of addition of AgOTf to **1** in CH₂Cl₂ at approx. 12 μM concentration. Excitation at wavelength of most intense absorption band (300-350 nm, present in all compounds). Inset: solutions of **1** in CH₂Cl₂ with 0 (left), 1 (middle) and 50 (right) equivalents of AgOTf; illumination by high-intensity 365 nm lamp.

Due to the stark contrast between the effects of protonation and Zn ions on **1-9**, we next investigated the effect of a Lewis acid on the fluorescence. Each compound was exposed to solutions of AlCl₃ in MeOH, and the emission spectra recorded (e.g., Figure 15 for **9**. See Figure 20 for spectra of **1-9**). Solvation to form Al(OMe)₃ and protons produces a dynamic system involving both metal and acid that could be of interest.

TAEBS **1**, **8**, and **9** showed response to Al(III) addition as a hypsochromic shift from 570 nm to ca. 395 nm with up to ten equivalents, followed thereafter by the generation of a third band at 475-490 nm. TAEB **7** showed the same behavior, but with initial appearance of the third band at as little as five equivalents. At 100 equivalents, **7** displayed the most relatively intense middle band. **1** exhibited much weaker behavior, with the middle band appearing only as a shoulder. TAEBS **2-6** did not show any such behavior, experiencing only a blue shift. This is presumably due once again to the inhibited conjugation caused by the position of the acceptor nitrogens. It is worth noting that the *ortho* isomers of both the 2- and 4-ethynylpyridyl triads showed the greatest amount of shifting. This may be due to the fact that they have the highest calculated dipoles, and thus present more attractive targets for the ion. Bidentate chelation is not believed to be involved, since the pyridyl nitrogens in **7** are oriented away from each other, whereas in **1** they are oriented closer together. Bidentate binding should thus cause increased sensitivity in **1** relative to **7**, rather than the other way around. As in the case of the Zn complexation studies above, these results should only be considered qualitative in nature due to the ambiguity of the ions involved. They do, however, imply a certain generality in the fundamental basis of the switching mechanism.

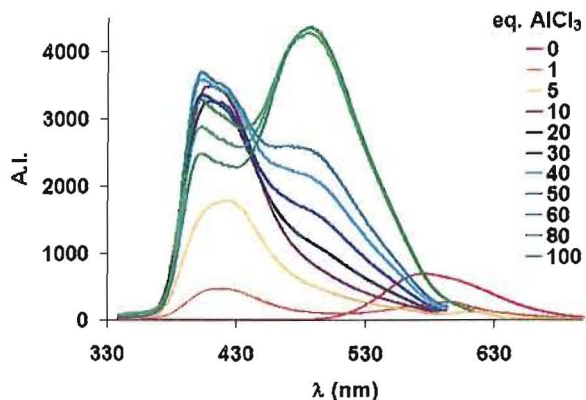


Figure 15. Example emission spectra of addition of AlCl_3 in MeOH to **9** at approx. 10-25 μM concentration. Peaks from 1x and 2x the excitation wavelength have been subtracted from each spectrum for clarity. Excitation at wavelength of most intense absorption band (300-320 nm, present under all conditions).

The effect of various metal salts was investigated by taking **1**, **5**, and **9** as a representative cross-section of the compounds and exposing them to excess ions of different types (Figure 16). The three possible results are blue shifting of fluorescence, red shifting, or quenching. For **9**, quenching was the most common effect, with a blue shift upon exposure to AlCl_3 . TAEB **5** on the other hand retained its fluorescence most often. Excess ZnCl_2 (without coordinating THF in this case) quenched **9**, but only red-shifted **1** and **5**. Ag ions caused the most notable differences in response: while **1** and **5** were blue-shifted in AgBF_4 solution, TAEB **9** experienced quenching. While **1** and **9** experienced a blue shift in AgOTf , **5** was actually red-shifted as well as partially quenched. The differences produced by varying the counterion are thus illustrated. The differential responses imply the potential of **1-9** to form components of a “sensing array”

for a host of applications.^{9,10a,27} Figure 17 provides a spectroscopic illustration of the effects of ZnCl_2 and AlCl_3 on **1**, **5**, and **9**.

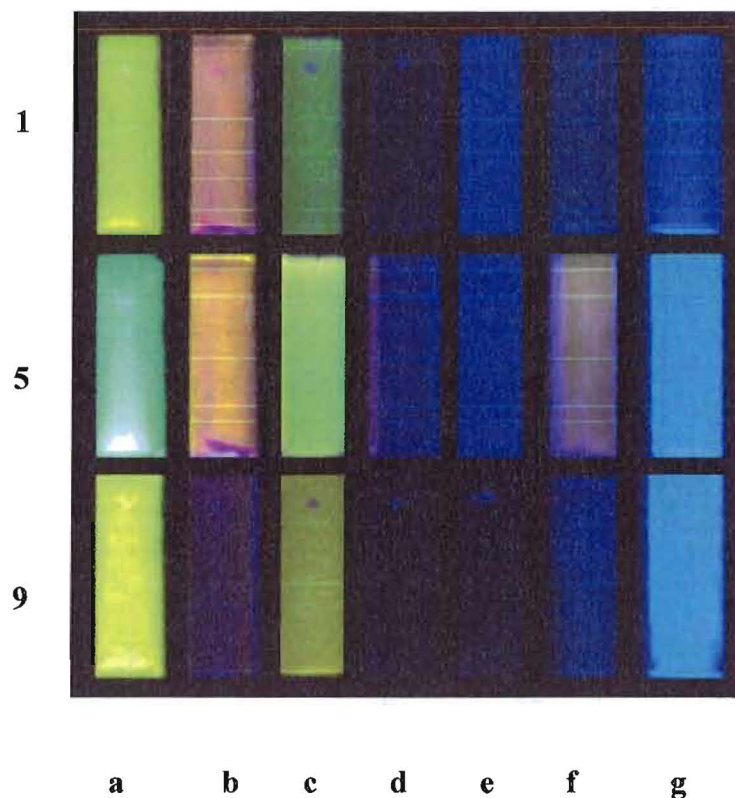


Figure 16. Effect of various metals on **1**, **5**, and **9** in CH_2Cl_2 : **a**, no ion; **b**, ZnCl_2 ; **c**, $\text{RuCl}_2(\text{bpy})_2$; **d**, $\text{PdCl}_2(\text{PhCN})_2$; **e**, AgBF_4 ; **f**, AgOTf ; **g**, AlCl_3 . Illumination by high-intensity 365 nm lamp.

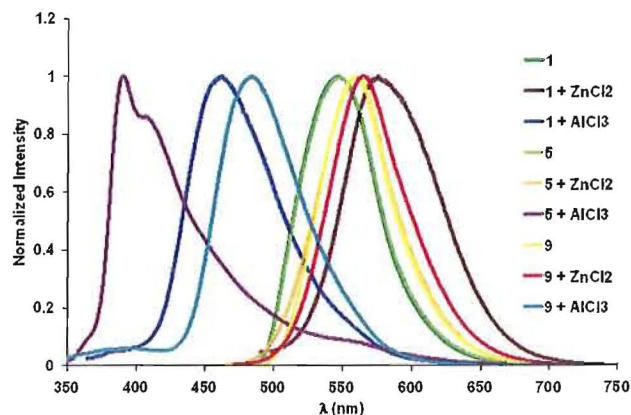


Figure 17. Normalized emission spectra of the effects of ZnCl_2 and AlCl_3 on **1**, **5**, and **9** in CH_2Cl_2 (columns **b** and **g** in Figure 16).

Conclusions

Donor/acceptor systems **1-9** display a number of unique and interesting optical properties due to the weak pyridyl acceptor group, including visibly fluorescent charge transfer, strong solvatochromism, and high quantum yields. These properties are not observed in the nitrophenyl acceptor-functionalized analogues we have previously reported.^{4a} The spectroscopic properties are susceptible to fine tuning via small structural variations of the chromophore topography, providing access to a wide array of optical band gaps for customized optical materials applications. Emissive data support theories regarding band gaps and acceptor strengths; namely, that acceptor strength is inversely proportional to quantum yield, and that high quantum yields are available even with spatially separated frontier molecular orbitals.^{4a,9} Data for **4-6** in particular imply encouraging potential for inductively-withdrawing electron acceptors, which we are currently investigating.²⁸ The TAEBs exhibit intramolecular charge transfer switching via

stepwise protonation in solution, providing support for the existing theory that the donor segment is more basic than the acceptor pyridines. This implies that spatially separate FMOs can be manipulated independently. Metal ion binding gives more complex data, and it is found that **1-9** bind stoichiometric amounts of Zn ion in solution only very weakly or not at all, in contrast to behavior reported for **18**.⁹ One possible contributor to this difference is the (possibly) less conjugation conferred by triple bonds versus double bonds.²⁴ AlCl₃ complexation provides data that is similar, but not identical to protonation, implying weak binding by the most conjugated compounds. Large excesses of the Al species produced intensely fluorescent solutions even in MeOH, in which quantum yields are expected to be low. This has potential consequences particularly in the area of OLEDs, which frequently contain Al ions.^{3b,c} Ag ion has a more impressive effect on **1**, first with likely bidentate chelation to adjacent pyridine nitrogens²⁶ followed by binding to the donor segments. This causes dramatic shifting in the emission spectra in a fashion that is the opposite of the effect of protonation. TAEBs **1-9** also respond differently to several different metal ions, providing potential as sensing arrays for a host of ions.^{9a,b,10a} Although the sensing effect is in some cases subtle, the high quantum yields of these weaker donor/acceptor systems may override sensitivity in overall attractiveness as materials components. We are currently using the insight attained herein to explore further functionalization options for maximization of the desirable optoelectronic properties, the results of which will be reported in the near future.

Experimental

General Methods. ^1H and ^{13}C NMR spectra were recorded in CDCl_3 unless otherwise noted using a 300 MHz (^1H : 299.94 MHz, ^{13}C : 75.43 MHz) spectrometer. Chemical shifts (δ) are expressed in ppm relative to the residual CHCl_3 (^1H : 7.26 ppm, ^{13}C : 77.0 ppm) reference. Coupling constants are expressed in hertz. Melting points were obtained in open-end capillary tubes and are uncorrected. THF was purified by distillation over potassium metal. All other chemicals were of reagent quality and used as obtained from manufacturers. Column chromatography was performed using N_2 or air pressure on silica gel (230-450 mesh). Pre-coated silica gel plates (200 \times 200 \times 0.50 mm) were used for analytical thin layer chromatography. Eluting solvents were reagent quality and used as obtained from the manufacturers. Reactions were carried out in an inert atmosphere (dry Ar) when necessary. All deprotected terminal alkynes were used directly without further purification.

General Alkyne Coupling Procedure A. Haloarene (1 equiv) and **16** (1.5 equiv per transformation unless otherwise noted) were dissolved in $i\text{Pr}_2\text{NH}:\text{THF}$ (1:1, 0.03 M) in a flask with KOH (aq, 50 wt.%, 20 equiv). The solution was purged for 30 min with bubbling Ar followed by addition of $\text{Pd}(\text{PPh}_3)_4$ (0.03 equiv per transformation) and CuI (0.06 equiv per transformation). The reaction mixture was purged another 20 min and then stirred at rt for 12-48 h under an Ar atmosphere. Upon completion, the mixture was concentrated, rediluted with CH_2Cl_2 , and filtered through a pad of silica gel. The solvent was removed in vacuo and the crude material was purified by column chromatography.

General Alkyne Coupling Procedure B. Donor-functionalized dibromoarene (1 equiv) was dissolved in *i*Pr₂NH:THF (1:1, 0.05 M) and the solution purged for 30 min with bubbling Ar. Pd(PPh₃)₄ (0.03 equiv per transformation) and CuI (0.06 equiv per transformation) were then added and the solution was purged another 20 min. Trimethylsilylacetylene (TMSA, 1.5 equiv per transformation unless otherwise noted) was injected and the solution was stirred at 65 °C for 12-48 h under an Ar atmosphere. Upon completion, the mixture was concentrated, rediluted with CH₂Cl₂, and filtered through a pad of silica gel. The solvent was removed in vacuo and the crude material was carried on to the next step without further purification.

General Alkyne Coupling Procedure C. The tetrayne product from procedure B was dissolved in THF (0.04 M) and purged for 30 min with bubbling Ar. Acceptor haloarene (3 equiv per transformation unless otherwise noted) was dissolved in *i*Pr₂NH:THF (1:1, 0.7 M) with KOH (aq, 50 wt.%, 20 equiv) and purged for 30 min with bubbling Ar. Pd(PPh₃)₄ (0.03 equiv per transformation) and CuI (0.06 equiv per transformation) were added to the second solution which was then purged another 20 min. The protected donor alkyne was added under an Ar atmosphere via slow injection over 8 h to the acceptor haloarene solution. The mixture was stirred at 65 °C for 8-12 h. Upon completion, the mixture was concentrated, rediluted with CH₂Cl₂, and filtered through a pad of silica gel. The solvent was removed in vacuo and the crude material was purified by column chromatography.

1,2-Dibromo-4,5-bis[(4'-*N,N*-dibutylaminophenyl)ethynyl]benzene (21). 1,2-Dibromo-4,5-diiodobenzene²⁹ (630 mg, 1.29 mmol) was reacted with donor alkyne **16**^{4a}

(798 mg, 2.65 mmol) using general procedure A. The crude material was chromatographed on silica gel (4:1 hexanes:CH₂Cl₂) to yield **21** (622 mg, 70%) as a yellow oil. ¹H NMR (CDCl₃): δ 7.71 (s, 2H), 7.39 (d, *J* = 8.8 Hz, 4H), 6.57 (d, *J* = 8.8 Hz, 4H), 3.29 (t, *J* = 7.5 Hz, 8H), 1.58 (quin, *J* = 6.3 Hz, 8H), 1.37 (sext, *J* = 7.6 Hz, 8H), 0.96 (t, *J* = 7.6 Hz, 12 H). ¹³C NMR (CDCl₃): δ 148.6, 135.6, 132.4, 128.9, 123.0, 112.5, 108.4, 97.7, 85.2, 51.0, 29.7, 20.6, 14.3. IR (NaCl): ν 2197, 1602, 1606, 1519 cm⁻¹. MS (APCI): *m/z* ([isotope], %) 762.8 (M⁺[⁷⁹Br⁸¹Br]+THF, 15), 760.8 (M⁺[⁷⁹Br⁷⁹Br]+THF, 26), 692.7 (M⁺[⁸¹Br⁸¹Br], 55), 690.8 (M⁺[⁷⁹Br⁸¹Br], 100), 688.7 (M⁺[⁷⁹Br⁷⁹Br], 48).

1,3-Dibromo-4,6-bis[(4'-*N,N*-dibutylaminophenyl)ethynyl]benzene (22). 1,3-Dibromo-4,6-diiodobenzene³⁰ (355 mg, 0.73 mmol) was reacted with donor alkyne **16** (450 mg, 1.49 mmol) using general procedure A. The crude material was chromatographed on silica gel (4:1 hexanes:CH₂Cl₂) to yield **22** (446 mg, 89%) as a red oil. ¹H NMR (CDCl₃): δ 7.81 (s, 1H), 7.63 (s, 1H), 7.38 (d, *J* = 9.0 Hz, 4H), 6.58 (d, *J* = 9.0 Hz, 4H), 3.29 (t, *J* = 7.8 Hz, 8H), 1.57 (quin, *J* = 8.7 Hz, 8H), 1.35 (sext, *J* = 7.6 Hz, 8H), 0.96 (t, *J* = 7.6 Hz, 12H). ¹³C NMR (CDCl₃): δ 148.6, 135.6, 134.0, 133.4, 125.9, 123.8, 111.4, 108.1, 97.4, 85.3, 51.0, 29.6, 20.6, 14.3. IR (NaCl): ν 2197, 1602, 1560, 1514, cm⁻¹. MS (APCI): *m/z* ([isotope], %) 692.7 (M⁺[⁸¹Br⁸¹Br], 58), 691.7 (M⁺[¹³C⁷⁹Br⁸¹Br], 40), 690.8 (M⁺[⁷⁹Br⁸¹Br], 100), 688.7 (M⁺[⁷⁹Br⁷⁹Br], 45).

1,4-Dibromo-2,5-bis[(4'-*N,N*-dibutylaminophenyl)ethynyl]benzene (17). 1,4-Dibromo-2,5-diiodobenzene³⁰ (1.41g, 2.89 mmol) was reacted with donor alkyne **16** (2.00g, 6.63 mmol) using general procedure A. The crude material was chromatographed

on silica gel (4:1 hexanes:CH₂Cl₂) to yield **17** (1.77g, 89%) as a red oil. Spectral data match those previously reported.³¹

1,2-Bis[(4'-N,N-dibutylaminophenyl)ethynyl]-4,5-bis(2-pyridylethynyl)benzene (1). TMSA (625 mg, 6.37 mmol) was coupled to **21** (1.50 g, 2.17 mmol) using general procedure B. The resulting red oil was coupled to 2-bromopyridine (1.96 g, 12.38 mmol) using general procedure C. The crude material was chromatographed on silica gel (99:1 CH₂Cl₂:MeOH) to yield **1** (236 mg, 17%) as a dark red oil. ¹H NMR (CDCl₃): δ 8.92 (d, *J* = 5.8 Hz, 2H), 7.73 (t, *J* = 8.0 Hz, 2H), 7.66 (s, 2H), 7.60 (d, *J* = 8.0 Hz, 2H), 7.42 (d, *J* = 9.2 Hz, 4H), 7.35 (t, *J* = 5.8 Hz, 2H), 6.59 (d, *J* = 9.2 Hz, 4H), 3.30 (t, *J* = 7.5 Hz, 8H), 1.59 (quin, *J* = 6.9 Hz, 8H), 1.38 (sext, *J* = 7.0 Hz, 8H), 0.97 (t, *J* = 7.0 Hz, 12H). ¹³C NMR (CDCl₃): δ 150.3, 148.6, 143.5, 136.5, 135.1, 133.5, 128.0, 126.9, 123.6, 123.2, 111.4, 108.6, 98.3, 94.1, 87.7, 86.3, 51.0, 29.6, 20.6, 14.3. IR (NaCl): ν 3041, 2192, 1605, 1601, 1518 cm⁻¹. MS (APCI): *m/z* ([isotope], %) 735.0 (M⁺, 100). UV (CH₂Cl₂) λ_{max} (log ε): 389 (4.45), 435 (sh, 4.32). Em. λ_{max}: 547.

1,3-Bis[(4'-N,N-dibutylaminophenyl)ethynyl]-4,6-bis(2-pyridylethynyl)benzene (2). TMSA (348 mg, 3.54 mmol) was coupled to **22** (830 mg, 1.20 mmol) using general procedure B. The resulting red oil was coupled to 2-bromopyridine (475 mg, 3.00 mmol) using general procedure C. The crude material was chromatographed on silica gel (99:1 CH₂Cl₂:MeOH) to yield **2** (356 mg, 79%) as a dark red-brown solid. Mp: 161-163 °C. ¹H NMR (CDCl₃): δ 8.66 (d, *J* = 4.5 Hz, 2H), 7.70-7.64 (m, 4H), 7.58 (s, 1H), 7.56 (s, 1H), 7.42 (d, *J* = 9.0 Hz, 4H), 7.25 (td, *J* = 7.5, 0.9 Hz, 2H), 6.56 (d, *J* = 9.0 Hz, 4H), 3.27 (t, *J* = 7.8 Hz, 8H), 1.56 (quin, *J* = 3.0 Hz, 8H), 1.34 (sext, *J* = 7.5 Hz, 8H), 0.95 (t, *J* = 7.5

Hz, 12H). ^{13}C NMR (CDCl_3): δ 150.5, 148.6, 143.8, 136.4, 133.6, 132.4, 128.7, 127.8, 123.1, 122.5, 111.4, 108.4, 100.2, 98.7, 93.7, 88.2, 86.1, 50.9, 29.6, 20.6, 14.3. IR (NaCl): ν 2186, 1648, 1605, 1568, 1521 cm^{-1} . MS (APCI): m/z ([isotope], %) 735.0 (M^+ , 100). UV (CH_2Cl_2) λ_{max} ($\log \epsilon$): 378 (4.67), 424 (4.68). Em. λ_{max} : 550.

1,4-Bis[(4'-*N,N*-dibutylaminophenyl)ethynyl]-2,5-bis(2-pyridylethynyl)benzene

(3). TMSA (24 mg, 0.24 mmol) was coupled to 17 (55 mg, 0.08 mmol) using general procedure B. The resulting red oil was coupled to 2-bromopyridine (38 mg, 0.24 mmol) using general procedure C. The crude material was concentrated in vacuo and chromatographed on silica gel (99:1 CH_2Cl_2 :MeOH) to yield 3 (35 mg, 60%) as a dark red solid. Mp: 158-161 $^\circ\text{C}$. ^1H NMR (CDCl_3): δ 8.66 (d, $J = 3.0$ Hz, 2H), 7.76 (s, 2H), 7.68 (td, $J = 7.5, 3.0$ Hz, 2H), 7.58 (d, $J = 7.5$ Hz, 2H), 7.43 (d, $J = 8.6$ Hz, 4H), 7.25 (td, $J = 7.5, 1.4$ Hz, 2H), 6.58 (d, $J = 8.6$ Hz, 4H), 3.29 (t, $J = 7.8$ Hz, 8H), 1.57 (quin, $J = 3.0$ Hz, 8H), 1.35 (sext, $J = 7.5$ Hz, 8H), 0.96 (t, $J = 7.5$ Hz, 12H). ^{13}C NMR (CDCl_3): δ 148.5, 143.7, 136.4, 135.1, 133.5, 132.6, 127.9, 126.1, 124.4, 123.5, 111.4, 108.5, 100.2, 98.1, 88.0, 85.9, 50.9, 29.6, 20.6, 14.3. IR (NaCl): ν 2194, 1603, 1602, 1560, 1522 cm^{-1} . MS (APCI): m/z ([isotope], %) 735.0 ($\text{M}^+ [^{13}\text{C}]$, 55), 734.7 (M^+ , 100). UV (CH_2Cl_2) λ_{max} ($\log \epsilon$): 383 (4.63), 446 (4.54). Em. λ_{max} : 550.

1,2-Bis[(4'-*N,N*-dibutylaminophenyl)ethynyl]-4,5-bis(3-pyridylethynyl)benzene

(4). TMSA (21 mg, 0.21 mmol) was coupled to 21 (49 mg, 0.07 mmol) using general procedure B. The resulting red oil was coupled to 3-bromopyridine (55 mg, 0.35 mmol) using general procedure C. The crude material was chromatographed on silica gel (99:1 CH_2Cl_2 :MeOH) to yield 4 (25 mg, 47%) as a viscous red oil. ^1H NMR (CDCl_3): δ 8.79 (s,

2H), 8.57 (d, $J = 4.5$ Hz, 2H), 7.82 (dt, $J = 7.8, 4.5$ Hz, 2H), 7.71 (s, 2H), 7.42 (d, $J = 9.3$ Hz, 4H), 7.30 (dd, $J = 7.8, 4.5$ Hz, 2H), 6.59 (d, $J = 9.3$ Hz, 4H), 3.30 (t, $J = 7.2$ Hz, 8H), 1.59 (quin, $J = 6.9$ Hz, 8H), 1.36 (sext, $J = 7.6$ Hz, 8H), 0.97 (t, $J = 7.6$ Hz, 12H). ^{13}C NMR ($(\text{CD}_3)_2\text{CO}$): δ 152.2, 149.5, 149.0, 148.9, 138.6, 134.6, 133.4, 126.7, 123.9, 123.5, 111.6, 108.2, 98.6, 91.8, 90.5, 86.0, 50.5, 29.5, 20.3, 13.7. IR (NaCl): ν 2194, 1606, 1522, 1519 cm^{-1} . MS (APCI): m/z ([isotope], %) 735.8 ($\text{M}^+[^{13}\text{C}]$, 55), 734.7 (M^+ , 100). UV (CH_2Cl_2) λ_{max} (log ϵ): 373 (4.82), 406 (4.71). Em. λ_{max} : 537.

1,3-Bis[(4'-*N,N*-dibutylaminophenyl)ethynyl]-4,6-bis(3-pyridylethynyl)benzene (5). TMSA (587 mg, 3.50 mmol) was coupled to **22** (830 mg, 1.20 mmol) using general procedure B. The resulting red oil was coupled to 3-bromopyridine (1.90 g, 12.0 mmol) using general procedure C. The crude material was chromatographed on silica gel (99:1 CH_2Cl_2 :MeOH) to yield **5** (516 mg, 59%) as a viscous red-brown oil. ^1H NMR (CDCl_3): δ 8.85 (s, 2H), 8.56 (d, $J = 5.1$ Hz, 2H), 7.82 (dt, $J = 8.1, 5.1$ Hz, 2H), 7.73 (s, 1H), 7.68 (s, 1H), 7.40 (d, $J = 8.7$ Hz, 4H), 7.28 (dd, $J = 8.1, 5.1$ Hz, 2H), 6.58 (d, $J = 8.7$ Hz, 4H), 3.28 (t, $J = 7.5$ Hz, 8H), 1.55 (quin, $J = 8.4$ Hz, 8H), 1.41 (sext, $J = 7.5$ Hz, 8H), 0.97 (t, $J = 7.5$ Hz, 12H). ^{13}C NMR (CDCl_3): δ 152.5, 148.9, 148.6, 138.8, 135.3, 134.3, 133.4, 127.4, 123.4, 122.7, 120.8, 111.5, 108.2, 98.6, 91.6, 91.2, 86.0, 50.9, 29.6, 20.6, 14.2. IR (NaCl): ν 2194, 1607, 1521 cm^{-1} . MS (APCI): m/z ([isotope], %) 735.8 ($\text{M}^+[^{13}\text{C}]$, 45), 734.7 (M^+ , 100). UV (CH_2Cl_2) λ_{max} (log ϵ): 374 (4.59), 424 (4.59). Em. λ_{max} : 547.

1,4-Bis[(4'-*N,N*-dibutylaminophenyl)ethynyl]-2,5-bis(3-pyridylethynyl)benzene (6). TMSA (35 mg, 0.36 mmol) was coupled to **17** (86 mg, 0.12 mmol) using general procedure B. The resulting red oil was coupled to 3-bromopyridine (175 mg, 1.10 mmol)

using general procedure C. The crude material was concentrated in vacuo and chromatographed on silica gel (99:1 CH₂Cl₂:MeOH) to yield **6** (46 mg, 51%) as a red-brown solid. Mp: 139.5-141 °C. ¹H NMR (CDCl₃): δ 8.84 (s, 2H), 8.58 (d, *J* = 3.4 Hz, 2H), 7.86 (dt, *J* = 7.8, 3.4 Hz, 2H), 7.72 (s, 2H), 7.38 (d, *J* = 8.8 Hz, 4H), 7.31 (dd, *J* = 7.8, 3.4 Hz, 2H), 6.58 (d, *J* = 8.8 Hz, 4H), 3.29 (t, *J* = 7.8 Hz, 8H), 1.58 (quin, *J* = 8.4 Hz, 8H), 1.36 (sext, *J* = 7.5 Hz, 8H), 0.97 (t, *J* = 7.5 Hz, 12H). ¹³C NMR (CDCl₃): δ 152.6, 149.0, 138.9, 134.8, 133.3, 125.7, 124.4, 123.1, 111.5, 108.3, 108.2, 100.2, 98.0, 91.5, 91.4, 85.8, 85.5, 50.9, 29.6, 20.6, 14.3. IR (NaCl): ν 2196, 1604, 1522 cm⁻¹. MS (APCI): *m/z* ([isotope], %) 735.8 (M⁺[¹³C], 51), 734.7 (M⁺, 100). UV (CH₂Cl₂) λ_{max} (log ε): 380 (4.52), 441 (4.48). Em. λ_{max}: 538.

1,2-Bis[(4'-*N,N*-dibutylaminophenyl)ethynyl]-4,5-bis(4-pyridylethynyl)benzene (7). TMSA (203 mg, 2.1 mmol) was coupled to **21** (476 mg, 0.69 mmol) using general procedure B. The resulting red oil was coupled to 4-bromopyridine hydrochloride (1.30 g, 6.69 mmol) using general procedure C. The crude material was chromatographed on silica gel (99:1 CH₂Cl₂:MeOH) to yield **7** (101 mg, 20%) as a viscous red-brown oil. ¹H NMR (CDCl₃): δ 8.60 (d, *J* = 4.5 Hz, 4H), 7.69 (s, 2H), 7.41 (d, *J* = 8.7 Hz, 4H), 7.37 (d, *J* = 5.7 Hz, 4H), 6.58 (d, *J* = 8.7 Hz, 4H), 3.29 (t, *J* = 7.5 Hz, 8H), 1.58 (quin, *J* = 7.8 Hz, 8H), 1.36 (sext, *J* = 7.3 Hz, 8H), 0.97 (t, *J* = 7.3 Hz, 12H). ¹³C NMR (CDCl₃): δ 150.1, 148.6, 135.0, 133.5, 131.4, 127.2, 125.7, 123.1, 111.4, 108.5, 98.8, 92.3, 91.9, 86.2, 50.9, 29.6, 20.6, 14.3. IR (NaCl): ν 2197, 1648, 1602, 1514 cm⁻¹. MS (APCI): *m/z* ([isotope], %) 737.0 (M⁺[¹³C¹³C], 18), 736.0 (M⁺[¹³C], 58), 735.0 (M⁺, 100). UV (CH₂Cl₂) λ_{max} (log ε): 377 (4.55), 407 (4.47). Em. λ_{max}: 558.

1,3-Bis[(4'-N,N-dibutylaminophenyl)ethynyl]-4,6-bis(4-pyridylethynyl)benzene

(8). TMSA (99 mg, 1.0 mmol) was coupled to **22** (233 mg, 0.34 mmol) using general procedure B. The resulting red oil was coupled to 4-bromopyridine hydrochloride (662 mg, 3.40 mmol) using general procedure C. The crude material was chromatographed on silica gel (99:1 CH₂Cl₂:MeOH) to yield **8** (61 mg, 54%) as an orange-brown solid. Mp: 145-147 °C. ¹H NMR (CDCl₃): δ 8.61 (s, 4H), 7.71 (s, 1H), 7.67 (s, 1H), 7.41 (d, *J* = 4.8 Hz, 4H), 7.37 (d, *J* = 8.7 Hz, 4H), 6.57 (d, *J* = 8.7 Hz, 4H), 3.29 (t, *J* = 7.5 Hz, 8H), 1.58 (quin, *J* = 7.8 Hz, 8H), 1.39 (sext, *J* = 7.3 Hz, 8H), 0.97 (t, *J* = 7.3 Hz, 12H). ¹³C NMR (CDCl₃): δ 150.0, 148.7, 135.6, 134.2, 133.4, 131.7, 128.1, 125.8, 122.3, 111.5, 108.1, 99.1, 92.8, 91.8, 85.9, 50.9, 29.6, 20.6, 14.3. IR (NaCl): ν 2192, 1648, 1607, 1565, 1519 cm⁻¹. MS (APCI): *m/z* ([isotope], %) 806.7 (M⁺+THF, 9), 734.7 (M⁺, 100). UV (CH₂Cl₂) λ_{max} (log ε): 380 (4.41), 432 (4.43). Em. λ_{max}: 553.

1,4-Bis[(4'-N,N-dibutylaminophenyl)ethynyl]-2,5-bis(4-pyridylethynyl)benzene

(9). TMSA (325 mg, 3.31 mmol) was coupled to **17** (762 mg, 1.10 mmol) using general procedure B. The resulting red oil was coupled to 4-bromopyridine hydrochloride (1.072 g, 5.52 mmol) using general procedure C. The crude material was chromatographed on silica gel (99:1 CH₂Cl₂:MeOH) to yield **9** (721 mg, 89%) as a red-brown solid. Mp: 172-174 °C. ¹H NMR (CDCl₃): δ 8.62 (s, 4H), 7.70 (s, 2H), 7.43 (d, *J* = 4.8 Hz, 4H), 7.36 (d, *J* = 9.0 Hz, 4H), 6.57 (d, *J* = 9.0 Hz, 4H), 3.29 (t, *J* = 7.8 Hz, 8H), 1.58 (quin, *J* = 8.1 Hz, 8H), 1.36 (sext, *J* = 7.5 Hz, 8H), 0.97 (t, *J* = 7.5 Hz, 12H). ¹³C NMR (CDCl₃): δ 150.0, 148.7, 134.9, 133.3, 131.6, 126.1, 125.9, 124.4, 111.4, 108.2, 98.4, 92.7, 92.2, 85.7, 50.9, 29.6, 20.6, 14.3. IR (NaCl): ν 2192, 1598, 1521 cm⁻¹. MS (APCI): *m/z* ([isotope], %)

737.0 ($M^+ [^{13}C^{13}C]$, 18), 736.0 ($M^+ [^{13}C]$, 57), 735.0 (M^+ , 100). UV (CH_2Cl_2) λ_{max} (log ϵ): 383 (4.77), 449 (4.59). Em. λ_{max} : 558.

TFA titration of 1-9. Solutions of 1-9 (35 μL , $\sim 250 \mu M$) were dissolved in spectrophotometric-grade MeOH (UV cutoff 204 nm) in four-sided quartz spectrophotometry cuvettes. Trifluoroacetic acid was diluted to concentrations ranging from 10^{-5} to 0.8 M in 10 mL MeOH. 2 mL aliquots were added to each solution of 1-9. The solutions were capped and shaken, and the fluorescence spectra were then taken immediately.

Zinc chloride complexation to 1-9. Solutions of 1-9 (3.5 mL, ~ 0.4 mM) were dissolved in spectrophotometric-grade CH_2Cl_2 (UV cutoff 250 nm) in four-sided quartz spectrophotometry cuvettes. 0.5 M $ZnCl_2$ in THF was diluted to 0.01 M with CH_2Cl_2 , and between 0.1 and 100 equiv were injected via microsyringe. The solutions were capped and shaken, and the UV and fluorescence spectra were then taken immediately.

Aluminum chloride addition to 1-9. Solutions of 1-9 (3.5 mL, $\sim 25 \mu M$) were dissolved in spectrophotometric-grade MeOH (UV cutoff 204 nm) in four-sided quartz spectrophotometry cuvettes. Anhydrous $AlCl_3$ (0.021 g, 0.16 mmol) was dissolved in anhydrous MeOH (100 mL). Between 1 and 100 equiv of this 0.0016 M Al(III) solution were injected into the solutions of 1-9 via microsyringe. The solutions were capped and shaken, and the fluorescence spectra were then taken immediately.

Silver triflate addition to 1. A solution of 1 (3.5 mL, $\sim 12 \mu M$) was dissolved in spectrophotometric-grade CH_2Cl_2 (UV cutoff 250 nm) in a four-sided quartz spectrophotometry cuvette. Anhydrous $AgOTf$ (0.0063 g, 0.025 mmol) was dissolved in

anhydrous CH_2Cl_2 (10 mL) with vigorous sonication for 30 min. Between 0.2 and 70 equiv of this 0.0025 M Ag(I) solution were injected into the solution of **1** via microsyringe. The solutions were capped and shaken, and the fluorescence spectra were then taken immediately.

Addition of excess metal salts to TAEBS 1, 5, and 9. Solutions of **1**, **5**, and **9** (5 mL, $\sim 60 \mu\text{M}$) were dissolved in spectrophotometric-grade CH_2Cl_2 (UV cutoff 250 nm) in 2 dram glass vials. Solid portions of each metal salt (at least 100 equiv each) were added to the vials. The vials were capped and shaken, then sonicated for 1 h. The supernatant solutions were decanted from remaining solids (where applicable) into new vials, and the solutions were visualized under a high-intensity 365 nm lamp (Figure 16). Solutions containing no ion, ZnCl_2 , and AlCl_3 were poured into four-sided quartz spectrophotometry cuvettes, and the spectra were taken.

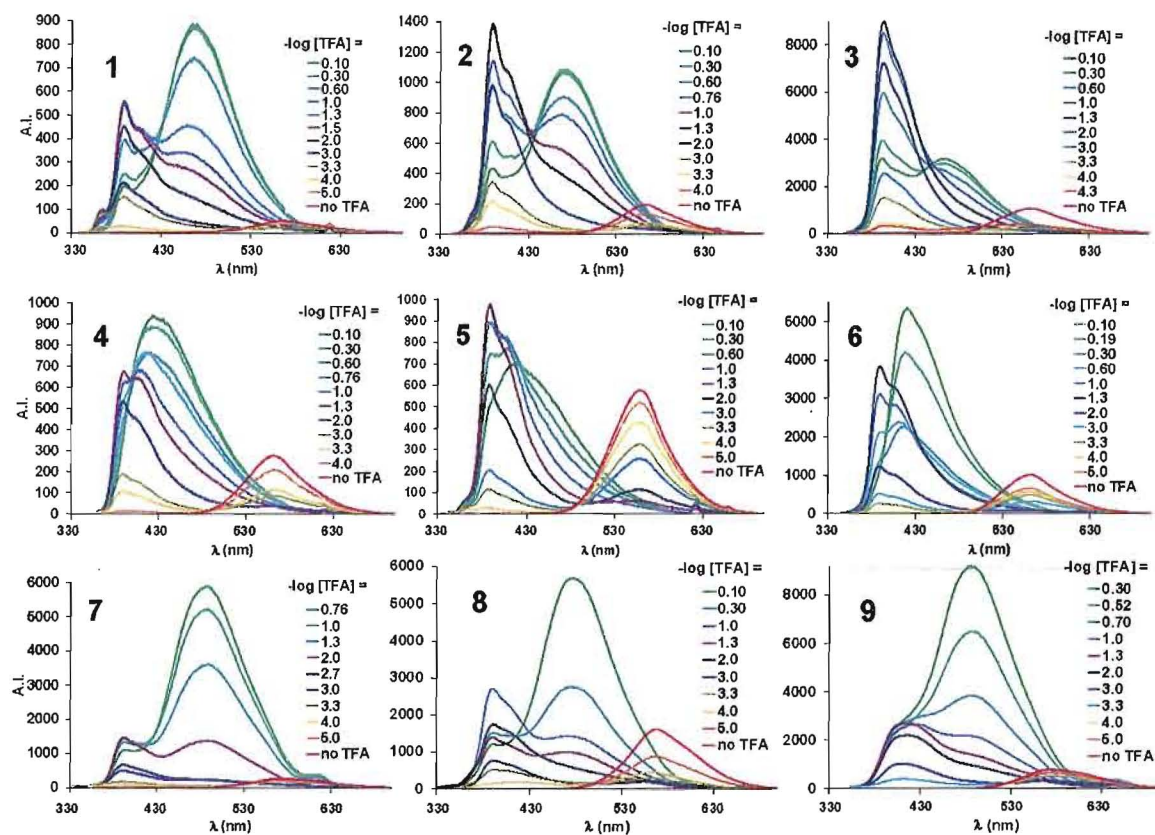


Figure 18. Emission spectra of TFA titration of 1-9 in MeOH. The small peaks appearing in the spectra past 600 nm arise from interference by doubling of the excitation wavelength. Peaks from the excitation wavelength have been subtracted from each spectrum when necessary for clarity. All spectra were recorded at approx. $4 \mu\text{M}$ concentration. Excitation at most intense absorption peak (300-350 nm, present in all compounds).

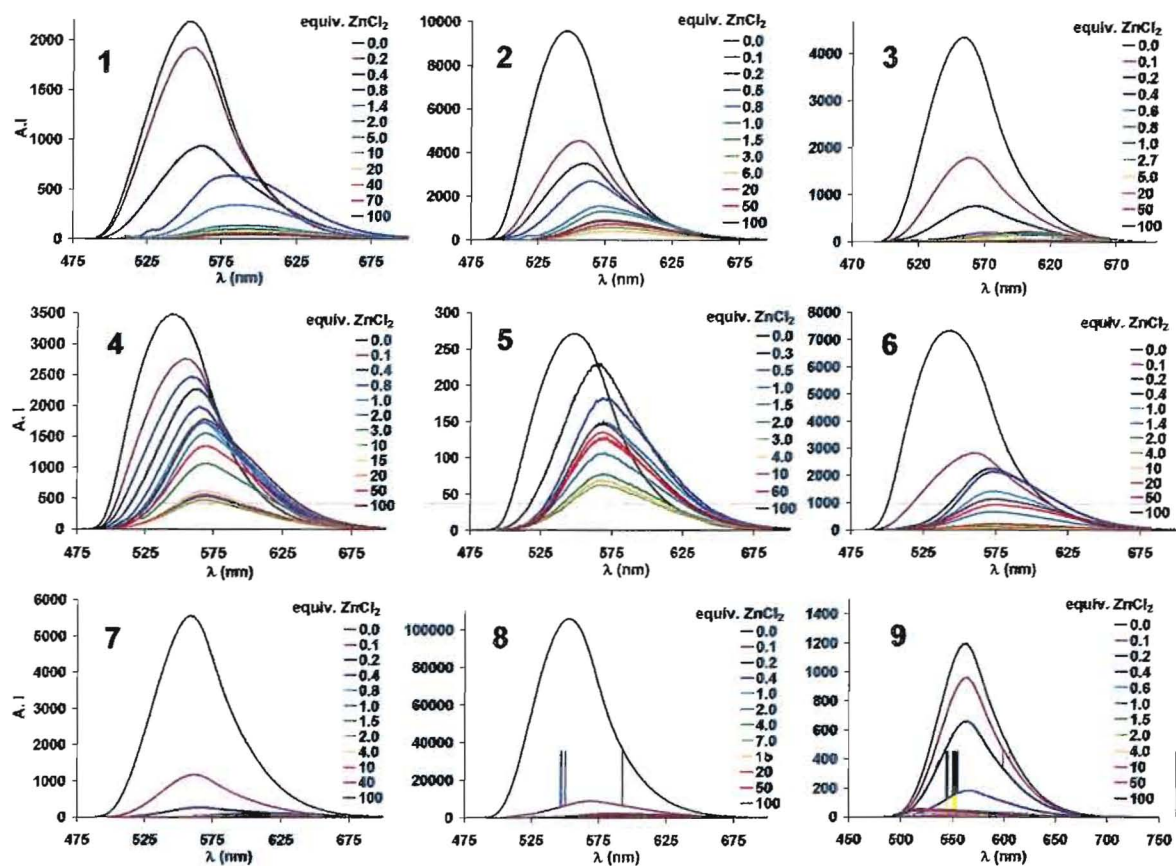


Figure 19. Emission spectra of ZnCl_2 complexation to 1-9 (left to right, top to bottom). All spectra were recorded in CH_2Cl_2 at approximately 0.4 mM concentration. Excitation at wavelength of lowest energy absorption peak (400-525 nm, present in all compounds).

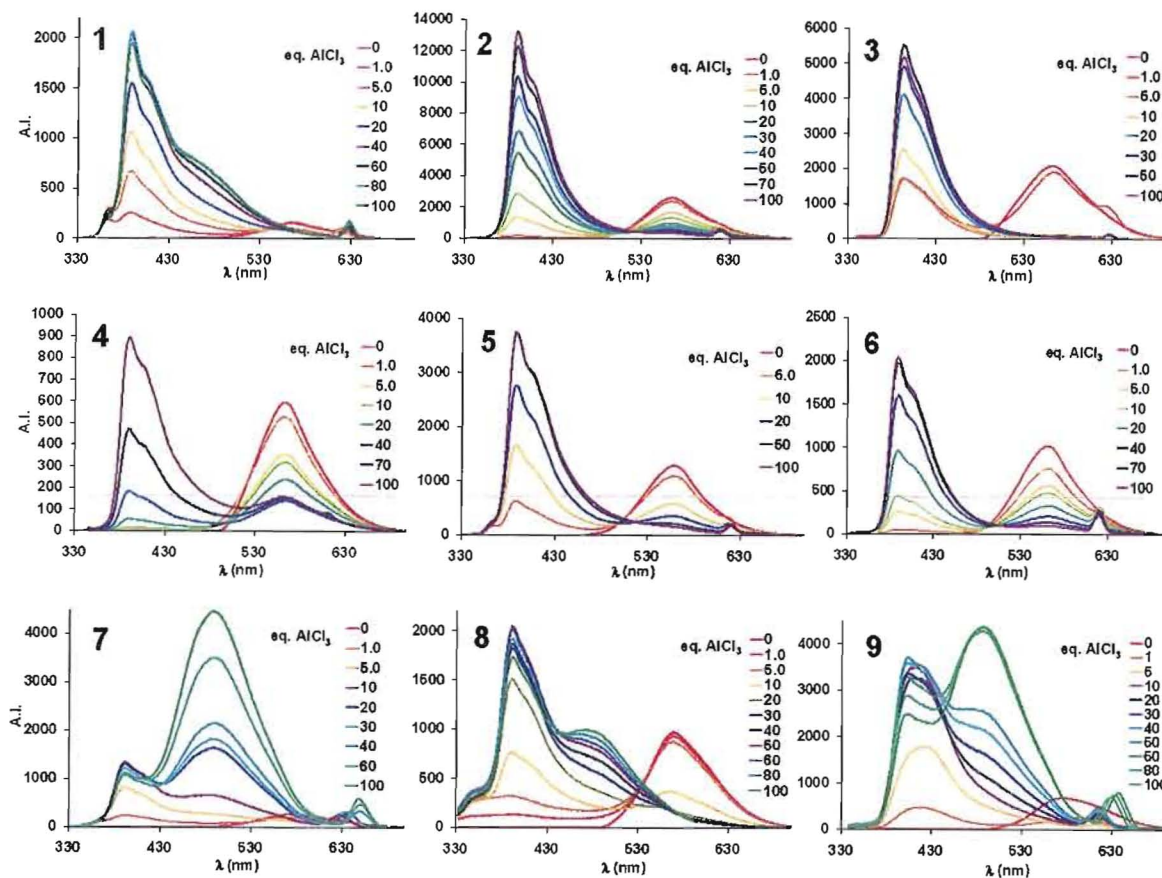


Figure 20. Emission spectra of addition of AlCl_3 in MeOH to **1-9** (left to right, top to bottom) at ca. $10\text{-}25\ \mu\text{M}$ concentration. The small peaks appearing in the spectra past 600 nm arise from interference by doubling of the excitation wavelength. Peaks from the excitation wavelength have been subtracted from each spectrum for clarity. Excitation at wavelength of most intense absorption band (300-320 nm, present in all compounds).

Bridge to Chapter III

Chapter III expands upon the emission switching effects in Chapter II to include dehydrobenzoannulene (DBA) architectures that consist of two donor groups conjugated to a single pyridine acceptor through acetylene linkers in a 15-membered macrocycle. The effect of enforced planarization on the spectroscopic profiles is examined, as well as the consequence of varying the position of the acceptor nitrogen relative to the conjugation pathways. The predicted overlapping FMOs in these molecules implies that partial protonation can induce enhanced intramolecular charge transfer behavior not present in the neutral species. The two-stage switching effect is observed to occur in a manner opposite to that observed for the acyclic molecules in Chapter II, further implying the ability to fine-tune the electronic properties of these types of chromophores to selected applications.

CHAPTER III

DYNAMIC PROTON-INDUCED EMISSION SWITCHING IN DONOR-FUNCTIONALIZED DEHYDROBENZOPYRID[15]ANNULENES

Introduction

This chapter was co-authored with Sean P. McClintock, who performed the molecular orbital computations and Professor Michael M. Haley, who conceptualized the project and provided editorial assistance. This chapter includes work that was published in the *Journal of Organic Chemistry* (2007, 72, 6692-6699, © 2007 American Chemical Society).

Highly conjugated, carbon-rich organic molecules have been the focus of extensive interest in recent years because of their unique optical and electronic properties.¹⁻³ In particular, chromophoric or fluorophoric systems possessing electronic and/or photonic transfer pathways are recognized as ideal candidates for components of analytical reagents and advanced optical devices.⁴⁻⁸ Their propensity to act as bulk materials or organic liquid crystal arrays also implies applications in OLED, organic semiconductor, and photoelectric cell design.

We have been investigating the optoelectronic properties of a special class of carbon-rich compounds, dehydrobenzoannulenes (DBAs, Figure 1a).^{4a-c} These fully conjugated macrocycles composed of acetylene-linked arenes represent attractive targets of fundamental study into aromaticity and enforced planarization. We have also performed studies on donor/acceptor-functionalized DBAs that undergo intramolecular charge transfer upon optical excitation, as well as studies of their acyclic tetrakis(arylethynyl)benzene analogues (TAEBs) with variation of the acceptor group. Most recently, we reported a systematic study of isomeric pyridine-derivatized bisdonor/bisacceptor TAEBs (Figure 1b).^{4d} We demonstrated that these systems underwent two-stage fluorescence emission shifting (to varying extents corresponding to charge transfer pathway

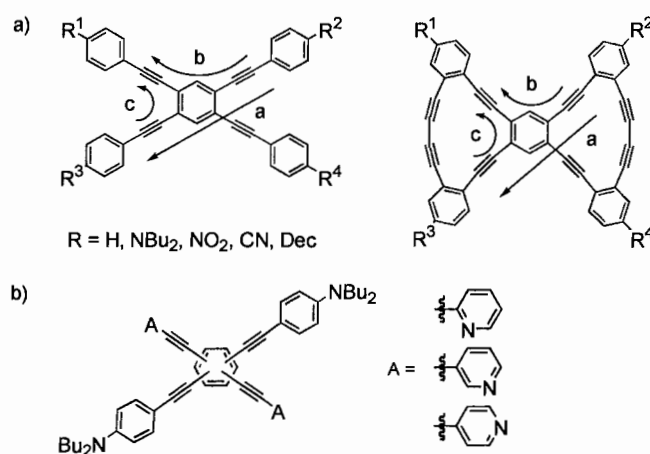


Figure 1. a) Conjugated pathways present in structurally related tetrakis(phenylethynyl)benzenes (TPEBs) and bis(dehydrobenzoannuleno)benzenes (DBAs); b) donor/acceptor tetrakis(arylethynyl)benzenes (TAEBs) with dibutylaniline donors and pyridine acceptors.

efficiency) upon titration with acid or addition of assorted metal ions, and that these shifts correlated to the relative energies of the spatially separate frontier molecular orbitals (FMOs). Thus, the segment-localized FMOs in conjugated donor/acceptor fluorophores could be manipulated independently.⁹

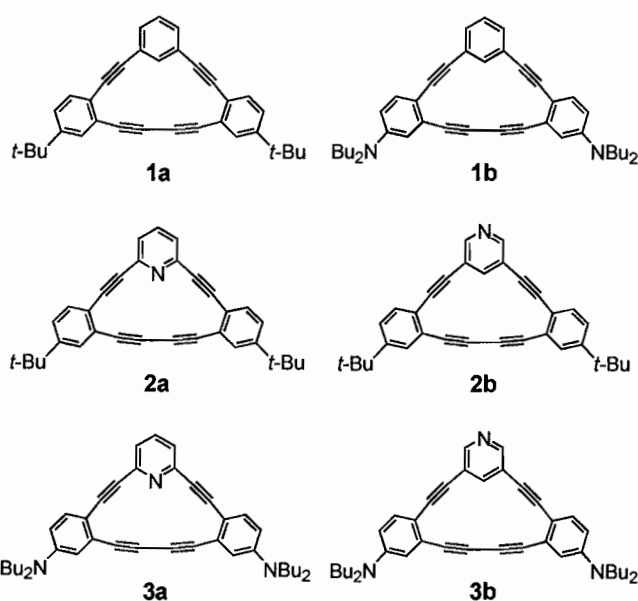


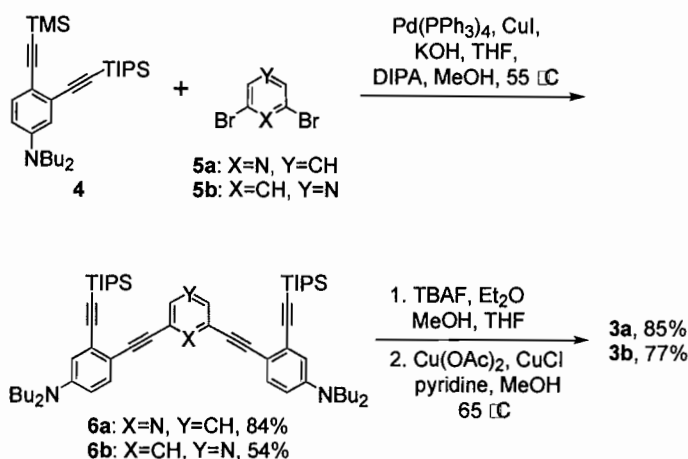
Figure 2. 15-membered carbon macrocycle DBAs (1), *t*-butyl functionalized DBPAs (2), and target donor-functionalized DBPAs (3).

We have previously examined DBAs of the type 1, incorporating solubilizing *t*-Bu groups or electron-donating *N*Bu₂ groups, as well as isomers of *t*-Bu-functionalized dehydrobenzopyridannulenes (DBPAs) 2, fused at either the 2,6- or 3,5- positions (Figure 2).^{10a-c} Tobe *et al.* have also prepared [15]DBAs in the course of examining more complex cyclophane architectures,^{10d} and Baxter *et al.* have synthesized several related

pyridannulene structures.^{5c} We now present donor-functionalized DBPAs of the type **3**, which incorporate the aforementioned switching behavior into 15-membered acetylenic macrocycles. As moderate strength acceptors, pyridines can participate in various degrees of intramolecular charge transfer, depending on the efficiency of the conjugated pathway from the donor to the acceptor nitrogen.^{4d} Since both donor and acceptor group(s) can be protonated, the ability to probe independent manipulation of the FMOs using shifts in the emission spectra can also be demonstrated.

Results and Discussion

Synthesis. Assembly of **3a** and **3b** is readily accomplished as shown in Scheme 1. Donor-functionalized alkyne segment **4**^{4a} is appended to either 2,6- or 3,5-dibromopyridine **5** using methanolic KOH to remove the more labile trimethylsilyl (TMS) group *in situ* to afford the bisdonor precursors **6a** and **6b**. Removal of the triisopropylsilyl (TIPS) groups with tetra-*n*-butylammonium fluoride (TBAF) followed by oxidative intramolecular homocoupling under Cu-mediated conditions furnished macrocycles **3a** and **3b** in 71% and 42% overall yield, respectively. It is notable that in both coupling steps, the more conjugated systems **a** proceed in somewhat higher yields, a trend also observed in preparation of **2a** and **2b**.^{10b}



Scheme 1. Preparation of DBPAs **3a** and **3b**.

In the strong donor/strong acceptor bisannulenes,^{4a} significant self-associative behavior was observed in their ¹H NMR spectra due to intermolecular π -stacking and dipole attraction between respective donor and acceptor groups. In **3a** and **3b**, no such behavior was observed: NMR signals remained constant over a several-fold concentration gradient. There were, however, noticeable upfield shifts of the signals from protons *ortho* to the monoacetylene linkages ($\Delta\delta = 0.1$ - 0.3 ppm) upon ring closure of **6a-b** to **3a-b**, with smaller upfield shifts in other signals (see experimental section). This effect is indicative of increased electron delocalization along the π -conjugated pathway. Upon cyclization to **3b**, there was a dramatic (0.91 ppm) downfield shift of the proton internal to the macrocycle, which was also observed in **2b**,^{10b} and is attributed to the anisotropy of the nearby triple bonds.

Crystals of **3a** and **3b** suitable for X-ray diffraction were obtained by evaporation from 5:1:1 and 5:3:1 solutions of hexanes:CH₂Cl₂:EtOAc, respectively. Both DBPAs are

planar structures with remarkably linear diyne bridges ($C_{sp}-C_{sp}$ bond angles for **3a**: 177-179°; **3b**: 177-178°; experimental section Figures 11 and 12). Most of the strain in the molecules is contained in the monoacetylene units, which are moderately distorted ($C_{sp}-C_{sp}$ bond angles for **3a**: 167-174°; **3b**: 163-171°). Overall, the structures closely resemble the purely hydrocarbon [15]DBA reported by Tobe *et al.*^{10d} In the solid state, **3b** packs in slipped π -stacking arrangement, similar to Tobe's annulene, whereas **3a** contains two symmetrically independent molecules arranged in zigzagging dimeric pairs. The packing differences are likely due to weak hydrogen bonding in **3b** between the pyridine nitrogen atom and an *ortho* pyridine proton on a neighboring molecule (N \cdots H-C distance 2.62 Å, Figure 12.)

Absorption and Emission Data. Electronic absorption and emission spectra of **3a-b** are shown in Figure 3a and summarized in Table 1, along with their respective precursors **6a-b** and *t*-butyl-functionalized analogues **2a-b**^{10b} for comparison. Cyclization/planarization to the macrocycle enhances π -orbital overlap, increasing the conjugation. This results in a 17-25 nm bathochromic shift in the absorption spectra of **3a-b** versus **6a-b**, accompanied by a significant loss of intensity of the lowest energy band, possibly indicating weak intramolecular charge transfer. This is in good agreement with our previously described donor/acceptor bisannulene series, as well as recent examples of weak donor/weak acceptor-functionalized DBAs.^{8f} The electron density from the donating groups results in a λ_{max} of the lowest energy bands in **3a** and **3b** that are 7 and 19 nm greater than **2a** and **2b**, respectively. It is somewhat surprising that the charge transfer bands for **3a** and **3b** are so similar, since **3b** does not contain a direct

resonance pathway for full conjugation, implying good inductive withdrawal by the pyridine ring as a unit.

Table 1. Electronic absorption and emission data for **2a-b**, **3a-b** and **6a-b**

compd	lowest energy abs λ_{max} [nm] (ϵ [$\text{M}^{-1}\text{cm}^{-1}$])	em λ_{max} [nm]	Stokes shift [cm^{-1}] (nm)]	Φ_{f}^a
2a	400 (sh) (1750) ^b	454 ^c	2974 (54)	0.16
2b	389 (3000) ^b	436 ^c	2771 (47)	0.20
6a	390 (49760±60)	427	2222 (37)	0.81
6b	383 (52910±190)	421	2357 (38)	0.85
3a	407 (17290±10)	490	4162 (83)	0.19
3b	~408 (sh) (12410±10)	494	~4267 (86)	0.17

^a Calculated relative to fluorescein at pH 8 (Ref. 11) with excitation at lowest energy abs λ_{max} . ^b Ref 10b. Error in ϵ values not given. ^c Maxima corrected from Ref. 10b due to instrument error.

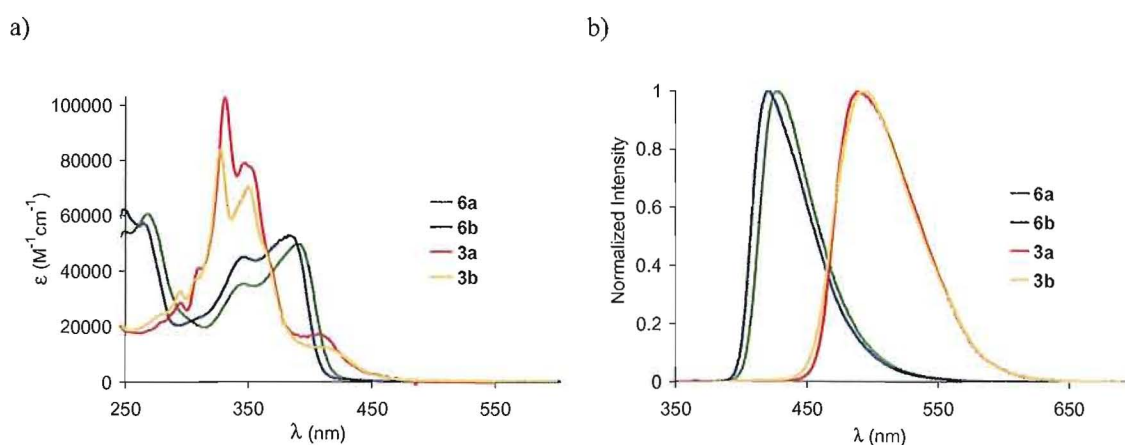


Figure 3. (a) Absorption and (b) emission spectra of DBPAs **3a-b** and precursors **6a-b** in CH_2Cl_2 at 20-30 μM concentration. Excitation at 365 nm.

Normalized emission spectra are shown in Figure 3b and Table 1. There is a dramatic red shift in both systems upon planarization. FMO plots (see next section) show significant LUMO density localized on the diacetylene bridges, so it is possible that cyclization has a more pronounced effect on the excited state energies, thus affecting the emission spectra more than the absorption. In the precursors, the more conjugated 2,6-fused system **6a** is more red-shifted, but in the annulenes the λ_{max} are very similar. This may be due to the larger predicted net dipole in **3b** (8.46 D vs. 4.25 D for **3a**, see experimental section Table 5). The large increase in Stokes shifts upon ring closure also indicates an increase in net dipole and the efficiency of the conjugated π -system.¹² Our previous DBAs studies generally show a *decrease* in Stokes shift upon planarization, but in some π -electron rich species an increase is seen when there is significant calculated LUMO density on the bridging pathway.^{4a} This also seems to be the case for the weak donor/acceptor systems here, and is likely due to the less effective cross-conjugated pathways present in the 15-membered macrocycles. Donor functionalization also results in maxima significantly red-shifted relative to **2a-b**,^{10b} in agreement with previous DBA behavior.^{4a}

There is little difference in Φ_f between **3a** and **3b**, likely reflecting the weak intramolecular charge transfer transitions dominating in both. This agrees with previous results wherein the all-donor analogues of the systems in Figure 1 show higher quantum yields than the donor/acceptor systems^{4,13} Interestingly, the values for **3a** and **3b** are comparable to **2a** and **2b**. One would expect functionalization with donor π -electrons to increase Φ_f . The emission spectra of **2a** and **2b** contain significant fine structure,

however, perhaps implying more complex vibronic interactions than are observed here. **2a** and **2b** also possess exceptionally long absorption cutoffs.^{10b} The remarkably high quantum yields of precursors **6a** and **6b** help illustrate in part the effect of enforced planarization on the conjugation, but it is likely that the increased fluorescence is also due in part to donor electron contribution from the TIPS groups. Examination of desilylated **6a-b**, however, showed no significant effect on either absorption or emission wavelengths (see experimental section Figure 8).

Molecular Orbital Plots. In our previously-described ethynylpyridine systems,^{4d} the ability to protonate the donor and acceptor segments independently resulted in a two-stage emission switching behavior, analogous to that first observed by Bunz and coworkers in related donor/acceptor cruciforms.^{9a,b} Initial protonation with trifluoroacetic acid (TFA) caused a dramatic blue shift in the spectra, followed by a more modest red shift with subsequent protonation. Since the HOMO and LUMO are calculated to be localized primarily on the donor and acceptor segments, respectively, protonation of the donor or acceptor nitrogens cause the shifts by affecting the relative energies of the orbitals. Molecules **3a** and **3b** are similar systems, but with enforced planarization and with only one acceptor unit for two donor units.

FMO plots of **3a'** and **3b'** were calculated using Gaussian03¹⁴ (B3LYP¹⁵ level of theory, 6-31G* basis set) with simplified structures that replaced the NBu₂ donor with NMe₂ (Figure 4). They predict largely overlapping HOMO and LUMO localizations in the neutral state, but protonation of the pyridine nitrogen and subsequent protonation of a donor nitrogen cause increasing spatial separation of the orbitals. Protonation of **3a'** to

3a'⁺ leaves the HOMO relatively unchanged and results in weak localization in the LUMO at the pyridine ring, but overall has little effect. Further protonation at one of the donor sites reveals a more separate orbital diagram in which the HOMO is localized largely on the neutral donor while the LUMO is spread over the protonated regions of the macrocycle, creating a more charge transfer-like system (although the FMOs are more separated in these cases, it is possible that both donor segments are in fact protonated in a dynamic equilibrium that does not lead to the orbital diagrams shown). Charge transfer is quenched by protonation of the final donor segment, causing overlapping molecular orbitals. Examination of **3b'** indicates that upon protonation the system exhibits more orbital localization than **3a'**, presumably due to the lack of a conjugated pathway. Protonation of the acceptor segment localizes the HOMO onto the two donor segments and the LUMO on the acceptor. Subsequent protonation of a donor segment results in localization of the HOMO around the neutral donor arene, while the LUMO is spread out between the two protonated segments. Both systems indicate that while the molecular orbitals are not fully separate, stepwise protonation of the systems may allow for manipulation of the orbitals and potentially their emission properties. The band gap energies for **3a'** and **3b'** were also calculated and found to be within 25 nm of the experimental band gaps for **3a** and **3b**, which is closer than calculated for previously examined DBAs (See experimental section Table 5).^{4a} Thus, stepwise protonation in **3a** and/or **3b** reflect an *induced* strong donor/acceptor species, implying enhanced charge-transfer character more akin to that predicted and observed in the ethynylpyridine systems, and therefore similar emission switching behavior for **3a-b**.

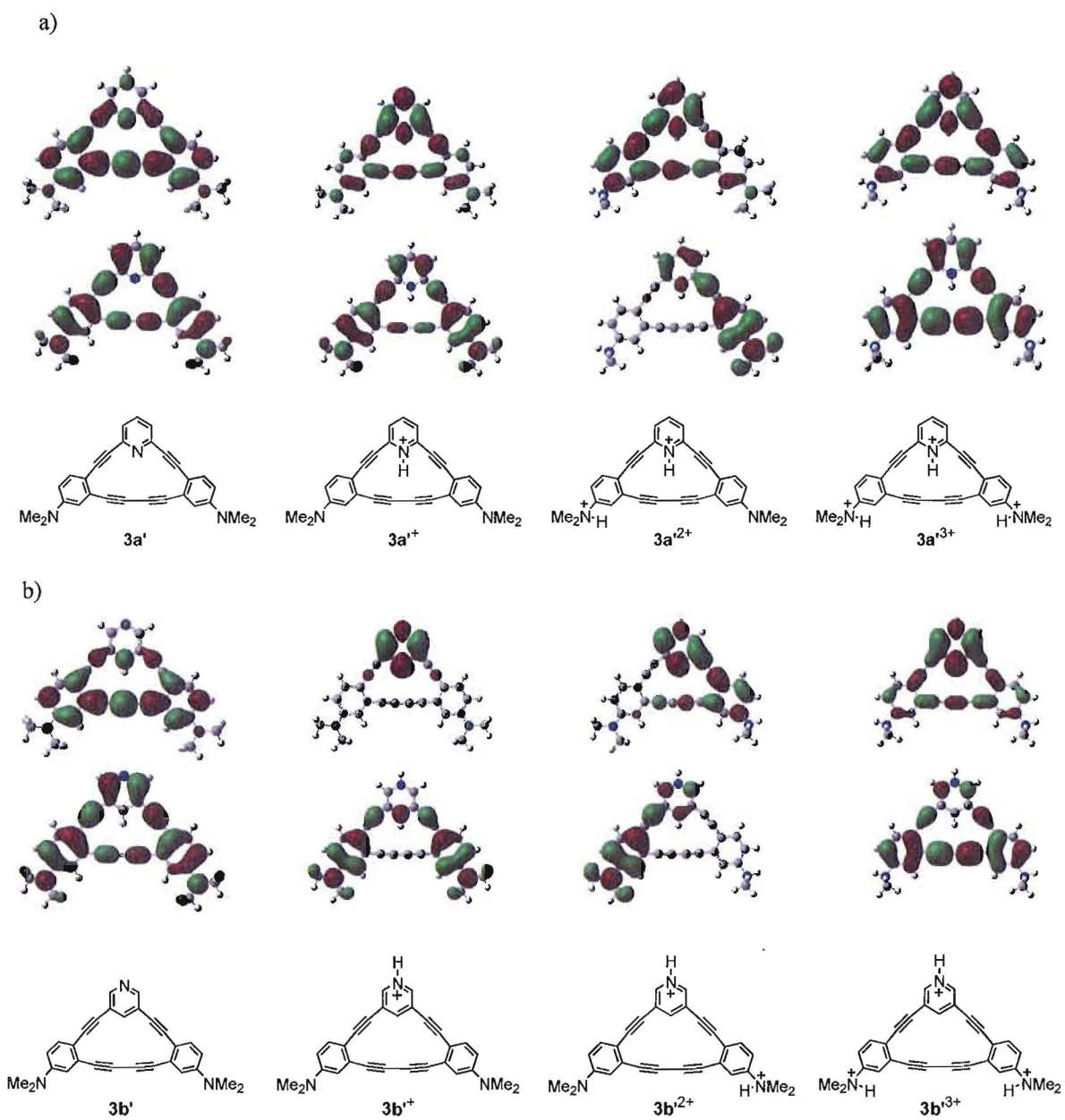


Figure 4. Molecular orbital plots (B3LYP/6-31G*) of simplified structures **3a'** (a) and **3b'** (b) of **3a** and **3b**, respectively, in the neutral, monoprotonated, diprotonated and triprotonated states. The lower plots represent the HOMOs, and the upper plots represent the LUMOs.

TFA Titrations. Trifluoroacetic acid (TFA) titration of **3a** in MeOH between $[\text{TFA}] = 10^{-5}$ and $10^{-0.3}$ M showed no such switching behavior, and resulted only in qualitative quenching of fluorescent intensity with no change in wavelength (see experimental section Figure 9). Repeating the titration of **3a** with TFA in CH_2Cl_2 , on the other hand, yielded far different results (Figure 5). At $[\text{TFA}] = 10^{-3}$ M, the original charge transfer band at 407 nm in the absorption spectrum is greatly enhanced, and two new bands at 494 and 619 nm appear. These bands reach maximum intensity at $[\text{TFA}] = 10^{-2}$ M, at which the solution attains a pale green color in ambient light. In the emission spectra, a rapid drop off of fluorescent intensity is accompanied by the simultaneous appearance of a low-intensity peak at ca. 670 nm, shifting from bright blue-green fluorescence to a dark, deep magenta at $[\text{TFA}] = 10^{-2}$ M. Further addition of TFA causes a gradual loss of the new bands in the absorption, until at $[\text{TFA}] = 10^{-0.3}$ M there are no bands past 400 nm. The solution fades from green to very light pink and finally a pale yellow. In the emission spectra, the red band is quenched along with the gradual appearance of a third peak around 540 nm, achieving a pale yellow-green fluorescence.

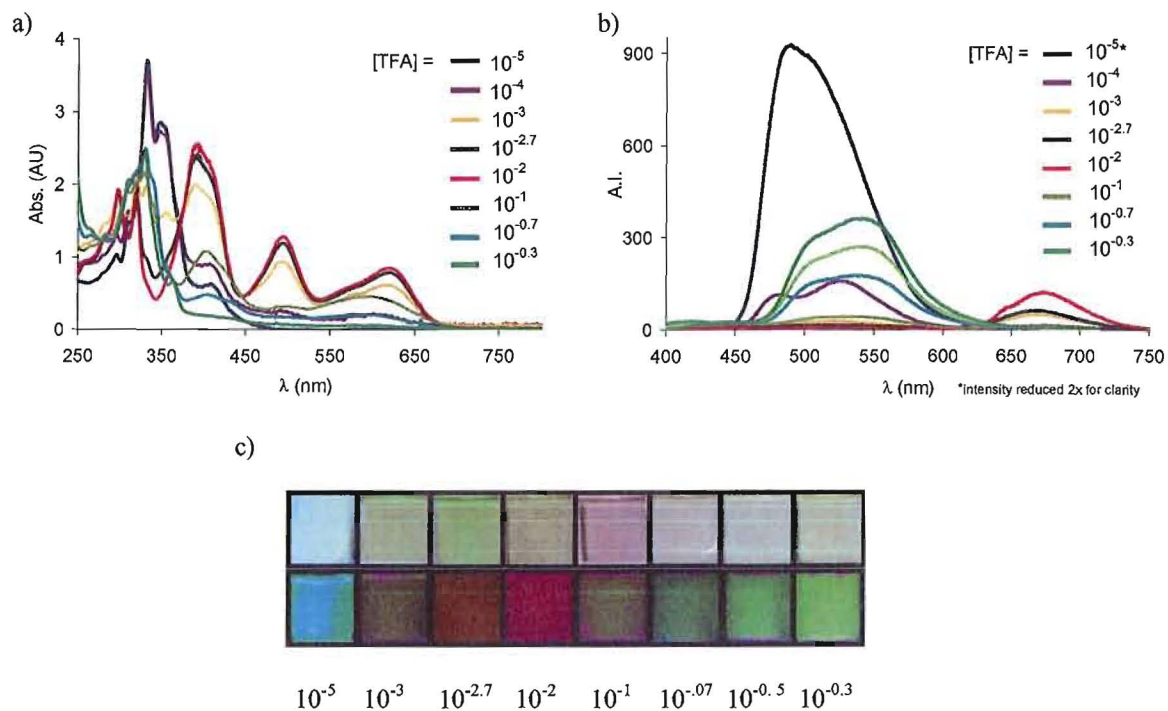


Figure 5. a) Absorption spectra of TFA titration of **3a** in CH_2Cl_2 at ca. $60 \mu\text{M}$ concentration. b) Emission spectra of TFA titration of **3a** in CH_2Cl_2 . Excitation at 365-385 nm. c) Solutions of **3a** in CH_2Cl_2 in ambient light against a white background (top) and under illumination by high-intensity 365 nm lamp in the dark (bottom) at indicated [TFA] (M).

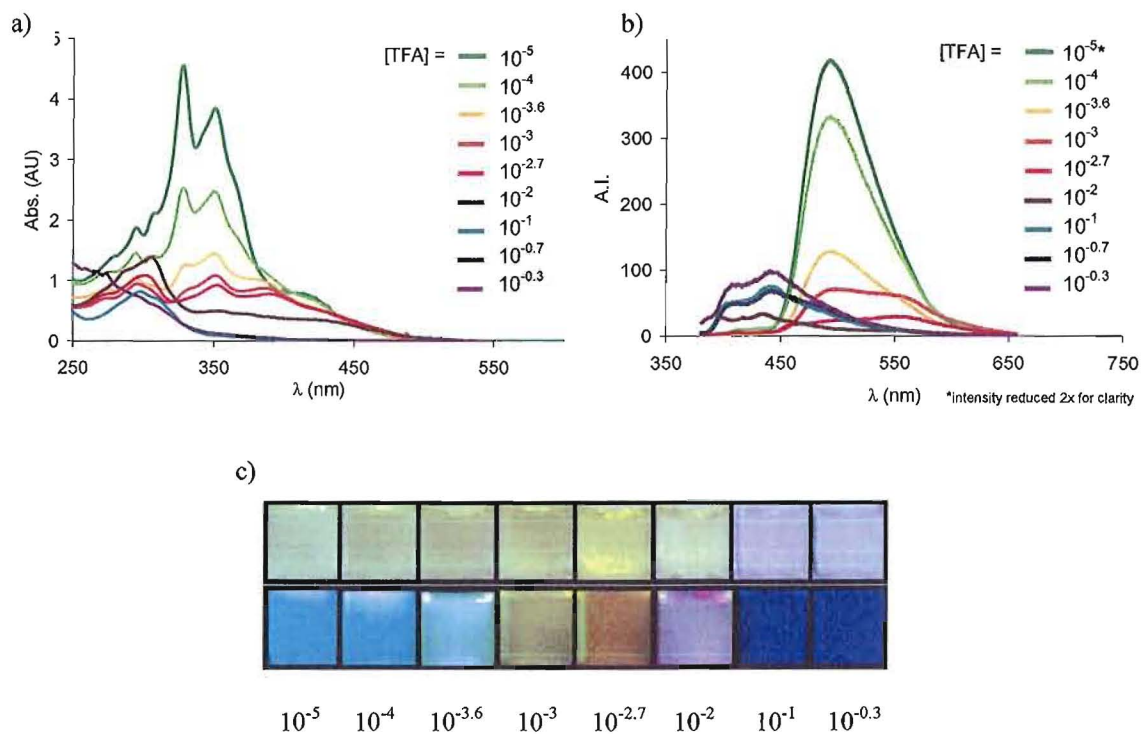


Figure 6. a) Absorption spectra of TFA titration of **3b** in CH_2Cl_2 at ca. $30 \mu\text{M}$ concentration. b) Emission spectra of TFA titration of **3b** in CH_2Cl_2 . Excitation at 365-400 nm. Interference peaks from excitation wavelength removed for clarity. c) Solutions of **3b** in CH_2Cl_2 in ambient light against a white background (top) and under illumination by high-intensity 365 nm lamp in the dark (bottom) at indicated [TFA] (M).

Table 2. Summary of TFA-induced emission shifting in **3a** and **3b** in CH_2Cl_2 .

cmpd	initial em λ_{max} (nm)	10^{-2} or $10^{-2.7}$ M TFA em λ_{max} (nm)	$\Delta\lambda_1$ (nm)	$10^{-0.3}$ M TFA em λ_{max} (nm)	$\Delta\lambda_2$ (nm)
3a	490	670	180	541	129
3b	494	560	66	445	115

Titration of **3b** (Figure 6) gave somewhat different results. In the initial stage, the lowest energy band in the absorption spectrum was suppressed and slightly red shifted to ca. 415 nm at 10^{-2} M TFA, while the fluorescence was significantly quenched at higher than 10^{-4} M, with a red shift of the emission maxima to about 560 nm. The solutions change from pale yellow-green to darker yellow in ambient light, and under UV illumination fade from fluorescent blue-green to a pale yellow-orange at $10^{-2.7}$ M TFA. Additional protonation eliminates any significant absorption past 400 nm, and at 10^{-2} M TFA the emission is suddenly blue-shifted past the neutral compound to around 445 nm. The solutions fade to colorless, with the generation of a bright blue fluorescence. The behavior of both compounds is summarized in Table 2. In contrast to our DBPAs, Baxter's pyridannulene systems, which lack donor group π -electrons, exhibited only red shifting and quenching with acidification.^{5c} Titration of acyclic precursors **6a** and **6b** resulted only in fluorescence quenching with no significant change in λ_{max} (see experimental section Figure 10).

We believe the behavior exhibited in **3a** and **3b** arise from predominantly stepwise protonation of the molecules. Because of the π -electron donation from the two NBu_2 groups, it is possible that the pyridine nitrogen is in general protonated first, causing the red shifts in the absorption and emission. Ionization of the acceptor should greatly enhance its electron withdrawal ability, potentially forming a strong charge transfer system with a low optical band gap. Subsequent protonation of the donor nitrogens then suppresses all charge transfer, leading to a system with only π - π^* transitions. The donor electrons also allow quick but qualitative evaluation of the

magnitude of the effect using fluorescence spectroscopy. This easily-accessible protonated state could potentially be exploited for advanced nonlinear optical applications. Several of our previously studied systems have exhibited significant nonlinear optical susceptibility, with two-photon absorption cross sections that rival literature standards.⁷ The greatly narrowed band gap in **3a** at 10^{-2} M TFA may display similar or even better results, particularly since the donor/strong acceptor DBAs^{4a} do not display band gaps as small, and acidification of solutions of them causes only blue shifts in both absorption and emission spectra. This effect is not observed to any significant extent in **3b**, likely due to the lack of fully conjugated pathways between the donors and the acceptor. Only a moderate red shift, followed by a dramatic blue shift in the emission is observed. These dynamic emission shifts thus can also serve as a qualitative probe of conjugation efficiency. Although it is not certain whether the red-shifted emission peaks correspond to mono- or diprotonated species, or an equilibrium mixture of both, in both sets of emission spectra the most acidic solutions' emission bands display a weak shoulder somewhat blue-shifted from the maxima. The two emissions may arise from states with either one or both donor nitrogens protonated, but the lack of clearly deconvoluted bands with distinct maxima implies that both are protonated nearly independently or in equilibrium (rather than discretely as in the above FMO calculations). This parallels both our previous work on the acyclic ethynylpyridines as well as Bunz' systems, where only one band for each protonation state was observed.^{9a,b} In those cases, the donors are believed to be protonated first, followed by the acceptors. Here, the cumulative donation by two NBu₂ groups to only one pyridine likely accounts for the

opposite behavior. The interesting lack of clearly discernable isosbestic points may imply dynamic equilibria during titration rather than distinct species, but the emission wavelengths clearly manifest switching behavior that takes place in predominantly two stages within similar [TFA] ranges for both **3a** and **3b**. Only in the emission spectra of **3a** is there seen a very weak iso-emissive region centered about 630 nm.

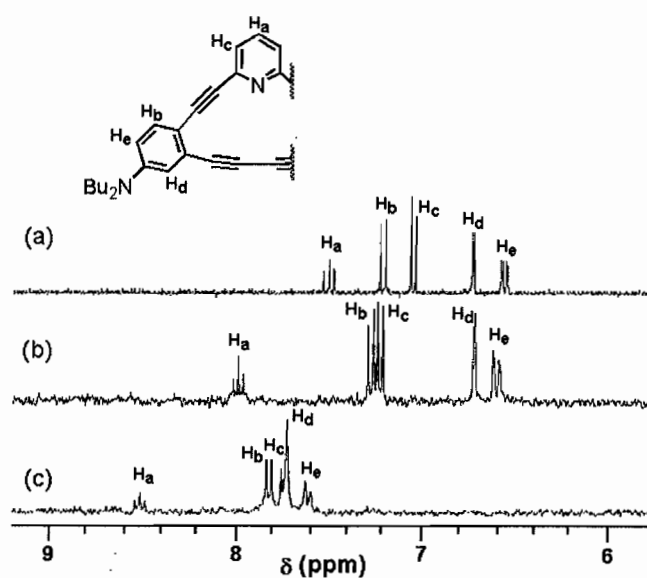


Figure 7. ^1H NMR spectra in CD_2Cl_2 expanded in the 6-9 ppm region of (a) top: **3a**; (b) middle: **3a** + 10^{-2} M TFA; (c) bottom: **3a** + $10^{-0.3}$ M TFA (exact H_b/H_c shifts indeterminate due to overlap).

To support the hypothesis that the pyridine nitrogen is predominantly protonated first, we prepared samples of **3a** in CD_2Cl_2 and observed the TFA-induced change in proton shifts of the ^1H NMR spectra. Figure 7 shows the 6-9 ppm region of solutions of **3a** alone and at 10^{-2} and $10^{-0.3}$ M TFA. Assignment of the protons is based on coupling

constants and previous data for **4**,^{4a} and is verified by correlation spectroscopy. Comparing the first two spectra clearly reveals significant downfield shifts of the pyridyl protons H_a ($\Delta\delta = 0.49$) and H_c ($\Delta\delta = 0.18$) and only slight shifts of the donor segment protons ($\Delta\delta = 0.01$ - 0.07), indicative of protonation of the pyridine nitrogen. At $10^{-0.3}$ M TFA, all protons are shifted far downfield. The greater degree of shifting in the donor segment protons ($\Delta\delta = 1.00$ for both H_d and H_e), in this case indicates protonation at one or both of the dibutylamino nitrogens and generation of an electron-deficient conjugated π -system. A similar but less dramatic stepwise shifting is observed for **3b**. The order of protonation is supported by computations, which indicate that the pyridine-protonated species are 19-31 kcal mol⁻¹ lower in energy than the donor-protonated species (See experimental section Figures 13 and 14).

Conclusions

We have prepared an isomeric pair of donor-functionalized DBPAs that visibly fluoresce and display weak intramolecular charge transfer behavior. The spectroscopic profiles of the readily-obtained molecules illustrate the effect of nitrogen placement in the pyridine acceptor on the degree of conjugation. The unusually large increases in Stokes shifts upon cyclization are believed to result from the combination of donor π -electrons, LUMO localization on the diacetylene bridge formed in the last synthetic step, and the cross-conjugated “kink” in the 15-membered macocycles. It has been demonstrated that fluorescence spectroscopy can be used to probe the behavior of a donor/acceptor fluorophore that can be protonated at both donor and acceptor sites. In particular, the

absorption and emission spectra for **3a** at moderate (10^{-2} M) acid concentration suggests a monoprotonated state with a particularly narrow optical band gap, prompting the question of its candidacy as a component in nonlinear optical devices. The dynamic emission switching bears striking resemblance to our and others' previous studies involving independent manipulation of frontier molecular orbitals, leading to potential applications as fluorescent ion sensors.^{9a,b,16} To our knowledge, this is the first reported instance of such behavior in conjugated acetylenic macrocycles. The calculated overlapping FMOs in neutral **3a** and **3b** further imply that independent manipulation of HOMOs and LUMOs may not require as dramatic of a spatial separation as previously assumed.

Experimental

General Methods. These have been described previously^{4a} and in Chapter I.

Precursor 6a. A mixture of 2,6-dibromopyridine (**5a**, 52 mg, 0.22 mmol), donor diyne **4^{4a}** (317 mg, 0.66 mmol), KOH (123 mg, 2.20 mmol), THF (20 mL), *i*-Pr₂NH (20 mL), and MeOH (1 mL) was bubbled with Ar with stirring for 30 min. Pd(PPh₃)₄ (15 mg, 0.013 mmol) and CuI (5 mg, 0.026 mmol) were quickly added and the mixture was bubbled for an additional 20 min. The temperature was raised to 55 °C and the reaction stirred until complete by TLC (ca. 18 h). The mixture was evaporated and the residue chromatographed on silica gel (2:1 hexanes:CH₂Cl₂) to yield **6a** (164 mg, 84%) as a yellow oil. ¹H NMR (300 MHz, CDCl₃): δ 7.53 (t, *J* = 7.2 Hz, 1H), 7.42 (d, *J* = 9.0 Hz, 2H), 7.34 (d, *J* = 7.8 Hz, 2H), 6.72 (d, *J* = 2.4 Hz, 2H), 6.54 (dd, *J* = 7.8, 2.4 Hz, 2H), 3.27 (t, *J* = 7.5 Hz, 8H), 1.56 (quin, *J* = 7.2 Hz, 8H), 1.35 (sext, *J* = 7.2 Hz, 8H), 1.15 (s,

42H), 0.96 (t, $J = 7.2$ Hz, 12H). ^{13}C NMR (75 MHz, CDCl_3): δ 148.1, 144.7, 135.7, 134.2, 127.4, 125.5, 115.4, 111.9, 110.8, 106.7, 93.5, 90.2, 90.2, 50.8, 29.5, 20.5, 19.0, 14.2, 11.7. IR (NaCl): ν 2955, 2937, 2858, 2202, 2147, 1655, 1639, 1594, 1572, 1552, 1534, 1509, 1465, 1438, 1397, 1367 cm^{-1} . MS (APCI): m/z ([isotope], %) 894.6 ($[\text{M}^+]$, 100), 895.6 ($[\text{M}^{+13}\text{C}]$, 78), 896.6 ($[\text{M}^{+2^{13}\text{C}}]$, 35). UV (CH_2Cl_2) λ_{max} (log ϵ): 346 (4.55), 390 (4.70). Em. λ_{max} : 427.

Precursor 6b. A mixture of 3,5-dibromopyridine (**5b**, 47 mg, 0.20 mmol), donor diyne **4^{4a}** (240 mg, 0.50 mmol), KOH (94 mg, 1.67 mmol), THF (20 mL), *i*-Pr₂NH (20 mL), and MeOH (1 mL) was bubbled with Ar with stirring for 30 min. Pd(PPh₃)₄ (14 mg, 0.012 mmol), and CuI (4.6 mg, 0.024 mmol) were quickly added and the mixture was bubbled for an additional 20 min. The temperature was raised to 55 °C and the reaction stirred until complete by TLC (ca. 18 h). The mixture was evaporated and the residue chromatographed on silica gel (2:1 hexanes: CH_2Cl_2) to yield **6b** (97 mg, 54%) as a yellow oil. ^1H NMR (300 MHz, CDCl_3): δ 8.55 (d, $J = 2.1$ Hz, 2H), 7.84 (t, $J = 2.1$ Hz, 1H), 7.32 (d, $J = 9.0$ Hz, 2H), 6.73 (d, $J = 2.8$ Hz, 2H), 6.55 (dd, $J = 9.0, 2.8$ Hz, 2H), 3.28 (t, $J = 7.8$ Hz, 8H), 1.57 (quin, $J = 7.5$ Hz, 8H), 1.38 (sext, $J = 7.8$ Hz, 8H), 1.17 (s, 42H), 0.96 (t, $J = 7.2$ Hz, 12H). ^{13}C NMR (75 MHz, CDCl_3): δ 150.0, 148.0, 140.5, 136.6, 127.1, 121.1, 115.5, 111.9, 110.9, 106.5, 93.8, 93.5, 86.7, 50.8, 29.5, 20.5, 19.0, 14.2, 11.6. IR (NaCl): ν 2952, 2938, 2859, 2208, 2151, 1718, 1593, 1568, 1536, 1503, 1464, 1432, 1396, 1371 cm^{-1} . MS (APCI): m/z ([isotope], %) 894.6 ($[\text{M}^+]$, 100), 895.6 ($[\text{M}^{+13}\text{C}]$, 70), 896.6 ($[\text{M}^{+2^{13}\text{C}}]$, 33). UV (CH_2Cl_2) λ_{max} (log ϵ): 348 (4.65), 383 (4.72). Em. λ_{max} : 421.

Annulene 3a. Precursor **6a** (120 mg, 0.13 mmol) was dissolved in THF (20 mL), Et₂O (20 mL), and MeOH (10 mL). TBAF (5.4 mL, 5.4 mmol, 1 M in THF) was added and the mixture stirred for ca. 18 h. The mixture was concentrated in vacuo, rediluted in Et₂O, and washed with H₂O (2×). The organic phase was dried (MgSO₄) and concentrated in vacuo to give an amber oil. The deprotected material was dissolved in pyridine (50 mL) and injected into a mixture of Cu(OAc)₂ (669 mg, 3.4 mmol) and CuCl (265 mg, 2.7 mmol) in pyridine (340 mL) and MeOH (50 mL) over 40 h with stirring at 65 °C. After injection was complete, the solution was stirred for an additional 24 h, then evaporated to a blue-green oil. The residue was redissolved in Et₂O and washed with H₂O (3×). The organic phase was dried (MgSO₄), concentrated in vacuo, and filtered through a pad of silica (1:1 hexanes: CH₂Cl₂) to yield **3a** (66 mg, 85%) as a bright yellow solid. Mp: 131-133 °C. ¹H NMR (CDCl₃): δ 7.49 (t, *J* = 7.8 Hz, 1H), 7.23 (d, *J* = 8.7 Hz, 2H), 7.07 (d, *J* = 7.8 Hz, 2H), 6.72 (d, *J* = 2.7 Hz, 2H), 6.51 (dd, *J* = 8.7, 2.7 Hz, 2H), 3.25 (t, *J* = 7.8 Hz, 8H), 1.54 (quin, *J* = 7.8 Hz, 8H), 1.34 (sext, *J* = 7.8 Hz, 8H), 0.96 (t, *J* = 7.2 Hz, 12H). ¹³C NMR (CDCl₃): δ 148.2, 145.4, 136.9, 131.7, 129.0, 121.2, 115.0, 112.3, 112.1, 94.1, 92.2, 82.3, 78.3, 51.0, 29.5, 20.5, 14.2. IR (NaCl): ν 2951, 2924, 2866, 2193, 1682, 1652, 1591, 1570, 1533, 1502, 1451, 1366 cm⁻¹. MS (APCI): *m/z* ([isotope], %) 580.4 ([M⁺], 100), 581.4 ([M⁺¹³C], 44), 582.4 ([M⁺²¹³C], 8). UV (CH₂Cl₂) λ_{max} (log ε): 347 (4.90), 407 (4.24). Em. λ_{max}: 490.

Annulene 3b. Precursor **6b** (90 mg, 0.10 mmol) was dissolved in THF (20 mL), Et₂O (20 mL), and MeOH (10 mL). TBAF (6.0 mL, 6.0 mmol, 1 M in THF) was added and the mixture stirred for ca. 18 h. The mixture was concentrated in vacuo, rediluted in Et₂O,

and washed with H₂O (2×). The organic phase was dried (MgSO₄) and concentrated in vacuo to give an amber oil. The deprotected material was dissolved in pyridine (37 mL) and injected into a mixture of Cu(OAc)₂ (499 mg, 2.5 mmol) and CuCl (198 mg, 2.0 mmol) in pyridine (254 mL) and MeOH (37 mL) over 40 h with stirring at 65 °C. After injection was complete, the solution was stirred for an additional 24 h, then evaporated to a blue-green oil. The residue was redissolved in Et₂O and washed in H₂O (3×). The organic phase was dried (MgSO₄), concentrated in vacuo, and filtered through a pad of silica (1:1 hexanes: CH₂Cl₂) to yield **3b** (25 mg, 77%) as a yellow solid. Mp: 181-183 °C. ¹H NMR (CDCl₃): δ 8.75 (t, *J* = 1.5 Hz, 1H), 8.39 (d, *J* = 1.5 Hz, 2H), 7.24 (d, *J* = 9.0 Hz, 2H), 6.77 (d, *J* = 2.4 Hz, 2H), 6.58 (dd, *J* = 9.0, 2.4 Hz, 2H), 3.27 (t, *J* = 8.1 Hz, 8H), 1.56 (quin, *J* = 8.1 Hz, 8H), 1.32 (sext, *J* = 7.5 Hz, 8H), 0.97 (t, *J* = 7.5 Hz, 12H). ¹³C NMR (CDCl₃): δ 150.5, 148.1, 145.4, 131.2, 127.7, 122.0, 115.3, 112.5, 112.2, 100.2, 98.1, 90.6, 83.2, 51.0, 29.5, 20.5, 14.3. IR (NaCl): ν 2951, 2925, 2866, 2218, 2191, 1771, 1739, 1696, 1684, 1650, 1594, 1567, 1557, 1538, 1504, 1455, 1399, 1365 cm⁻¹. MS (APCI): *m/z* ([isotope], %) 580.4 ([M⁺], 100), 581.4 ([M⁺¹³C], 37), 582.3 ([M⁺2¹³C], 11). UV (CH₂Cl₂) λ_{max} (log ε): 352 (4.70), 408 (4.09). Em. λ_{max}: 494.

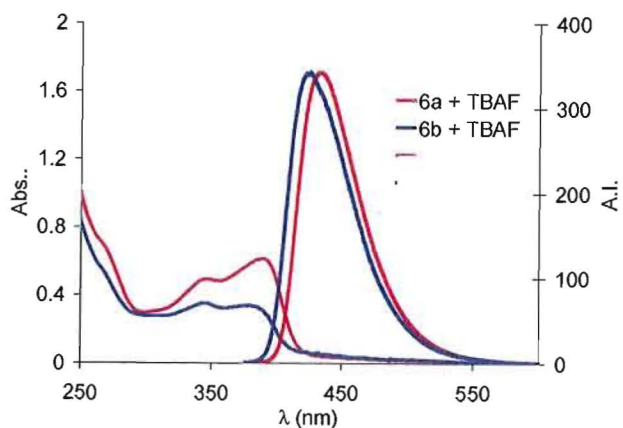


Figure 8. Absorption (left) and emission (right) spectra of **6a** and **6b** treated with excess TBAF in CH_2Cl_2 . Excitation at 365 nm.

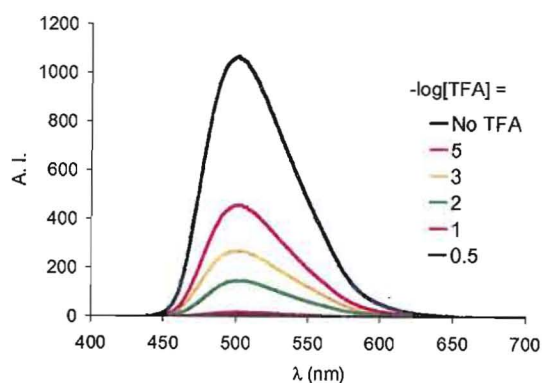


Figure 9. Emission spectra of TFA titration of **3a** in MeOH at indicated $-\log[\text{TFA}]$. Excitation at 365 nm.

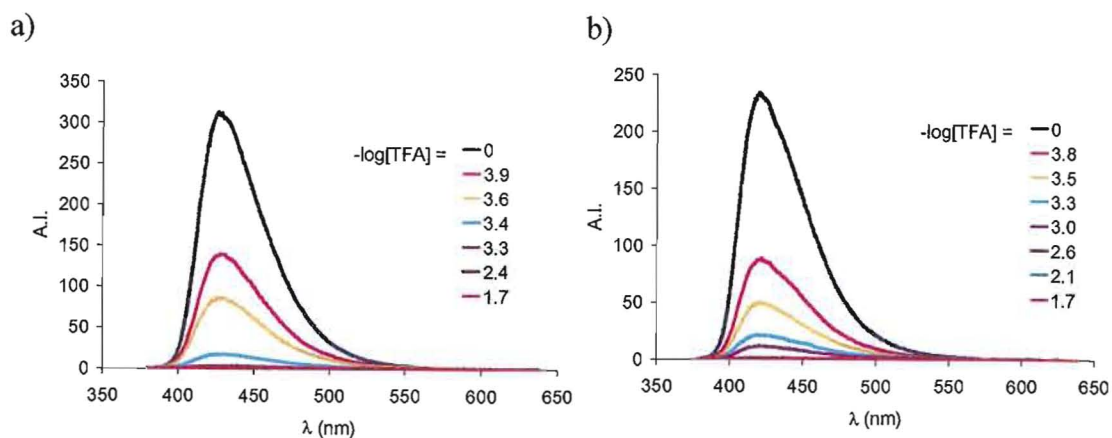


Figure 10. Emission spectra of TFA titration of a) **6a** and b) **6b** in CH_2Cl_2 at indicated $-\log[\text{TFA}]$. Excitation at 365 nm.

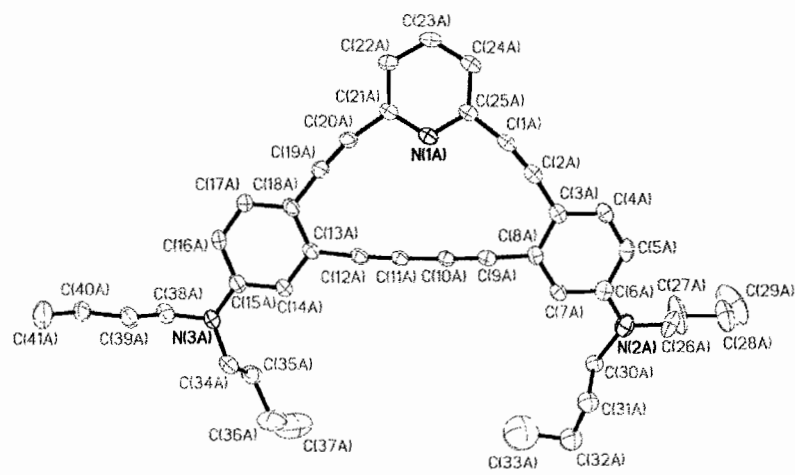
Crystallographic Data. X-ray diffraction experiments for **3a** and **3b** were carried out on a Bruker Smart Apex diffractometer at 173(2) K using MoK α radiation ($\lambda = 0.71070$ Å). Absorption corrections were done by SADABS[*]. The structure was solved using direct methods and refined with full-matrix least-squares methods based on F^2 . Non-hydrogen atoms were refined with anisotropic thermal parameters. The H atoms were treated in calculated positions. Some of carbon atoms in the terminal –Bu groups are disordered over two positions in ratio 1:1. The disordered groups were refined with restrictions on the C–C distances; in the refinement the standard C–C distances were used as targets for the C–C bonds. The hexane solvent molecule in **3a** is highly disordered around an inversion center and was treated by SQUEEZE[**]; corrections of the X-ray data by SQUEEZE are 238 electron/cell; the required value is 200 electron/cell for four hexane molecules in the full unit cell. All calculations were performed using the SHELXTL package (v. 6.10) [***].

[*] G. M. Sheldrick, *Bruker/Siemens Area Detector Absorption Correction Program*, Bruker AXS, Madison, WI, 1998.

[**] Van der Sluis, P.; Spek, A. L. *Acta Cryst A* **1990**, *A46*, 194-201.

[***] SHELXTL-6.10 "Program for Structure Solution, Refinement and Presentation"
BRUKER AXS Inc., 5465 East Cheryl Parkway, Madison, WI 53711-5373 USA

a)



b)

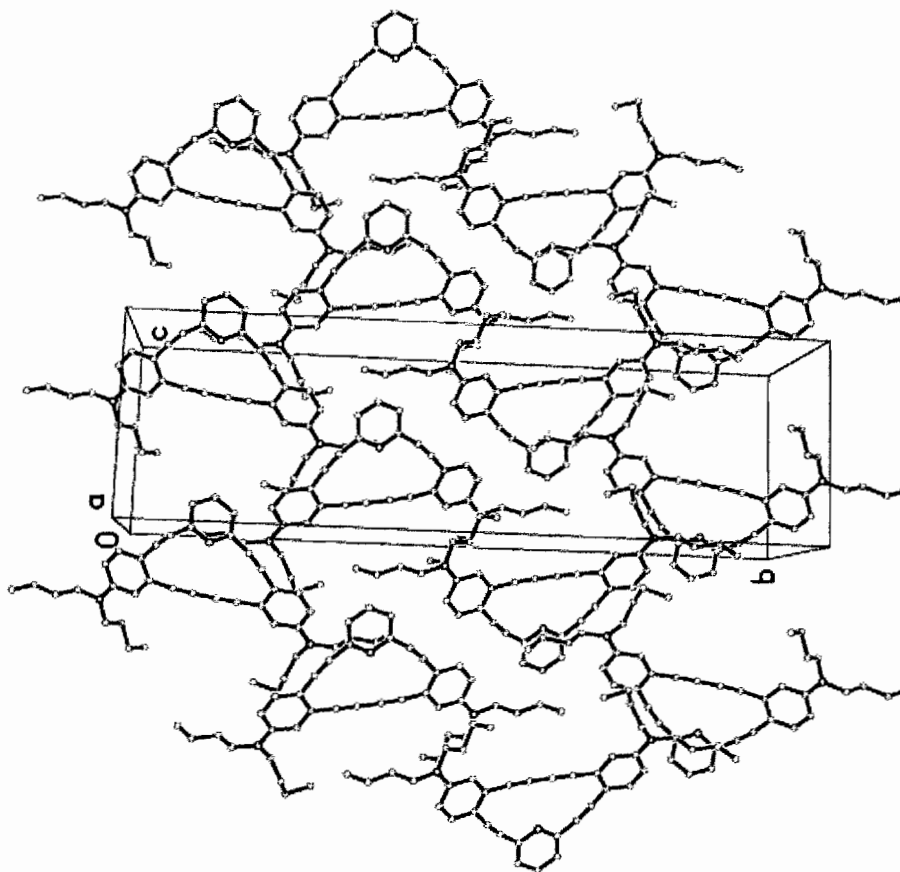
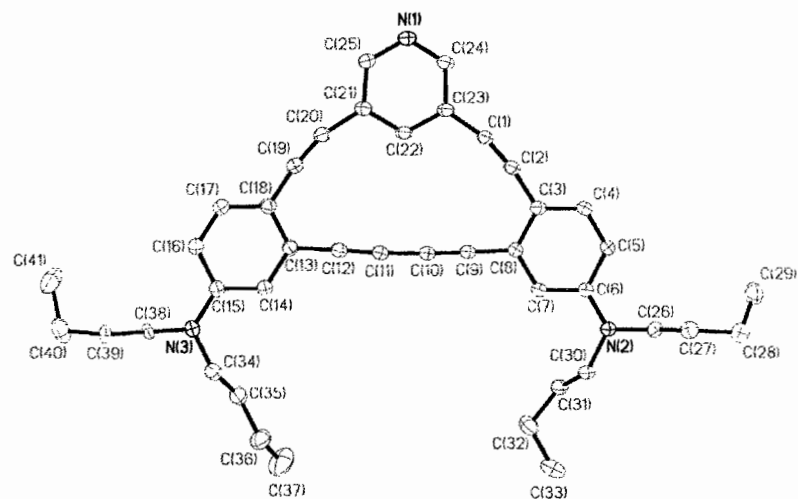


Figure 11. a) X-ray crystal structure and b) packing in **3a**. Ellipsoids at 30% probability. Hexane solvent molecule removed for clarity.

Table 3. Crystal data and structure refinement for **3a**.

Empirical formula	C _{29.33} H _{34.67} N ₂	
Formula weight	415.26	
Temperature	173(2) K	
Wavelength	0.71073 Å	
Crystal system	Monoclinic	
Space group	P2(1)/c	
Unit cell dimensions	a = 17.086(5) Å	α = 90°.
	b = 38.818(12) Å	β = 96.540(5)°.
	c = 11.632(4) Å	γ = 90°.
Volume	7665(4) Å ³	
Z	12	
Density (calculated)	1.080 Mg/m ³	
Absorption coefficient	0.062 mm ⁻¹	
F(000)	2696	
Crystal size	0.40 x 0.14 x 0.08 mm ³	
Theta range for data collection	1.05 to 25.00°.	
Index ranges	-20 ≤ h ≤ 20, -46 ≤ k ≤ 46, -13 ≤ l ≤ 13	
Reflections collected	72718	
Independent reflections	13493 [R(int) = 0.0846]	
Completeness to theta = 25.00°	99.9 %	
Absorption correction	Semi-empirical from equivalents	
Max. and min. transmission	0.9950 and 0.9755	
Refinement method	Full-matrix least-squares on F ²	
Data / restraints / parameters	13493 / 19 / 792	
Goodness-of-fit on F ²	1.041	
Final R indices [I > 2σ(I)]	R1 = 0.0981, wR2 = 0.2457	
R indices (all data)	R1 = 0.1590, wR2 = 0.2805	
Largest diff. peak and hole	0.699 and -0.322 e.Å ⁻³	

a)



b)

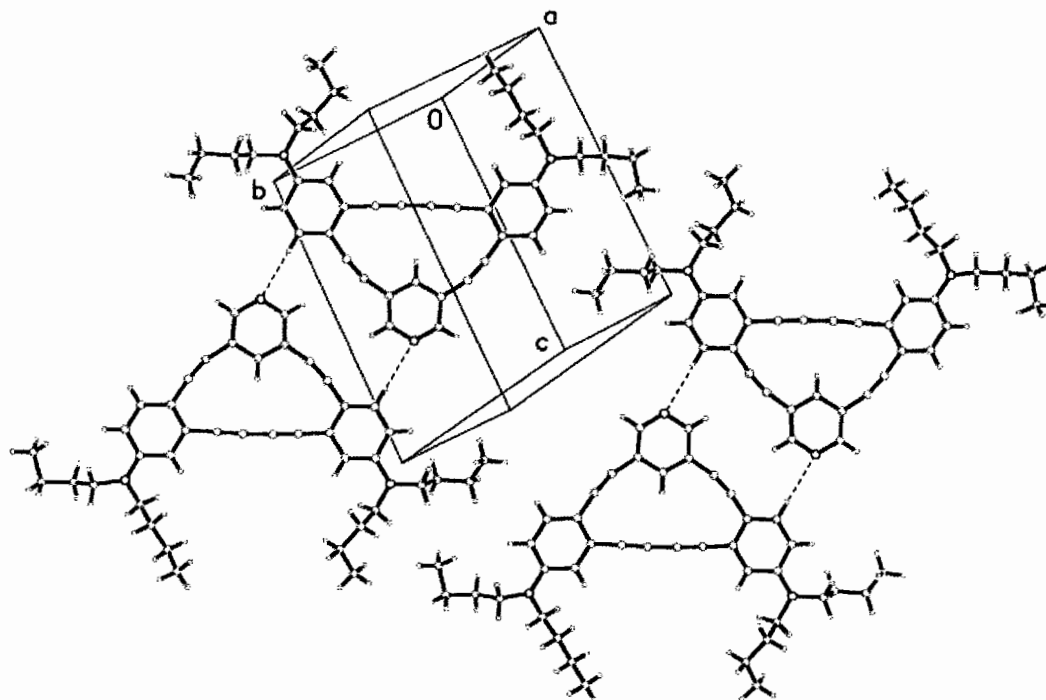


Figure 12. a) Molecular structure and b) packing in **3b**. Ellipsoids at 30% probability. Hexane solvent molecule removed for clarity.

Table 4. Crystal data and structure refinement for **3b**.

Empirical formula	C43 H49 N3 O	
Formula weight	623.85	
Temperature	173(2) K	
Wavelength	0.71073 Å	
Crystal system	Triclinic	
Space group	P-1	
Unit cell dimensions	a = 9.182(2) Å	$\alpha = 75.347(4)^\circ$.
	b = 14.218(4) Å	$\beta = 82.272(4)^\circ$.
	c = 14.920(4) Å	$\gamma = 76.899(4)^\circ$.
Volume	1829.2(8) Å ³	
Z	2	
Density (calculated)	1.133 Mg/m ³	
Absorption coefficient	0.067 mm ⁻¹	
F(000)	672	
Crystal size	0.25 x 0.16 x 0.11 mm ³	
Theta range for data collection	1.42 to 25.00°.	
Index ranges	-10 ≤ h ≤ 10, -16 ≤ k ≤ 16, -17 ≤ l ≤ 17	
Reflections collected	17672	
Independent reflections	6418 [R(int) = 0.0182]	
Completeness to theta = 25.00°	99.8 %	
Absorption correction	Semi-empirical from equivalents	
Max. and min. transmission	0.9926 and 0.9833	
Refinement method	Full-matrix least-squares on F ²	
Data / restraints / parameters	6418 / 0 / 415	
Goodness-of-fit on F ²	1.051	
Final R indices [I > 2σ(I)]	R1 = 0.0488, wR2 = 0.1403	
R indices (all data)	R1 = 0.0604, wR2 = 0.1498	
Largest diff. peak and hole	0.358 and -0.316 e.Å ⁻³	

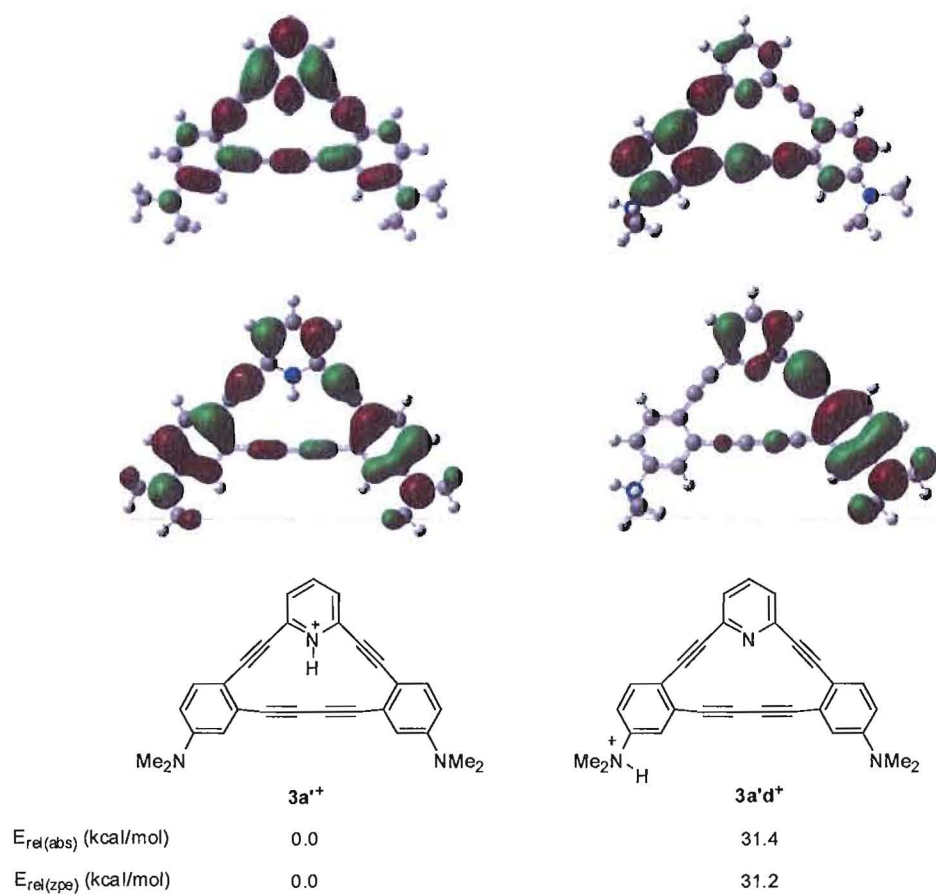


Figure 13. Calculated (B3LYP/6-31G*) molecular orbitals and relative energies of **3a³⁺** and **3a^{d+}**.

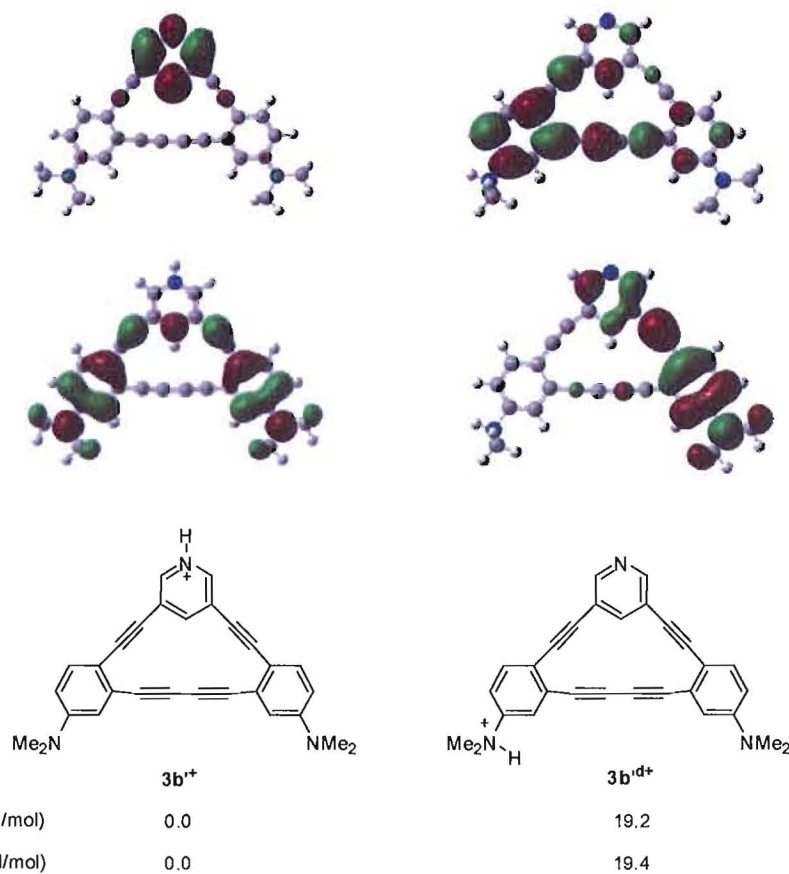


Figure 14. Calculated (B3LYP/6-31G*) molecular orbitals and relative energies of **3b'⁺** and **3b'^{d+}**.

Table 5. Calculated band gap energies of **3a'/3a'⁺** and **3b'/3b'⁺**.

Molecule	E (HOMO) ^a	E (LUMO) ^a	E (eV)	Wavelength (nm)	Calc. Dipole
3a'	-0.176	-0.057	3.2381804	383.1473	4.2455
3a'⁺	-0.283	-0.194	2.4218324	512.2981	0.0115
3b'	-0.182	-0.064	3.2109688	386.3943	8.4635
3b'⁺	-0.276	-0.189	2.3674092	524.0751	5.6664

^a in Hartrees.

Bridge to Chapter IV

Chapter IV examines a series of tetrakis(phenylethynyl)benzenes (TPEBs) and bis[14] and bis[15]DBAs functionalized with di-*n*-butylamino donor groups and various fluorinated acceptor groups. This work takes advantage of the efficient inductive electron withdrawal ability of fluorines, which occurs solely through the σ -framework of the acceptor units, rather than via resonance as with the directly conjugated 2- and 4-pyridyl groups examined previously. The apparent efficiency of the cross-conjugated 3-pyridyl systems implies good potential for these weaker donor/acceptor fluorophores and may additionally impart greater stability and processability versus the more directly conjugated known nitro- and cyano-functionalized analogues, which will also be discussed along with and in comparison to the novel compounds of this original work. Again, the effects of enforced planarization on the conjugated systems will be examined by comparison between the DBAs and their related TPEBs.

CHAPTER IV

STRUCTURE-PROPERTY RELATIONSHIPS OF FLUORINATED DONOR/ACCEPTOR TETRAKIS(PHENYLETHYNYL)BENZENES AND BIS(DEHYDROBENZOANNULENO)BENZENES

Introduction

This chapter was co-authored with John M. Monson, who assisted with synthesis of certain compounds, and Professor Michael M. Haley, who conceptualized the project and provided editorial assistance. This chapter includes work that was published in the *Journal of Organic Chemistry* (2008, ASAP Article, © 2008, American Chemical Society).

Donor/acceptor-substituted tetrakis(phenylethynyl)benzenes (TPEBs)¹ are two-dimensional, carbon-rich chromophores² which exhibit a high degree of conjugation, and consequently possess multiple pathways for intramolecular electronic and photonic transfer. These cruciform-shaped molecules exhibit spatial separation of their frontier molecular orbitals, making TPEBs excellent candidates for a variety of advanced materials applications, such as organic light-emitting diodes, thin film organic transistors, solar cells, and optical storage devices.³⁻⁵ Carbon-rich cruciforms already possess

demonstrated potential as nonlinear optical/two-photon absorption⁶ and fluorescent sensing materials.⁷

Our previous studies have focused on the syntheses and spectroscopic characteristics of bisdonor/bisacceptor TPEBs incorporating dibutylaniline groups as the donor groups and nitrophenyl,^{1a,b} pyridyl,^{1c} or benzonitrile^{1a,d} groups as the acceptors. We showed that adjusting the identity of the acceptor group and topology of the chromophore led to predictable variations in the electronic absorption and emission profiles. These small structural variations allow fine-tuning of optical band gap energies and emissive wavelengths for customized optical materials applications. To date though, we have not examined inductive accepting groups that participate in charge transfer through the σ -framework only.⁸ Such structures may display similar optical behavior, but with greater chemical stability or bulk processing characteristics. Herein we describe further studies in acceptor group variation with the addition of benzotrifluoride- and pentafluorophenyl-functionalized donor/acceptor TPEBs (**1-9**, Figure 1) and the impact of the variations on the optical properties. Of particular interest is comparison of the properties of the inductive fluoro accepting groups of **1-9** to those of the nitrile (**10-12**) and nitro (**13-15**) resonance acceptors. By undertaking parallel investigations of chromophores with both one (**1-3**) and two (**4-6**) trifluoromethyl groups per acceptor arene, we can also evaluate the cumulative effect of the number of acceptors per arene ring. Since the electron withdrawal is through-bond only, the position of the $-\text{CF}_3$ groups relative to the acetylene bridge should have little (if any) impact on the optical properties, allowing us to maintain symmetry and thus avoid dissimilar net dipole effects between isomers.

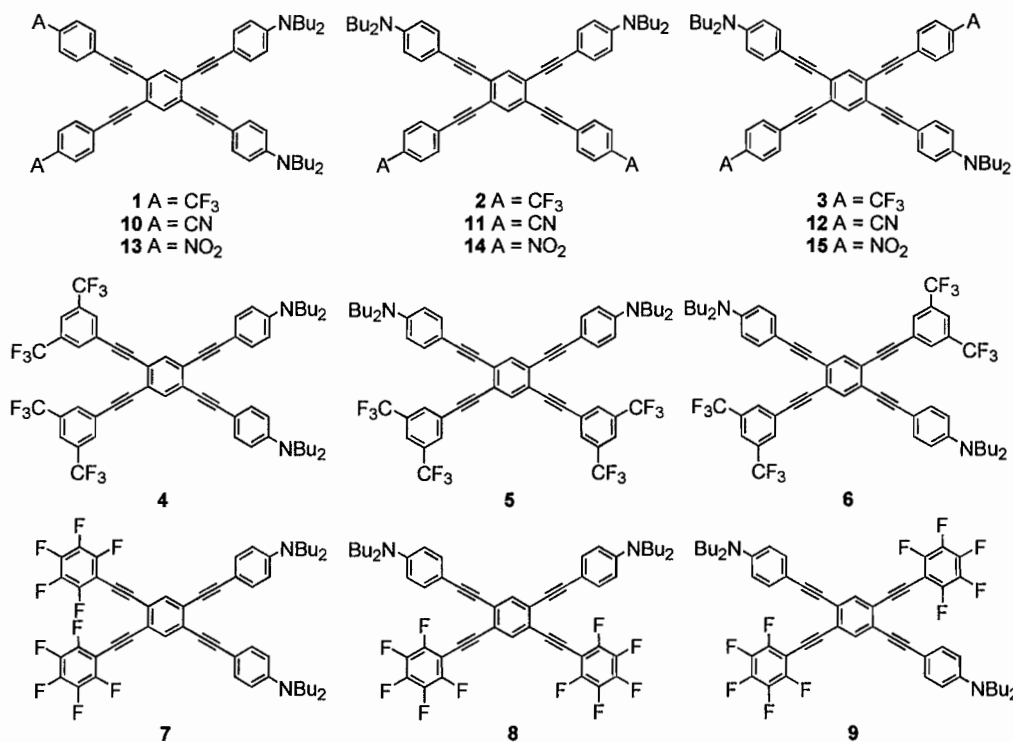


Figure 1. Target donor/acceptor TPEBs **1-9** with benzotrifluoride and perfluorophenyl acceptor units, and known nitrophenyl and benzonitrile acceptor TPEBs **10-15**.

We have had a longstanding interest in the effects of enforced planarization on the photophysics and materials properties of phenyl-acetylene scaffolding.⁹ Accordingly, we also targeted bis(dehydrobenzo[14]- and [15]annuleno)benzene (bisDBA) macrocycle analogues of **1-3** (i.e., **16-21**, Figure 2), in an attempt to derive structure-property characteristics from comparison both to the acyclic variants as well as the previously reported nitro-functionalized DBAs (**22-26**).^{1b} In addition to planarization, **16-21** possess additional conjugated chromophore pathways, and [15]DBAs **19-21** contain a cross-conjugated pathway at the central arene.

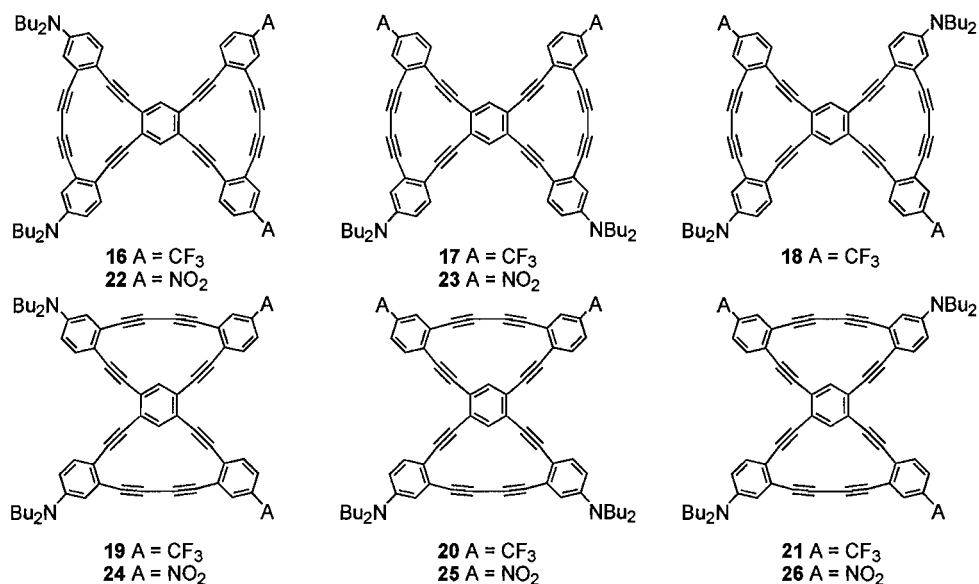


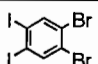
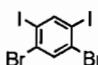
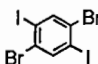
Figure 2. Target donor/acceptor DBAs **16-21** with dibutylaniline donors and trifluoromethyl acceptors and previously reported^{1b} nitro-functionalized DBAs **22-26**.

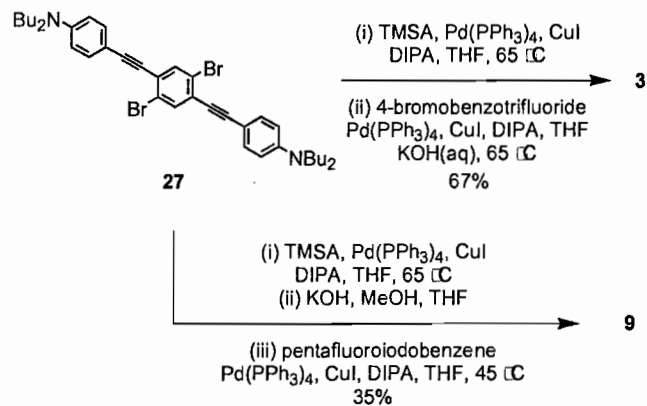
Results and Discussion

Synthesis. Scheme 1 illustrates the modular synthesis of **1-9**.

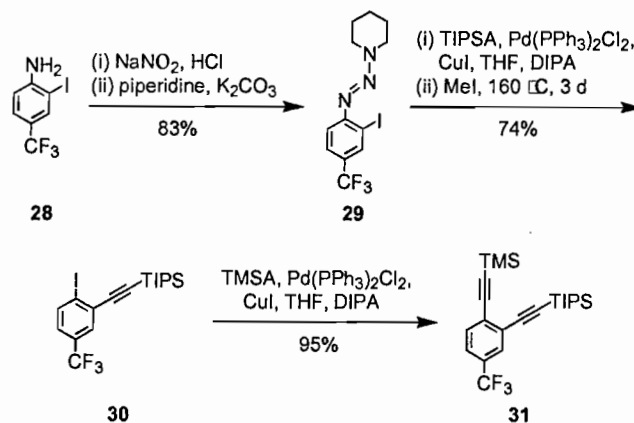
Trimethylsilylacetylene (TMSA) was cross-coupled¹⁰ to donor bromide **27**^{1c} at 65 °C, which was followed by an in situ deprotection/twofold cross-coupling¹¹ of the acceptor haloarene. In this way, TPEBs **1-6** were prepared from only three key intermediates, similar to the ethynylpyridine analogues.^{1c} In the case of **7-9**, stepwise deprotection after TMSA coupling to **27** was necessary to avoid nucleophilic substitution of the fluorinated arenes by alkoxide generated under the in situ deprotection conditions (Scheme 1, bottom).^{7b,12} A complete listing of yields is given in Table 1.

Table 1. Yields for preparation of TPEBs 1-9.

haloar- ene	donor coupling ^a	TMSA/4- bromo- benzotrifluoride coupling (pdt)	TMSA/3,5- bis(trifluoro- methyl)bromobenzene coupling (pdt)	TMSA/pentafluoro- iodobenzene coupling (pdt)
	70%	80% (1)	42% (4)	43% (7)
	89%	80% (2)	40% (5)	42% (8)
	89%	67% (3)	22% (6)	35% (9)

^a Reference 1c.**Scheme 1.** Representative syntheses of donor/acceptor TPEBs 3 and 9.

Scheme 2. Synthesis of acceptor segment **31**



BisDBAs **16-21** were prepared by the same general routes described for the nitro-functionalized analogues.^{1b,13} Donor and acceptor segments were synthesized separately and appended to the central arenes in a stepwise fashion. The differentially silylated bisalkyne acceptor segment was prepared from iodoaniline **28** (Scheme 2) first by conversion to triazene **29**. Sonogashira cross-coupling of triisopropylsilylacetylene (TIPSA) followed by displacement of the triazene at high temperature afforded iodoarene **30**. A second coupling of TMSA provided segment **31** in good overall yield. Selective deprotection of **31** under mildly basic conditions followed by coupling to isomers of dibromodiodobenzene furnished the acceptor-functionalized intermediates (e.g., **32**, Scheme 3). Cross-coupling of donor diyne **33**^{1b} at elevated temperature afforded the bisannulene precycles. Removal of the TIPS groups with TBAF followed by selective macrocyclization under either Pd- or Cu-mediated conditions gave the [14]- or [15]-membered bisDBAs, respectively.^{1f} For example, precycle **34** can be converted to either bisDBA **17** or **20**. Yields are given in Table 2. Compounds deriving from the 1,5-

dibromo-2,4-diiodobenzene starting arene (the “*meta*” isomers) consistently proceeded in higher yields. This is likely due to the lack of steric hindrance during the two-fold couplings as well as having withdrawing groups (bromo in the first case, acceptor segments in the second case) *para* to the coupling site on the arene, since the Sonogashira reaction has a well-known preference for electron-poor arenes.⁹

Scheme 3. Representative synthesis of DBAs 17 and 20

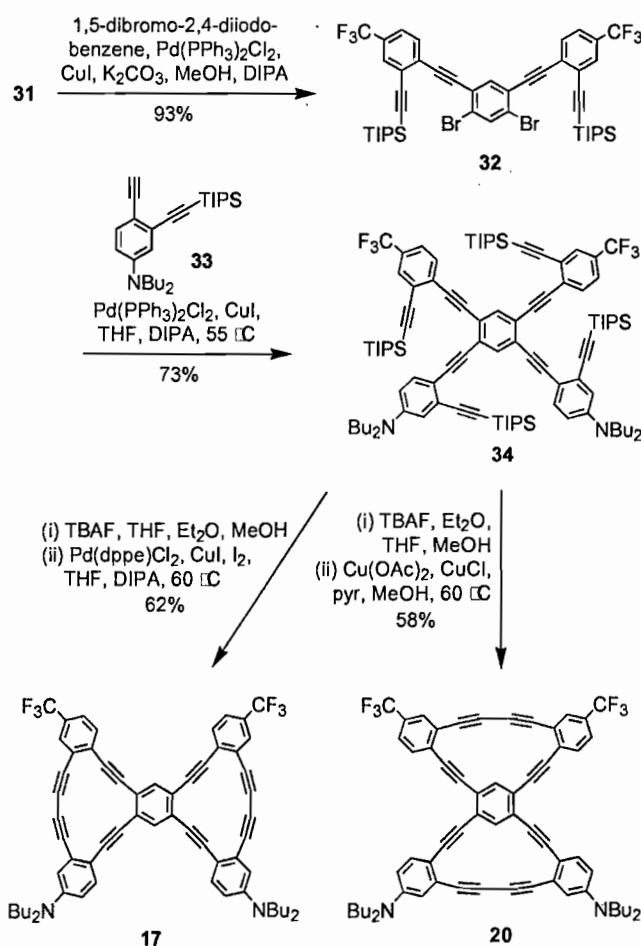
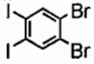
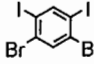
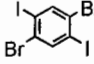


Table 2. Yields for preparation of DBAs 16-21.

haloarene	acceptor coupling	donor coupling	cyclization	bisDBA
	92%	18%	14%	16
			64%	19
	93%	73%	62%	17
			58%	20
	86%	37%	33%	18
			60%	21

Electronic Absorption Spectra. The electronic absorption spectra of TPEBs 1-9 in dichloromethane are shown in Figure 3, along with the spectra of known 10-15 for comparison.^{1a,b,d} Lowest-energy bands, along with the emission data, are given in Table 3. The next higher bands are listed in the experimental section. All donor/acceptor-functionalized systems display a characteristic broad, low-energy band in the 400-500 nm region with extinction coefficients of ca. 20,000-60,000 M⁻¹ cm⁻¹, indicative of intramolecular charge transfer.^{1,13,14} Calculated molecular orbital plots for 13-15 and 22-26 show dramatic spatial separation of frontier molecular orbitals (FMOs) upon donor/acceptor functionalization.^{1b} Calculations of the FMOs of the ethynylpyridine analogues show similar but weakened charge transfer polarization.^{1c} With this in mind, we expect the same properties in the cases of 1-9. The trend in longest wavelength λ_{\max} , which is correlated to the optical band gap, holds across the substitution isomers of each acceptor variant triad: isomers in which like groups are *ortho* to each other (1, 4, and 7, as well as 10 and 13) display the highest energy band gaps, whereas isomers in which they

are *para* (**3**, **6**, and **9**, as well as **12** and **15**) display the lowest. TPEBs **7-9** with perfluorinated arene acceptor rings exhibit the smallest band gaps of the acyclic compounds presented here. It is notable that **9** has a λ_{max} that appears at least as red-shifted as **15**, but in the latter case the band is a shoulder and too broadened for accurate comparison. The λ_{max} cutoff for **15**, however, extends well past 550 nm. Previous studies¹ indicate an inverse relationship with ground state net dipole: the TPEBs with the lowest calculated net dipole (the *para* isomers) show the most red-shifted absorbance and hence smallest band gap, while those with the highest (the *ortho* isomers) are the most blue-shifted. This trend contradicts conventional theories, which predict a strong correlation between band gap energy and conjugation efficiency:¹⁴ the *ortho* and *meta* isomers, which have two linear charge transfer conduits, possess the larger optical band gaps, while the *para* isomers have charge transfer pathways with bent geometries but the smallest band gaps. These results parallel the findings of Diederich et al.,¹⁵ who discovered similar contradictions in the case of donor-substituted cyanoethynylethenes, and warned of the limitations of UV/Vis spectrophotometry as a measure of conjugation. Meier et al. described similar effects with elongated phenyl-acetylenic chromophores.¹⁶ In both cases, the usefulness of UV/Vis data is relegated to probing only the change in charge transfer on going from the ground state to the excited state, and not as a measure of conjugation, for which other methods including ground state geometry and energy calculations are more appropriate.

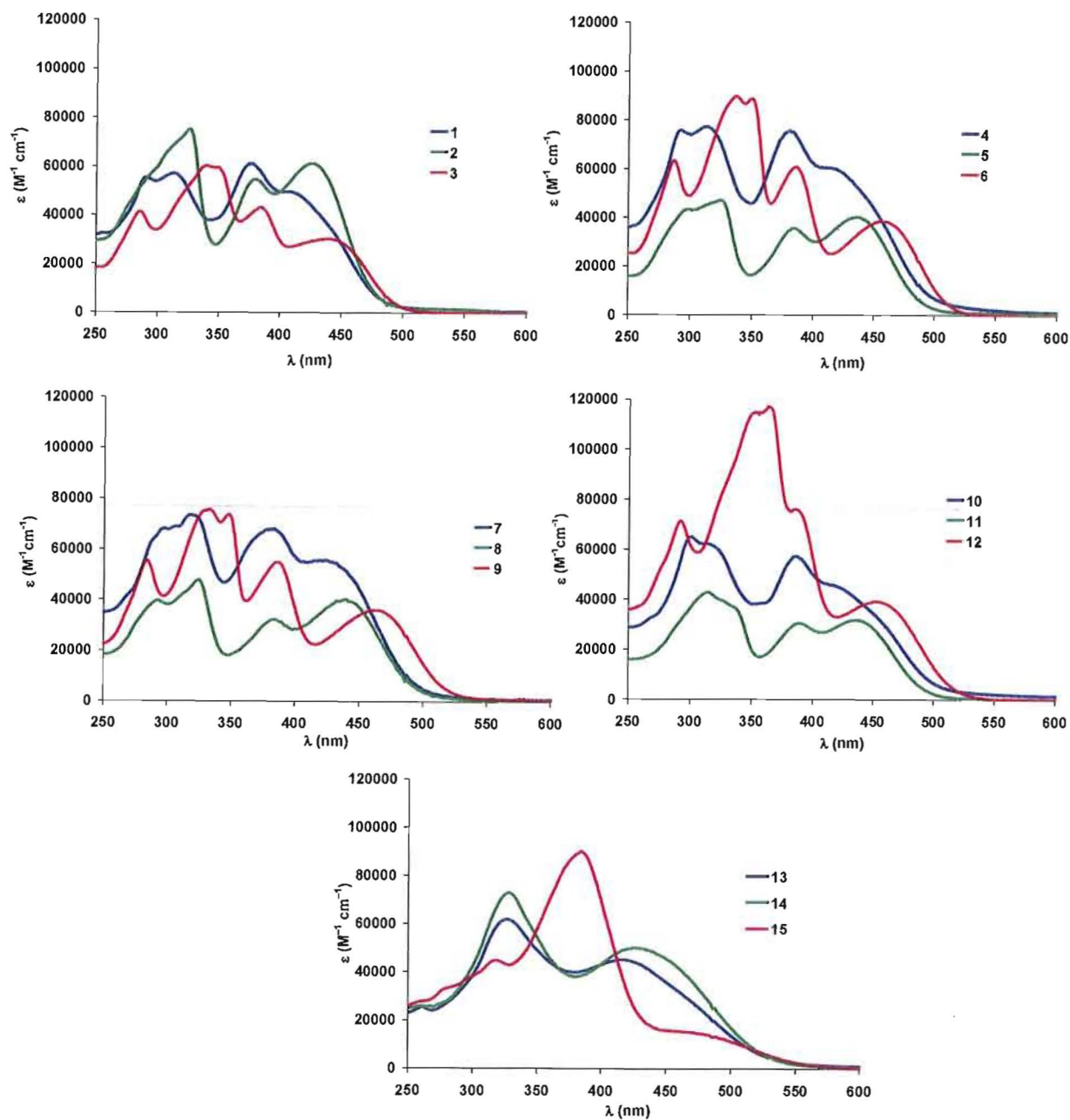


Figure 3. Electronic absorption spectra of (a) 1-3, (b) 4-6, (c) 7-9, (d) 10-12,^{1d} and (e) 13-15.^{5,6} All spectra recorded in CH_2Cl_2 at analyte concentrations of 15-25 μM .

Table 3. Electronic absorption and emission data for TPEBs 1-15.

compd	Lowest Energy Abs λ_{\max} [nm] (ϵ [M^{-1} cm^{-1}])	Em λ_{\max} [nm]	Stokes Shift	Φ_F^a
1	407 ^b (49,560)	544	137	0.44
2	427 (61,120)	541	114	0.38
3	438 (30,380)	546	108	0.50
4	410 ^b (60,380)	556	146	0.31
5	433 (25,460)	552	119	0.34
6	456 (38,510)	561	105	0.25
7	423 (55,690)	556	133	0.17
8	438 (40,090)	555	117	0.30
9	462 (36,100)	563	101	0.14
10	416 ^b (45,700)	563	147	0.26
11	435 (31,640)	557	122	0.35
12	454 (39,250)	563	109	0.25
13	417 (45,200)	563	146	<0.01
14	426 (50,100)	552	126	<0.01
15	448 ^b (15,690)	557	109	<0.01

^a calculated relative to fluorescein at pH=8. ^b approximate value as band is only a shoulder.

Even with these limitations, it is likely that TPEBs 1-9 participate in a good degree of intramolecular charge transfer. The benzonitrile accepting group is weak relative to the nitrophenyl group,¹⁶ yet produces band gaps in the same general range and extinction coefficient (compare Figures 3d and e and *cf.* Table 3). Equally impressive are the benzotrifluoride acceptor systems 1-6, with band gaps averaging only a few nm more

blue-shifted. Since there are no viable resonance forms for the charge-separated excited state (which may in fact be distinct from a neutral excited state¹⁷), electron withdrawal occurs principally via induction through the σ -framework. This would intuitively imply a larger optical band gap, and hence a dramatic hypsochromic shift in the absorbance spectra. From Figures 3a-c, however, this is not entirely the case: TPEBs **1-9** display the same charge transfer properties as the resonance acceptors with bands in the same region of the UV/Vis spectrum. The intensities of the longest wavelength bands are comparatively high ($\epsilon = 50,000\text{-}60,000 \text{ M}^{-1} \text{ cm}^{-1}$) for **1**, **2**, **4**, and **7**, all of which have linear charge transfer pathways. Taken together, these data provide further illustration of the potential limitations of electronic absorption spectra in evaluating the complex interrelationships between optical band gap, conjugation, and charge transfer.

Comparison of **1-3** to **4-6** reveals the cumulative effect of the number of acceptor groups. TPEBs **1-3** possess one $-\text{CF}_3$ group per acceptor arene *para* to the acetylene bridge, while **4-6** possess two $-\text{CF}_3$ groups at the *meta* positions. Increasing the number of acceptor groups results in a 3-24 nm bathochromic shift in the absorption spectrum, depending on substitution isomer and solvent. Shifts are most dramatic in the *para* isomer **6** and least in the *ortho* isomer **4**. The inductive nature of the electron acceptors should negate any effect of the relative positions of the $-\text{CF}_3$ groups on the acceptor arene, allowing observation of the effect of changing only the number of acceptor units. Furthermore, use of symmetric acceptor units should eliminate any skewing effect of dissimilar net dipoles on the absorption and emission data. A reasonable inference from

the data therefore is that “acceptor density” can be used to provide further fine-tuning of the net acceptor strength and hence the optoelectronic properties.

Absorption spectra of DBAs **16-21** are shown in Figure 4 and data given in Table 4. There is a 27-67 nm (depending on isomer) bathochromic shift in the lowest energy band upon planarization compared to **1-3**, reflecting the enhanced conjugation effects from increased π -orbital overlap.¹ The bis[15]DBAs **19-21** are red shifted by between 5 and 24 nm relative to bis[14]DBAs **16-18**. A side-by-side comparison of the spectra of TPEBs, bis[14]DBAs and bis[15]DBAs is exemplified in Figure 5. The lowest energy bands in **16-21** are at somewhat shorter wavelengths than **22-26** due to the weaker inductive acceptors. It is noteworthy that the *ortho* to *meta* to *para* isomer trend in band wavelength holds for **16-18**, but not for **19-21**: **19** is slightly red shifted from **20**. Also of note is the relative sharpness of these bands compared to the corresponding broad bands in **16-18**, which may represent increased vibronic fine structure both from the rigidified molecular geometry as well as the cross-conjugated pathway.^{1c} BisDBAs **19-21** also possess somewhat higher molar extinction coefficients than **16-18**. This effect was also observed in **22-26**, and is likely due to the greater linearity of the phenyl-acetylene pathways in [15]DBAs compared to [14]DBAs, which have been shown by computation and X-ray crystallography to possess greater distortion of the sp-carbon bond angles.^{1b} Also as in **22-26**, the *meta* isomers show the most intense charge transfer band, and the *para* isomers the least. It is uncertain why this is the case, but as with the TPEBs, the *para* isomers represent quadrupolar chromophores, which may experience significant solvent

stabilization of the excited state similar to a highly dipolar chromophore, e.g., the *ortho* isomers.¹⁵

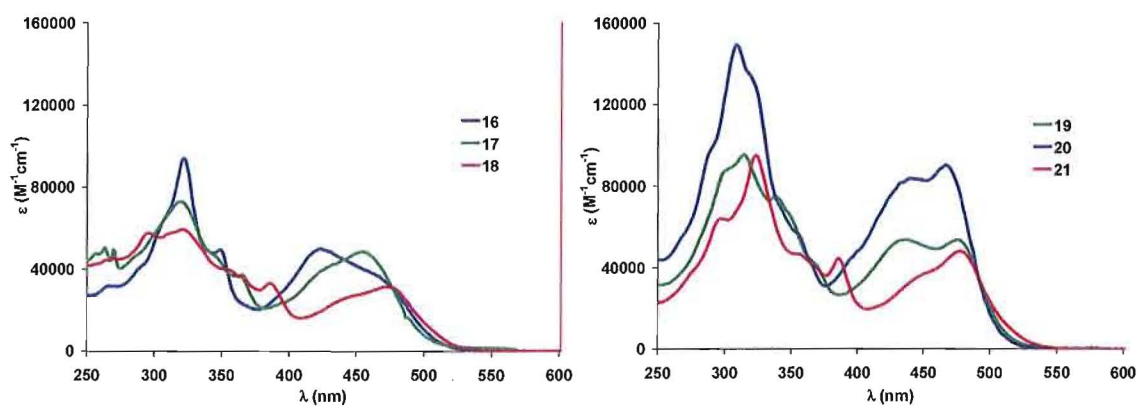


Figure 4. Electronic absorption spectra of (a) **16-18** and (b) **19-21**. All spectra recorded in CH₂Cl₂ at analyte concentrations of 10-20 μ M.

Table 4. Electronic absorption and emission data for BisDBAs **16-21**.

compd	Lowest Energy Abs λ_{\max} [nm] (ϵ [$M^{-1}cm^{-1}$])	Em λ_{\max} [nm]	Stokes Shift	Φ_F^a
16	450 ^b (41,430)	554	104	0.35
17	454 (48,310)	544	90	0.46
18	472 (31,480)	555	83	0.33
19	474 (53,300)	550	76	0.23
20	466 (90,020)	551	85	0.15
21	477 (48,080)	558	81	0.25

^a calculated relative to fluorescein at pH=8. ^b approximate value as band is only a shoulder.

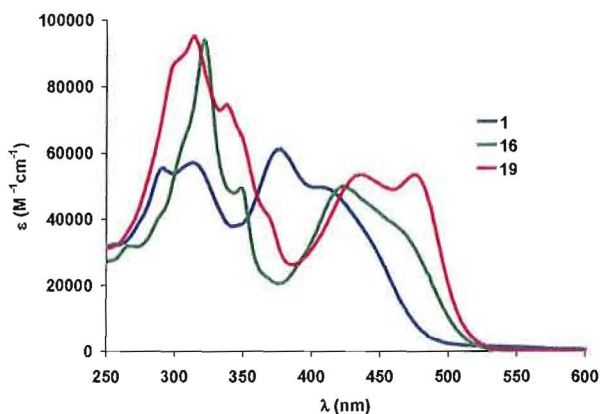


Figure 5. Electronic absorption spectra of TPEB 1, bis[14]DBA 16 and bis[15]DBA 19.

Electronic Emission Spectra. The electronic emission spectra of TPEBs 1-12 in CH_2Cl_2 and benzene are shown in Figure 6 and the data given in Tables 3 and 5. All compounds display strong fluorescence solvatochromism, experiencing bathochromic shifts of 29-55 nm in switching to the more polar solvent. In each case, the *ortho* isomers experience the greatest solvatochromism, and the *para* isomers the least. We do not suspect that the effect is due to formation of dimers or higher aggregates in solution: experiments reveal no observable concentration dependence of ^1H NMR proton shifts or emission wavelength over a 100-fold concentration gradient (e.g., 0.13-13 mM). This parallels our previously published data concerning the nitrophenyl analogues 13-15: significant aggregation requires enforced planarization to the corresponding bis(dehydrobenzo-annuleno)benzenes (*vide infra*).^{1b} Variation in substitution isomer has little effect on emission wavelength in CH_2Cl_2 , although the trend of *meta* < *ortho* < *para*, in order of increasing wavelength, holds for all compounds. In benzene the order is *ortho* < *meta* < *para*. Since this positive solvatochromism results from solvent

stabilization of the charge transfer excited state,^{18a-g} we are led to the intuitive inference that the *ortho* isomers experience the greatest stabilization in the excited state by the more polar solvent and possess the greatest net dipole in the ground state. The Stokes shift trends in CH₂Cl₂ support this hypothesis: higher dipole moments lead to greater excited state stabilization by polar solvents, resulting in higher Stokes shifts.^{18f,g} Emission wavelengths are more spread out in benzene, perhaps more accurately reflecting the variations in electronic states with substitution isomer.

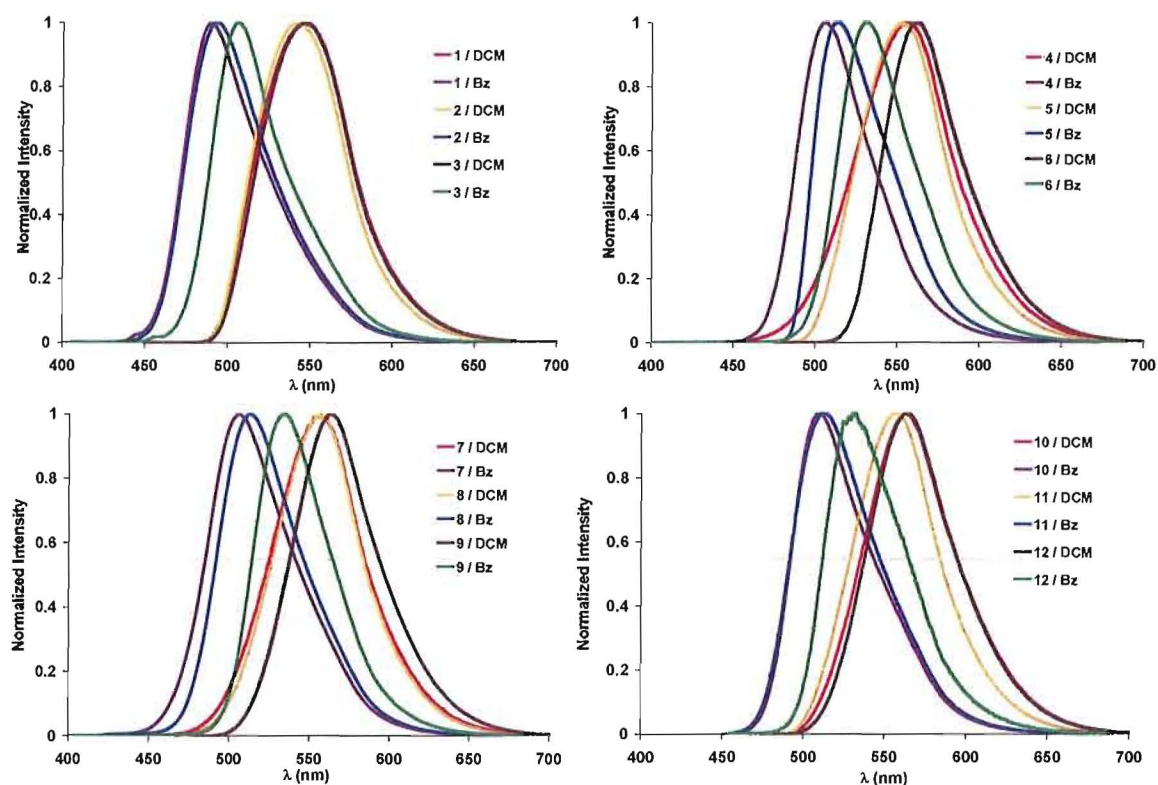


Figure 6. Electronic emission spectra of (a) **1-3**, (b) **4-6**, (c) **7-9**, and (d) **10-12** in CH_2Cl_2 (DCM) and benzene (Bz). All spectra were recorded at analyte concentrations of 15-25 μM with excitation at 450 nm.

The emission spectra of **1-6** in CH_2Cl_2 expanded in the 520-600 nm region are shown in Figure 7 and illustrate the overall effect of both isomer and number of acceptor groups. The most red-shifted of the benzotrifluoride TPEBs, **3**, is 6 nm behind **5**, the most blue-shifted of the bis(trifluoromethyl)phenyl compounds, showing that choice of acceptor strength is more effective at tuning fluorescence than choice of substitution isomer. TPEB **6** is conspicuously red-shifted relative to **1-5**, emitting at nearly the same wavelength as **10** and **12**, both of which are resonance acceptors. Note as well in Table 3

the similarity in extinction coefficient, showing that the strongly inductive acceptor group displays optical band gaps (and potential nonlinear optical susceptibilities) comparable to that of the relatively weak resonance acceptors. These similarities extend also to **13-15**, which have been shown to possess attractive NLO characteristics.⁶

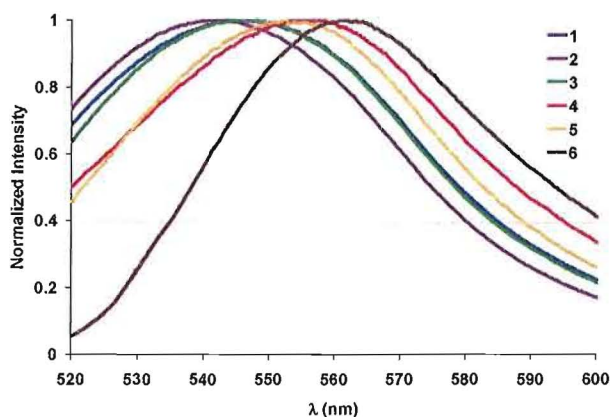


Figure 7. Expanded electronic emission spectra of **1-6** in CH_2Cl_2 .

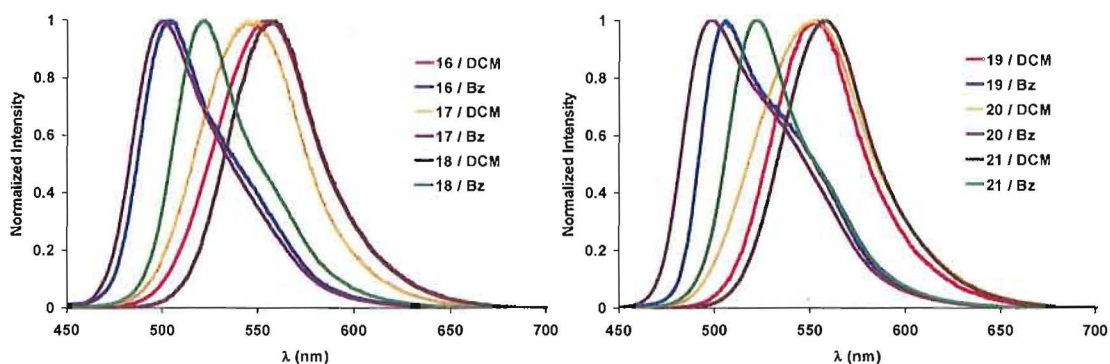


Figure 8. Electronic emission spectra of (a) **16-19** and (b) **19-21** in CH_2Cl_2 (DCM) and benzene (Bz). All spectra were recorded at analyte concentrations of 15-25 μM with excitation at 450 nm.

The electronic emission spectra of **16-21** in CH₂Cl₂ and benzene are shown in Figure 8 and the data tabulated in Tables 4 and 5. The bisDBAs exhibit the same dramatic solvatochromism as the TPEBs (see experimental section Figure 12 for additional representative spectra). Planarization has much less effect on the emission than the absorption, however. Maxima rarely differ from **1-3** in either solvent by more than 12 nm, and never by more than 20 nm. This may imply that planarization has less of an effect on the lowest vibrational level of the first excited state than the ground state. Consequently, Stokes shifts are smaller for all isomers. In benzene, the *para* isomers are again conspicuously red shifted relative to the *ortho* and *meta* isomers. In the cases of the DBAs the wavelength order in both solvents is *meta* < *ortho* < *para*. This may indicate an enhanced dipole in the *ortho* DBAs upon planarization from **1**. The bisDBAs presented here are significantly (60-80 nm) blue shifted relative to **22-26**, which emit in toluene in the orange-red region (all emission of **22-26** is quenched in CH₂Cl₂).^{1b} This large difference is likely due to a much lower-lying excited state in the strong resonance acceptor systems. Segment-localized FMOs explain this effect: when the HOMO is localized on the donor segment and the LUMO is localized on the acceptor segment, changes in the strength or type of either group can affect each MO nearly independently.^{1c,7} Here, we retain the strong donor group and switch to a weaker acceptor group. Accordingly, a greater effect is seen in the emission spectra than the absorption spectra.

Table 5. Electronic emission data for **1-12** and **16-21** in benzene.

compd	λ_{em} (nm) ^a
1	490
2	493
3	506
4	506
5	514
6	531
7	505
8	512
9	534
10	508
11	512
12	530
16	504
17	501
18	521
19	503
20	499
21	522

^aExcitation at 450 nm.

The fluorescence quantum yields of **1-12** and **16-21** in CH₂Cl₂ were calculated from the steady-state spectroscopic measurements using the techniques described by Drushel et al.^{18h} The values are given in Tables 3 and 4, and the quantum yields are also shown graphically in Figure 9 (**13-15** and **22-26** are calculated to have quantum yields of <0.01).^{1b} The general trend follows the concept of decreasing quantum yield with increasing acceptor strength: as band gaps narrow, nonradiative de-excitation via dissipative/vibronic coupling becomes more accessible.^{1b,c,19} In most cases presented here, the *meta* isomers show the highest Φ_f , possibly for the same reasons they exhibit higher charge transfer band intensities in the absorption spectra. Notable exceptions are **2** and **20**, although it is unclear why these are the case. As noted above, however, conjugation pathways in **19-21** are structurally more similar to those in **1-3** than are **16-18**, so the cause for the deviation may be the same in both systems. From this data, **7-9** appear to exhibit qualitative acceptor strength equal to or greater than even the benzonitrile analogues. If the absorption spectrum can be taken as a quantitative measure of excitation band gaps, then we have in **1-9**, and especially in **3**, TPEBs that exhibit relatively narrow band gaps *and* high quantum yields. Thus, it is demonstrated once again that correct choice of acceptor identity can optimize various desired optical properties for specialized applications. The bis[14]DBAs exhibit quantum yields comparable to **1-3**, while the bis[15]DBAs are consistently lower. This was also observed for the all-donor analogues,^{1b} and may indicate increased π - π^* -like character of the S₀→S₁ transition for **16-21** relative to **22-26**. Quantum yields in benzene have been calculated for many of the

TPEB compounds,^{1d} and are generally higher than in dichloromethane due to decreased solvent and dipole interaction with lower internal and external conversion rate constants.

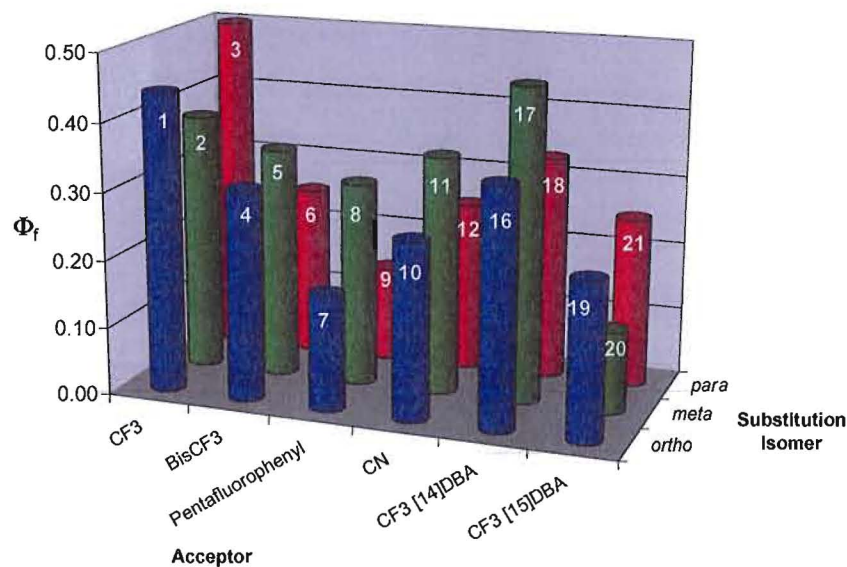


Figure 9. Quantum yield trends for TPEBs 1-12 and bisDBAs 16-21 in CH₂Cl₂.

Film Spectra. Because of the potential for these systems to serve as components of organic optical devices, as well as the striking emission solvent sensitivity, we determined the absorption and emission profiles of thin films to examine how the solid state properties compared to those in solution. Compounds 1-9 were drop-cast from CH₂Cl₂ solution onto cleaned glass microscope cover slides and the resulting films were placed under vacuum for 1 h to remove residual solvent. The resulting absorption and emission spectra are shown in Figure 10 and the relevant maxima are listed in Table 6. The features of the absorption spectra are considerably broadened compared to the

solution-phase spectra, but in general the absorption profiles retain their characteristic band shapes. The lowest energy λ_{max} for most compounds remains remarkably similar to that in CH_2Cl_2 , typically with shifts of less than 12 nm. For **1-3** and **7-9**, the λ_{max} are either equal to or lower than in CH_2Cl_2 , possibly reflecting less interaction between the molecules and the substrate, resulting in slightly larger band gaps. TPEB **4** shows a charge transfer band potentially red-shifted by a few nm, but as in all *ortho* isomers, the band overlaps with the next highest band, making the exact determination of the λ_{max} difficult. TPEB **5**, however, displays an 18 nm red-shift relative to CH_2Cl_2 . TPEB **6** exhibits a band ca. 10 nm blue-shifted from CH_2Cl_2 , but also shows an additional anomalous band at 495 nm. Additional solid-state samples of **6** also showed this band. While not an artifact, we are currently at a loss to explain this origin of this new peak.

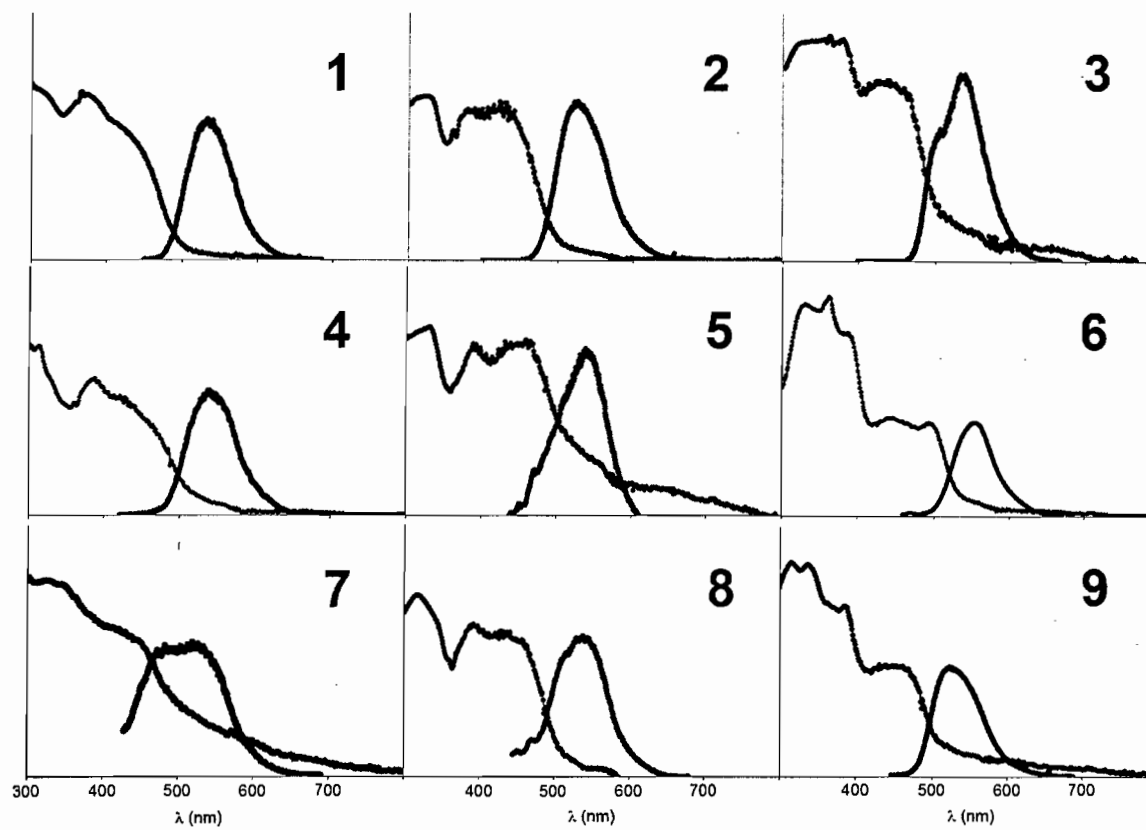


Figure 10. Absorption (left) and normalized emission (right) spectra of drop-cast films of 1-9.

Table 6. Electronic absorption and emission data for films of TPEBs 1-9.

compd	Lowest Energy Abs λ_{\max} (nm)	Em λ_{\max} (nm)	Stokes shift
1	405	534	129
2	427	527	100
3	438	538	100
4	422	540	118
5	451	539	88
6	446, 495	556	110, 61
7	415	529	114
8	437	539	102
9	452	525	73

The emission spectra of the thin films consistently display maxima between 5 and 16 nm blue-shifted from those in CH_2Cl_2 , with the exception of **7**, with an emission λ_{\max} almost halfway between CH_2Cl_2 and benzene and an additional shoulder around 487 nm, and **9**, which is significantly blue-shifted from benzene. As a group, the aryl perfluoride acceptor compounds **7-9** exhibit the most consistent blue-shifting relative to solvent spectra, implying the least amount of surface interaction of the systems examined here.

Self-Association. As stated above, aggregation of the TPEB skeleton in solution requires enforced planarization to the corresponding bis(dehydrobenzoannuleno)benzenes. In prior studies, bisDBAs **22-26** were observed to exhibit significant aggregation due to pi-stacking and dipole-dipole attraction between donor and acceptor rings, which resulted in dramatic (over 1 ppm) upfield shifts of ^1H NMR signals with increasing concentration and association constants of up to $K_2 = 5000$

M^{-1} .^{1b} In the case of **26**, the molecule rapidly decomposed in deacidified $CDCl_3$, possibly due to topochemical diacetylene polymerization induced by the strong association.²⁰ Similar experiments show that **16-21** do not display such extreme behavior, exhibiting only relatively small (0.005-0.249 ppm, average 0.06 ppm) proton shifts over a several hundred-fold concentration gradient (0.27-9.9 mM). We calculated the association constants for the protons of DBA **19** as the most dramatic example (Figures 11, see also Figure 14),²¹ assuming that the monomer-dimer equilibrium was the predominant process as was the case in **22-26**. The small values (Table 7) likely reflect both a much smaller degree of intermolecular attraction as well as much greater solvent interaction relative to **22-26**. Unlike **26**, **16-21** are completely stable to polymerization when left in $CDCl_3$ solution for several days. It is likely that the weaker acceptor groups cannot induce the degree of aggregation necessary for decomposition/polymerization. This greater stability implies better processability for materials based on inductive $-CF_3$ acceptors versus strong resonance acceptors, although a larger optical band gap is achieved.

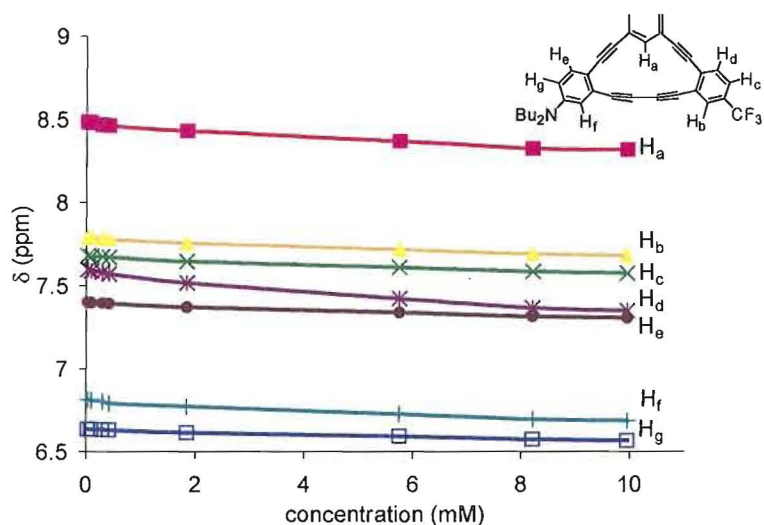


Figure 11. Concentration-dependent chemical shifts of the aromatic protons of DBA **19** in CDCl_3 at $20\text{ }^\circ\text{C}$.

Table 7. Calculated association constants K_2 (M^{-1}) of DBA **19** protons^a in CDCl_3 at $20\text{ }^\circ\text{C}$.^b

H _a	H _b	H _c	H _d	H _e	H _f	H _g
204 ± 11	170 ± 35	162 ± 20	236 ± 78	161 ± 54	178 ± 36	137 ± 51

^a Protons labeled in Figure 11. ^bValues calculated using the methods described in reference 21.

Conclusions

Two-dimensional donor/acceptor tetrakis(phenylethynyl)benzenes **1-9** and bis(dehydro-benzoannuleno)benzenes **16-21** have been prepared. The fluorinated acceptor groups, while weaker than previously-reported nitrile- or nitro-functionalized

analogues **10-15** and **22-26**,^{1a,b,d} lead to strongly fluorescent intramolecular charge transfer. TPEBs **1-9** display band gaps very near **10-15**, while retaining high fluorescence quantum yields for relatively small chromophores, providing unique and promising candidates for nonlinear optical device materials.⁶ The inductive $-\text{CF}_3$ acceptor group is quite effective at participating in ICT behavior, despite the lack of a formal resonance pathway for full conjugation. This may imply that electronic transitions with both $\pi-\pi^*$ and formal charge transfer characteristics dominate, producing a “best of both worlds” situation that could be exploited in materials design.^{7,21,22} The bis $-\text{CF}_3$ acceptors show significant bathochromic shifts relative to a single $-\text{CF}_3$ group, demonstrating the cumulative effect of acceptor strength and “acceptor density.” The pentafluorophenyl acceptor TPEBs show the most red-shifting of absorption and emission wavelengths, and approach the benzonitrile and nitrophenyl systems in terms of band gap narrowing ability. In thin films, on the other hand, their spectra indicate the least amount of substrate interaction of the compounds studied herein.

BisDBAs **16-21** represent planarized versions of fluorophores **1-3**, with enhanced conjugation efficiency from greater π -orbital overlap, and accordingly smaller optical band gaps. They exhibit higher quantum yields and greater solution stability than our previously examined D/A DBAs. Additionally, the full isomer/ring size array is accessible in **16-21**, whereas the nitro analogue of **18** could not be isolated.

Our results support findings by Diederich et al.¹⁵ questioning the utility of UV/Vis data alone as a measure of conjugation pathway efficiency. One possible explanation for the lower experimental band gaps in the systems with bent charge transfer pathways is

that fundamentally different transitions dominate in the quadrupolar chromophores, causing dramatically different optical behavior than is observed in the dipolar analogues.^{6c} It may be that the HOMO-LUMO transition is in fact not the lowest energy transition for these molecules. On the other hand, Stokes shift seems well correlated to conjugation pathway efficiency, with the *ortho* isomers displaying the highest values, and (presumably) the highest ground state net dipoles.

The effectiveness of the $-\text{CF}_3$ acceptor has led us to investigate its utility in further studies involving modification of the *donor* group to one containing a *meta* electron transport pathway. Donor/acceptor systems with such geometries have been shown to possess intriguing potential as unidirectional one-electron wires for use in solar electrochemical cells^{17,23} and provide insight into excited-state behavior.^{18f,24} The results of these new studies will be reported in due course.

Experimental

General Methods. These are described in reference 1b and Chapter I.

General Alkyne Coupling Procedure A. Haloarene (1 equiv) and TMSA (1.5 equiv per transformation unless otherwise noted) were dissolved in *i*Pr₂NH:THF (1:1, 0.05 M) and the solution purged for 30 min with bubbling Ar. Pd(PPh₃)₄ (0.03 equiv per transformation) and CuI (0.06 equiv per transformation) were added and the solution was purged another 20 min. The reaction mixture was stirred at 65 °C for 12-48 h under an Ar atmosphere. Upon completion, the mixture was concentrated and filtered through a pad of

silica gel eluting with hexanes. The solvent was removed in vacuo and the crude material was used without further purification.

General Alkyne Coupling Procedure B. Acceptor haloarene (3 equiv per transformation unless otherwise noted) and KOH (aq, 50 wt %, 10 equiv) were dissolved in *i*Pr₂NH:THF (1:1, 0.03 M) and the solution was purged for 30 min with bubbling Ar. Pd(PPh₃)₄ (0.03 equiv per transformation) and CuI (0.06 equiv per transformation) were added and the solution was purged another 20 min. Trimethylsilyl-protected diyne (1 equiv) was purged in THF solution for 50 min with bubbling Ar, and then injected via syringe pump into the stirred haloarene solution over 12 h at 65 °C under an Ar atmosphere. The reaction mixture was stirred an additional 12-48 h until complete by TLC. The mixture was then concentrated, rediluted with CH₂Cl₂, and filtered through a pad of silica gel. The solvent was removed in vacuo and the crude material was purified by column chromatography.

General Alkyne Coupling Procedure C. Acceptor segment **31** (2.3 equiv) and the appropriate isomer of dibromodiodobenzene (1 equiv) were dissolved in *i*Pr₂NH:THF:MeOH (3:3:1, 0.003 M) and the solution was purged for 30 min with bubbling Ar. PdCl₂(PPh₃)₂ (0.03 equiv per transformation), CuI (0.06 equiv per transformation) and K₂CO₃ (8 equiv per transformation) were added and the solution was purged another 20 min. The reaction mixture was stirred at room temperature for 24-48 h under an Ar atmosphere until complete by TLC. The mixture was then concentrated, rediluted with hexanes, and filtered through a pad of silica gel. The solvent was removed in vacuo and the crude material was used without further purification.

General Alkyne Coupling Procedure D. Acceptor-functionalized tetrayne, PdCl₂(PPh₃)₂ (0.03 equiv per transformation), and CuI (0.06 equiv per transformation) were dissolved in *i*Pr₂NH:THF (1:1, 0.008 M) and the solution was purged for 30 min under bubbling Ar. Diyne **33**^{1b} (2.3 equiv) was dissolved in THF (0.04 M), the solution was purged for 30 min under bubbling Ar, and then injected via syringe pump into the stirred polyynes solution over 8 h at 55 °C under an Ar atmosphere. The reaction was stirred an additional 12-24 h until complete by TLC. The mixture was then concentrated, rediluted with hexanes:CH₂Cl₂ (4:1), and filtered through a pad of silica gel. The solvent was removed in vacuo, and the crude material was purified by column chromatography.

General Pd-catalyzed Cyclization Procedure E. Annulene precycle was dissolved in THF, Et₂O and MeOH (2:1:0.01, 0.005 M) and Bu₄NF (TBAF, 1.0 M soln in THF, 10 equiv) was added. The solution was stirred at room temperature until complete by TLC (typically <1 h). The reaction mixture was then concentrated, dissolved in Et₂O, and washed with H₂O (3 x 50 mL). The organic phase was collected, dried over MgSO₄, and filtered through a pad of silica gel eluting with hexanes. The solvent was removed in vacuo and deprotected precycle was dissolved in THF (0.005 M). PdCl₂(dppe) (0.1 equiv per transformation), CuI (0.2 equiv per transformation), and I₂ (0.25 equiv per transformation) were dissolved in *i*Pr₂NH:THF (1.4:1, ~0.5 L per mmol precycle). To this mixture, the deprotected precycle solution was injected via syringe pump over 40 h at 60 °C. The reaction mixture was stirred until complete by TLC, then concentrated, rediluted in hexanes:CH₂Cl₂ (4:1) and filtered through a pad of silica gel. The solvent was removed in vacuo and the product was triturated with hexanes.

General Cu-mediated Cyclization Procedure F. Annulene precycle was dissolved in THF, Et₂O and MeOH (2:1:0.01, 0.005 M) and TBAF (1.0 M soln in THF, 10 equiv) was added. The solution was stirred at room temperature until complete by TLC (typically <1 h). The reaction mixture was then concentrated, dissolved in Et₂O, and washed with H₂O (3 x 50 mL). The organic phase was collected, dried with MgSO₄, and filtered through a pad of silica gel eluting with hexanes. The solvent was removed in vacuo and deprotected precycle was dissolved in pyridine (0.005 M). Cu(OAc)₂ (12.5 equiv per transformation), and CuCl (10 equiv per transformation) were dissolved in pyridine:MeOH (1.5:1, ~2.5 L per mmol precycle). To this mixture, the deprotected precycle solution was injected via syringe pump over 40 h at 60 °C. The reaction mixture was stirred until complete by TLC, then concentrated, rediluted in hexanes:CH₂Cl₂ (4:1) and filtered through a pad of silica gel. The solvent was removed in vacuo and the product was triturated with hexanes.

1,2-Bis[(4'-*N,N*-dibutylaminophenyl)ethynyl]-4,5-bis[(4'-trifluoromethyl)phenyl]ethynyl]benzene (1). TMSA (22 mg, 0.22 mmol) was coupled to 1,2-dibromo-4,5-bis[(4'-*N,N*-dibutylaminophenyl)ethynyl]benzene^{1c} (50 mg, 0.073 mmol) using general procedure A. The resulting red oil was coupled to 4-bromobenzotrifluoride (83 mg, 0.37 mmol) using general procedure B. The crude material was concentrated in vacuo and chromatographed on silica gel (7:3 hexanes:CH₂Cl₂) to yield **1** (51 mg, 80%) as a dark red oil. ¹H NMR (CDCl₃): δ 7.71 (s, 2H), 7.61-7.65 (m, 8H), 7.42 (d, *J* = 9.0 Hz, 4H), 6.59 (d, *J* = 9.0 Hz, 4H), 3.30 (t, *J* = 7.8 Hz, 8H), 1.60 (quin, *J* = 7.5 Hz, 8H), 1.39 (sext, *J* = 7.8 Hz, 8H), 0.98 (t, *J* = 7.8 Hz, 12H). ¹³C NMR (CDCl₃): δ 148.6, 134.9, 133.5,

132.1, 130.7, 130.2, 127.2, 126.8, 125.7, 123.5, 111.4, 108.6, 98.3, 93.3, 90.3, 86.2, 51.0, 29.6, 20.6, 14.3. IR (NaCl): ν 3059, 2196, 1772, 1648, 1605, 1519 cm^{-1} . MS (APCI): m/z ([isotope], %) 871.4 ($\text{M}^+ [2^{13}\text{C}]$, 30), 870.4 ($\text{M}^+ [^{13}\text{C}]$, 55), 869.4 (M^+ , 100). UV (CH_2Cl_2) λ_{max} (log ϵ): 377 (4.79), 407 (sh, 4.70). Em. λ_{max} : 544.

1,5-Bis[(4'-*N,N*-dibutylaminophenyl)ethynyl]-2,4-bis[(4'-trifluoromethylphenyl)ethynyl]benzene (2). TMSA (77 mg, 0.79 mmol) was coupled to 1,5-dibromo-2,4-bis[(4'-*N,N*-dibutylamino]phenylethynyl)benzene^{1c} (181 mg, 0.26 mmol) using general procedure A. The resulting red oil was coupled to 4-bromobenzotrifluoride (590 mg, 2.6 mmol) using general procedure B. The crude material was chromatographed on silica gel (3:2 hexanes: CH_2Cl_2) to yield **2** (181 mg, 80%) as a bright yellow solid. Mp: 118-120 °C. ¹H NMR (CDCl_3): δ 7.72-7.59 (m, 10H), 7.39 (d, $J = 9.0$ Hz, 4H), 6.58 (d, $J = 9.0$ Hz, 4H), 3.31 (t, $J = 7.2$ Hz, 8H), 1.60 (quin, $J = 7.5$ Hz, 8H), 1.38 (sext, $J = 7.8$ Hz, 8H), 0.98 (t, $J = 7.8$ Hz, 12H). ¹³C NMR (CDCl_3): δ 148.6, 135.3, 134.2, 133.4, 132.5, 127.5, 127.4, 126.1, 125.6, 125.5, 122.9, 111.4, 108.3, 98.5, 93.3, 90.7, 86.1, 51.0, 29.6, 20.6, 14.3. IR (NaCl): ν 2187, 1596, 1519 cm^{-1} . MS (APCI): m/z ([isotope], %) 871.3 ($\text{M}^+ [2^{13}\text{C}]$, 15), 870.5 ($\text{M}^+ [^{13}\text{C}]$, 65), 869.2 (M^+ , 100). UV (CH_2Cl_2) λ_{max} (log ϵ): 380 (4.74), 427 (4.79). Em. λ_{max} : 541.

1,4-Bis[(4'-*N,N*-dibutylaminophenyl)ethynyl]-2,5-bis[(4'-trifluoromethylphenyl)ethynyl]benzene (3). TMSA (130 mg, 1.3 mmol) was coupled to diyne **16**^{1c} (304 mg, 0.44 mmol) using general procedure A. The resulting red oil was coupled to 4-bromobenzotrifluoride (990 mg, 4.4 mmol) using general procedure B. The crude material was chromatographed on silica gel (4:1 hexanes: CH_2Cl_2) to yield **3** (255

mg, 67%) as a bright yellow solid. Mp: 125-127 °C (dec). ^1H NMR (CDCl_3): δ 7.71 (s, 2H), 7.60-7.70 (m, 8H), 7.40 (d, $J = 8.4$ Hz, 4H), 6.60 (d, $J = 8.4$ Hz, 4H), 3.32 (t, $J = 7.5$ Hz, 8H), 1.61 (quin, $J = 6.6$ Hz, 8H), 1.39 (sext, $J = 7.2$ Hz, 8H), 1.00 (t, $J = 7.2$ Hz, 12H). ^{13}C NMR (CDCl_3): δ 148.6, 134.8, 133.4, 132.2, 127.4, 125.9, 125.6, 125.5, 124.6, 111.5, 108.4, 98.0, 93.6, 90.8, 86.0, 51.0, 29.7, 20.6, 14.3. IR (NaCl): ν 2197, 1602, 1519, cm^{-1} . MS (APCI): m/z ([isotope], %) 871.3 ($\text{M}^+[2^{13}\text{C}]$, 18), 870.5 ($\text{M}^+[^{13}\text{C}]$, 62), 869.2 (M^+ , 100). UV (CH_2Cl_2) λ_{max} (log ϵ): 383 (4.64), 440 (4.48). Em. λ_{max} : 546.

1,2-Bis[(4'-*N,N*-dibutylaminophenyl)ethynyl]-4,5-bis[(3',5'-bis(trifluoromethyl)phenyl)-ethynyl]benzene (4). TMSA (91 mg, 0.93 mmol) was coupled to 1,2-dibromo-4,5-bis[(4'-*N,N*-dibutylaminophenyl)ethynyl]benzene^{1c} (214 mg, 0.31 mmol) using general procedure A. The resulting red oil was coupled to 3,5-bis(trifluoromethyl)bromobenzene (908 mg, 3.1 mmol) using general procedure B. The crude material was chromatographed on silica gel (4:1 hexanes: CH_2Cl_2) to yield **4** (130 mg, 42%) as a dark red oil. ^1H NMR (CDCl_3): δ 7.93 (s, 4H), 7.84 (s, 2H), 7.72 (s, 2H), 7.43 (d, $J = 9.0$ Hz, 4H), 6.60 (d, $J = 9.0$ Hz, 4H), 3.31 (t, $J = 7.8$ Hz, 8H), 1.60 (quin, $J = 7.5$ Hz, 8H), 1.39 (sext, $J = 7.5$ Hz, 8H), 0.97 (t, $J = 7.5$ Hz, 12H). ^{13}C NMR (CDCl_3): δ 148.6, 134.9, 133.6, 132.7, 132.2, 131.5, 127.4, 125.5, 124.9, 122.8, 122.3, 111.4, 108.4, 98.9, 91.7, 91.1, 86.1, 51.0, 29.6, 20.6, 14.3. IR (NaCl): ν 2196, 1608, 1605, 1526 cm^{-1} . MS (APCI): m/z ([isotope], %) 1007.3 ($\text{M}^+[2^{13}\text{C}]$, 21), 1006.3 ($\text{M}^+[^{13}\text{C}]$, 65), 1005.3 (M^+ , 100). UV (CH_2Cl_2) λ_{max} (log ϵ): 380 (4.88), 410 (sh, 4.78). Em. λ_{max} : 556.

1,5-Bis[(4'-*N,N*-dibutylaminophenyl)ethynyl]-2,4-bis[(3',5'-bis(trifluoromethyl)phenyl)-ethynyl]benzene (5). TMSA (94 mg, 0.96 mmol) was

coupled to 1,5-dibromo-2,4-bis([4'-*N,N*-dibutylamino]phenylethynyl)benzene^{1c} (220 mg, 0.32 mmol) using general procedure A. The resulting red oil was coupled to 3,5-bis(trifluoromethyl)bromobenzene (931 mg, 3.2 mmol) using general procedure B. The crude material was chromatographed on silica gel (4:1 hexanes:CH₂Cl₂) to yield **5** (127 mg, 40%) as a bright yellow solid. Mp: 173-175 °C. ¹H NMR (CDCl₃): δ 8.02 (s, 4H), 7.83 (s, 2H), 7.72 (s, 1H), 7.67 (s, 1H), 7.39 (d, *J* = 8.4 Hz, 4H), 6.58 (d, *J* = 8.4 Hz, 4H), 3.30 (t, *J* = 7.5 Hz, 8H), 1.57 (quin, *J* = 7.8 Hz, 8H), 1.40 (sext, *J* = 7.2 Hz, 8H), 0.98 (t, *J* = 7.2 Hz, 12H). ¹³C NMR (CDCl₃): δ 148.8, 135.2, 133.8, 133.3, 132.5, 131.8, 128.3, 125.9, 125.0, 122.2, 121.6, 111.5, 107.9, 99.4, 91.7, 91.5, 85.9, 51.0, 29.6, 20.5, 14.2. IR (NaCl): ν 2186, 1596, 1662, 1601, 1580 cm⁻¹. MS (APCI): *m/z* ([isotope], %) 1007.3 (M⁺[2¹³C], 17), 1006.3 (M⁺[¹³C], 53), 1005.3 (M⁺, 100). UV (CH₂Cl₂) λ_{max} (log ε): 384 (4.55), 435 (4.60). Em. λ_{max}: 552.

1,4-Bis[(4'-*N,N*-dibutylaminophenyl)ethynyl]-2,5-bis[(3',5'-bis(trifluoromethyl)phenyl)-ethynyl]benzene (6**).** TMSA (83 mg, 0.84 mmol) was coupled to **16**¹ (193 mg, 0.28 mmol) using general procedure A. The resulting red oil was coupled to 3,5-bis(trifluoromethyl)bromo-benzene (410 mg, 1.4 mmol) using general procedure B. The crude material was chromatographed on silica gel (5:1 hexanes:CH₂Cl₂) to yield **6** (61 mg, 22%) as a bright yellow solid. Mp: 165-167 °C. ¹H NMR (CDCl₃): δ 8.02 (s, 4H), 7.84 (s, 2H), 7.71 (s, 2H), 7.39 (d, *J* = 9.0 Hz, 4H), 6.58 (d, *J* = 9.0 Hz, 4H), 3.30 (t, *J* = 8.1 Hz, 8H), 1.59 (quin, *J* = 9.3 Hz, 8H), 1.37 (sext, *J* = 7.8 Hz, 8H), 0.98 (t, *J* = 7.8 Hz, 12H). ¹³C NMR (CDCl₃): δ 148.7, 134.5, 133.2, 132.1, 131.8, 126.0, 125.0, 124.4, 122.0, 121.4, 111.5, 107.9, 98.6, 91.9, 91.7, 85.7, 51.0, 29.5,

20.5; 14.2. IR (NaCl): ν 2200, 1601, 1519 cm^{-1} . MS (APCI): m/z ([isotope], %) 1006.5 ($\text{M}^+ [^{13}\text{C}]$, 35), 1005.5 (M^+ , 100). UV (CH_2Cl_2) λ_{max} (log ϵ): 385 (4.78), 456 (4.59). Em. λ_{max} : 561.

1,2-Bis[(4'-*N,N*-dibutylaminophenyl)ethynyl]-bis-4,5-(2',3',4',5',6'-pentafluorophenyl-ethynyl)benzene (7). TMSA (28 mg, 0.28 mmol) was coupled to 1,2-dibromo-4,5-bis[(4'-*N,N*-dibutylaminophenyl)ethynyl]benzene^{1c} (66 mg, 0.095 mmol) using general procedure A. The resulting red oil was desilylated by dissolving in THF:MeOH (5:1, 20 mL) with KOH (27 mg, 0.4 mmol) and stirring for 2 h. The red solution was concentrated in vacuo and filtered through a pad of silica with CH_2Cl_2 . After reconcentration, the red oil was immediately coupled to pentafluoroiodobenzene (139 mg, 0.47 mmol) using general procedure B with omission of KOH in the reaction mixture and injection of the deprotected alkyne over 18 h at 45 °C. The crude material was chromatographed on silica gel (5:1 hexanes: CH_2Cl_2) to yield **7** (38 mg, 43%) as a bright yellow-orange solid. Mp: 130-170 °C (dec). ^1H NMR (CDCl_3): δ 7.74 (s, 2H), 7.42 (d, $J = 9.0$ Hz, 4H), 6.59 (d, $J = 9.0$ Hz, 4H), 3.30 (t, $J = 7.5$ Hz, 8H), 1.59 (quin, $J = 9.3$ Hz, 8H), 1.37 (sext, $J = 7.5$ Hz, 8H), 0.97 (t, $J = 7.5$ Hz, 12H). ^{13}C NMR (CDCl_3): δ 148.6, 145.6, 143.3, 136.3, 135.1, 133.5, 129.0, 127.6, 122.3, 111.4, 108.4, 100.3, 99.0, 86.1, 78.5, 51.0, 29.6, 20.6, 14.3. IR (NaCl): ν 2280, 2200, 1729, 1691, 1645, 1611, 1554, 1512 cm^{-1} . MS (APCI): m/z ([isotope], %) 914.0 ($\text{M}^+ [2^{13}\text{C}]$, 20), 913.5 ($\text{M}^+ [^{13}\text{C}]$, 50), 912.2 (M^+ , 100). UV (CH_2Cl_2) λ_{max} (log ϵ): 383 (4.83), 423 (4.75). Em. λ_{max} : 556.

1,5-Bis[(4'-*N,N*-dibutylaminophenyl)ethynyl]-bis-2,4-(2',3',4',5',6'-pentafluorophenyl-ethynyl)benzene (8). TMSA (97 mg, 0.99 mmol) was coupled to

1,5-dibromo-2,4-bis[(4'-*N,N*-dibutylaminophenyl)ethynyl]benzene^{1c} (228 mg, 0.33 mmol) using general procedure A. The resulting red oil was desilylated by dissolving in THF:MeOH (5:1, 40 mL) with KOH (93 mg, 1.65 mmol) and stirring for 2 h. The red solution was concentrated in vacuo and filtered through a pad of silica with CH₂Cl₂. After reconcentration, the red oil was immediately coupled to pentafluoriodobenzene (485 mg, 1.63 mmol) using general procedure B with omission of KOH in the reaction mixture and injection of the deprotected alkyne over 18 h at 45 °C. The crude material was chromatographed on silica gel (5:1 hexanes:CH₂Cl₂) to yield **8** (126 mg, 42%) as a bright yellow solid. Mp: 130-170 °C (dec). ¹H NMR (CDCl₃): δ 7.76 (s, 1H), 7.71 (s, 1H), 7.39 (d, *J* = 8.7 Hz, 4H), 6.59 (d, *J* = 8.7 Hz, 4H), 3.30 (t, *J* = 7.2 Hz, 8H), 1.59 (quin, *J* = 7.5 Hz, 8H), 1.39 (sext, *J* = 7.5 Hz, 8H), 0.97 (t, *J* = 7.5 Hz, 12H). ¹³C NMR (CDCl₃): δ 148.7, 133.6, 132.3, 131.4, 130.8, 128.2, 125.7, 125.0, 121.1, 111.3, 110.4, 103.5, 97.0, 92.1, 89.8, 85.7, 50.9, 29.5, 20.5, 14.2. IR (NaCl): ν 2276, 2192, 1730, 1696, 1642, 1558 cm⁻¹. MS (APCI): *m/z* ([isotope], %) 915.0 (M⁺ [2¹³C], 22), 914.5 (M⁺ [¹³C], 49), 913.2 (M⁺, 100). UV (CH₂Cl₂) λ_{max} (log ε): 383 (4.51), 438 (4.60). Em. λ_{max}: 555.

1,4-Bis[(4'-*N,N*-dibutylaminophenyl)ethynyl]-2,5-bis(2',3',4',5',6'-pentafluorophenylethynyl)benzene (9). TMSA (94 mg, 0.96 mmol) was coupled to diyne **16**^{1c} (221 mg, 0.32 mmol) using general procedure A. The resulting red oil was desilylated by dissolving in THF:MeOH (5:1, 40 mL) with KOH (90 mg, 1.6 mmol) and stirring for 2 h. The red solution was concentrated in vacuo and filtered through a pad of silica with CH₂Cl₂. After reconcentration, the red oil was immediately coupled to pentafluoriodobenzene (470 mg, 1.60 mmol) using general procedure B with omission

of KOH in the reaction mixture and injection of the deprotected alkyne over 18 h at 45 °C. The crude material was chromatographed on silica gel (5:1 hexanes:CH₂Cl₂) to yield **9** (100 mg, 35%) as a bright yellow solid. Mp: 130-170 °C (dec). ¹H NMR (CDCl₃): δ 7.72 (s, 2H), 7.38 (d, *J* = 9.0 Hz, 4H), 6.58 (d, *J* = 9.0 Hz, 4H), 3.30 (t, *J* = 7.5 Hz, 8H), 1.59 (quin, *J* = 8.1 Hz, 8H), 1.38 (sext, *J* = 7.5 Hz, 8H), 0.97 (t, *J* = 7.5 Hz, 12H). ¹³C NMR (CDCl₃): δ 149.5, 148.5, 146.9, 139.5, 135.5, 133.5, 125.5, 123.8, 111.2, 111.2, 108.3, 100.2, 98.6, 85.4, 78.4, 50.9, 29.6, 20.6, 14.2. IR (NaCl): ν 3014, 2281, 2187, 1728, 1689, 1575, 1571, 1524 cm⁻¹. MS (APCI): *m/z* ([isotope], %) 915.5 (M⁺[²¹³C], 16), 914.5 (M⁺[¹³C], 50), 913.2 (M⁺, 100). UV (CH₂Cl₂) λ_{max} (log ε): 385 (4.74), 462 (4.56). Em. λ_{max}: 563.

Acceptor triazene 29. Aniline **28** (6.71 g, 23 mmol) and CH₃CN (5 mL) was cooled in an ice salt bath to -5 °C and conc. HCl (21 mL) was added dropwise. A solution NaNO₂ (3.85 g, 56 mmol) in H₂O (3 mL) was added dropwise maintaining the temperature below 0 °C. Upon completion, the reaction mixture was stirred at -5 °C for 15 min more. In a separate flask, K₂CO₃ (18.3 g, 130 mmol) and piperidine (21.5 g, 302 mmol) were dissolved in CH₃CN (110 mL) and H₂O (300 mL) and cooled to 0 °C in an ice salt bath. The reaction mixture was transferred into the basic solution via canula while maintaining temperature below 5 °C, and then left stirring open to air for 12 h while warming to rt. The mixture was then concentrated and taken up in Et₂O, then washed successively with H₂O, brine solution, and H₂O (100 mL each). The organic phase was dried over MgSO₄ and filtered through a pad of silica gel eluting with hexanes:CH₂Cl₂ (7:3). The solvent was removed in vacuo to yield **29** (7.4 g, 83%) as an orange oil. ¹H

NMR (CDCl₃): δ 8.08 (s, 1H), 7.52 (d, 1H, $J = 5.1$ Hz), 7.45 (d, 1H, $J = 5.1$ Hz), 3.97 (s, 2H), 3.84 (s, 2H), 1.75 (m, 6H). ¹³C NMR (CDCl₃): δ 153.0, 136.4, 136.3, 126.0, 125.9, 117.4, 96.0, 53.4, 44.6, 26.7, 24.4. IR (NaCl): ν 2938, 2853, 1600, 1423, 1388, 1320, 1253, 1164, 1118, 1075 cm⁻¹. MS (APCI): m/z ([isotope], %) 383.0 (M⁺, 100), 384.0 (M⁺ [¹³C], 9).

Acceptor iodide 30. Triazene **29** (7.3 g, 19 mmol), PdCl₂(PPh₃)₂ (134 mg, 0.19 mmol), and CuI (0.073 g, 0.38 mmol) were dissolved in THF (75 mL) and *i*-Pr₂NH (75 mL), and the solution was purged with bubbling Ar for 30 min. TIPSA (6.4 mL, 29 mmol) was injected via syringe, and the reaction mixture was left stirring 24 h at room temperature under an atmosphere of Ar. The reaction mixture was then concentrated, rediluted in hexanes:CH₂Cl₂ (2:1) and filtered through a pad of silica gel. The solvent was removed in vacuo, and the crude material was redissolved in MeI (30 mL). The solution was stirred for 72 h at 155 °C in a high pressure reaction vessel. The reaction mixture was then cooled, concentrated, rediluted in hexanes:CH₂Cl₂ (4:1) and filtered through a pad of silica gel. The solvent was removed in vacuo to yield **30** (6.4 g, 74%) as a red oil. ¹H NMR (CDCl₃): 7.96 (d, 1H, $J = 9.0$ Hz), 7.68 (d, 1H, $J = 2.7$ Hz), 7.20 (dd, 1H, $J = 9.0, 2.7$ Hz), 1.17 (s, 21H). ¹³C NMR (CDCl₃): δ 139.6, 131.3, 129.7, 125.7, 106.9, 105.4, 98.0, 90.5, 81.8, 18.9, 11.5. IR (NaCl): ν 2952, 2889, 2160, 1597, 1565, 1462, 1395, 1328, 1280, 1252, 1209, 1177, 1126, 1082 cm⁻¹. MS (APCI): m/z ([isotope], %) 452.4 (M⁺, 100), 453.3 (M⁺ [¹³C], 31).

Acceptor segment 31. Iodoarene **30** (6.4 g, 14 mmol), PdCl₂(PPh₃)₂ (390 mg, 0.56 mmol), and CuI (0.11 g, 1.1 mmol) were dissolved in THF (100 mL) and *i*Pr₂NH (100

mL), and the solution was purged with bubbling Ar for 30 min. TMSA (4 mL, 28 mmol) was injected via syringe, and the reaction mixture was stirred 24 h at room temperature under an atmosphere of Ar. The reaction mixture was then concentrated, rediluted in hexanes:CH₂Cl₂ (2:1) and filtered through a pad of silica gel. The solvent was removed in vacuo to yield **31** (5.6 g, 95%) as a yellow solid. Mp: 65-69 °C. ¹H NMR (CDCl₃): δ 7.69 (s, 1H), 7.57 (d, 1 H, *J* = 8.1 Hz), 7.46 (d, 1 H, *J* = 8.1 Hz), 1.16 (s, 21 H), 0.26 (s, 9H). ¹³C NMR (CDCl₃): δ 133.5, 129.9, 129.3, 126.7, 124.5, 122.0, 104.0, 102.3, 101.5, 97.4, 81.8, 18.9, 11.6, 0.03. IR (NaCl): ν 2955, 2944, 2890, 2865, 2156, 2058, 1608, 1464, 1406, 1331, 1262, 1248, 1136, 1172 cm⁻¹. MS (APCI): *m/z* ([isotope], %) 422.2 (M⁺, 100), 423.3 (M⁺ [¹³C], 56).

Acceptor-functionalized aryl bromide 32. Diyne **31** (200 mg, 0.54 mmol) was coupled to 1,5-dibromo-2,4-diiodobenzene (100 mg, 0.24 mmol) using general procedure C to yield **32** (205 mg, 93%) as a yellow solid. Mp: 52-53 °C. ¹H NMR (CDCl₃): δ 7.92 (s, 1H), 7.77 (s, 2H), 7.74 (s, 1H), 7.67 (d, 2H, *J* = 8.1 Hz), 7.56 (d, 2H, *J* = 8.1 Hz), 1.10 (s, 42H). ¹³C NMR (CDCl₃): δ 137.7, 136.1, 133.2, 132.9, 130.7, 129.9, 128.6, 127.0, 126.1, 124.8, 124.5, 103.7, 98.2, 92.8, 92.0, 18.9, 11.5. IR (NaCl): ν 2944, 2890, 2867, 2157, 1614, 1490, 1452, 1382, 1324, 1258, 1200, 1130, 1068 cm⁻¹. MS (APCI): *m/z* ([isotope], %) 931.1 (M⁺, [2⁷⁹Br], 90), 932.2 (M⁺ [⁷⁹Br⁸¹Br], 100), 933.2 (M⁺ [2⁸¹Br], 57).

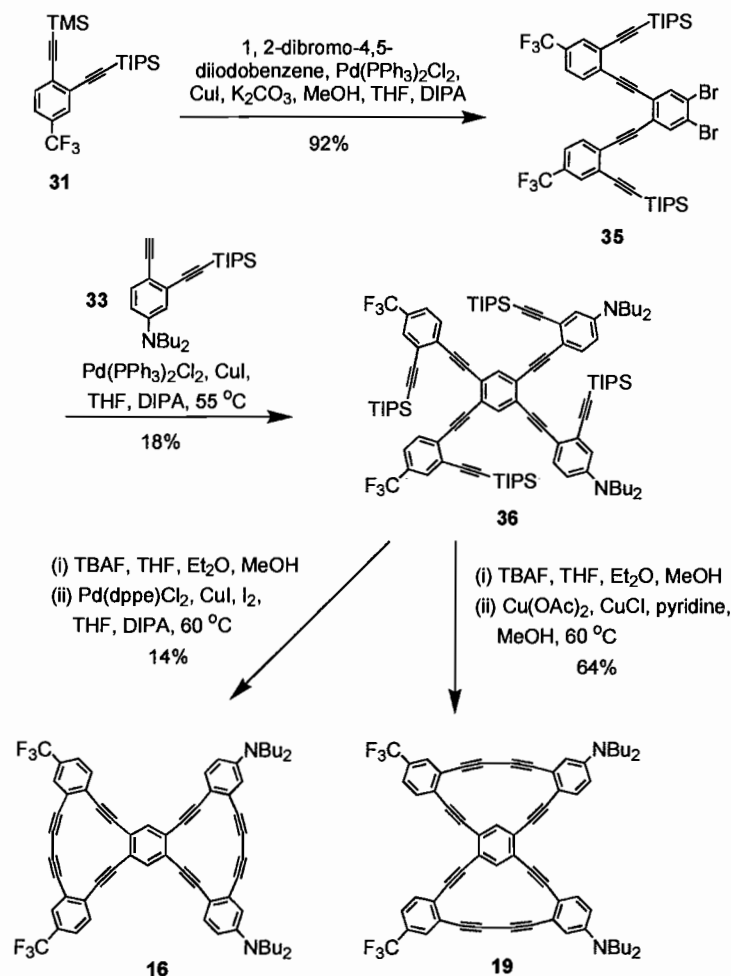
BisDBA precursor 34. Diyne **33**^{1b} (478 mg, 1.15 mmol) was coupled to tetrayne **32** (446 mg, 0.48 mmol) using general procedure D to yield **34** (555 mg, 73%) as an amorphous yellow solid. ¹H NMR (CDCl₃, 500 MHz): δ 7.72, (s, 1H), 7.68 (s, 1H), 7.63 (d, 2H, *J* = 8.0 Hz), 7.44 (d, 2H, *J* = 8.0 Hz), 7.27 (d, 2H, *J* = 7.0 Hz), 6.72 (d, 2H, *J* = 2.5

Hz), 6.48 (dd, 2H, $J = 7.0, 2.5$ Hz), 3.27 (t, 8H, $J = 7.0$ Hz), 1.56 (m, 8H, $J = 7.5$ Hz), 1.35 (m, 8H, $J = 7.5$ Hz), 0.96 (t, 12H, $J = 7.5$ Hz). ^{13}C NMR (CDCl_3): δ 148.0, 135.4, 135.2, 133.8, 133.5, 133.3, 129.7, 129.5, 127.4, 127.1, 126.6, 124.5, 123.6, 115.4, 111.9, 111.6, 111.3, 106.5, 103.9, 97.8, 96.6, 94.3, 93.8, 92.2, 88.6, 50.8, 29.5, 20.5, 18.9, 14.2, 11.6, 11.5. IR (NaCl): ν 2961, 2945, 2885, 2863, 2198, 2150, 1591, 1509, 1470, 1392, 1363, 1322, 1249, 1170, 1132, 1094, 1068 cm^{-1} . UV (CH_2Cl_2) λ_{max} (log ϵ): 315 (4.84), 422 (4.62). Em. λ_{max} : 533. MS (APCI): m/z ([isotope], %) 1588.6 (M^+ , 80), 1589.7 (M^+ [^{13}C], 100), 1590.8 (M^+ [2^{13}C], 91).

BisDBA 17. Octayne **34** (220 mg, 0.138 mmol) was cyclized using general procedure E to yield **17** (82 mg, 62%) as a red solid. Mp: 160-174 °C (dec). ^1H NMR (CDCl_3): δ 8.34 (s, 1H), 8.27 (s, 1H), 8.03 (d, 2H, $J = 7.8$ Hz), 7.83 (s, 2H), 7.75 (d, 2H, $J = 7.8$ Hz), 7.69 (d, 2H, $J = 8.7$ Hz), 6.78 (s, 2H), 6.76 (d, 2H, $J = 8.7$ Hz), 3.33 (t, 8H, $J = 7.8$ Hz), 1.62 (m, 8H, $J = 6$ Hz), 1.40 (m, 8H, $J = 7.8$ Hz), 1.00 (t, 12H, $J = 7.5$ Hz). ^{13}C NMR (CDCl_3 , 500 MHz): δ 148.0, 134.9, 133.6, 132.8, 129.7, 129.5, 126.3, 126.1, 125.0, 124.0, 123.5, 122.7, 119.9, 115.3, 112.9, 111.5, 111.2, 97.7, 96.1, 93.0, 91.5, 87.9, 83.9, 82.0, 78.9, 51.0, 29.5, 20.6, 14.3. IR (NaCl): ν 2958, 2931, 2876, 2186, 2168, 1599, 1531, 1510, 1497, 1456, 1369, 1342, 1315, 1172, 1129 cm^{-1} . UV (CH_2Cl_2) λ_{max} (log ϵ): 322 (4.86), 454 (4.68). Em. λ_{max} : 544. MS (APCI): m/z ([isotope], %) 960.2 (M^+ , 100), 961.2 (M^+ [^{13}C], 87), 962.3 (M^+ [2^{13}C], 25).

BisDBA 20. Octayne **34** (220 mg, 0.138 mmol) was cyclized using general procedure F to yield **20** (77 mg, 58%) as a yellow solid. Mp: 160-170 °C (dec). ^1H NMR (CDCl_3): δ 8.64 (s, 1H), 8.25 (s, 1H), 7.75 (s, 2H), 7.62 (d, 2H, $J = 8.1$ Hz), 7.54 (d, 2H, $J = 8.1$

Hz), 7.37 (d, 2H, $J = 9.3$ Hz), 6.78 (s, 2H), 6.58 (d, 2H, $J = 9.3$ Hz), 3.28 (t, 8H, $J = 6.6$ Hz), 1.59 (m, 8H), 1.38 (m, 8H, $J = 7.5$ Hz), 0.99 (t, 12H, $J = 7.2$ Hz). ^{13}C NMR (CDCl_3 , 500 MHz): δ 148.0, 131.7, 131.3, 130.5, 129.7, 129.5, 129.4, 127.7, 126.9, 125.6, 124.8, 122.5, 120.3, 119.5, 115.0, 112.8, 112.2, 99.0, 98.5, 94.2, 93.1, 83.2, 81.9, 79.5, 77.5, 50.9, 29.5, 20.5, 14.2. IR (NaCl): ν 2957, 2932, 2871, 2183, 1593, 1531, 1328, 1292, 1169, 1119, 1063 cm^{-1} . UV (CH_2Cl_2) λ_{max} (log ϵ): 310 (5.17), 4.41 (4.92), 466 (4.95). Em. λ_{max} : 551. MS (APCI): m/z ([isotope], %) 960.3 (M^+ , 92), 961.1 (M^+ [^{13}C], 100), 962.5 (M^+ [2^{13}C], 12).

Scheme 4. Synthesis of bisDBAs **16** and **19**.

Acceptor-functionalized aryl bromide 35. Diyne **31** (200 mg, 0.54 mmol) was coupled to 1,2-dibromo-4,5-diiodobenzene (100 mg, 0.24 mmol) using general procedure C to yield **35** (177 mg, 92%) as an orange oil. $^1\text{H NMR}$ (CDCl_3): δ 7.82 (s, 2H), 7.76 (s, 2H), 7.58 (d, $J = 8.1$, 2H), 7.49 (d, $J = 8.1$ Hz, 2H), 1.12 (s, 42H). $^{13}\text{C NMR}$ (CDCl_3): δ 136.6, 132.9, 131.1, 133.1, 129.6, 128.7, 126.9, 125.8, 125.3, 124.8, 103.7, 100.2, 98.3, 91.8, 18.9, 11.5. IR (NaCl): ν 2952, 2890, 2855, 2723, 2188, 2152, 2037, 1599, 1498, 1456, 1405, 1362, 1320, 1250, 1200, 1169, 1130, 1110, 1076, 990, 917, 882, 839, 754,

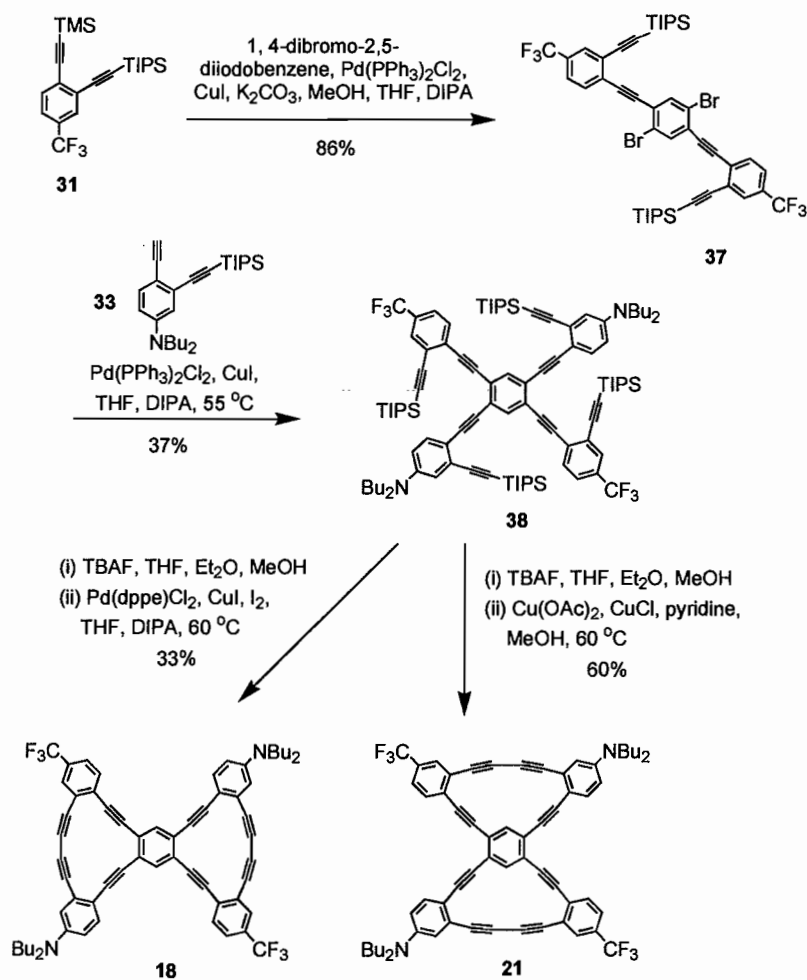
680, 572, 494 cm^{-1} . MS (APCI): m/z ([isotope], %) 931.2 (M^+ , $[\text{2}^{79}\text{Br}]$, 80), 932.2 (M^+ $[\text{79}\text{Br}^{81}\text{Br}]$, 100), 933.2 (M^+ $[\text{2}^{81}\text{Br}]$, 69).

DBA precursor 36. Diyne **33**^{1b} (132 mg, 0.32 mmol) was coupled to **35** (100 mg, 0.107 mmol) using general procedure D to yield **36** (30 mg, 18%) as a yellow oil. ^1H NMR (CDCl_3): δ 7.73 (s, 2H), 7.69 (s, 2H), 7.57 (d, $J = 7.8$ Hz, 2H), 7.46 (d, $J = 7.8$ Hz, 2H), 7.34 (d, $J = 9.0$ Hz, 2H), 6.72 (d, $J = 2.7$ Hz, 2H), 6.51 (dd, $J = 9.0, 2.7$ Hz, 2H), 3.27 (t, $J = 7.0$ Hz, 8H), 1.35 (quin, $J = 7.0$ Hz, 8H), 1.10 (sext, $J = 7.8$ Hz, 8H), 1.08 (s, 84H), 0.96 (t, $J = 7.0$ Hz, 12H). ^{13}C NMR (CDCl_3): δ 147.9, 135.6, 134.0, 133.8, 132.9, 130.3, 130.1, 129.5, 127.1, 126.9, 126.7, 124.6, 123.6, 122.7, 115.4, 111.9, 106.6, 103.8, 98.0, 96.4, 93.9, 93.6, 92.1, 88.9, 50.8, 29.6, 20.5, 18.9, 18.8, 14.2, 11.7, 11.6, 11.5. IR (NaCl): ν 2956, 2937, 2859, 2894, 2200, 2153, 1591, 1533, 1514, 1459, 1366, 1324, 1169, 1122, 1099, 1072, 882, 746, 680 cm^{-1} . UV (CH_2Cl_2) λ_{max} (log ϵ): 314 (4.74), 385 (4.63), 420 (4.65). Em. λ_{max} : 534. MS (APCI): m/z ([isotope], %) 1588.6 (M^+ , 81), 1589.7 (M^+ $[\text{13}\text{C}]$, 100), 1590.8 (M^+ $[\text{2}^{13}\text{C}]$, 70).

BisDBA 16. Octayne **36** (30 mg, 0.019 mmol) was cyclized using general procedure E to yield **16** (3 mg, 14%) as a yellow solid. Mp: 150-165 $^\circ\text{C}$ (dec). ^1H NMR (CDCl_3): δ 8.35 (s, 2H), 8.07 (d, $J = 8.1$ Hz, 2H), 7.86 (s, 2H), 7.76 (d, $J = 9.0$ Hz, 2H), 7.74 (d, $J = 6.6$ Hz, 2H), 6.78 (s, 2H), 6.76 (d, $J = 9.0$ Hz, 2H), 3.34 (t, $J = 6.9$ Hz, 8H), 1.62 (quin, $J = 7.5$ Hz, 8H), 1.40 (sext, $J = 7.5$ Hz, 8H), 1.00 (t, $J = 7.2$ Hz, 12H). ^{13}C NMR (CDCl_3 , 500 MHz): δ 148.2, 145.4, 143.0, 134.8, 133.7, 132.7, 130.0, 126.5, 125.9, 125.5, 124.6, 123.4, 120.8, 115.0, 112.6, 111.5, 97.8, 96.0, 93.7, 91.8, 86.5, 85.2, 81.5, 79.4, 51.0, 30.0, 21.0, 14.2. IR (NaCl): ν 2952, 2925, 2871, 2851, 2192, 2130, 1735, 1591, 1537, 1502,

1463, 1432, 1397, 1366, 1211, 1169, 1138, 1091, 924, 847, 812 cm^{-1} . UV (CH_2Cl_2) λ_{max} (log ϵ): 322 (4.97), 424 (4.70), 450 (4.62). Em. λ_{max} : 554. MS (APCI): m/z ([isotope], %) 960.2 (M^+ , 100), 961.1 (M^+ [^{13}C], 58), 962.3 (M^+ [2^{13}C], 19).

BisDBA 19. Octayne **36** (33 mg, 0.021 mmol) was cyclized using general procedure F to yield **19** (13 mg, 64%) as a yellow solid. Mp: 150-170 $^{\circ}\text{C}$ (dec). ^1H NMR (CDCl_3 , 500 MHz): δ 8.32 (s, 2H), 7.68 (s, 2H), 7.57 (d, $J = 8.5$ Hz, 2H), 7.35 (d, $J = 8.5$ Hz, 2H), 7.30 (d, $J = 8.0$ Hz, 2H), 6.68 (s, 2H), 6.56 (d, $J = 8.0$ Hz, 2H), 3.27 (t, $J = 8.0$ Hz, 8H), 1.57 (quin, $J = 7.0$ Hz, 8H), 1.41 (sext, $J = 7.0$ Hz, 8H), 1.00 (t, $J = 7.0$ Hz, 12H). ^{13}C NMR (CDCl_3 , 500 MHz): δ 148.0, 145.2, 142.4, 141.4, 131.7, 130.8, 129.7, 127.3, 127.2, 125.3, 123.5, 122.6, 120.8, 115.3, 112.9, 112.7, 98.6, 97.7, 94.6, 93.3, 84.5, 80.7, 80.2, 76.8, 50.9, 29.5, 20.5, 14.2. IR (NaCl): ν 2951, 2917, 2847, 2186, 1736, 1588, 1540, 1496, 1468, 1394, 1369, 1331, 1306, 1259, 1223, 1170, 1126, 1078 cm^{-1} . UV (CH_2Cl_2) λ_{max} (log ϵ): 316 (4.97), 436 (4.73), 474 (4.73). Em. λ_{max} : 550. MS (APCI): m/z ([isotope], %) 960.2 (M^+ , 100), 961.1 (M^+ [^{13}C], 78), 962.3 (M^+ [2^{13}C], 10).

Scheme 5. Synthesis of bisDBAs **18** and **21**.

Acceptor-functionalized aryl bromide 37. Diyne **31** (200 mg, 0.54 mmol) was coupled to 1,4-dibromo-2,5-diiodobenzene (100 mg, 0.24 mmol) using general procedure C to yield **37** (188 mg, 86%) as a yellow solid. Mp: 156-158 °C. ¹H NMR (CDCl₃): δ 7.80 (s, 2H), 7.76 (s, 2H), 7.69 (d, 2H, *J* = 8.1 Hz), 7.55 (d, 2H, *J* = 8.1 Hz), 1.14 (s, 42H). ¹³C NMR (CDCl₃): δ 136.7, 133.0, 129.9, 129.8, 128.5, 127.0, 126.6, 124.8, 124.7,

123.9, 103.9, 98.5, 94.7, 92.1, 18.5, 11.3. IR (NaCl) ν 2943, 2865, 2152, 1608, 1468, 1406, 1327, 1270, 1171, 1130, 1117, 1068, 911 cm^{-1} . MS (APCI): m/z ([isotope], %) 931.2 (M^+ , [2⁷⁹Br], 41), 932.0 (M^+ [7⁹Br⁸¹Br], 100), 933.2 (M^+ [2⁸¹Br], 52).

DBA precursor 38. Diyne **33**^{1b} (71 mg, 0.17 mmol) was coupled to **37** (54 mg, 0.058 mmol) using general procedure D to yield **38** (36 mg, 37%) as a yellow oil. ¹H NMR (CDCl_3): δ 7.71 (s, 2H), 7.68 (s, 2H), 7.63 (d, $J = 8.1$ Hz, 2H), 7.45 (d, $J = 8.1$ Hz, 2H), 7.28 (d, $J = 9.0$ Hz, 2H), 6.71 (d, $J = 2.7$ Hz, 2H), 6.49 (dd, $J = 9.0, 2.7$ Hz, 2H), 3.27 (t, $J = 7.8$ Hz, 8H), 1.56 (quin, $J = 7.8$ Hz, 8H), 1.36 (sext, $J = 7.8$ Hz, 8H), 1.06 (s, 84H), 0.96 (t, $J = 7.2$ Hz, 12H). ¹³C NMR (CDCl_3): δ 147.9, 135.4, 133.8, 133.3, 130.2, 129.9, 129.7, 129.6, 127.0, 126.6, 126.0, 124.9, 124.5, 115.4, 111.9, 111.6, 106.6, 103.9, 97.9, 96.2, 94.3, 93.7, 92.5, 88.5, 50.8, 29.5, 20.5, 18.9, 14.1, 11.6, 11.5. IR (NaCl): 2956, 2939, 2861, 2890, 2205, 2156, 1595, 1513, 1327, 1323, 1171, 1130, 878 cm^{-1} . UV (CH_2Cl_2) λ_{max} (log ϵ): 351 (4.69), 371 (4.66), 435 (4.38). Em. λ_{max} : 539. MS (APCI): m/z ([isotope], %) 1588.6 (M^+ , 68), 1589.7 (M^+ [¹³C], 100), 1590.8 (M^+ [2¹³C], 63).

BisDBA 18. Octayne **38** (35 mg, 0.022 mmol) was cyclized using general procedure E to yield **18** (7 mg, 33%) as an insoluble red solid. Upon isolation this compound exhibited very poor solubility, thus precluding acquisition of ¹³C NMR data. Mp: 165-180 °C (dec). ¹H NMR (CDCl_3 , 500 MHz): δ 8.48 (s, 2H), 7.79 (s, 2H), 7.67 (d, $J = 8.1$ Hz, 2H), 7.60 (d, $J = 8.1$ Hz, 2H), 7.38 (d, 2H, $J = 9.0$ Hz), 6.82 (s, 2H), 6.64 (d, $J = 2.7$ Hz, 2H), 3.31 (m, 8H), 1.53 (m, 8H), 1.40 (m, 8H), 1.00 (m, 12H). IR (NaCl): ν 2954, 2923, 2847, 2180, 2136, 1736, 1595, 1497, 1460, 1367 cm^{-1} . UV (CH_2Cl_2) λ_{max} (log ϵ):

323 (4.77), 387 (4.52), 472 (4.50). Em. λ_{\max} : 555. MS (APCI): m/z ([isotope], %) 960.0 (M^+ , 82), 961.1 (M^+ [^{13}C], 100), 962.1 (M^+ [2^{13}C], 60).

BisDBA 21. Octayne **38** (100 mg, 0.0628 mmol) was cyclized using general procedure F to give **21** (36 mg, 60%) as an insoluble red solid. Upon isolation this compound exhibited very poor solubility, thus precluding acquisition of ^{13}C NMR data. Mp: 164-175 °C (dec). ^1H NMR (CDCl_3): δ 8.47 (s, 2H), 7.78 (s, 2H), 7.70 (d, 2H, $J=8.1$ Hz), 7.58 (d, 2H, $J=8.1$ Hz), 7.39 (d, 2H, $J=9.3$ Hz), 6.80 (s, 2H), 6.63 (d, 2H, $J=9.3$ Hz), 3.30 (t, 8H, $J=7.0$ Hz), 1.55 (m, 8H), 1.36 (m, 8H, $J=7.2$ Hz), 0.99 (t, 12H, $J=6.6$ Hz). IR (NaCl) ν 2951, 2935, 2874, 2865, 2186, 1590, 1537, 1510, 1310, 1124 cm^{-1} . UV (CH_2Cl_2) λ_{\max} (log ϵ): 325 (4.97), 386 (4.64), 477 (4.68). Em. λ_{\max} : 558. MS (APCI): m/z ([isotope], %) 960.2 (M^+ , 100), 961.2 (M^+ [^{13}C], 68), 962.2 (M^+ [2^{13}C], 47).

Solid-state Optical Measurements. Compounds **1-9** were drop-cast from solutions in CH_2Cl_2 (~1 mM) onto cleaned (70:30 H_2SO_4 : H_2O_2 solution followed by distilled water and nitrogen dried) glass microscope cover slides with rt deposition times of ~30 s. The resulting films were placed under vacuum for 1 h to remove residual solvent and were not annealed. Substrates were cut to fit the spectrophotometers used for the solution-phase spectra prior to coating and were placed either orthogonal to the detector (for absorption) or at a 45° angle to the source and detector (for emission). A cleaned, uncoated glass substrate was used as the blank for the absorption spectra, and displayed no significant absorption past 300 nm.

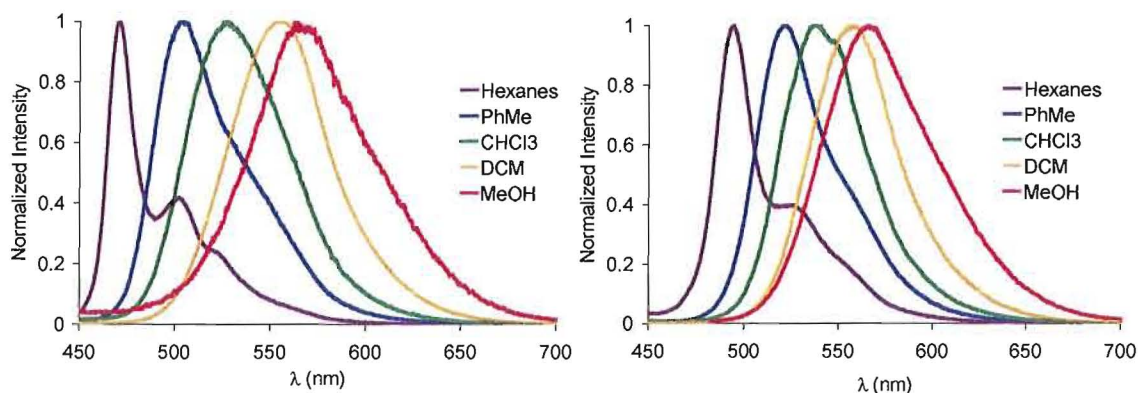


Figure 12. Emission spectra of **16** (left) and **18** (right) in various solvents. Excitation at 365 nm.

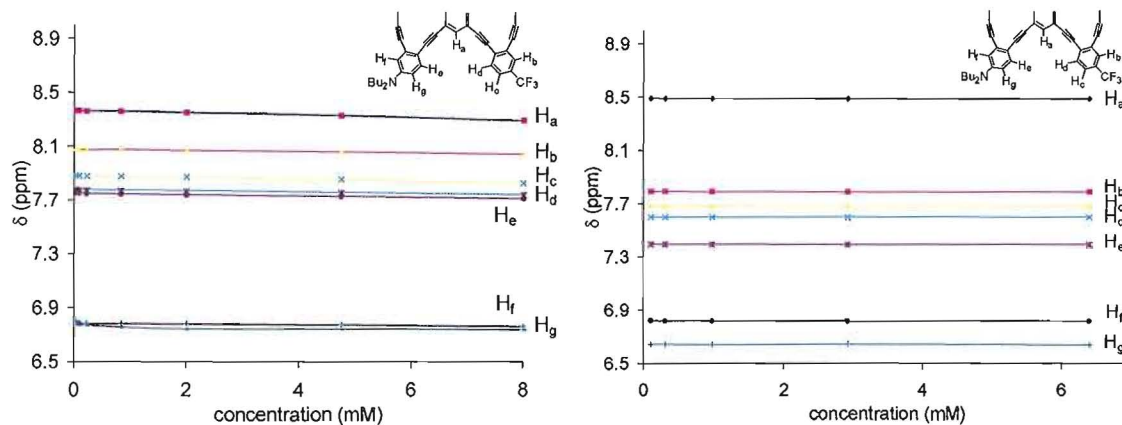


Figure 13. Concentration-dependent chemical shifts of the aromatic protons of **16** (left) and **18** (right) in CDCl_3 at 20 °C.

Bridge to Chapter V

Having described the optoelectronic properties of bis[14] and bis[15]DBAs functionalized with donor groups and weak acceptor groups and made comparison to their nitro-functionalized analogues, Chapter V expands the range of study to include 18-membered DBA structures with nitro acceptor groups. These larger systems experience no ring strain from triple bond distortion, and possess longer chromophore lengths than the [14] and [15]DBAs. Comparison can also be made to earlier mono[18]DBA systems prepared in the Haley lab several years ago. The electronic and physical consequences of fusing a second [18]DBA unit to the molecule and varying the various topologies of donor/acceptor substitution can lead to important structure-property relationship correlations, especially having to do with optical band gap, a significant parameter in nonlinear optical materials design.

CHAPTER V

CHARGE TRANSFER PATHWAY TOPOLOGY-OPTICAL BAND GAP CORRELATIONS IN DONOR/ACCEPTOR-FUNCTIONALIZED BIS(DEHYDROBENZO[18]ANNULENO)BENZENES

Introduction

This chapter was co-authored with Professor Michael M. Haley, who conceptualized the project and provided editorial assistance. This chapter includes work that has been accepted in the *Journal of Organic and Biomolecular Chemistry* (© 2008, Royal Society of Chemistry).

The last decade has seen a dramatic expansion in the study of a special class of carbon-rich conjugated macrocycles, dehydrobenzoannulenes (DBAs), due in part to their demonstrated unique optical, electronics, and materials properties, as well as the increasing synthetic accessibility of desired molecular topologies and site-specific functionalization.¹ These planar phenylacetylenic macrocycles display a host of intriguing characteristics, including enhanced π -orbital overlap, intermolecular π -stacking, and highly tunable dipole and symmetries.² They thus possess potential in a wide array of applications such as fluorimetric sensing, organic electronics,

organopolymers, and nonlinear optical (NLO) device components.³ Large DBA assemblies have been shown to approximate the expected properties of theoretical all-carbon networks graphyne and graphdiyne, and to serve as precursors for nanoporous materials.⁴ We have previously reported DBA systems functionalized with electron donating and accepting groups in a site-specific manner (e.g., Figure 1^{1b}) in order to induce varying degrees of intramolecular charge transfer (ICT),^{2b} and have shown that a particular DBA structure's two-photon absorption (TPA) cross-section, a key parameter in third-order NLO materials, is often closely correlated to its ICT optical band gap in the steady-state one-photon absorption spectrum.^{3c,d} Thus, we have sought to elucidate structure-property relationships in donor/acceptor-functionalized DBAs for the design of customized NLO materials that also possess high molar extinction coefficients. We have demonstrated that while chromophore length affects optical band gap for these systems, the *number* of chromophores (defined here as a linear conjugated pathway) affects the extinction coefficient.^{1b,5} To that end, we now present a series of two-dimensional conjugated quadrupolar bis(dehydrobenzoannuleno)[18]benzenes (1-7, Figure 2) functionalized with donor and acceptor groups at their peripheries. It is hoped that probing the photophysical effects of small variations in functional group orientation and conjugated charge transfer pathway topology will lead to an improved understanding of structure-property relationships, with the ultimate application toward the rational design of the next generation of organic electronics.

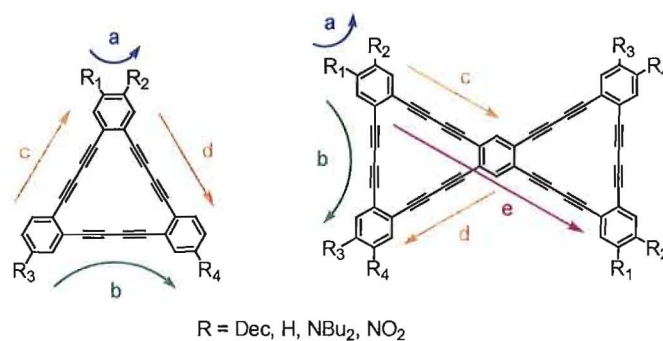


Figure 1. Previously studied mono[18]DBAs with various conjugated pathways a-d^{1b} and target bis[18]DBAs with conjugated pathways a-e.

BisDBAs **1-7** represent an expansion of our previous work on donor/acceptor-functionalized mono[18]DBAs.^{1b} The fusion of two chromophore units into one molecule is expected to lead to similar optical band gaps in the absorption spectrum, but with higher molar extinction coefficients. Of the six target molecules, only **2** and **6** contain an element of asymmetry and possess a net dipole. Furthermore, **1** is an all-donor analogue, and is believed to exhibit only non-ICT π - π^* excitations.^{2b} These molecules thus represent good targets for comparison to **3-5** and **7**.

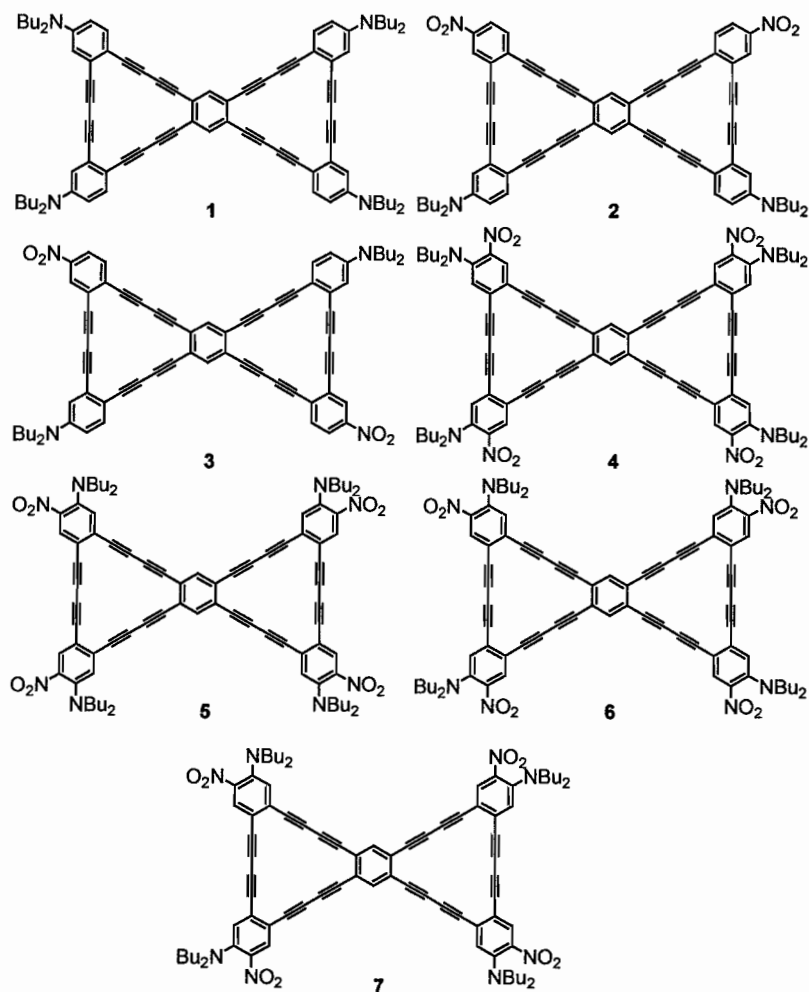


Figure 2. Target Bis[18]DBAs 1-7.

Results and Discussion

Synthesis. Synthesis of 1-7 is accomplished using a highly modular approach based on successive palladium-catalyzed Sonogashira cross-coupling reactions. Donor/acceptor-alkyne segments 8-11 (Figure 3, described previously^{1b,c}) can be appended to 1,2,4,5-tetraiodobenzene (e.g., Scheme 1) or an appropriate isomer of dibromodiiodobenzene (e.g., Scheme 2) using our selective *in situ* desilylation/cross-

soupling protocol. Undesired dimerization of the alkyne segments can be avoided to varying degrees of success by slowly injecting a solution of the segment into the reaction mixture over a period of 8-12 h. Further desilylation followed by an oxidative intramolecular homocoupling under palladium-catalyzed aerobic conditions furnishes the corresponding bis[18]DBA in a wide range of yields (Table 1). It is believed that the variation in isolated yield is due to a significant degree of intermolecular oligomerization. Certain topologies (**2** and **3**) have proven unstable, and rapidly decompose in solution. Consequently, only small amounts of these isomers could be prepared. This behavior was also observed for several of our smaller bis[14]- and bis[15]DBAs^{2b} with similar donor/acceptor topologies (to such an extent that the 14-membered analogue of **3** could not be isolated at all), and is believed to be due to an uncontrolled topochemical 1,3-diacetylene polymerization promoted by strong intermolecular self-association and π -stacking (*vide infra*). The extreme insolubility of **2** and **3** also precludes extensive chromatographic purification; trituration of the crude product with THF has been found to be the only viable alternative. With these limitations in mind, **4-7** were assembled specifically to increase the donor/acceptor pathways and to avoid the strong polarization that leads to this degradative polymerization. The additional alkylamino groups also greatly increase solubility. Due to anticipated synthetic and solubility issues, an all-acceptor analogue was not pursued. DBAs **4-7** are both soluble and stable in CH₂Cl₂ and CHCl₃, and do not undergo decomposition even when left in solution for several days.

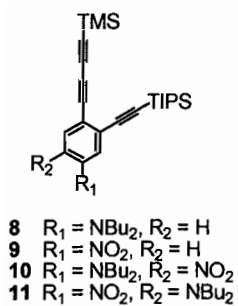
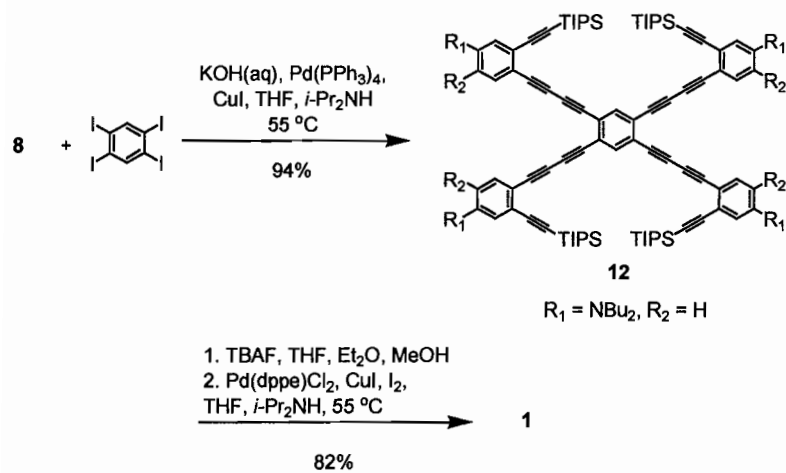


Figure 3. Differentially silylated donor/acceptor alkyne segments **8-11**.^{1b,c}

Scheme 1. Synthesis of DBA **1**.



Scheme 2. Synthesis of DBA7.

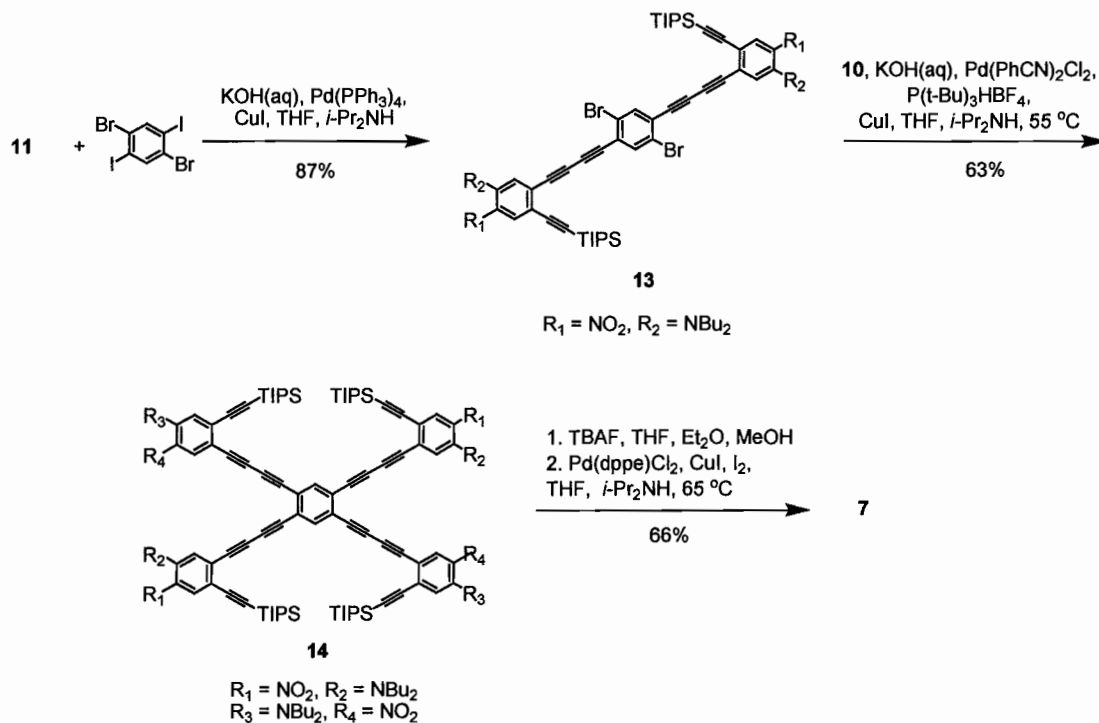


Table 1. Yields for alkyne segment couplings and cyclization to DBAs 1-7.

arene	1 st coupled segment (pdt, yield)	2 nd coupled segment (pdt, yield)	DBA (yield)
	8 (12, 94%)	-	1 (82%)
	10 (15, 70%)	-	4 (60%)
	11 (16, 92%)	-	5 (49%)
	9 (17, 86%)	8 (18, 18%)	2 (10%)
	11 (19, 78%)	10 (20, 21%)	6 (19%)
	9 (21, 71%)	8 (22, 24%)	3 (9%)
	11 (13, 87%)	10 (14, 63%)	7 (66%)

Electronic Absorption Spectra. The UV-visible absorption spectra of **1-7** are given in Figure 4. All compounds display longest-wavelength absorption maxima between 450 and 520 nm (Table 2). With the exception of tetradonor **1**, all contain strong donor/acceptor functionalization. Frontier molecular orbital plots of these types of systems consistently predict strong localization of the HOMO on the donor-functionalized alkyne chromophore segments and the LUMO on the acceptor segments, implying intramolecular charge transfer as the lowest energy transition.^{2,3a} The low, broadened peaks in this region for **2-7**, often accompanied by bathochromic shifts relative to **1**, are indicative of ICT behavior and are consistent with our previous DBA studies. In all compounds, conversion from the acyclic precursors to the corresponding bisDBA results in a bathochromic shift in the absorption spectra (example spectra, Figure 5). This is likely due to an enhanced conjugation effect from the enforced planarization. It is notable that for DBAs **1** and **4**, with donor groups situated along the longest linear chromophore path, cyclization causes an increase in molar extinction coefficient in the longest wavelength band in addition to a bathochromic shift, whereas in the other systems a corresponding decrease is seen. This is presumably due to enhanced ICT and delocalization in the planarized macrocycles.

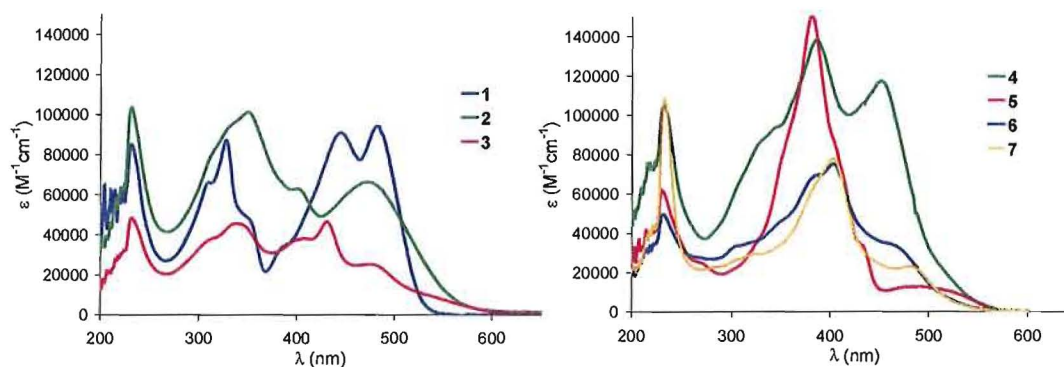


Figure 4. Electronic absorption spectra of DBAs **1-3** and **4-7** in CH_2Cl_2 .

Table 2. Lowest energy absorptions in **1-7**.

DBA	longest wavelength λ_{max} [nm] (ϵ [$\text{M}^{-1}\text{cm}^{-1}$])	approximate λ_{cutoff} [nm]
1	481 (94030)	560
2	471 (66170)	626
3	^a 517 (12530)	656
4	451 (117070)	569
5	490 (12680)	567
6	^a 456 (34590)	575
7	480 (22870)	571

^aapproximate λ_{max} as band is only a shoulder.

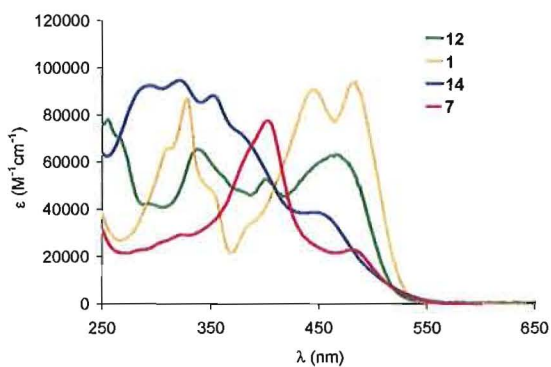


Figure 5. Electronic absorption spectra of acyclic precursors **12** and **14** and their respective DBAs **1** and **7**.

Comparing two-donor/two-acceptor DBAs **2** and **3** to tetradonor **1**, we see a significant broadening of the corresponding bands, with absorption cutoffs extending past 600 nm. In the case of **3**, the lowest discernible band exists as a shoulder beginning near 517 nm, indicating a narrowed optical band gap relative to **1**. Interestingly, the ICT band in **2** is slightly blue-shifted from **1**. This was initially a surprising result, since **2** contains two long, linear conjugated pathways from the donor groups to the acceptor groups; one might intuitively expect such a topology to exhibit a significantly narrowed band gap. This result is consistent, however, with previous observations by Meier *et al.*,^{6a} who also noted hypsochromic shifts in the absorption spectra of certain extended chromophores upon strong donor/acceptor functionalization. In those cases, the nearly complete lack of calculated Franck-Condon overlap actually resulted in predominantly non-HOMO-LUMO transitions as the lowest energy absorptions. Furthermore, Diederich and coworkers have observed a lack of correlation between optical band gap and conjugated pathway efficiency for certain donor/acceptor cyanoethynylethene systems,^{6b} finding instead that quadrupolar compounds with bent donor/acceptor pathways (analogous to pathway *c-d* in Figure 1) often display smaller band gaps than corresponding dipolar analogues with linear pathways (path *e* in Figure 1). Our own systematic structure-property studies involving isomeric permutations of particular acyclic donor/acceptor motifs have confirmed this phenomenon.^{2b,3} Note that **3** is quadrupolar rather than dipolar, and exhibits the smallest band gap of the DBAs presented here. This property could potentially have consequences for the future design of organic NLO materials, particularly those that rely on good two-photon absorption (TPA) parameters. We have

shown that systems with either symmetric multi-chromophore units or strong donor/acceptor-functionalization can display particularly high TPA cross-sections.^{1c,3c-e} The DBAs presented here, which possess both qualities, are expected to follow suit.

The absorption spectra of the four-donor/four-acceptor DBAs **4-7** provide further insight into structural effects on band gap. Each of these compounds contains four donor groups and four acceptor groups; only the orientation of them with respect to the DBA skeleton varies. Here only **6** possesses a net dipole, while all the others are quadrupolar, thus allowing us to investigate only the effects of conjugated pathway topology on the band gap. It is interesting to note that **4-7** all display absorption cutoffs at nearly the same wavelength. The most striking feature, however, is the high molar extinction coefficient in **4**, whose spectrum somewhat resembles tetradonor **1**. This is not surprising, since the four donor groups lie along the longest conjugated chromophores as in **1**, with the acceptor groups along the bridging diacetylenes. **5-7** display more characteristic low-intensity ICT bands red-shifted from **4**, with **5** possessing the smallest band gap. DBA **5** most resembles a ‘tetraacceptor’ system, with acceptor groups along the longest conjugated pathway, and donors along the diacetylene bridges. DBAs **6** and **7** lie in between these two extremes. In this case, the dipolar DBA **6**, which contains only linear donor- π -acceptor pathways, is only slightly red-shifted from **4**, while **7** (with only two linear ICT pathways) and **5** (with no linear ICT pathways) are more red-shifted. Thus, we are led to the conclusion that for these systems, a supposedly ‘efficient’ linear donor- π -acceptor conjugated chromophore does not lead to the lowest energy charge transfer transition.

Comparing all the spectra of **1-7**, we can note that placing like groups along a longest chromophore (donor- π -donor or acceptor- π -acceptor) results in the smallest band gaps, with acceptor- π -acceptor arrangements being particularly effective. This makes sense when considering the likely FMO localizations (which were not computed for these systems here, but for which there is extensive precedent from our earlier studies^{1,2a,3,6}): rather than exhibiting the behavior of a donor atom transferring electron density to an acceptor atom, the spectra imply a transition from an electron-rich chromophore to an electron-poor chromophore, wherein two directly conjugated donor groups contribute to generate the former, and two acceptor groups contribute to the latter. The band gap is thus more dependent on the length of the linear chromophores, and hence is smaller for the quadrupolar systems than for the dipolar ones. This “synergistic cooperation” was also observed for our previously-reported mono[18]DBAs:^{1b} the smallest band gaps occurred when a donor was conjugated to a donor and an acceptor to an acceptor. Linear donor/acceptor pathways exhibited larger band gaps. In those cases, however, the necessary asymmetry of most of the DBAs could lead to potential skewing from dissimilar net dipole effects which are not present in most of the bis[18]DBAs presented here. Finally, our most bathochromic systems here, **3** and **5**, display charge transfer bands with molar extinction coefficients roughly double those of analogous mono[18]DBAs, but in the same 490-530 nm region. In donor-functionalized systems, the bisDBAs display both higher extinction coefficients from fusion of a second annulenic unit *and* longer wavelength absorptions from extension of the chromophore lengths.

Electronic Emission Spectra. Many of the DBAs and donor/acceptor systems we have presented in the past exhibit efficient fluorescence.^{2,3a,b} Small structural variations of the conjugated pathways (e.g., chromophore topology, polarization, planarity, donor or acceptor strength, protonation or metal ion complexation ability, etc.) can fine-tune both emission wavelength and quantum yield. In donor/nitro-functionalized systems, however, the high internal conversion rate caused by mixing of vibronic states as well as solvent interaction effectively quenches fluorescence.^{3b} The only highly emissive DBA presented here is therefore tetradonor **1** ($\Phi_f = 0.34$ in CH_2Cl_2). The long, electron-rich conjugated pathways and the lack of a net dipole likely result in an excited state that is highly polarized relative to the ground state. The photophysical manifestation of this is a dramatic degree of fluorescence solvatochromism (Figure 6), with emission maxima ranging from 486 nm in hexane to 587 nm in acetone. The absorption spectra by contrast (Table 3), display only slight solvent dependence, implying that the effect is enhanced by relaxation to increasingly low-lying vibrational levels of the S_1 state after initial excitation (note the gradual loss of vibronic fine structure in Figure 6 as solvent polarity increases). In contrast, DBA **4**, which also has its donor groups along the longest chromophores but also acceptors along the diacetylene bridges, is only slightly fluorescent, displaying jagged, irregular peaks and much less solvent dependence (Figure 7). DBAs **2**, **3**, and **5-7** do not fluoresce at all. No concentration dependence was noted in either absorption or emission spectra for any compound.

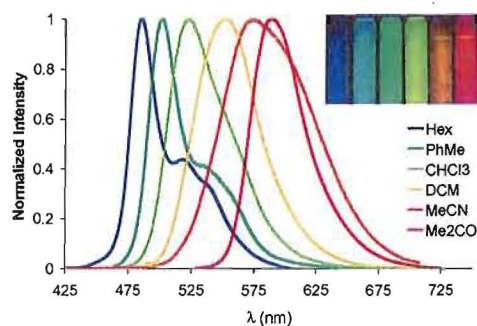


Figure 6. Emission spectra of **1** in hexanes (Hex), toluene (PhMe), chloroform (CHCl_3), dichloromethane (DCM), acetonitrile (MeCN), and acetone (Me_2CO). Excitation at 365 nm. Inset: photographs of solutions of **1** in various corresponding solvents (left to right) under illumination by high-intensity 365 nm lamp.

Table 3. Lowest energy absorption and emission wavelengths of **1** in various solvents.

solvent	absorption λ_{max} (nm)	emission λ_{max} (nm)
hexanes	466	486
toluene	471	502
chloroform	478	522
dichloromethane	481	551
acetonitrile	482	575
acetone	479	587

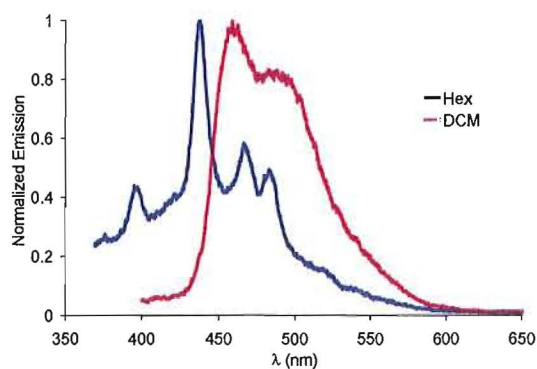


Figure 7. Normalized electronic emission spectra of DBA **4** in hexanes (Hex) and dichloromethane (DCM). Excitation at 358 and 385 nm, respectively.

Self-Association. Our previously reported bis[14] and bis[15]DBAs (e.g., **23** and **24**, Figure 8),^{2b} also functionalized with dibutylamino and nitro groups, displayed a significant degree of intermolecular self-association in solution, presumably due to π -stacking enhanced by attraction between donor and acceptor groups between molecules. The aggregation was manifested by upfield shifts of the ¹H-NMR signals of the aromatic protons with increasing concentration. It has been confirmed that the monomer-dimer equilibrium is the dominant process in these systems, and hence dimerization constants could be calculated from the concentration-dependent chemical shifts. This effect was not observed in DBAs **1** or **4-7**, or in equimolar mixtures of **4** and **5** (which could theoretically form dimer aggregates when respective donor and acceptor groups from each molecule are π -stacked). It is believed that the *ortho* relationship between the alkylamino and nitro groups on each arene ring can prevent strong polarization (dipolar or quadrupolar) and effectively “cancel out” any long-range intermolecular attraction. Tetradonor **1** possesses no acceptor groups to enhance π -stacking via intermolecular attraction.

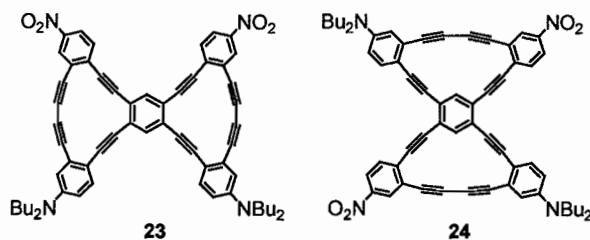


Figure 8. Examples of previously reported bis[14] and bis[15]DBAs that display self-association in solution.^{2b}

DBA **2** underwent rapid degradation in CDCl_3 solution, so concentration-dependent experiments could not be conducted. DBA **3**, however, remained stable long enough for several concentration-dependence data points to be collected (Figure 9). The protons residing on the donor and acceptor arene rings experienced the greatest degree of upfield shifts, and the central arene ring protons experienced the least, indicating the greatest degree of change in the shielding environment where the donors of one molecule interact with the acceptors of another, and vice versa. The gradual upfield shifts were fitted to curves using the HypNMR program⁷ from which a dimerization constant of $515 \pm 31 \text{ M}^{-1}$ was extracted. This value is only slightly larger than for the smaller analogous DBA **23** ($326 \pm 51 \text{ M}^{-1}$), and may be due to more efficient stacking due to increased π -orbital overlap in the strain-free bis[18]DBA.

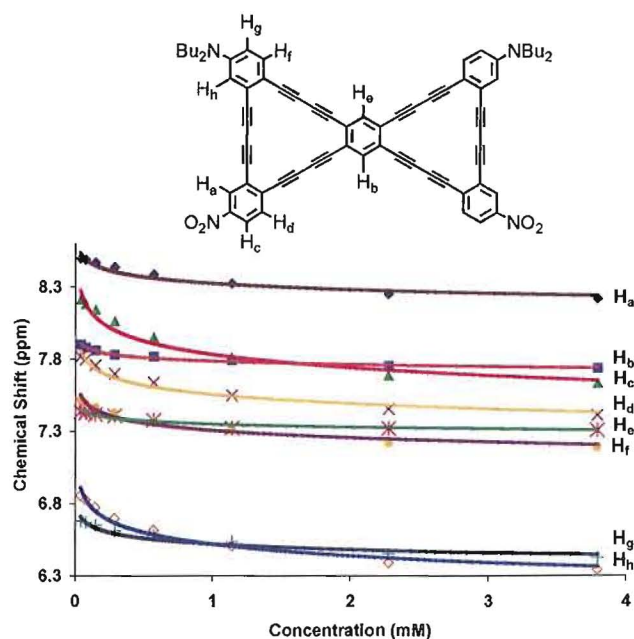


FIGURE 9. Concentration-dependent chemical shifts of the aromatic protons of DBA **3** in CDCl_3 at 20 °C.

Conclusions

Bis[18]DBAs **1-7** represent an important systematic investigation into the effects of conjugation pathway topology, chromophore length, and symmetry on the optical band gaps of carbon-rich intramolecular charge transfer systems. We have demonstrated that quadrupolar chromophores with linear donor- π -donor and acceptor- π -acceptor pathways can exhibit narrowed band gaps versus donor- π -acceptor analogues, and comparison to our earlier mono[18]DBAs shows that while extending the length of a donor-functionalized system results in absorption red shifts, increasing the number of chromophore units in the system causes an increase in molar extinction coefficient. Our studies also support observations in other systems that strong donor/acceptor functionalization of an extended chromophore can actually lead to increased band gaps due to lack of Franck-Condon overlap of segment-isolated FMOs.⁶ It has been shown in the past that highly conjugated organic molecules often exhibit high TPA cross-sections, especially when possessing either high symmetry or donor/acceptor functionalization.^{1c,3c-}

^e The systems presented here satisfy both conditions, so it is expected that they will display particularly favorable results, and we hope to report the outcome of these experiments in the near future.

Experimental

General Methods. These have been described in previously.^{2b} Synthesis of segments **8-11** have been described previously.^{1b}

General Alkyne Coupling Procedure A. Alkyne segment **8,10**, or **11** (5.0 equiv) and 1,2,4,5-tetraiodobenzene (1 equiv) were dissolved in *i*Pr₂NH:THF (3:3, 0.003 M) and the solution was purged for 30 min with bubbling Ar. PdCl₂(PPh₃)₂ (0.03 equiv per transformation), CuI (0.06 equiv per transformation) and aqueous KOH (5 equiv per transformation) were added and the solution was purged another 20 min. The reaction mixture was stirred at 55 °C for 24-48 h under an Ar atmosphere until complete by TLC. The mixture was then concentrated, rediluted with hexanes, and filtered through a pad of silica gel. The solvent was removed in vacuo and the crude material was used without further purification.

General Alkyne Coupling Procedure B. Acceptor segment **9** or **11** (2.5 equiv) and the appropriate isomer of dibromodiodobenzene (1 equiv) were dissolved in *i*Pr₂NH:THF (3:3, 0.003 M) and the solution was purged for 30 min with bubbling Ar. PdCl₂(PPh₃)₂ (0.03 equiv per transformation), CuI (0.06 equiv per transformation) and aqueous potassium carbonate (5 equiv per transformation) were added and the solution was purged another 20 min. The reaction mixture was stirred at room temperature for 24-48 h under an Ar atmosphere until complete by TLC. The mixture was then concentrated, rediluted with hexanes, and filtered through a pad of silica gel. The solvent was removed in vacuo and the crude material was used without further purification.

General Alkyne Coupling Procedure C. Acceptor-functionalized tetrayne **13**, **17**, **19** or **21**, and aqueous KOH (5 equiv per transformation) were dissolved in *i*Pr₂NH:THF (3:2, 0.004 M) and the solution was purged for 30 min with bubbling Ar. Pd(PhCN)₂Cl₂ (0.03 equiv per transformation), P(*t*-Bu)₃HBF₄ (0.07 equiv per transformation) and CuI

(0.06 equiv per transformation) were added and the solution was purged for another 20 min under bubbling Ar. Donor segment **8** or **10** (2.5 equiv) was dissolved in THF (0.04 M), the solution was purged for 30 min under bubbling Ar, and then injected via syringe pump into the stirred polyne solution over 8 h at 55 °C under an Ar atmosphere. The reaction was stirred until complete by TLC. The mixture was then concentrated, rediluted with hexanes:CH₂Cl₂ (4:1), and filtered through a pad of silica gel. The solvent was removed in vacuo, and the crude material was purified by column chromatography.

General Pd-catalyzed Cyclization Procedure D. Annulene precycle was dissolved in THF, Et₂O and MeOH (2:1:0.01, 0.005 M) and Bu₄NF (TBAF, 1.0 M soln in THF, 10 equiv) was added. The solution was stirred at room temperature until complete by TLC (typically <1 h). The reaction mixture was then concentrated, dissolved in Et₂O, and washed with H₂O (3 x 50 mL). The organic phase was collected, dried over MgSO₄, and filtered through a pad of silica gel eluting with hexanes. The solvent was removed in vacuo and deprotected precycle was dissolved in THF (0.005 M). PdCl₂(dppe) (0.1 equiv per transformation), CuI (0.2 equiv per transformation), and I₂ (0.25 equiv per transformation) were dissolved in *i*Pr₂NH:THF (1.4:1, ~0.5 L per mmol precycle). To this mixture, the deprotected precycle solution was injected via syringe pump over 40 h at 65 °C. The reaction mixture was stirred until complete by TLC, then concentrated, rediluted in hexanes:CH₂Cl₂ (3:1) and filtered through a pad of silica gel. The solvent was removed in vacuo and the product was triturated with hexanes.

DBA precursor 12. Segment **8** (306 mg, 0.605 mmol) was cross-coupled to 1,2,4,5-tetraiodobenzene (78 mg, 0.134 mmol) at 55 °C using general alkyne coupling procedure

A (12 h). The crude material was purified by column chromatography (4:1 hexanes:CH₂Cl₂) to give **12** (227 mg, 94%) as a dark red oil. ¹H NMR (CDCl₃): δ 7.51 (s, 2H), 7.35 (d, *J* = 9.0 Hz, 4H), 6.66 (d, *J* = 2.7 Hz, 4H), 6.49 (dd, *J* = 9.0, 2.7 Hz), 3.27 (t, *J* = 7.5 Hz, 16H), 1.54 (quin, *J* = 7.5 Hz, 16H), 1.34 (sext, *J* = 7.2 Hz, 16H), 1.18 (s, 84H), 0.96 (t, *J* = 7.2 Hz, 24H). ¹³C NMR (CDCl₃): δ 148.30, 137.66, 134.58, 128.57, 125.49, 114.89, 111.72, 110.40, 105.84, 94.59, 85.37, 81.84, 78.87, 75.99, 50.78, 29.50, 20.48, 18.97, 14.16, 11.60. IR (NaCl): ν 2959, 2935, 2856, 2191, 2155, 1589, 1530, 1479, 1365, 1223, 1113 cm⁻¹. MS (APCI): *m/z* (%) 1719.2 (M⁺-TIPS+THF, 65), 1720.2 (M⁺¹³C-TIPS+THF, 93), 1721.2 (M⁺2¹³C-TIPS+THF, 100). UV (CH₂Cl₂) λ_{max} (log ε): 400 (4.73), 466 (4.81). Em. λ_{max}: 551. Φ_f = 0.18.

Tetradonor DBA 1. Precursor **12** (136 mg, 0.075 mmol) was subjected to general Pd-catalyzed cyclization procedure D (40 h). The crude material was purified by filtration through a pad of silica gel followed by concentration in vacuo and trituration with hexanes to afford 72 mg (82%) of **1** as a brick red powder. Once purified, the product exhibited very poor solubility, thus precluding acquisition of ¹³C NMR data. Mp: 200-220 °C (dec). ¹H NMR (CDCl₃): δ 7.78 (s, 2H), 7.49 (d, *J* = 8.7 Hz, 4H), 6.84 (s, 4H), 6.66 (d, *J* = 11.4 Hz, 4H), 3.30 (t, *J* = 6.9 Hz, 16H), 1.59 (m, 16H), 1.40 (sext, *J* = 7.8 Hz, 16H), 0.99 (t, *J* = 7.2 Hz, 24H). ¹H NMR (300 MHz, THF-*d*₈): δ 7.84 (s, 2H), 7.50 (d, *J* = 9.0 Hz, 4H), 6.92 (s, 4H), 6.80 (d, *J* = 9.0 Hz, 4H), 3.39 (t, *J* = 7.8 Hz, 16H), 1.63 (m, 16H), 1.40 (sext, *J* = 7.5 Hz, 16H), 0.99 (t, *J* = 7.5 Hz, 24H). IR (KBr): ν 2956, 2929, 2871, 2136, 1591, 1590, 1482, 1368, 1218, 1110 cm⁻¹. UV (CH₂Cl₂) λ_{max} (log ε): 445 (4.96), 481 (4.98). Em. λ_{max}: 551. Φ_f = 0.34.

Acceptor-functionalized arene 17. Segment **9** (500 mg, 1.18 mmol) was cross-coupled to 1,3,-dibromo-4,6-diiodobenzene (173 mg, 0.36 mmol) at rt for 24 h using general alkyne coupling procedure B. The crude material was purified by column chromatography (4:1 hexanes:CH₂Cl₂) to give **17** (285 mg, 86%) as a yellow powder. Once purified, the product exhibited very poor solubility, thus precluding acquisition of mass spectrometry data. Mp: 170-173 °C. ¹H NMR (CDCl₃): δ 8.32 (d, *J* = 2.2 Hz, 2H), 8.12 (dd, *J* = 9.0, 2.2 Hz, 2H), 7.91 (s, 1H), 7.67 (s, 1H), 7.66 (d, *J* = 9.0 Hz, 2H), 1.18 (s, 42H). ¹³C NMR (CDCl₃): δ 147.53, 138.81, 136.69, 133.87, 133.71, 128.89, 127.84, 127.42, 123.71, 122.86, 102.42, 100.49, 81.75, 81.11, 80.96, 79.45, 18.96, 11.46. IR (KBr): ν 2941, 2863, 2150, 1592, 1521, 1455, 1345, 1106, 1062, 884, 853, 814, 745, 723, 680 cm⁻¹.

DBA precursor 18. Acceptor-functionalized arene **17** (430 mg, 0.860 mmol) was cross-coupled with segment **8** (270 mg, 0.289 mmol) at 55 °C for 72 h using general alkyne coupling procedure C (injection over 12 h). The crude material was purified by column chromatography (4:1 hexanes:CH₂Cl₂) to give **18** (85 mg, 18%) as a red oil. ¹H NMR (CDCl₃): δ 8.32 (t, *J* = 2.1 Hz, 2H), 8.12 (m, 2H), 7.73 (s, 1H), 7.68 (dd, *J* = 9.0, 2.1 Hz, 2H), 7.59 (s, 1H), 7.33 (dd, *J* = 9.0, 2.7 Hz, 2H), 6.68 (d, *J* = 2.7 Hz, 2H), 6.50 (dd, *J* = 9.3, 2.7 Hz, 2H), 3.28 (t, *J* = 7.8 Hz, 8H), 1.56 (quin, *J* = 5.4 Hz, 8H), 1.32 (sext, *J* = 7.8 Hz, 8H), 1.16 (s, 84H), 0.96 (t, *J* = 7.2 Hz, 12H). ¹³C NMR (CDCl₃): δ 148.9, 147.5, 140.4, 134.5, 133.9, 130.7, 130.4, 128.9, 127.8, 127.4, 125.2, 122.9, 116.5, 115.0, 113.6, 108.2, 105.8, 104.6, 102.4, 100.4, 100.2, 89.7, 86.7, 84.0, 81.9, 81.2, 81.0, 79.4, 50.8, 29.5, 20.5, 19.0, 14.2, 11.5 ppm. IR (KBr): ν 2955, 2934, 2886, 2861, 2185, 2149, 1655,

1630, 1568, 1557, 1539, 1517, 1499, 1477, 1452, 1346 cm^{-1} . MS (APCI): m/z (%) 1639.5 (M^+ , 72), 1640.5 ($M+1$, 100), 1641 ($M+2$, 90). UV (CH_2Cl_2) λ_{max} ($\log \epsilon$): 342 (5.05), 363 (5.04), 471 (4.71).

DBA 2. Precursor **18** (80 mg, 0.049 mmol) was subjected to general Pd-catalyzed cyclization procedure D (36 h). The crude material was purified by filtration through a pad of silica gel followed by concentration in vacuo and trituration with hexanes to afford 4.9 mg (10%) of **3** as a red powder. Once purified, the product exhibited very poor solubility, thus precluding acquisition of ^{13}C NMR data. Mp: 160-180 $^\circ\text{C}$ (dec). ^1H NMR (CDCl_3): δ 8.40 (s, 2H), 8.05 (s, 1H), 7.98 (d, $J = 7.8$ Hz, 2H), 7.82 (s, 1H), 7.67 (d, $J = 9.0$ Hz, 2H), 7.39 (d, $J = 9.3$ Hz, 2H), 6.65 (s, 2H), 6.59 (d, $J = 9.0$ Hz, 2H), 3.26 (t, $J = 8.4$ Hz, 8H), 1.56 (m, 8H), 1.42 (sext, $J = 8.2$ Hz, 8H), 1.00 (t, $J = 8.2$ Hz, 12H). IR (KBr): ν 2947, 2924, 2852, 2184, 1719, 1590, 1512, 1461, 1334, 1261, 1214, 1018, 196 cm^{-1} . MS (APCI): m/z (%) 1012.5 (29), 1010.0 (M^+ , 54), 968.8 (40), 921.7 (30), 690.3 (65), 604.0 (100). UV (CH_2Cl_2) λ_{max} ($\log \epsilon$): 400 (4.80), 471 (4.82).

Acceptor-functionalized arene 21. Segment **9** (203 mg, 0.479 mmol) was cross-coupled to 1,4,-dibromo-2,5-diiodobenzene (96 mg, 0.197 mmol) at rt for 36 h using general alkyne coupling procedure B. The crude material was purified by column chromatography (5:1 hexanes: CH_2Cl_2) to give **21** (131 mg, 71%) as an insoluble yellow powder. Mp: 192.5-195.8 $^\circ\text{C}$ (dec). ^1H NMR (CDCl_3): δ 8.33 (d, $J = 2.1$ Hz, 2H), 8.12 (dd, $J = 8.8, 2.1$ Hz, 2H), 7.74 (s, 2H), 7.68 (d, $J = 8.8$ Hz, 2H), 1.18 (s, 42H). ^{13}C NMR (CDCl_3): δ 147.56, 137.69, 133.88, 130.60, 128.95, 127.41, 126.34, 124.63, 122.86, 102.38, 100.60, 82.01, 81.60, 81.22, 81.21, 18.94, 11.45. IR (KBr): ν 2941, 2863, 1653,

1569, 1522, 1458, 1437, 1344, 1067, 995, 883, 835, 815, 743, 679 cm^{-1} . MS (APCI): m/z (%) 932.2 ($\text{M}^{+79}\text{Br}^{79}\text{Br}$, 68), 934.2 ($\text{M}^{+79}\text{Br}^{81}\text{Br}$, 100), 935.2 ($\text{M}^{+13}\text{C}^{79}\text{Br}^{81}\text{Br}$, 81), 936.2 ($\text{M}^{+81}\text{Br}^{81}\text{Br}$, 58).

DBA precursor 22. Acceptor-functionalized arene **21** (770 mg, 1.52 mmol) was cross-coupled with segment **8** (474 mg, 0.507 mmol) at 55 °C for 72 h using general alkyne coupling procedure C (injection over 6 h). The crude material was purified by column chromatography (9:1 hexanes: CH_2Cl_2) to give **22** (193 mg, 24%) as a red oil. ^1H NMR (CDCl_3): δ 8.32 (d, $J = 2.2$ Hz, 2H), 8.10 (dd, $J = 8.6, 2.2$ Hz, 2H), 7.68 (d, $J = 8.6$ Hz, 2H), 7.57 (s, 2H), 7.34 (d, $J = 8.8$ Hz, 2H), 6.68 (d, $J = 2.4$ Hz, 2H), 6.50 (dd, $J = 8.8, 2.4$ Hz, 2H), 3.28 (t, $J = 7.8$ Hz, 8H), 1.53 (quin, $J = 7.2$ Hz, 8H), 1.34 (sext, $J = 7.4$ Hz, 8H), 1.18 (s, 84H), 0.96 (t, $J = 7.4$ Hz, 12H). IR (KBr): ν 2954, 2934, 2879, 2180, 1649, 1590, 1562, 1537, 1518, 1488, 1346 cm^{-1} . MS (APCI): m/z (%) 1639.5 (M^+ , 70), 1640.5 ($\text{M}+1$, 100), 1641 ($\text{M}+2$, 81).

DBA 3. Precursor **22** (90 mg, 0.055 mmol) was subjected to general Pd-catalyzed cyclization procedure D (25 h). The crude material was purified by filtration through a pad of silica gel followed by concentration in vacuo and trituration with hexanes to afford 5.0 mg (9%) of **3** as a red powder. Once purified, the product exhibited very poor solubility, thus precluding acquisition of ^{13}C NMR data. Mp: 160-180 °C (dec). ^1H NMR (CDCl_3): δ 8.34 (d, $J = 2.1$ Hz, 2H), 7.97 (dd, $J = 6.6, 2.1$ Hz, 2H), 7.69 (s, 2H), 7.58 (d, $J = 8.7$ Hz, 2H), 7.32 (d, $J = 8.7$ Hz, 2H), 6.63 (s, 2H), 6.52 (d, $J = 10.5$ Hz, 2H), 3.21 (t, $J = 8.4$ Hz, 8H), 1.55 (m, 8H), 1.39 (sext, $J = 7.0$ Hz, 8H), 0.99 (t, $J = 7.0$ Hz, 12H). IR (KBr): ν 2956, 2924, 2853, 2348, 1734, 1635, 1576, 1522, 1465, 1344, 1214, 1092, 458

cm^{-1} . MS (APCI): m/z (%) 1012.5 (35), 1010.0 (M^+ , 51), 968.8 (30), 690.3 (44), 604.0 (100). UV (CH_2Cl_2) λ_{max} ($\log \epsilon$): 431 (4.67), 475 (4.40), 517(sh) (4.10).

DBA precursor 15. Segment **10** (71 mg, 0.129 mmol) was cross-coupled to 1,2,4,5-tetraiodobenzene (15 mg, 0.026 mmol) at 55 °C using general alkyne coupling procedure A (12 h). The crude material was purified by column chromatography (4:1 hexanes: CH_2Cl_2) to give **15** (113 mg, 70%) as a dark red oil. ^1H NMR (CDCl_3): δ 7.90 (s, 4H), 7.57 (s, 2H), 7.10 (s, 4H), 3.15 (t, $J = 7.2$ Hz, 16H), 1.53 (quin, $J = 6.6$ Hz, 16H), 1.28 (sext, $J = 7.5$ Hz, 16H), 1.24 (s, 84H), 0.89 (t, $J = 7.5$ Hz, 24H). ^{13}C NMR (CDCl_3): δ 145.26, 139.56, 137.89, 131.67, 131.39, 125.62, 124.16, 113.55, 103.58, 99.90, 82.42, 81.32, 79.14, 77.22, 51.76, 29.72, 20.26, 18.93, 14.04, $\overline{11.53}$. IR (NaCl): ν 2958, 2926, 2861, 2204, 1652, 1596, 1539, 1504, 1475, 1456, 1416 cm^{-1} . MS (APCI): m/z (%) 1984.6 (M^+H^+ , 66), 1986.1 ($\text{M}^{+13}\text{CH}^+\text{H}^+$, 100). UV (CH_2Cl_2) λ_{max} ($\log \epsilon$): 288 (5.01), 329 (5.00), 354 (4.99), 384 (4.89), 432 (4.88).

DBA 4. Precursor **15** (108 mg, 0.054 mmol) was subjected to general Pd-catalyzed cyclization procedure D (40 h). The crude material was purified by filtration through a pad of silica gel followed by concentration in vacuo and trituration with hexanes to afford 44 mg (60%) of **4** as a bright orange powder. Mp: 170-190 °C (dec). ^1H NMR (CD_2Cl_2): δ 8.00 (s, 4H), 7.83 (s, 2H), 7.31 (s, 4H), 3.18 (t, $J = 7.5$ Hz, 16H), 1.55 (quin, $J = 7.5$ Hz, 16H), 1.28 (sext, $J = 7.5$ Hz, 16H), 0.89 (t, $J = 7.5$ Hz, 24H). ^{13}C NMR (CD_2Cl_2): δ 144.98, 140.03, 136.40, 131.74, 128.80, 125.19, 124.71, 113.05, 82.38, 81.74, 80.88, 79.80, 79.04, 77.24, 51.94, 29.65, 20.26, 13.79. IR (NaCl): ν 2952, 2926, 2868, 2191,

1595, 1543, 1502, 1476, 1457, 1431 cm^{-1} . UV (CH_2Cl_2) λ_{max} ($\log \epsilon$): 387 (5.14), 451 (5.07). Em. λ_{max} : 459.

DBA precursor 16. Segment **11** (260 mg, 0.472 mmol) was cross-coupled to 1,2,4,5-tetraiodobenzene (46 mg, 0.079 mmol) at 55 °C using general alkyne coupling procedure A (12 h). The crude material was purified by column chromatography (4:1 hexanes: CH_2Cl_2) to give **16** (143 mg, 92%) as a dark red oil. ^1H NMR (CDCl_3): δ 7.82 (s, 4H), 7.64 (s, 2H), 7.21 (s, 4H), 3.11 (t, $J = 4.2$ Hz, 16H), 1.49 (quin, $J = 3.9$ Hz, 16H), 1.26 (sext, $J = 4.5$ Hz, 16H), 1.14 (s, 84H), 0.87 (t, $J = 4.2$ Hz, 24H). ^{13}C NMR (CDCl_3): δ 144.29, 140.94, 138.23, 130.59, 128.60, 125.70, 125.20, 117.01, 102.96, 96.11, 82.64, 81.03, 79.97, 79.40, 51.92, 29.71, 20.26, 18.96, 14.03, 11.53. IR (NaCl): ν 2982, 2963, 2882, 2209, 2179, 1717, 1624, 1458, 1436, 1362, 1344, 1318 cm^{-1} . MS (APCI): m/z (%) 1983.5 (M^+ , 70), 1984.4 (M^+H^+ , 72), 1985.6 ($\text{M}^{+13}\text{CH}^+$, 100). UV (CH_2Cl_2) λ_{max} ($\log \epsilon$): 318 (5.16), 360 (4.98), 467 (4.25).

DBA 5. Precursor **16** (117 mg, 0.059 mmol) was subjected to general Pd-catalyzed cyclization procedure D (40 h). The crude material was purified by filtration through a pad of silica gel followed by concentration in vacuo and trituration with hexanes to afford 38 mg (49%) of **5** as a deep red powder. Mp: 165-180 °C (dec). ^1H NMR (CDCl_3): δ 7.96 (s, 4H), 7.82 (s, 2H), 7.29 (s, 4H), 3.18 (t, $J = 7.5$ Hz, 16H), 1.57 (quin, $J = 6.9$ Hz, 16H), 1.30 (sext, $J = 7.2$ Hz, 16H), 0.92 (t, $J = 7.5$ Hz, 24H). ^{13}C NMR (CDCl_3): δ 144.66, 140.26, 137.08, 131.23, 128.73, 125.77, 124.60, 114.15, 100.23, 81.91, 81.22, 80.35, 79.75, 79.65, 51.94, 29.72, 20.33, 14.08. IR (NaCl): ν 2954, 2924, 2868, 2198,

2148, 1638, 1594, 1531, 1482, 1435, 1369 cm^{-1} . UV (CH_2Cl_2) λ_{max} ($\log \epsilon$): 381 (5.17), 490 (4.10).

Acceptor-functionalized arene 19. Segment 11 (260 mg, 0.472 mmol) was cross-coupled to 1,3-dibromo-4,6-diiodobenzene (96 mg, 0.197 mmol) at rt for 16 h using general alkyne coupling procedure B. The crude material was purified by column chromatography (9:1 hexanes: CH_2Cl_2) to give **19** (183 mg, 78%) as a red-orange oil. ^1H NMR (CDCl_3): δ 7.89 (s, 1H), 7.82 (s, 2H), 7.61 (s, 1H), 7.21 (s, 2H), 3.12 (t, $J = 7.2$ Hz, 8H), 1.51 (quin, $J = 6.9$ Hz, 8H), 1.25 (sext, $J = 6.9$ Hz, 8H), 1.16 (s, 42H), 0.88 (t, $J = 7.2$ Hz, 12H). ^{13}C NMR (CDCl_3): δ 144.28, 140.91, 138.72, 136.58, 130.60, 128.61, 127.57, 125.25, 123.88, 116.91, 103.01, 96.05, 81.76, 79.87, 79.75, 79.10, 51.96, 29.72, 20.30, 18.98, 14.05, 11.54. IR (KBr): ν 2955, 2927, 2860, 2158, 2144, 1652, 1599, 1540, 1508, 1453, 1365, 1340, 1278 cm^{-1} . MS (APCI): m/z (%) 1188.2 ($\text{MH}^{+79}\text{Br}^{79}\text{Br}$, 40), 1189.2 ($\text{MH}^{+79}\text{Br}^{81}\text{Br}$, 100), 1190.2 ($\text{MH}^{+13}\text{C}^{81}\text{Br}^{81}\text{Br}$, 87).

DBA precursor 20. Segment 10 (104 mg, 0.189 mmol) was cross-coupled to acceptor-functionalized arene **19** (90 mg, 0.076 mmol) at 55 $^\circ\text{C}$ using general alkyne coupling procedure C (8 h). The crude material was purified by column chromatography (5:1 hexanes: CH_2Cl_2) to give **20** (32 mg, 21%) as a dark red oil. ^1H NMR (CDCl_3): δ 7.90 (s, 2H), 7.82 (s, 2H), 7.60 (s, 1H), 7.59 (s, 1H), 7.22 (s, 2H), 7.10 (s, 2H), 3.13 (m, 16H), 1.50 (m, 16H), 1.25 (m, 16H), 1.16 (s, 42H), 1.14 (s, 42H), 0.89 (m, 24H). ^{13}C NMR (CDCl_3): δ 145.32, 144.31, 140.98, 139.56, 138.09, 138.01, 131.66, 131.39, 130.58, 128.79, 126.16, 125.35, 125.21, 124.13, 117.08, 113.31, 104.36, 103.57, 102.99, 99.89, 96.11, 82.75, 82.42, 81.72, 80.68, 80.30, 79.61, 78.90, 51.98, 51.77, 29.95, 29.72, 20.27,

18.94, 14.01, 11.53. IR (NaCl): ν 2954, 2935, 2888, 2859, 2218, 2142, 1653, 1599, 1537, 1504, 1493, 1454, 1367, 1338, 1276 cm^{-1} . UV (CH_2Cl_2) λ_{max} (log ϵ): 320 (5.01), 354 (4.94), 427 (4.69).

DBA 6. Precursor **20** (32 mg, 0.016 mmol) was subjected to general Pd-catalyzed cyclization procedure D (40 h). The crude material was purified by filtration through a pad of silica gel followed by concentration in vacuo and trituration with hexanes to afford 4 mg (19%) of **6** as a dark orange-red solid. Mp: 150-170 °C (dec). ^1H NMR (CD_2Cl_2): δ 8.01 (s, 2H), 7.99 (s, 2H), 7.88 (s, 1H), 7.87 (s, 1H), 7.35 (s, 2H), 7.31 (s, 2H), 3.20 (m, 16H), 1.57 (m, 16H), 1.31 (m, 16H), 0.91 (m, 24H). IR (NaCl): ν 2958, 2927, 2868, 2851, 2210, 1709, 1594, 1535, 1493, 1457, 1426, 1339 cm^{-1} . UV (CH_2Cl_2) λ_{max} (log ϵ): 382 (4.84), 404 (4.87), 456 (4.54).

Acceptor-functionalized arene 13. Segment **11** (198 mg, 0.359 mmol) was cross-coupled to 1,4-dibromo-2,6-diiodobenzene (72 mg, 0.148 mmol) at rt for 16 h using general alkyne coupling procedure B. The crude material was purified by column chromatography (4:1 hexanes: CH_2Cl_2) to give **13** (153 mg, 87%) as a red oil. ^1H NMR (CDCl_3): δ 7.82 (s, 2H), 7.72 (s, 2H), 7.20 (s, 2H), 3.12 (t, $J = 6.9$ Hz, 8H), 1.53 (quin, $J = 7.5$ Hz, 8H), 1.29 (sext, $J = 7.5$ Hz, 8H), 1.15 (s, 42H), 0.88 (t, $J = 7.2$ Hz, 12H). ^{13}C NMR (CDCl_3): δ 144.25, 140.92, 137.61, 130.59, 128.52, 126.35, 125.21, 124.54, 116.94, 102.96, 96.13, 81.84, 81.51, 80.07, 78.98, 51.96, 29.71, 20.29, 18.98, 14.06, 11.54. IR (KBr): ν 2958, 2937, 2860, 2150, 1652, 15991, 1540, 1506, 1472, 1457, 1338, 1277 cm^{-1} . MS (APCI): m/z (%) 1187.3 ($\text{M}^{+79}\text{Br}^{79}\text{Br}$, 42), 1189.3 ($\text{MH}^{+79}\text{Br}^{81}\text{Br}$, 100), 1190.3 ($\text{MH}^{+13}\text{C}^{81}\text{Br}^{81}\text{Br}$, 65).

DBA Precursor 14. Segment **10** (106 mg, 0.192 mmol) was cross-coupled to acceptor-functionalized arene **13** (106 mg, 0.089 mmol) at 55 °C using general alkyne coupling procedure C (10 h). The crude material was purified by column chromatography (4:1 hexanes:CH₂Cl₂) to give **14** (111 mg, 63%) as a dark red oil. ¹H NMR (CDCl₃): δ 7.90 (s, 2H), 7.82 (s, 2H), 7.60 (s, 1H), 7.22 (s, 2H), 7.10 (s, 2H), 3.13 (m, 16H), 1.52 (m, 16H), 1.29 (m, 16H), 1.16 (s, 42H), 1.14 (s, 42H), 0.88 (m, 24H). ¹³C NMR (CDCl₃): δ 145.32, 144.30, 140.91, 139.50, 138.01, 131.68, 131.62, 130.59, 128.79, 125.81, 125.55, 125.33, 124.11, 117.03, 113.25, 103.56, 102.98, 100.25, 99.87, 96.09, 82.71, 82.44, 81.63, 80.76, 80.29, 79.60, 78.86, 51.96, 51.76, 29.71, 20.26, 18.94, 14.02, 11.53. IR (NaCl): ν 2953, 2932, 2891, 2856, 2218, 2147, 1595, 1536, 1505, 1487, 1466, 1428, 1337, 1274 cm⁻¹. UV (CH₂Cl₂) λ_{max} (log ε): 294 (4.97), 322 (4.98), 353 (4.94), 445 (4.59).

DBA 7. Precursor **14** (65 mg, 0.033 mmol) was subjected to general Pd-catalyzed cyclization procedure D (40 h). The crude material was purified by filtration through a pad of silica gel followed by concentration in vacuo and trituration with hexanes to afford 29 mg (66%) of **7** as a dark orange powder. Mp: 160-180 °C (dec). ¹H NMR (CD₂Cl₂): δ 8.01 (s, 2H), 8.00 (s, 2H), 7.88 (s, 2H), 7.36 (s, 2H), 7.32 (s, 2H), 3.20 (m, 16H), 1.55 (m, 16H), 1.29 (m, 16H), 0.91 (m, 24H). ¹³C NMR (CDCl₃): δ 145.09, 139.86, 139.75, 139.50, 137.46, 136.69, 131.72, 129.77, 129.41, 125.77, 125.25, 124.25, 124.06, 113.15, 113.03, 82.14, 81.92, 81.35, 81.27, 80.94, 80.78, 80.71, 80.19, 79.83, 79.41, 77.46, 77.41, 51.70, 29.71, 20.33, 14.05. IR (NaCl): ν 2955, 2924, 2868, 2213, 1651, 1592, 1535, 1479, 1431, 1370 cm⁻¹. UV (CH₂Cl₂) λ_{max} (log ε): 403 (4.89), 479 (4.36).

CHAPTER VI

CONCLUDING SUMMARY

The ever-expanding role of carbon in areas traditionally reserved for silicon or various metals heralds an end to the old distinctions between organic and inorganic chemistry. The recent surge of organic materials research, supported in part by new developments in carbon-carbon bond forming techniques, opens up entirely new frontiers of study in the fields of nanoscale devices, biological imaging, and quantum computing. In this dissertation it has been demonstrated that donor/acceptor-functionalization of rigidified, highly conjugated carbon systems provides access to a powerful method of manipulating electronic and photonic transport for customized applications in these and other areas. We have shown that isomeric arrays of D/A arylacetylenes, with only small structural variations, can exhibit very different degrees of optoelectronic properties based on systematic adjustments to the donor/acceptor pathway topology, and can be used to fine-tune properties such as optical band gap, emission wavelength, net dipole and quantum yield almost independently. It has also been demonstrated that these functionalizations often lead to FMO localization on respective donor and acceptor segments, with the result that stepwise protonation or metal ion complexation of one type of group (donor or acceptor) followed by the other is reflected in the absorption and/or

emission spectra by dynamic switching of the spectral maxima. Thus it is shown that such switching can be used as a probe of properties such as conjugation efficiency and electronic environment, and may prove useful as fluorimetric ion sensors.

We have also examined the effects of enforced planarization on a variety of D/A mono- and bisdehydrobenzoannulene structures. The effects of enhanced π -orbital overlap in the conjugated macrocycles on spectroscopic and materials properties imply good utility in the next generation of organic electronics. In particular, the relative ease of synthesis, visibly fluorescent intramolecular charge transfer, and moderately narrow optical band gaps exhibited by TPEBs and DBAs with fluorinated acceptor groups provide exciting motivation for future design of organic fluorophores for applications ranging from dyes to display technologies. The series of larger bis[18]DBAs functionalized with donor and acceptor groups in a systematic variation of arrangements clearly demonstrates how small changes in the charge transfer pathways can affect the optical band gaps. In these systems, the long electron-poor chromophores, conjugated to electron-rich chromophores, predicts extremely high two-photon absorption cross-sections, and hence excellent utility in future nonlinear optical devices.

The structure-property relationships discovered in these studies represents a unique toolbox for understanding the complex interrelationships between conjugation and donor/acceptor electron transport in carbon-rich systems, and the insight gained herein will prove invaluable to the rational design of new, high-performance organic materials that could very well far outstrip their inorganic counterparts in both cost and performance.

APPENDIX A

DYNAMIC PROTON-INDUCED EMISSION SWITCHING IN DONOR-FUNCTIONALIZED BIS(DEHYDROBENZO[18]ANNULENO)BENZENE

Introduction

Conjugated fluorophores rich in π -electrons have been recognized as ideal candidates for organic materials, organic electronics components, nonlinear optical materials, and fluorescent sensor dyes.¹⁻⁹ Small structural variations in a particular molecular architecture can elucidate important structure-property relationships essential for fine-tuning the photophysical spectroscopic profiles to targeted applications.^{4,9} To that end, we have been investigating the π -electronic behavior of a class of carbon-rich conjugated chromophores, dehydrobenzoannulenes (DBAs).^{4,10} These carbocyclic molecules contain multiple pathways for intramolecular electronic and photonic transport and exhibit enhanced π -orbital overlap due to enforced planarization, often leading to bulk organic material behavior. For example, we have recently demonstrated the formation of ordered self-assembled monolayers of 18-membered DBA derivatives visualized at the liquid-solid interface via STM imaging,^{4f} and have shown the ability of large DBA networks to approximate the materials properties of certain theoretical carbon

allotropes.^{4h} Furthermore, we have shown that functionalization with strong electron-donating groups results in low-lying excited states that provide efficient emission and are highly sensitive to molecular and electronic environment. We^{4d,g} and others^{9a,b} have reported several planarized DBA systems, as well as analogous acyclic arylacetylenes (e.g., **1** and **2**, Figure 1), that exhibit an intriguing ability to switch their emissive wavelengths in one direction or the other based on independent manipulation of the energy levels of the frontier molecular orbitals (FMOs) through the titrimetric introduction of ions. In the conjugated acyclic systems,^{4d,9a,b} the effect relied on donor/acceptor functionalization, with the calculated localizations of the HOMO and LUMO on the donor and acceptor segments, respectively. In the case of our recently examined pyridine-derivatized DBAs,^{4g} the effect was observed even though the FMOs were predicted to mostly overlap. Herein we report similar dynamic emission switching via acid titration of a solely donor-functionalized bis(dehydrobenzo[18]annuleno)benzene (**3**, Figure 1).

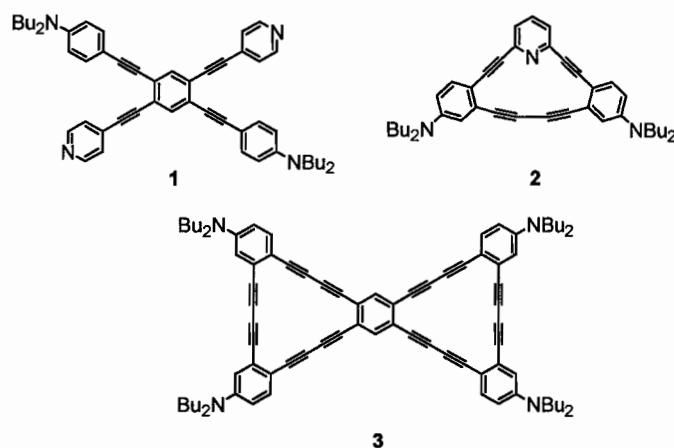
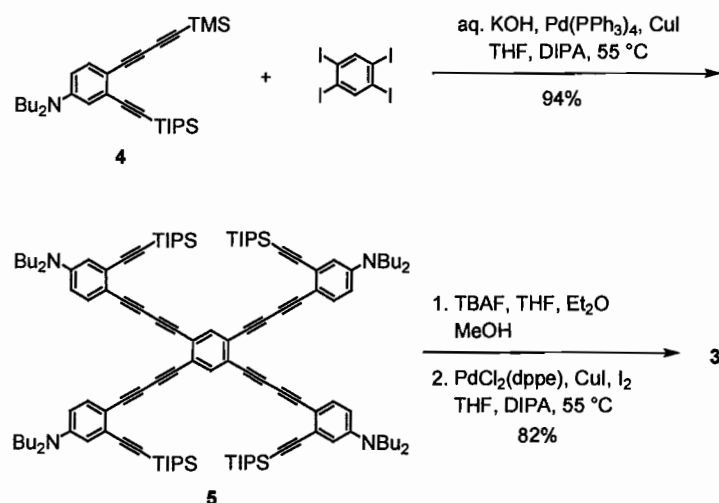


Figure 1. Cruciform^{4d} (**1**) and annulenic^{4g} (**2**) donor/pyridyl acetylene systems and donor-functionalized bis[18]DBA **3**.

Results and Discussion

Synthesis. The synthesis of bisDBA **3** was described in Chapter V, and is illustrated again in Scheme 1. Selective in situ desilylation of triyne **4**¹⁰ and fourfold cross-coupling to 1,2,4,5-tetraiodobenzene afforded dodecayne **5** in excellent yield. Removal of the TIPS groups with TBAF and acetylenic homocoupling using our recently described procedure^{4b} furnished the brick red annulene **3** also in high yield. Upon cyclization, the longest wavelength absorption in the UV spectrum red shifts from 466 to 481 nm, indicating increased π -electron delocalization along the conjugated pathways (Figure 2), while the emission wavelength remains at 551 nm. The quantum yield, however, increases dramatically from 0.18 to 0.34, likely due to the increased orbital overlap resulting from enforced planarization.

Scheme 1. Synthesis of DBA **3**.



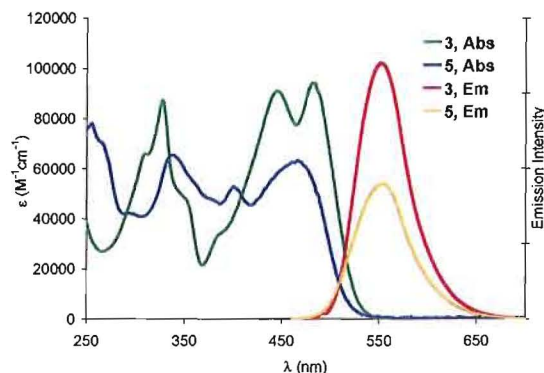


Figure 2. Electronic absorption (left) and emission (right) spectra of DBA **3** and its precursor **5** in CH_2Cl_2 .

TFA Titration. In our previous systems, emission switching was caused by stepwise protonation (or in some cases, metal ion complexation) of first one type of group (donor or acceptor, depending on structure), causing a dramatic red or blue shift in the fluorescence spectrum, followed by the other group, causing a shift in the opposite direction with further addition of ion.^{4e,f} Here, only donating dibutylamino groups are present, so protonation may not proceed in a site-specific, stepwise fashion, but protonation of one or more of the nitrogens (thus generating a positively-charged inductive *acceptor* unit) may still result in a transient donor/acceptor system with intramolecular charge transfer-like behavior.

Accordingly, dilute solutions of **3** in CH_2Cl_2 (0.05 mg mL^{-1}) were exposed to varying concentrations of trifluoroacetic acid (TFA) ranging from 10^{-5} to $10^{-0.3}$ M, and the effects on the fluorescence spectra were observed (Figure 3, left). Initial addition of TFA causes a gradual 47 nm red shift in the emission spectrum with a qualitative loss of fluorescent intensity (Table 1). The solutions shift in fluorescence color from yellow to a

dark orange-red. Between $10^{-2.3}$ and $10^{-2.0}$ M TFA (depending on the excitation wavelength), a new, blue-shifted band at 434 nm appears, and the dual emission leads to a bright purple-pink fluorescence. With further TFA addition this new band, possessing vibronic fine structure typical of π - π^* transitions for these systems, becomes dominant, suppressing the bathochromic band and shifting the solutions to bright blue fluorescence. The spectrum of the final strongly acidic solution closely resembles that of the decyl-functionalized parent analogue.^{4f} Addition of *i*-Pr₂NH gradually reverses the protonation to regenerate the original spectrum, albeit at a lower relative intensity (see Supporting Information Figure S3). In the electronic absorption spectra, the longest wavelength band is gradually suppressed as [TFA] increases, with no significant change in λ_{max} as new peaks at 377, 411 and 426 nm appear. In the excitation spectra a similar effect is seen: the longest wavelength peaks diminish, and between $10^{-2.3}$ and $10^{-2.0}$ M TFA the new hypsochromic peaks gradually increase.

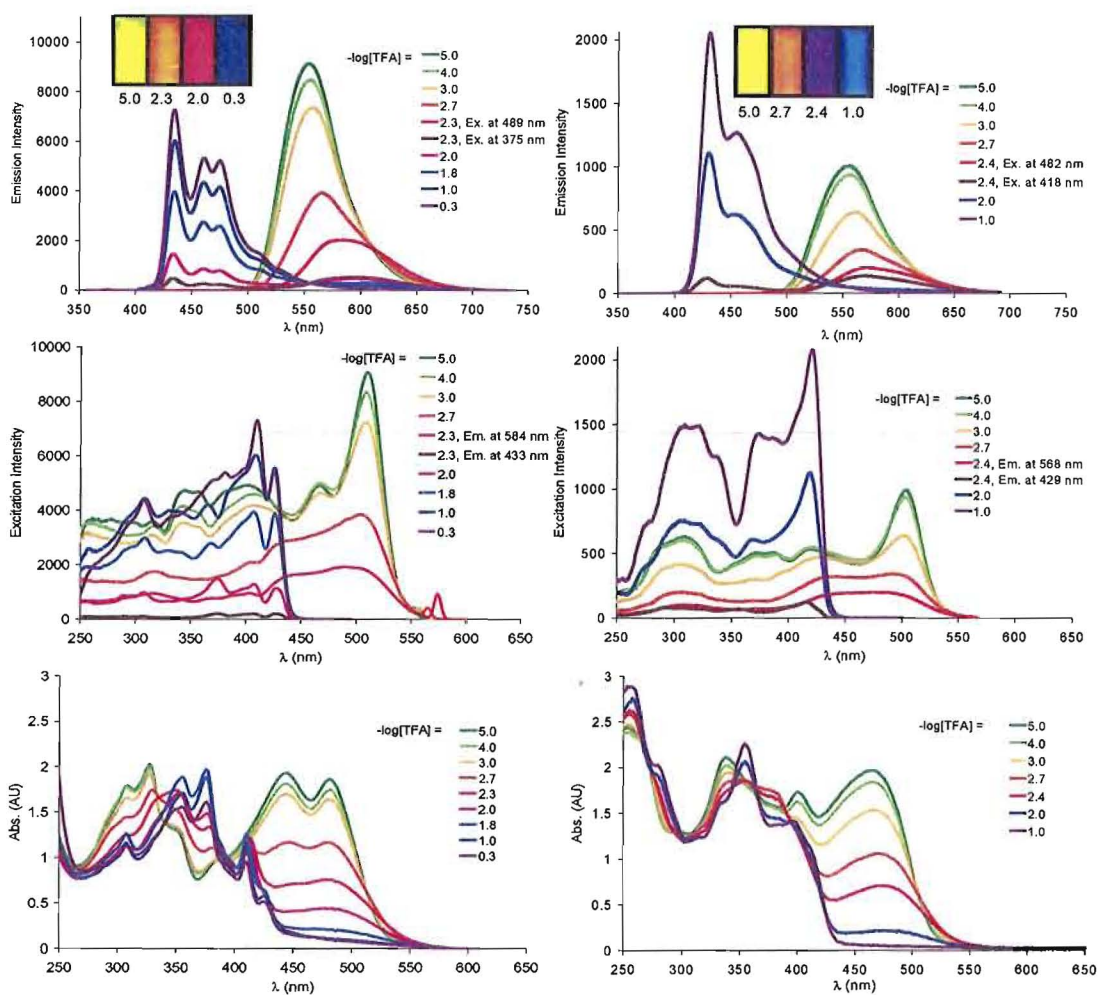


Figure 3. Emission (top), excitation (middle) and absorption (bottom) spectra of TFA titration of DBA **3** (left) and precursor **5** (right) in CH_2Cl_2 . No significant shifting between 0 and 10^{-5} M TFA. Insets: photographs of vials of analyte at indicated $-\log[\text{TFA}]$ under illumination by high-intensity 365 nm lamp.

We believe this effect reflects an incremental protonation of the electron-donating dibutylamino groups at the periphery of the annulene, with partial protonation resulting in an induced intramolecular charge transfer system wherein protonated donor groups become transient acceptor groups. Donor/acceptor-functionalized DBAs typically exhibit large bathochromic shifts in their emission spectra relative to the all-donor versions as the energy of the lowest vibrational levels of the S_1 state decrease, along with a corresponding decrease in the longest wavelength absorption.^{4a} There are three distinct iso-emissive points in the emission spectra: the first three spectra at 10^{-5} , 10^{-4} , and 10^{-3} M TFA converge at 603 nm; the third, fourth and fifth at 10^{-3} , $10^{-2.7}$, and $10^{-2.3}$ (with 507 nm excitation) M TFA converge at 613 nm, and all the remaining spectra at 556 nm. These points may indicate switching between distinct protonation states, although with four donor groups it is difficult to assign each spectrum to a dominant species. The lack of any bathochromic shifting after $10^{-2.3}$ M TFA implies that this acid concentration represents a triprotonated state, with three dibutylammonium acceptor groups and one dibutylamino donor. Additional TFA suppresses the 600 nm band and promotes the 434 nm band. The fact that the 434 nm band grows in intensity but does not shift in wavelength further implies that only two species are involved between $10^{-2.3}$ and $10^{-0.3}$ M TFA. Since the titration is observed on a logarithmic scale of acid concentration, the protonation of **3** is clearly not stoichiometric, since 10^{-5} M TFA represents 0.24 equivalents of the acid, $10^{-2.7}$ M 47 equivalents, and at $10^{-0.3}$ M nearly 12000 equivalents, which we assume to generate fully protonated annulene. The lack of such distinct maxima for the mono- and diprotonated species may imply that initial protonation takes

place at the donor sites nearly independently and in rapid equilibrium, causing a gradual red shifting with two very close iso-emissive points. This behavior is similar to that observed in our previous acyclic donor/acceptor ethynylpyridine systems (e.g., **1**).^{4d}

Table 1. Summary of TFA-induced spectral shifting in DBA **3**.

$-\log[\text{TFA}]$	equiv. TFA ^a	excitation λ_{max} (nm) ^b	emission λ_{max} (nm) ^c
5.0	0.24	509	553
4.0	2.4	508	554
3.0	24	509	558
2.7	47	504	566
2.3	120	489	584
2.3	120	375	433, 598
2.0	240	374	433, 597
1.8	370	407	434, 600
1.0	2400	408	434
0.3	12000	409	434

^a 8.5×10^{-8} mol **3**. ^bFrom excitation spectra in Figure 3. ^cInitial $\Phi_f = 0.34$ in CH_2Cl_2 .

Table 2. Summary of TFA-induced spectral shifting in DBA precursor **5**.

$-\log[\text{TFA}]$	equiv. TFA ^a	excitation λ_{max} (nm) ^b	emission λ_{max} (nm) ^c
5.0	0.36	502	556
4.0	3.6	502	556
3.0	36	500	560
2.7	72	490	566
2.4	140	490	572
2.4	140	415	429, 568
2.0	360	418	429
1.0	3600	420	430

^a 5.5×10^{-8} mol **5**. ^bFrom excitation spectra in Figure 3. ^cInitial $\Phi_f = 0.18$ in CH_2Cl_2 .

To examine the contribution of the enforced planarity of the DBA system, we also titrated the acyclic precursor **5** (Figure 3, right, and Table 2). The spectra are very similar to the titration of **3**, but in this case only a 16 nm red shift was observed in the emission, and the most bathochromic maximum at 572 nm was not observed at greater than $10^{-2.4}$ M TFA. The planarity of **3** may lead to a more highly polarized excited state that can emit at longer wavelengths than the acyclic precursor. Unlike DBA **3**, the fully protonated species of **5** emits at a higher relative intensity than the neutral molecule, likely due to the extra electron donating ability of the TIPS protecting groups. Neutral **5** also possesses a lower fluorescence quantum yield (0.18) than **3** in (0.34) CH_2Cl_2 . Along with longest-wavelength band suppression, a slight bathochromic shift from 463 to 477 nm was observed in the absorption spectrum which was not seen for **3**. Since **5** can rotate about its carbon-carbon single bond axes, it could potentially undergo rotational relaxation to a twisted intramolecular charge transfer (TICT) state with a smaller optical band gap upon formation of a transient donor/acceptor species.

The emission shifts presented here are observed even when the excitation wavelength is held constant, resulting in spectra with only somewhat altered relative intensities. We also observe the effect with several of our previously published donor-functionalized systems, both cyclic and acyclic (Figures 4 and 5). Thus the generality of the effect is illustrated and the potential utility in fluorometric sensing devices is enhanced.

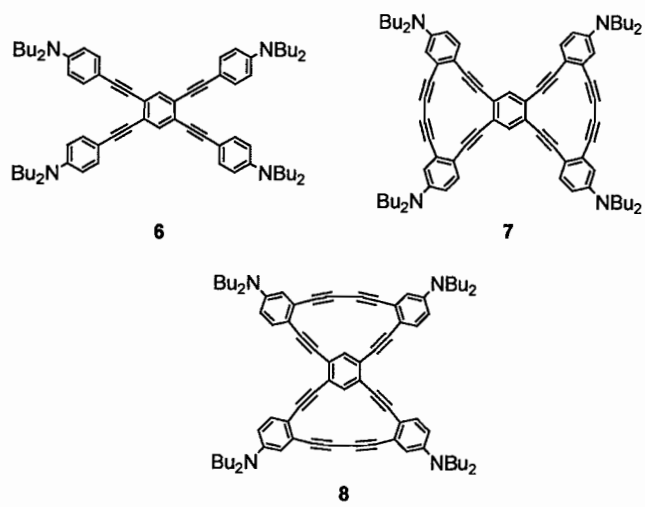


Figure 4. Donor-functionalized tetrakis(phenylethynyl)benzene **6** and tetradonor bis[14] and [15]DBAs **7** and **8**, respectively.^{4a}

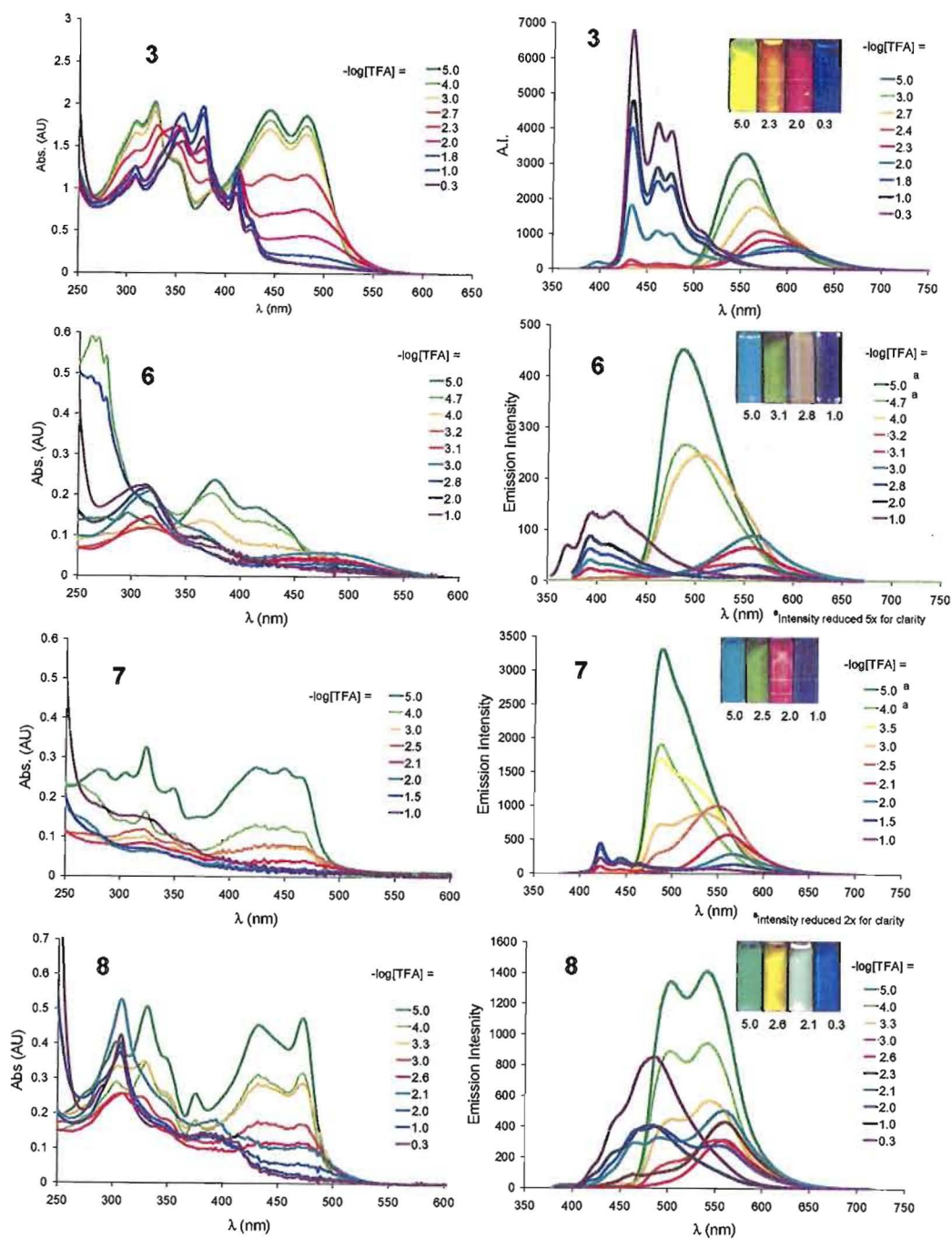


Figure 5. Electronic absorption (left) and emission (right) spectra of **3** and **6-8** in CH_2Cl_2 at indicated [TFA]. Excitation wavelength held constant at 365 nm. Insets: photographs of vials of analyte at indicated $-\log[\text{TFA}]$ under illumination by higher-intensity 365 nm

lamp. Note significant red-shifting in absorption spectra of **6** and the white fluorescence in **8** at $10^{-2.1}$ M TFA due to overlap of emission bands across a wide wavelength range.

Finally, the emission shifting in all compounds is reversible by stepwise back-titration with the organic base di-isopropylamine in a roughly stoichiometric fashion (Figure 6).

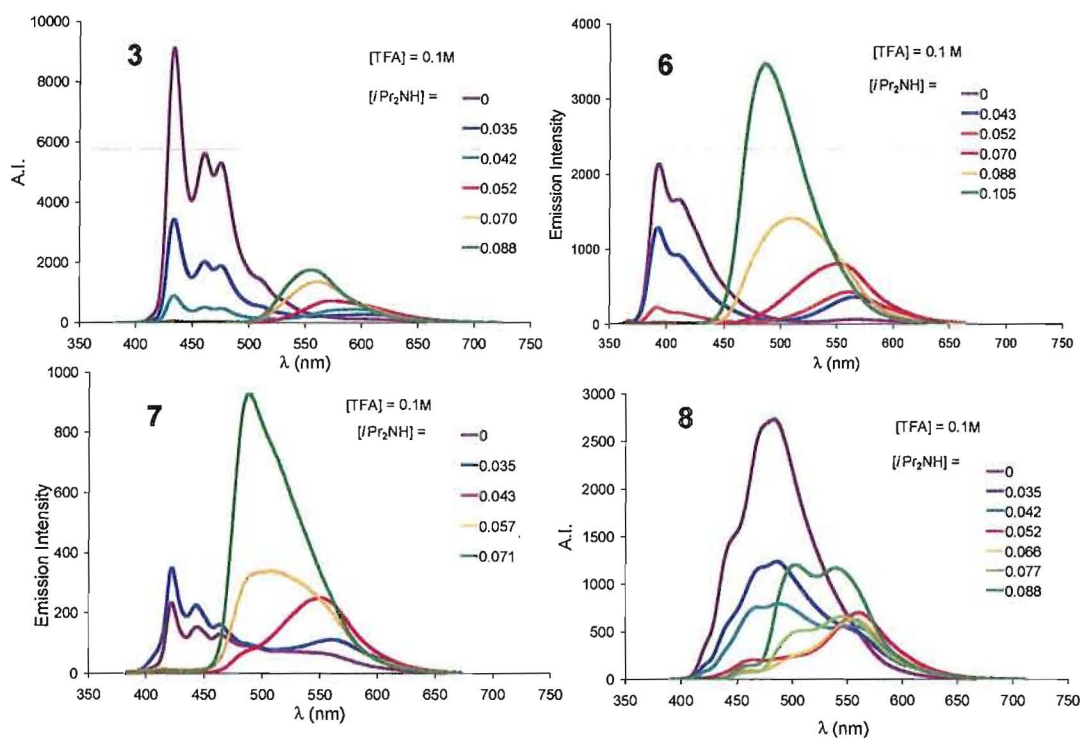


Figure 6. Emission spectra of $i\text{-Pr}_2\text{NH}$ addition to 0.1 M TFA solutions of **3** and **6-8** in CH_2Cl_2 . Excitation at 365 nm.

Conclusions

The dramatic spectroscopic switching displayed by these compounds is surprising, given the predicted overlapping FMOs. It is possible that partial protonation of the donor groups results in transient donor/acceptor systems with intramolecular charge transfer properties, and modifies the HOMO and LUMO to adopt more spatially separate localizations similar to those calculated in our donor/acceptor-functionalized DBAs and donor/pyridyl-functionalized TPEBs.^{4a-f} This sensitivity of the emission profiles to functional group environment could potentially be exploited for optoelectronic devices or fluorescent sensor arrays,¹¹ and represents an interesting structure-property investigation into a versatile class of conjugated organic materials.

APPENDIX B

COMPUTATIONAL DETAILS

CHAPTER II

Cartesian Coordinates of Calculated Structures	C -0.106282 -4.505210 -2.357529
	H -0.148729 -4.592091 -1.275842
	H -0.148729 -4.592091 1.275842
1'	C -0.106282 -4.505210 2.357529
B3LYP/6-31G* = -1761.10313110 au	C 0.000000 -3.221753 2.937578
	C 0.000000 -2.048666 2.140788
	C 0.000000 -1.037670 1.460302
N 0.136505 7.287798 -2.363025	C 0.000000 -3.147429 4.344649
N 0.136505 7.287798 2.363025	C -0.106714 -5.651744 3.134865
C 0.000000 6.008152 2.948373	C 0.000000 -4.288046 5.130710
C 0.000000 4.839170 2.143346	C 0.000000 -5.578671 4.549058
C 0.000000 3.831571 1.460025	C 0.000000 -3.147429 -4.344649
C 0.000000 2.625267 0.713766	C 0.000000 -4.288046 -5.130710
C 0.000000 2.625267 -0.713766	C 0.000000 -5.578671 -4.549058
C 0.000000 1.397596 -1.390487	C -0.106714 -5.651744 -3.134865
C 0.000000 0.166749 -0.716072	C 0.149550 8.430091 -3.150533
C 0.000000 0.166749 0.716072	C 0.000000 8.294891 -4.536546
C 0.000000 1.397596 1.390487	C 0.000000 7.045631 -5.150075
C 0.000000 6.008152 -2.948373	C 0.000000 5.907008 -4.357151
C 0.000000 4.839170 -2.143346	C 0.149550 8.430091 3.150533
C 0.000000 3.831571 -1.460025	C 0.000000 8.294891 4.536546
C 0.000000 -1.037670 -1.460302	C 0.000000 7.045631 5.150075
C 0.000000 -2.048666 -2.140788	C 0.000000 5.907008 4.357151
C 0.000000 -3.221753 -2.937578	

H 0.000000 1.397009 -2.474827	C 0.000000 4.605097 -1.997338
H 0.000000 1.397009 2.474827	C 0.000000 3.440768 -1.185733
H 0.000000 -2.172449 4.820283	C 0.000000 2.435063 -0.497980
H -0.146806 -6.613769 2.638333	C 0.000000 1.229616 0.248687
H 0.000000 -4.174704 6.206791	C 0.000000 1.227519 1.677735
N 0.000000 -6.718006 5.329593	C 0.000000 0.000000 2.354660
H 0.000000 -2.172449 -4.820283	C 0.000000 -1.227519 1.677735
H 0.000000 -4.174704 -6.206791	C 0.000000 -1.229616 0.248687
N 0.000000 -6.718006 -5.329593	C 0.000000 0.000000 -0.426360
H -0.146806 -6.613769 -2.638333	C 0.000000 4.637555 3.885601
H 0.225497 9.419083 -2.715819	C 0.000000 3.438165 3.111126
H -0.101788 6.985898 -6.229391	C 0.000000 2.435271 2.423500
H -0.124445 4.926110 -4.814161	C 0.000000 -2.435271 2.423500
H 0.225497 9.419083 2.715819	C 0.000000 -3.438165 3.111126
H -0.101788 6.985898 6.229391	C 0.000000 -4.637555 3.885601
H -0.124445 4.926110 4.814161	C 0.000000 -5.890677 3.242303
C 0.000000 -8.027900 4.702057	H 0.000000 -5.934940 2.158135
C 0.112869 -6.613242 6.768020	H 0.000000 -6.000628 -0.353951
H 0.887148 -8.183278 4.110641	C 0.000000 -5.897325 -1.435038
H -0.889933 -8.177809 4.039221	C 0.000000 -4.605097 -1.997338
H 0.000000 -8.796785 5.475398	C 0.000000 -3.440768 -1.185733
H -0.681020 -6.009754 7.226704	C 0.000000 -2.435063 -0.497980
H 1.080479 -6.163652 7.037178	C 0.000000 -4.512292 -3.404169
H 0.000000 -7.610661 7.208269	C 0.000000 -7.034542 -2.227177
C 0.000000 -8.027900 -4.702057	C 0.000000 -5.642338 -4.206148
C 0.112869 -6.613242 -6.768020	C 0.000000 -6.941359 -3.640782
H -0.889933 -8.177809 -4.039221	N 0.000000 -4.511630 5.231668
H 0.887148 -8.183278 -4.110641	C 0.000000 -5.633440 5.953902
H 0.000000 -8.796785 -5.475398	C 0.000000 -6.919731 5.407782
H 1.080479 -6.163652 -7.037178	C 0.000000 -7.043974 4.018481
H -0.681020 -6.009754 -7.226704	C 0.000000 7.043974 4.018481
H 0.000000 -7.610661 -7.208269	C 0.000000 6.919731 5.407782
H 0.121204 9.208217 5.114462	C 0.000000 5.633440 5.953902
H 0.121204 9.208217 -5.114462	N 0.000000 4.511630 5.231668
	C 0.000000 7.034542 -2.227177
	C 0.000000 6.941359 -3.640782
	C 0.000000 5.642338 -4.206148
	C 0.000000 4.512292 -3.404169
	H 0.000000 0.000000 3.439075
	H 0.000000 0.000000 -1.510643
	H 0.000000 -3.530038 -3.867294
	H 0.000000 -8.003933 -1.743282
	H 0.000000 -5.513956 -5.281923
	N 0.000000 -8.070320 -4.436149

2'
B3LYP/6-31G* = -1761.10563643 au

C 0.000000 5.890677 3.242303
H 0.000000 5.934940 2.158135
H 0.000000 6.000628 -0.353951
C 0.000000 5.897325 -1.435038

H 0.000000 -5.497874 7.034640	C 0.479223 1.306227 0.000000
H 0.000000 -8.023304 3.547207	C -5.332267 -1.268981 0.000000
H 0.000000 8.023304 3.547207	C -3.952128 -0.940257 0.000000
H 0.000000 5.497874 7.034640	C -2.770048 -0.644771 0.000000
H 0.000000 8.003933 -1.743282	C 1.889269 -2.109941 0.000000
N 0.000000 8.070320 -4.436149	C 2.693510 -3.022669 0.000000
H 0.000000 5.513956 -5.281923	C 3.633199 -4.085831 0.000000
H 0.000000 3.530038 -3.867294	C 4.989063 -3.827105 0.393530
C 0.000000 7.941322 -5.882498	H 5.299049 -2.808338 0.601561
C 0.000000 9.389313 -3.829096	H 5.981249 -0.671342 -0.692499
C 0.000000 -9.389313 -3.829096	C 6.303318 0.321659 -0.392336
C 0.000000 -7.941322 -5.882498	C 5.332267 1.268981 0.000000
H -0.888886 7.406192 -6.245908	C 3.952128 0.940257 0.000000
H 0.888886 7.406192 -6.245908	C 2.770048 0.644771 0.000000
H 0.000000 8.935720 -6.331807	C 5.786280 2.553945 0.350957
H 0.888995 9.552314 -3.203183	C 7.652596 0.633851 -0.413262
H -0.888995 9.552314 -3.203183	C 7.133678 2.876314 0.335596
H 0.000000 10.146340 -4.614977	C 8.111502 1.922213 0.000000
H -0.888995 -9.552314 -3.203183	N 3.230433 -5.415079 -0.165514
H 0.888995 -9.552314 -3.203183	C 4.151781 -6.452286 -0.128613
H 0.000000 -10.146340 -4.614977	C 5.483942 -6.162334 0.168912
H 0.888886 -7.406192 -6.245908	C 5.913811 -4.860929 0.431933
H -0.888886 -7.406192 -6.245908	C -7.652596 -0.633851 0.413262
H 0.000000 -8.935720 -6.331807	C -8.111502 -1.922213 0.000000
H 0.000000 -7.791799 6.054728	C -7.133678 -2.876314 -0.335596
H 0.000000 7.791799 6.054728	C -5.786280 -2.553945 -0.350957
	C -5.913811 4.860929 -0.431933
	C -5.483942 6.162334 -0.168912
	C -4.151781 6.452286 0.128613
	N -3.230433 5.415079 0.165514
	H -0.744616 -2.362473 0.000000
	H 0.744616 2.362473 0.000000
	H 5.061556 3.306879 0.646217
	H 8.356786 -0.128092 -0.724813
	H 7.429298 3.879454 0.617976
	N 9.456101 2.234425 0.000000
	H 3.860682 -7.476731 -0.324954
	H 6.956571 -4.680904 0.662168
	H -8.356786 0.128092 0.724813
	N -9.456101 -2.234425 0.000000
	H -7.429298 -3.879454 -0.617976
	H -5.061556 -3.306879 -0.646217
	H -6.956571 4.680904 -0.662168
	H -3.860682 7.476731 0.324954

3'
B3LYP/6-31G* = -1761.10637570 au

C -6.303318 -0.321659 0.392336	
H -5.981249 0.671342 0.692499	
H -5.299049 2.808338 -0.601561	
C -4.989063 3.827105 -0.393530	
C -3.633199 4.085831 0.000000	
C -2.693510 3.022669 0.000000	
C -1.889269 2.109941 0.000000	
C -0.951534 1.045449 0.000000	
C -1.392339 -0.315410 0.000000	
C -0.479223 -1.306227 0.000000	
C 0.951534 -1.045449 0.000000	
C 1.392339 0.315410 0.000000	

C 10.425503 1.266231 -0.529342
 C 9.887376 3.590491 0.249749
 H 10.258765 1.000763 -1.584008
 H 10.397705 0.341600 0.000000
 H 11.428037 1.687543 -0.440087
 H 9.573016 3.901348 1.254627
 H 9.491033 4.320734 -0.471603
 H 10.976993 3.635474 0.214127
 C -9.887376 -3.590491 -0.249749
 C -10.425503 -1.266231 0.529342
 H -9.491033 -4.320734 0.471603
 H -9.573016 -3.901348 -1.254627
 H -10.976993 -3.635474 -0.214127
 H -10.397705 -0.341600 0.000000
 H -10.258765 -1.000763 1.584008
 H -11.428037 -1.687543 0.440087
 H -6.240299 6.937054 -0.190128
 H 6.240299 -6.937054 0.190128

4'

B3LYP/6-31G* = -1761.10965641 au

C -0.014476 7.296917 2.350075
 H -0.017006 7.383259 1.265256
 H -0.017006 7.383259 -1.265256
 C -0.014476 7.296917 -2.350075
 C -0.004968 6.014766 -2.941146
 C 0.001355 4.839064 -2.143402
 C 0.007060 3.831562 -1.460977
 C 0.013643 2.624014 -0.714011
 C 0.013643 2.624014 0.714011
 C 0.020496 1.395929 1.388979
 C 0.027268 0.165211 0.715017
 C 0.027268 0.165211 -0.715017
 C 0.020496 1.395929 -1.388979
 C -0.004968 6.014766 2.941146
 C 0.001355 4.839064 2.143402
 C 0.007060 3.831562 1.460977
 C 0.031637 -1.040458 1.460373
 C 0.033716 -2.051220 2.140493
 C 0.034417 -3.226748 2.935713
 C 0.097947 -4.508660 2.353935

H 0.146464 -4.593344 1.272319
 H 0.146464 -4.593344 -1.272319
 C 0.097947 -4.508660 -2.353935
 C 0.034417 -3.226748 -2.935713
 C 0.033716 -2.051220 -2.140493
 C 0.031637 -1.040458 -1.460373
 C -0.035249 -3.157529 -4.341917
 C 0.095293 -5.658167 -3.128357
 C -0.039498 -4.300731 -5.125374
 C 0.033835 -5.589228 -4.541744
 C -0.035249 -3.157529 4.341917
 C -0.039498 -4.300731 5.125374
 C 0.033835 -5.589228 4.541744
 C 0.095293 -5.658167 3.128357
 N -0.020747 8.436424 3.039869
 C -0.017760 8.352783 4.377378
 C -0.008508 7.141632 5.072093
 C -0.002024 5.955564 4.347430
 N -0.020747 8.436424 -3.039869
 C -0.017760 8.352783 -4.377378
 C -0.008508 7.141632 -5.072093
 C -0.002024 5.955564 -4.347430
 H 0.020472 1.395667 2.473394
 H 0.020472 1.395667 -2.473394
 H -0.091569 -2.183982 -4.819826
 H 0.139506 -6.618567 -2.628945
 H -0.100861 -4.189583 -6.201251
 N 0.050264 -6.732471 -5.320976
 H -0.091569 -2.183982 4.819826
 H -0.100861 -4.189583 6.201251
 N 0.050264 -6.732471 5.320976
 H 0.139506 -6.618567 2.628945
 H -0.006444 7.131752 6.158078
 H 0.005283 4.991035 4.845952
 H -0.006444 7.131752 -6.158078
 H 0.005283 4.991035 -4.845952
 C -0.019599 -8.038204 -4.687929
 C -0.172703 -6.631927 -6.753247
 H -0.947643 -8.180298 -4.112488
 H 0.827644 -8.195217 -4.008626
 H 0.026170 -8.811511 -5.456781
 H 0.594041 -6.009645 -7.231560
 H -1.157896 -6.205722 -6.998090
 H -0.113068 -7.627853 -7.195672

C -0.019599 -8.038204 4.687929
C -0.172703 -6.631927 6.753247
H 0.827644 -8.195217 4.008626
H -0.947643 -8.180298 4.112488
H 0.026170 -8.811511 5.456781
H -1.157896 -6.205722 6.998090
H 0.594041 -6.009645 7.231560
H -0.113068 -7.627853 7.195672
H -0.023002 9.298913 -4.915670
H -0.023002 9.298913 4.915670

5'

B3LYP/6-31G* = -1761.11098394 au

C -5.902164 3.062376 -0.336672
H -5.894621 2.004835 -0.593332
H -5.946560 -0.249993 0.438633
C -5.929324 -1.322022 0.266878
C -4.692562 -1.959829 0.040085
C -3.479580 -1.223887 0.020027
C -2.445372 -0.579946 0.003401
C -1.231614 0.151332 -0.003830
C -1.225784 1.581115 0.019934
C 0.002550 2.255667 0.027536
C 1.227744 1.576288 0.005243
C 1.226310 0.146542 -0.017385
C -0.003508 -0.526737 -0.023267
C -4.686335 3.698434 -0.002461
C -3.467653 2.968393 0.014546
C -2.438111 2.319891 0.022596
C 2.444736 2.306825 -0.012939
C 3.484350 2.938217 -0.044818
C 4.707072 3.659953 -0.093278
C 5.920691 3.035591 -0.438275
H 5.931097 1.976804 -0.679208
H 5.897281 -0.291189 0.671701
C 5.907008 -1.337276 0.379487
C 4.695804 -1.953271 0.004285
C 3.476915 -1.225806 -0.012531
C 2.439648 -0.587226 -0.021918

C 4.743911 -3.318003 -0.343629
C 7.101675 -2.039717 0.401261
C 5.933907 -4.028601 -0.327662
C 7.153691 -3.407829 0.037388
C 4.752055 5.040114 0.200292
N 5.864268 5.773805 0.171128
C 7.006617 5.155494 -0.158870
C 7.083675 3.796353 -0.469877
N -7.083572 3.677785 -0.367739
C -7.110338 4.983611 -0.065696
C -5.972317 5.717956 0.273318
C -4.742717 5.070015 0.306747
C -7.119189 -2.031626 0.280159
C -7.138263 -3.432793 0.071309
C -5.895418 -4.072208 -0.160543
C -4.710596 -3.353279 -0.171257
H 0.004917 3.340176 0.041020
H -0.005887 -1.611002 -0.035570
H 3.825704 -3.822535 -0.629398
H 8.001884 -1.520640 0.707634
H 5.913541 -5.077037 -0.599459
N 8.347147 -4.107148 0.034584
H 3.833553 5.557596 0.470155
H 8.036803 3.347417 -0.733756
H -6.051556 6.775573 0.507075
H -3.832848 5.601886 0.567710
H -8.041663 -1.490810 0.452689
N -8.321363 -4.147439 0.097403
H -5.854489 -5.140345 -0.336307
H -3.773855 -3.871921 -0.352770
C -8.321303 -5.558743 -0.247727
C -9.589109 -3.443315 0.195541
C 9.548585 -3.485437 0.565329
C 8.343770 -5.540525 -0.204458
H -7.676712 -6.133550 0.429368
H -7.979346 -5.740714 -1.278303
H -9.335256 -5.950668 -0.151443
H -9.756476 -2.758639 -0.649784
H -9.649190 -2.858509 1.122120
H -10.402090 -4.171218 0.210297
H 9.449830 -3.214877 1.627961
H 9.805238 -2.576610 0.006590
H 10.384280 -4.180419 0.467195
H 7.916652 -5.776904 -1.186962

H 7.773716 -6.095284 0.556865
 H 9.371741 -5.906946 -0.194598
 H 7.899731 5.777737 -0.175410
 H -8.087520 5.462229 -0.097944

6'

B3LYP/6-31G* = -1761.11104730 au

C 6.321617 -0.256857 -0.199137
 H 6.012037 0.770878 -0.363700
 H 5.242184 2.911058 0.662669
 C 4.928845 3.913691 0.378222
 C 3.583532 4.137068 0.011663
 C 2.648762 3.067053 -0.002805
 C 1.868918 2.133258 -0.010473
 C 0.943312 1.056064 -0.011101
 C 1.393980 -0.300366 0.018252
 C 0.432204 -1.321680 0.030957
 C -0.943312 -1.056064 0.011101
 C -1.393980 0.300366 -0.018252
 C -0.432204 1.321680 -0.030957
 C 5.337069 -1.244606 0.007142
 C 3.956420 -0.916096 0.017609
 C 2.774172 -0.621633 0.023771
 C -1.868918 -2.133258 0.010473
 C -2.648762 -3.067053 0.002805
 C -3.583532 -4.137068 -0.011663
 C -4.928845 -3.913691 -0.378222
 H -5.242184 -2.911058 -0.662669
 H -6.012037 -0.770878 0.363700
 C -6.321617 0.256857 0.199137
 C -5.337069 1.244606 -0.007142
 C -3.956420 0.916096 -0.017609
 C -2.774172 0.621633 -0.023771
 C -5.778454 2.569775 -0.195593
 C -7.671490 0.569682 0.210596
 C -7.126245 2.893036 -0.186078
 C -8.116782 1.899153 0.008422
 C -3.221235 -5.452021 0.333921
 C -4.190719 -6.447952 0.302840
 C -5.492267 -6.107407 -0.070496
 N -5.862548 -4.864011 -0.407613

C 7.671490 -0.569682 -0.210596
 C 8.116782 -1.899153 -0.008422
 C 7.126245 -2.893036 0.186078
 C 5.778454 -2.569775 0.195593
 N 5.862548 4.864011 0.407613
 C 5.492267 6.107407 0.070496
 C 4.190719 6.447952 -0.302840
 C 3.221235 5.452021 -0.333921
 H 0.766287 -2.353255 0.049510
 H -0.766287 2.353255 -0.049510
 H -5.043382 3.354181 -0.349998
 H -8.385059 -0.227605 0.379454
 H -7.410856 3.928193 -0.331319
 N -9.463579 2.213100 -0.003177
 H -2.197352 -5.671327 0.621032
 H -3.945686 -7.473096 0.564563
 H 8.385059 0.227605 -0.379454
 N 9.463579 -2.213100 0.003177
 H 7.410856 -3.928193 0.331319
 H 5.043382 -3.354181 0.349998
 H 3.945686 7.473096 -0.564563
 H 2.197352 5.671327 -0.621032
 C -10.445830 1.195596 0.331177
 C -9.880355 3.603514 -0.063838
 H -10.324850 0.812302 1.356152
 H -10.384880 0.344140 -0.357989
 H -11.446590 1.622110 0.243006
 H -9.517570 4.088019 -0.979275
 H -9.520443 4.189410 0.795994
 H -10.970660 3.649999 -0.074822
 C 9.880355 -3.603514 0.063838
 C 10.445830 -1.195596 -0.331177
 H 9.520443 -4.189410 -0.795994
 H 9.517570 -4.088019 0.979275
 H 10.970660 -3.649999 0.074822
 H 10.384880 -0.344140 0.357989
 H 10.324850 -0.812302 -1.356152
 H 11.446590 -1.622110 -0.243006
 H 6.273910 6.864334 0.102016
 H -6.273910 -6.864334 -0.102016

7'

B3LYP/6-31G* = -1761.10994771 au

C -7.339193 2.184876 -0.373301
 H -7.352384 1.137675 -0.657732
 H -7.345728 -1.143203 0.678949
 C -7.332670 -2.190878 0.396257
 C -6.124915 -2.810181 0.021815
 C -4.902900 -2.083529 -0.006718
 C -3.866552 -1.446661 -0.023110
 C -2.650768 -0.713121 -0.026934
 C -2.651535 0.715019 0.011456
 C -1.426193 1.393079 0.027137
 C -0.196198 0.717985 0.002393
 C -0.195452 -0.712633 -0.032335
 C -1.424459 -1.389405 -0.050254
 C -6.129652 2.806108 -0.007972
 C -4.905986 2.081839 0.009368
 C -3.868425 1.446822 0.016872
 C 1.015488 1.452241 -0.001305
 C 2.049543 2.096113 -0.020809
 C 3.263334 2.830389 -0.050576
 C 4.491203 2.197779 -0.333272
 H 4.499211 1.131076 -0.537298
 H 4.478449 -1.154208 0.642711
 C 4.482797 -2.204226 0.365144
 C 3.268166 -2.819661 0.000000
 C 2.052575 -2.087595 -0.022758
 C 1.017520 -1.445315 -0.035867
 C 3.308865 -4.189024 -0.330656
 C 5.673760 -2.912504 0.394113
 C 4.495270 -4.905166 -0.307592
 C 5.718460 -4.285521 0.047968
 C 3.290518 4.217077 0.200360
 C 4.475507 4.935168 0.173570
 C 5.709295 4.301898 -0.115762
 C 5.681299 2.907221 -0.363845
 C -8.509075 2.939015 -0.372708
 N -8.567204 4.236958 -0.043583
 C -7.412436 4.823211 0.301062
 C -6.183819 4.169708 0.336027
 C -8.500881 -2.947514 0.406981
 N -8.559025 -4.246185 0.080734

C -7.405967 -4.830576 -0.272711
 C -6.179107 -4.174514 -0.319316
 H -1.426722 2.477265 0.049959
 H -1.423559 -2.473598 -0.072957
 H 2.387754 -4.692710 -0.608490
 H 6.577196 -2.393904 0.691651
 H 4.469502 -5.956839 -0.566013
 N 6.908319 -4.990822 0.052682
 H 2.360640 4.731344 0.424421
 H 4.441716 5.998082 0.379833
 N 6.891420 5.016698 -0.158831
 H 6.597466 2.372744 -0.584237
 H -9.453611 2.475623 -0.653507
 H -7.473487 5.877853 0.565176
 H -5.281486 4.698553 0.624984
 H -9.443982 -2.485630 0.695006
 H -7.466987 -5.885829 -0.534380
 H -5.278125 -4.701970 -0.614951
 C 8.113934 -4.368103 0.572296
 C 6.897883 -6.426934 -0.169720
 H 8.018596 -4.082116 1.631206
 H 8.374305 -3.468478 0.000401
 H 8.945749 -5.068853 0.482540
 H 6.469205 -6.672665 -1.149238
 H 6.325409 -6.969796 0.598247
 H 7.924035 -6.798257 -0.155828
 C 8.152807 4.320309 -0.343664
 C 6.902173 6.422859 0.206802
 H 8.173490 3.776183 -1.296884
 H 8.356136 3.599666 0.463110
 H 8.965080 5.048866 -0.360360
 H 6.584368 6.588424 1.247508
 H 6.243307 7.010034 -0.445866
 H 7.914616 6.814189 0.094464

8'

B3LYP/6-31G* = -1761.11018624 au

C 0.000000 5.910937 3.245818
 H 0.000000 6.004794 2.164854
 H 0.000000 5.993216 -0.346031
 C 0.000000 5.903559 -1.428300

C 0.000000 4.618226 -2.007015	H 0.000000 -3.636014 5.769137
C 0.000000 3.445999 -1.208324	H 0.000000 -5.767002 7.055043
C 0.000000 2.435817 -0.526790	H 0.000000 -8.031746 3.612479
C 0.000000 1.230230 0.217323	H 0.000000 8.031746 3.612479
C 0.000000 1.227884 1.647237	H 0.000000 5.767002 7.055043
C 0.000000 0.000000 2.322789	H 0.000000 3.636014 5.769137
C 0.000000 -1.227884 1.647237	H 0.000000 8.013242 -1.710467
C 0.000000 -1.230230 0.217323	N 0.000000 8.111661 -4.401786
C 0.000000 0.000000 -0.456996	H 0.000000 5.566299 -5.280055
C 0.000000 4.637421 3.845727	H 0.000000 3.565328 -3.890056
C 0.000000 3.450181 3.064378	C 0.000000 8.001508 -5.850113
C 0.000000 2.435987 2.392028	C 0.000000 9.423623 -3.778107
C 0.000000 -2.435987 2.392028	C 0.000000 -9.423623 -3.778107
C 0.000000 -3.450181 3.064378	C 0.000000 -8.001508 -5.850113
C 0.000000 -4.637421 3.845727	H -0.889042 7.471414 -6.220092
C 0.000000 -5.910937 3.245818	H 0.889042 7.471414 -6.220092
H 0.000000 -6.004794 2.164854	H 0.000000 9.001694 -6.286132
H 0.000000 -5.993216 -0.346031	H 0.889131 9.578425 -3.150678
C 0.000000 -5.903559 -1.428300	H -0.889131 9.578425 -3.150678
C 0.000000 -4.618226 -2.007015	H 0.000000 10.190060 -4.554675
C 0.000000 -3.445999 -1.208324	H -0.889131 -9.578425 -3.150678
C 0.000000 -2.435817 -0.526790	H 0.889131 -9.578425 -3.150678
C 0.000000 -4.541868 -3.414997	H 0.000000 -10.190060 -4.554675
C 0.000000 -7.049919 -2.206166	H 0.889042 -7.471414 -6.220092
C 0.000000 -5.681384 -4.202825	H -0.889042 -7.471414 -6.220092
C 0.000000 -6.973800 -3.621282	H 0.000000 -9.001694 -6.286132
C 0.000000 -4.590424 5.252903	
C 0.000000 -5.785490 5.966263	
N 0.000000 -7.000397 5.400109	
C 0.000000 -7.039064 4.060368	
C 0.000000 7.039064 4.060368	
N 0.000000 7.000397 5.400109	
C 0.000000 5.785490 5.966263	
C 0.000000 4.590424 5.252903	
C 0.000000 7.049919 -2.206166	
C 0.000000 6.973800 -3.621282	
C 0.000000 5.681384 -4.202825	
C 0.000000 4.541868 -3.414997	
H 0.000000 0.000000 3.407330	
H 0.000000 0.000000 -1.541215	
H 0.000000 -3.565328 -3.890056	
H 0.000000 -8.013242 -1.710467	
H 0.000000 -5.566299 -5.280055	
N 0.000000 -8.111661 -4.401786	
	9'
	B3LYP/6-31G* = -1761.11035922 au
	C 5.818382 -2.455019 -0.342045
	H 5.864231 -1.403408 -0.609874
	H 5.954580 0.848593 0.686919
	C 5.995040 1.902005 0.429312
	C 4.819793 2.590735 0.073062
	C 3.563046 1.926842 0.032044
	C 2.498529 1.338910 0.006141
	C 1.252450 0.657863 -0.007317
	C 1.199995 -0.770686 0.021479
	C -0.058472 -1.390393 0.031256

C -1.252450 -0.657863 0.007317
C -1.199995 0.770686 -0.021479
C 0.058472 1.390393 -0.031256
C 4.573248 -3.019980 0.001943
C 3.389960 -2.236527 0.017865
C 2.381706 -1.552723 0.027246
C -2.498529 -1.338910 -0.006141
C -3.563046 -1.926842 -0.032044
C -4.819793 -2.590735 -0.073062
C -5.995040 -1.902005 -0.429312
H -5.954580 -0.848593 -0.686919
H -5.864231 1.403408 0.609874
C -5.818382 2.455019 0.342045
C -4.573248 3.019980 -0.001943
C -3.389960 2.236527 -0.017865
C -2.381706 1.552723 -0.027246
C -4.550024 4.392729 -0.320460
C -6.977893 3.213781 0.361901
C -5.704176 5.159736 -0.305561
C -6.957812 4.590868 0.029186
C -4.942710 -3.957954 0.236922
C -6.201591 -4.549458 0.179802
N -7.324132 -3.899038 -0.156331
C -7.200095 -2.597892 -0.453376
C 6.977893 -3.213781 -0.361901
C 6.957812 -4.590868 -0.029186
C 5.704176 -5.159736 0.305561
C 4.550024 -4.392729 0.320460
C 7.200095 2.597892 0.453376
N 7.324132 3.899038 0.156331
C 6.201591 4.549458 -0.179802
C 4.942710 3.957954 -0.236922
H -0.108122 -2.473553 0.048265
H 0.108122 2.473553 -0.048265
H -3.604385 4.857914 -0.582602
H -7.907202 2.732585 0.641888
H -5.629875 6.211276 -0.554961
N -8.114468 5.347526 0.027483
H -4.069144 -4.537358 0.517259
H -6.315863 -5.605913 0.417684
H -8.119053 -2.082124 -0.727937
H 7.907202 -2.732585 -0.641888
N 8.114468 -5.347526 -0.027483
H 5.629875 -6.211276 0.554961
H 3.604385 -4.857914 0.582602
H 8.119053 2.082124 0.727937
H 6.315863 5.605913 -0.417684
H 4.069144 4.537358 -0.517259
C -9.359686 4.767184 0.500997
C -8.041060 6.781038 -0.197637
H -9.303080 4.452439 1.554230
H -9.645388 3.893630 -0.098835
H -10.156920 5.506742 0.409444
H -7.602769 7.007863 -1.177897
H -7.443932 7.297537 0.569408
H -9.049418 7.198016 -0.181549
C 8.041060 -6.781038 0.197637
C 9.359686 -4.767184 -0.500997
H 7.443932 -7.297537 -0.569408
H 7.602769 -7.007863 1.177897
H 9.049418 -7.198016 0.181549
H 9.645388 -3.893630 0.098835
H 9.303080 -4.452439 -1.554230
H 10.156920 -5.506742 -0.409444

CHAPTER III

Cartesian Coordinates of Calculated Structures

3a'

Point Group: C1

B3LYP/6-31G* = -1281.75529194 au

B3LYP/6-31G* Zero Point Corrected Energy = -1281.338508 au

NIMAG = 0

C	1.15837600	3.56160800	0.01147800
C	-1.15837800	3.56160800	0.01147600
C	2.31337100	2.71825600	0.00313400
C	3.11663500	1.80473300	-0.00540900
C	3.92943000	0.64410800	-0.01676600
C	-2.31337300	2.71825600	0.00313300
C	-3.11663700	1.80473300	-0.00545000
C	-3.92943200	0.64410800	-0.01678800
C	-3.31832000	-0.64845900	-0.03350200
C	-1.90156300	-0.76919800	-0.03560000
C	-0.67992400	-0.80378600	-0.03638500
C	0.67992300	-0.80378600	-0.03638200
C	1.90156200	-0.76919800	-0.03559300
C	3.31831900	-0.64845800	-0.03349500
C	5.33220900	0.70142800	-0.00624300
C	6.11559400	-0.44228100	-0.01468200
C	5.52566900	-1.73031800	-0.04210100
C	4.11639100	-1.80031100	-0.04223500
C	-5.33221100	0.70142800	-0.00626900
C	-6.11559500	-0.44228200	-0.01468900
C	-5.52567000	-1.73032000	-0.04208700
C	-4.11639200	-1.80031200	-0.04222500
H	5.81261700	1.67511000	0.01294900
H	7.19294200	-0.33196900	0.00011700
N	6.30137100	-2.87615800	-0.07300000
H	3.61109800	-2.75727400	-0.04715700
H	-5.81261800	1.67511000	0.01290700
H	-7.19294400	-0.33197000	0.00010600

N	-6.30136700	-2.87616100	-0.07296300
H	-3.61109900	-2.75727600	-0.04713600
C	1.20621100	4.96805300	0.02631100
C	-1.20621400	4.96805300	0.02631000
C	-0.00000100	5.66600900	0.03360500
H	-0.00000100	6.75277200	0.04501800
C	7.74027500	-2.77586500	0.10233900
C	5.66795500	-4.17877900	0.04604400
C	-7.74027600	-2.77587200	0.10233500
C	-5.66794300	-4.17877900	0.04606500
H	8.01860900	-2.33771300	1.07341800
H	8.19519100	-2.16565500	-0.68797400
H	8.17791200	-3.77379900	0.04125800
H	4.94820800	-4.34343700	-0.76520200
H	5.13750600	-4.30589100	1.00253400
H	6.43156200	-4.95520800	-0.02700900
H	-8.19518200	-2.16570600	-0.68801700
H	-8.01863400	-2.33767400	1.07338600
H	-8.17790200	-3.77381400	0.04129800
H	-5.13747000	-4.30588500	1.00254100
H	-4.94821400	-4.34343500	-0.76519800
H	-6.43154800	-4.95521200	-0.02696600
N	-0.00000100	2.87866300	0.00418000
H	-2.16068100	5.48411600	0.03182200
H	2.16067800	5.48411600	0.03182200

3a⁺

Point Group: C1

B3LYP/6-31G* = -1282.18331855 au

B3LYP/6-31G* Zero Point Corrected Energy = -1281.751962 au

NIMAG = 0

C	1.21962900	3.55789200	-0.00011000
C	-1.21962900	3.55789200	-0.00010800
C	2.33009800	2.70587800	-0.00056600
C	3.10690600	1.76148700	-0.00039700
C	3.92359300	0.62115800	-0.00027200
C	-2.33009800	2.70587800	-0.00056000
C	-3.10690600	1.76148700	-0.00041600
C	-3.92359300	0.62115800	-0.00028500
C	-3.31916800	-0.67954300	-0.00046600
C	-1.90193900	-0.80063800	-0.00064100
C	-0.68033600	-0.84835900	-0.00101800
C	0.68033600	-0.84835900	-0.00101800

C	1.90193900	-0.80063800	-0.00064000
C	3.31916800	-0.67954300	-0.00046200
C	5.33136100	0.69715200	-0.00002300
C	6.11840100	-0.43595500	0.00014000
C	5.53640400	-1.73570400	0.00013500
C	4.11863900	-1.82050300	-0.00031700
C	-5.33136100	0.69715200	-0.00004000
C	-6.11840100	-0.43595500	0.00013000
C	-5.53640400	-1.73570400	0.00013500
C	-4.11863900	-1.82050300	-0.00031400
H	5.80262100	1.67489900	-0.00004400
H	7.19438900	-0.31972600	0.00009400
N	6.31034000	-2.85958600	0.00042400
H	3.62605400	-2.78350800	-0.00049600
H	-5.80262100	1.67489900	-0.00007000
H	-7.19438900	-0.31972600	0.00008200
N	-6.31034000	-2.85958600	0.00043100
H	-3.62605400	-2.78350800	-0.00048500
C	1.21853700	4.95833500	0.00062500
C	-1.21853700	4.95833500	0.00062700
C	0.00000000	5.63860600	0.00099000
H	0.00000000	6.72434000	0.00157000
C	7.76646000	-2.75054900	0.00179100
C	5.69293000	-4.18229300	-0.00047000
C	-7.76646000	-2.75055000	0.00179600
C	-5.69292900	-4.18229300	-0.00045100
H	8.12878400	-2.22191900	0.89232700
H	8.13083800	-2.22443600	-0.88943100
H	8.19847000	-3.75098200	0.00375500
H	5.07144600	-4.33510300	-0.89182300
H	5.07082100	-4.33608500	0.89028800
H	6.47545900	-4.94069400	-0.00064900
H	-8.13083700	-2.22444200	-0.88942900
H	-8.12878600	-2.22191600	0.89232900
H	-8.19847000	-3.75098300	0.00376400
H	-5.07082200	-4.33607800	0.89030900
H	-5.07144300	-4.33510900	-0.89180100
H	-6.47545700	-4.94069400	-0.00062700
N	0.00000000	2.92739800	-0.00046600
H	-2.16401000	5.48570900	0.00090300
H	2.16400900	5.48570900	0.00089900
H	0.00000000	1.90984900	-0.00096000

3a²⁺

Point Group: C1

B3LYP/6-31G* = -1282.47379682 au

B3LYP/6-31G* Zero Point Corrected Energy = -1282.028261 au

NIMAG = 0

C	-1.16664300	3.61279200	-0.00017400
C	1.26705700	3.57290000	-0.00022300
C	-2.29215200	2.75257800	-0.00025100
C	-3.08113800	1.82810600	-0.00008500
C	-3.92705300	0.68850300	-0.00005800
C	2.36324800	2.71566000	-0.00040500
C	3.12280800	1.75330200	-0.00022400
C	3.91995400	0.60737500	0.00005500
C	3.30182900	-0.69050300	-0.00009300
C	1.88335000	-0.79582700	-0.00027000
C	0.66036800	-0.83516000	-0.00008800
C	-0.69818300	-0.82220400	-0.00002900
C	-1.92030400	-0.76012100	-0.00002400
C	-3.32913500	-0.61389800	-0.00000400
C	-5.32419600	0.81539800	-0.00004500
C	-6.14182000	-0.31141900	0.00001500
C	-5.54775000	-1.57245100	0.00007400
C	-4.16894900	-1.74354500	0.00006100
C	5.33187600	0.66465300	0.00055300
C	6.10257800	-0.47662400	0.00066000
C	5.50694300	-1.77357700	0.00005300
C	4.08258700	-1.84108700	-0.00001900
H	-5.76906400	1.80439000	-0.00008700
H	-7.22259600	-0.19216400	0.00001900
N	-6.44099200	-2.76719600	0.00016100
H	-3.71193800	-2.72710800	0.00010100
H	5.81584400	1.63590200	0.00088800
H	7.17966800	-0.37313500	0.00117600
N	6.26327700	-2.89976100	-0.00020700
H	3.58049900	-2.79914700	0.00020600
C	-1.16524300	4.99887500	0.00011200
C	1.27225100	4.98503500	0.00008100
C	0.07098400	5.67525600	0.00023700
H	0.07971000	6.76069900	0.00046800
C	-6.30991600	-3.60601200	-1.25541400
C	-6.30986000	-3.60586000	1.25583000
C	7.72564600	-2.80949700	0.00057800
C	5.63417200	-4.22091100	-0.00094400
H	-5.31508400	-4.04997500	-1.27632000

H	-6.45371500	-2.95726000	-2.11971900
H	-7.07089300	-4.38765600	-1.22834700
H	-6.45360200	-2.95700200	2.12006500
H	-5.31503300	-4.04983500	1.27673700
H	-7.07084900	-4.38749800	1.22890200
H	8.09051100	-2.28783800	0.89293000
H	8.09145200	-2.28738500	-0.89113500
H	8.14342300	-3.81518300	0.00062100
H	5.01386900	-4.36601100	-0.89350300
H	5.01445000	-4.36739100	0.89181300
H	6.41095700	-4.98420200	-0.00178700
N	0.03954400	2.96046200	-0.00035800
H	2.22363100	5.50289600	0.00018600
H	-2.10473600	5.53711000	0.00024500
H	0.03002900	1.94354500	-0.00054500
H	-7.39919900	-2.40070000	0.00016000

3a³⁺

Point Group: C1

B3LYP/6-31G* = -1282.69606824 au

B3LYP/6-31G* Zero Point Corrected Energy = -1282.236267 au

NIMAG = 0

C	-1.16664300	3.61279200	-0.00017400
C	1.26705700	3.57290000	-0.00022300
C	-2.29215200	2.75257800	-0.00025100
C	-3.08113800	1.82810600	-0.00008500
C	-3.92705300	0.68850300	-0.00005800
C	2.36324800	2.71566000	-0.00040500
C	3.12280800	1.75330200	-0.00022400
C	3.91995400	0.60737500	0.00005500
C	3.30182900	-0.69050300	-0.00009300
C	1.88335000	-0.79582700	-0.00027000
C	0.66036800	-0.83516000	-0.00008800
C	-0.69818300	-0.82220400	-0.00002900
C	-1.92030400	-0.76012100	-0.00002400
C	-3.32913500	-0.61389800	-0.00000400
C	-5.32419600	0.81539800	-0.00004500
C	-6.14182000	-0.31141900	0.00001500
C	-5.54775000	-1.57245100	0.00007400
C	-4.16894900	-1.74354500	0.00006100
C	5.33187600	0.66465300	0.00055300

C	6.10257800	-0.47662400	0.00066000
C	5.50694300	-1.77357700	0.00005300
C	4.08258700	-1.84108700	-0.00001900
H	-5.76906400	1.80439000	-0.00008700
H	-7.22259600	-0.19216400	0.00001900
N	-6.44099200	-2.76719600	0.00016100
H	-3.71193800	-2.72710800	0.00010100
H	5.81584400	1.63590200	0.00088800
H	7.17966800	-0.37313500	0.00117600
N	6.26327700	-2.89976100	-0.00020700
H	3.58049900	-2.79914700	0.00020600
C	-1.16524300	4.99887500	0.00011200
C	1.27225100	4.98503500	0.00008100
C	0.07098400	5.67525600	0.00023700
H	0.07971000	6.76069900	0.00046800
C	-6.30991600	-3.60601200	-1.25541400
C	-6.30986000	-3.60586000	1.25583000
C	7.72564600	-2.80949700	0.00057800
C	5.63417200	-4.22091100	-0.00094400
H	-5.31508400	-4.04997500	-1.27632000
H	-6.45371500	-2.95726000	-2.11971900
H	-7.07089300	-4.38765600	-1.22834700
H	-6.45360200	-2.95700200	2.12006500
H	-5.31503300	-4.04983500	1.27673700
H	-7.07084900	-4.38749800	1.22890200
H	8.09051100	-2.28783800	0.89293000
H	8.09145200	-2.28738500	-0.89113500
H	8.14342300	-3.81518300	0.00062100
H	5.01386900	-4.36601100	-0.89350300
H	5.01445000	-4.36739100	0.89181300
H	6.41095700	-4.98420200	-0.00178700
N	0.03954400	2.96046200	-0.00035800
H	2.22363100	5.50289600	0.00018600
H	-2.10473600	5.53711000	0.00024500
H	0.03002900	1.94354500	-0.00054500
H	-7.39919900	-2.40070000	0.00016000

3a^{d+}

Point Group: C1

B3LYP/6-31G* = -1282.13330775 au

B3LYP/6-31G* Zero Point Corrected Energy = -1281.702314 au

NIMAG = 0

C	-1.14864900	3.60101000	0.00004900
C	1.16253700	3.56926600	-0.00004300
C	-2.30753000	2.75754000	0.00001300
C	-3.13231000	1.86460600	0.00007800
C	-3.94711300	0.70939700	0.00006200
C	2.30963700	2.72094600	-0.00017400
C	3.11077200	1.80547000	-0.00012500
C	3.92050200	0.64502200	-0.00012000
C	3.30689900	-0.64654200	-0.00016400
C	1.89034300	-0.75090600	-0.00020500
C	0.66732000	-0.77030300	-0.00016400
C	-0.68804800	-0.75052900	-0.00012500
C	-1.91141000	-0.71136600	-0.00008600
C	-3.31770000	-0.58480600	-0.00001900
C	-5.34958900	0.79193600	0.00013500
C	-6.14284700	-0.35178700	0.00012100
C	-5.51482500	-1.59576100	0.00003700
C	-4.13333300	-1.73246400	-0.00003300
C	5.32413100	0.69421900	-0.00004400
C	6.09718900	-0.45488700	-0.00002700
C	5.50324400	-1.74439400	-0.00009400
C	4.09090800	-1.80674100	-0.00015000
H	-5.81640200	1.77080000	0.00020100
H	-7.22711800	-0.26204600	0.00017600
N	-6.37609000	-2.81518500	0.00002200
H	-3.65094400	-2.70443200	-0.00009700
H	5.81206600	1.66385300	0.00000000
H	7.17509000	-0.35163100	0.00002600
N	6.26976300	-2.88533500	-0.00010800
H	3.58114800	-2.76127400	-0.00016300
C	-1.19450300	5.00344400	0.00024100
C	1.21633500	4.97819100	0.00014500
C	0.02061700	5.69039400	0.00028500
H	0.03315400	6.77633700	0.00043200
C	-6.21909300	-3.64659700	-1.25218100
C	-6.21897100	-3.64671400	1.25213300
C	7.72255900	-2.79021400	0.00037700
C	5.63315400	-4.19312500	-0.00007600
H	-5.20646100	-4.04771100	-1.27736000
H	-6.38594000	-3.00010800	-2.11384600
H	-6.94799200	-4.45884500	-1.22832600
H	-6.38574600	-3.00030900	2.11387400

H	-5.20633300	-4.04781900	1.27718200
H	-6.94786400	-4.45896700	1.22826700
H	8.09564000	-2.26595600	0.89050400
H	8.09621300	-2.26585900	-0.88944800
H	8.14618200	-3.79500800	0.00045300
H	5.00590600	-4.34031000	-0.89013700
H	5.00620500	-4.34048400	0.89017900
H	6.40261400	-4.96581100	-0.00029900
N	-0.00364500	2.89868400	-0.00010200
H	2.17505700	5.48589700	0.00018200
H	-2.14434800	5.52731600	0.00035400
H	-7.34166200	-2.47060300	0.00008600

3b'

Point Group: C1

B3LYP/6-31G* = -1281.75839526 au

B3LYP/6-31G* Zero Point Corrected Energy = -1281.340840 au

NIMAG = 0

C	1.21586500	3.58951600	0.01109100
C	-1.21586600	3.58951500	0.01109100
C	2.39046100	2.78414000	0.00321500
C	3.16650100	1.84550000	-0.00517300
C	3.95416600	0.66732700	-0.01610000
C	-2.39046200	2.78414000	0.00321600
C	-3.16650200	1.84550000	-0.00520900
C	-3.95416700	0.66732700	-0.01612100
C	-3.32109000	-0.61470500	-0.03218100
C	-1.90201500	-0.72188900	-0.03392900
C	-0.68071800	-0.79527800	-0.03500500
C	0.68071800	-0.79527800	-0.03500400
C	1.90201500	-0.72188900	-0.03392600
C	3.32109000	-0.61470400	-0.03217500
C	5.35835300	0.69740300	-0.00582900
C	6.11986200	-0.46045500	-0.01416900
C	5.50768200	-1.73832200	-0.04127700
C	4.09775800	-1.78203800	-0.04074000
C	-5.35835300	0.69740300	-0.00585400
C	-6.11986200	-0.46045600	-0.01417900
C	-5.50768200	-1.73832200	-0.04126800
C	-4.09775800	-1.78203800	-0.04073100
H	5.85673800	1.66183600	0.01299600
H	7.19899300	-0.36960800	0.00045300
N	6.26245500	-2.89728500	-0.07232200

H	3.57498900	-2.72955000	-0.04496200
H	-5.85673900	1.66183600	0.01295600
H	-7.19899400	-0.36960800	0.00043900
N	-6.26245300	-2.89728600	-0.07229400
H	-3.57498900	-2.72955200	-0.04494200
C	1.15175400	4.99638200	0.02657800
C	-1.15175500	4.99638200	0.02657900
C	7.70356600	-2.82311200	0.10093900
C	5.60529700	-4.18848600	0.04281900
C	-7.70356700	-2.82311400	0.10093800
C	-5.60529200	-4.18848600	0.04284300
H	7.99075500	-2.38952400	1.07134000
H	8.16863400	-2.22221600	-0.69056300
H	8.12248000	-3.82897000	0.04029000
H	4.88331500	-4.33779900	-0.76947000
H	5.07218200	-4.30832200	0.99874800
H	6.35456500	-4.97847700	-0.03174100
H	-8.16862700	-2.22225100	-0.69059400
H	-7.99077400	-2.38949000	1.07131800
H	-8.12247500	-3.82897700	0.04032200
H	-5.07216500	-4.30831500	0.99876500
H	-4.88332000	-4.33780200	-0.76945500
H	-6.35456000	-4.97847800	-0.03170200
H	-2.06521800	5.58746000	0.03324300
H	2.06521700	5.58746100	0.03324100
C	0.00000000	2.89596500	0.00325100
H	0.00000000	1.81403500	-0.00855000
N	-0.00000100	5.67582000	0.03400200

3b⁺

Point Group: C1

B3LYP/6-31G* = -1282.16261524 au

B3LYP/6-31G* Zero Point Corrected Energy = -1281.731256 au

NIMAG = 0

C	1.23658200	3.54133000	-0.00022300
C	-1.23658200	3.54133000	-0.00021600
C	2.40277300	2.75205100	-0.00035000
C	3.16355400	1.79562800	-0.00017300
C	3.95346000	0.63312200	-0.00007200
C	-2.40277300	2.75205100	-0.00033500
C	-3.16355400	1.79562800	-0.00016700
C	-3.95346000	0.63312200	-0.00006800
C	-3.31991800	-0.65396800	-0.00007200

C	-1.90181900	-0.75672200	-0.00009000
C	-0.68011800	-0.82206300	-0.00013800
C	0.68011900	-0.82206300	-0.00013900
C	1.90181900	-0.75672200	-0.00009200
C	3.31991800	-0.65396800	-0.00007400
C	5.36219100	0.67493500	0.00003000
C	6.12416900	-0.47562600	0.00011000
C	5.51352300	-1.76178000	0.00011200
C	4.09718500	-1.81380600	0.00001100
C	-5.36219100	0.67493500	0.00003300
C	-6.12416900	-0.47562600	0.00011200
C	-5.51352300	-1.76178000	0.00011300
C	-4.09718500	-1.81380600	0.00001100
H	5.85599200	1.64161200	0.00001200
H	7.20266900	-0.38345500	0.00012200
N	6.26454800	-2.90425100	0.00022700
H	3.58227300	-2.76513900	0.00005800
H	-5.85599200	1.64161200	0.00001600
H	-7.20266900	-0.38345500	0.00012400
N	-6.26454800	-2.90425100	0.00022600
H	-3.58227300	-2.76513900	0.00005800
C	1.20086700	4.94695300	0.00009700
C	-1.20086700	4.94695300	0.00010400
C	7.72143800	-2.82728000	0.00063900
C	5.61657200	-4.21088200	-0.00030400
C	-7.72143800	-2.82727900	0.00063900
C	-5.61657200	-4.21088200	-0.00030500
H	8.09776500	-2.30774100	0.89113600
H	8.09841100	-2.30873200	-0.89017800
H	8.13137200	-3.83715800	0.00137900
H	4.99038800	-4.34978000	-0.89103100
H	4.99039900	-4.35055200	0.89031700
H	6.38072700	-4.98806500	-0.00065600
H	-8.09841100	-2.30873000	-0.89017700
H	-8.09776500	-2.30774300	0.89113700
H	-8.13137300	-3.83715700	0.00137800
H	-4.99040000	-4.35055300	0.89031600
H	-4.99038800	-4.34977900	-0.89103200
H	-6.38072700	-4.98806500	-0.00065800
H	-2.08111600	5.57559500	0.00026000
H	2.08111600	5.57559500	0.00024800
N	0.00000000	5.56583200	0.00023300
C	0.00000000	2.86906700	-0.00042300
H	0.00000000	1.78651200	-0.00070100

H 0.00000000 6.58190100 0.00046300

3b²⁺

Point Group: C1

B3LYP/6-31G* = -1282.46078361 au

B3LYP/6-31G* Zero Point Corrected Energy = -1282.015003 au

NIMAG = 0

C	1.19190200	3.59071300	-0.00003300
C	-1.27630500	3.56342300	0.00012300
C	2.36851800	2.79257600	-0.00001600
C	3.14915000	1.86039900	-0.00010000
C	3.96147000	0.69776000	-0.00010900
C	-2.42558400	2.76047400	0.00027900
C	-3.16728000	1.78637600	0.00021100
C	-3.94358400	0.62096800	0.00015800
C	-3.30273000	-0.66584800	0.00021500
C	-1.88440000	-0.75501700	0.00028000
C	-0.66096200	-0.80856500	0.00022200
C	0.69646400	-0.79313200	0.00017000
C	1.91873500	-0.71465600	0.00011500
C	3.32808600	-0.59005300	0.00002700
C	5.36305300	0.78340800	-0.00022900
C	6.15078900	-0.36299500	-0.00020600
C	5.52206600	-1.60835500	-0.00006300
C	4.14100200	-1.74177900	0.00005300
C	-5.35481400	0.65037200	0.00001200
C	-6.10477400	-0.50575600	-0.00005600
C	-5.48675200	-1.79175500	0.00001600
C	-4.06525000	-1.83247500	0.00014600
H	5.83432900	1.76011100	-0.00033300
H	7.23445000	-0.27329000	-0.00029600
N	6.38286200	-2.82723400	-0.00003700
H	3.65742600	-2.71269000	0.00015800
H	-5.85751500	1.61209700	-0.00003700
H	-7.18372200	-0.42176700	-0.00014800
N	-6.22612800	-2.93255700	-0.00004700
H	-3.54456400	-2.78057600	0.00015600
C	1.15839100	4.99290000	-0.00024000
C	-1.24353000	4.96965200	-0.00008000
C	6.22842000	-3.66141200	1.25518300
C	6.22821600	-3.66161100	-1.25509900
C	-7.68844700	-2.86760100	-0.00049900

C	-5.57201900	-4.23969200	0.00010800
H	5.22123800	-4.07652900	1.27608700
H	6.38958600	-3.01622500	2.11906400
H	6.96687800	-4.46446300	1.22936300
H	6.38903300	-3.01651500	-2.11911300
H	5.22109800	-4.07690100	-1.27566800
H	6.96681600	-4.46453300	-1.22937300
H	-8.06464400	-2.35257400	-0.89237700
H	-8.06521600	-2.35275400	0.89124300
H	-8.08863900	-3.88063200	-0.00073300
H	-4.94796800	-4.37396300	0.89222400
H	-4.94828000	-4.37437700	-0.89217100
H	-6.33334500	-5.01869300	0.00044000
H	-2.12860700	5.59274900	-0.00011600
H	2.03454900	5.62732800	-0.00039100
H	7.35045000	-2.48654900	-0.00014300
C	-0.02628500	2.90339100	0.00016800
H	-0.01737500	1.82112100	0.00034700
N	-0.04911400	5.60004500	-0.00024600
H	-0.06059100	6.61758300	-0.00038900

3b³⁺

Point Group: C1

B3LYP/6-31G* = -1282.69191164 au

B3LYP/6-31G* Zero Point Corrected Energy = -1282.231656 au

NIMAG = 0

C	-1.23078600	3.61478200	-0.00050800
C	1.23078600	3.61478200	-0.00050800
C	-2.39545400	2.80259000	-0.00045400
C	-3.14709900	1.84677500	-0.00035700
C	-3.95205400	0.67754800	-0.00015700
C	2.39545400	2.80259000	-0.00045500
C	3.14709900	1.84677500	-0.00035500
C	3.95205400	0.67754800	-0.00015600
C	3.31956100	-0.60826200	0.00008200
C	1.90269300	-0.72381300	0.00012600
C	0.68076300	-0.79039500	0.00010800
C	-0.68076300	-0.79039500	0.00010800
C	-1.90269300	-0.72381300	0.00012700
C	-3.31956100	-0.60826200	0.00008200
C	-5.35351700	0.76197700	-0.00020000
C	-6.13609300	-0.38824200	-0.00000900

C	-5.50975900	-1.63458500	0.00021800
C	-4.12559800	-1.76337600	0.00026500
C	5.35351700	0.76197700	-0.00019900
C	6.13609300	-0.38824200	-0.00000900
C	5.50975900	-1.63458500	0.00021700
C	4.12559800	-1.76337600	0.00026400
H	-5.82902500	1.73663900	-0.00038600
H	-7.21973500	-0.29792300	-0.00004600
N	-6.37239800	-2.85083400	0.00041500
H	-3.64136100	-2.73385800	0.00044000
H	5.82902500	1.73663900	-0.00038400
H	7.21973500	-0.29792300	-0.00004500
N	6.37239800	-2.85083400	0.00041300
H	3.64136100	-2.73385800	0.00043800
C	-1.20043600	5.01402400	-0.00053400
C	1.20043600	5.01402400	-0.00053400
C	-6.22365100	-3.68800800	-1.25691100
C	-6.22360800	-3.68763400	1.25798300
C	6.22365100	-3.68800700	-1.25691500
C	6.22360800	-3.68763600	1.25798000
H	-5.22082300	-4.11386600	-1.27642300
H	-6.38229400	-3.04394700	-2.12223500
H	-6.96962700	-4.48387600	-1.22797000
H	-6.38213200	-3.04329900	2.12312400
H	-5.22081000	-4.11356300	1.27754100
H	-6.96964400	-4.48345700	1.22934600
H	6.38229400	-3.04394500	-2.12223800
H	5.22082300	-4.11386500	-1.27642700
H	6.96962800	-4.48387400	-1.22797400
H	5.22081000	-4.11356400	1.27753700
H	6.38213200	-3.04330200	2.12312100
H	6.96964400	-4.48345900	1.22934200
H	2.08256900	5.64248200	-0.00054200
H	-2.08256900	5.64248200	-0.00054100
H	-7.34043200	-2.50966000	0.00038100
H	7.34043200	-2.50966000	0.00037900
N	0.00000000	5.63590300	-0.00055000
C	0.00000000	2.93932000	-0.00051300
H	0.00000000	1.85696600	-0.00050700
H	0.00000000	6.65555100	-0.00057200

3b^{d+}

Point Group: C1

B3LYP/6-31G* = -1282.131934 au

B3LYP/6-31G* Zero Point Corrected Energy = -1281.700309 au
NIMAG = 0

C	1.19657400	3.62013200	0.00022000
C	-1.23232600	3.60722800	-0.00007300
C	2.36724900	2.81268400	0.00013800
C	3.16773200	1.89487100	0.00014600
C	3.96383000	0.72850100	0.00014600
C	-2.40088100	2.79641200	-0.00048300
C	-3.16333200	1.84650800	-0.00077800
C	-3.94441800	0.66623100	-0.00088000
C	-3.30822900	-0.61496100	-0.00122100
C	-1.89059500	-0.71023900	-0.00120900
C	-0.66742600	-0.77613100	-0.00104500
C	0.68986800	-0.76149000	-0.00083900
C	1.91213000	-0.67914500	-0.00065000
C	3.32163400	-0.55996100	-0.00025200
C	5.36871600	0.79308300	0.00055900
C	6.14729300	-0.35926000	0.00060100
C	5.50643500	-1.59734200	0.00020100
C	4.12346300	-1.71701800	-0.00022900
C	-5.34940600	0.68788800	-0.00044200
C	-6.10078900	-0.47489000	-0.00050300
C	-5.48450000	-1.75431400	-0.00136800
C	-4.07200000	-1.79036200	-0.00131300
H	5.84705900	1.76629900	0.00086500
H	7.23248600	-0.28119000	0.00092500
N	6.35424600	-2.82567600	0.00028700
H	3.62987300	-2.68337800	-0.00055200
H	-5.85508200	1.64824800	0.00009600
H	-7.18034900	-0.39072600	0.00013900
N	-6.23040200	-2.90828700	-0.00234400
H	-3.54495900	-2.73543700	-0.00125700
C	1.13733800	5.02751900	0.00087900
C	-1.16712200	5.01544400	0.00062800
C	6.18857800	-3.65594800	1.25249400
C	6.18947700	-3.65555500	-1.25230700
C	-7.68512500	-2.83967100	0.00348400
C	-5.56976800	-4.20416300	0.00158500
H	5.17209500	-4.04729700	1.27707600
H	6.36173000	-3.01158800	2.11452200
H	6.90940000	-4.47532900	1.22848600
H	6.36307900	-3.01088100	-2.11400800
H	5.17307200	-4.04706000	-1.27765500

H	6.91040600	-4.47483600	-1.22810800
H	-8.07090000	-2.31924200	-0.88327100
H	-8.06495400	-2.32607900	0.89692700
H	-8.08987700	-3.85212800	0.00062900
H	-4.94372800	-4.33938000	0.89450500
H	-4.93666800	-4.34003700	-0.88607600
H	-6.32473700	-4.99089900	-0.00138500
H	-2.08020800	5.60622800	0.00081000
H	2.04874200	5.62102500	0.00130600
H	7.32352900	-2.49145700	0.00068200
C	-0.01416900	2.91871000	-0.00030300
H	-0.01149100	1.83701700	-0.00083400
N	-0.01668800	5.69818800	0.00106700

BIBLIOGRAPHY

Chapter I

- (1) Sondheimer, F.; Wolovsky, R. *J. Am. Chem. Soc.* **1962**, *84*, 260.
- (2) (a) Nakagawa, M. *The Chemistry of Annulenes: From the Standpoint of Organic Chemistry*; Osaka University Press: Suita, Japan, **1996**. (b) Nakagawa, M. *Pure Appl. Chem.* **1975**, *44*, 885.
- (3) *Inter alia*: (a) Staab, H. A.; Meissner, U. E.; Gensler, A. *Chem. Ber.* **1979**, *112*, 3907. (b) Staab, H. A.; Meissner, U. E.; Weinacht, W.; Gensler, A. *Chem. Ber.* **1979**, *112*, 3895. (c) Meissner, U. E.; Bravo, R.; Staab, H. A. *Liebigs Ann.* **1983**, 687.
- (4) (a) Sondheimer, F. *Acc. Chem. Res.* **1972**, *5*, 81. (b) Sondheimer, F. *Pure Appl. Chem.* **1971**, *28*, 331.
- (5) Darby, N.; Kim, C. U.; Salaün, J. A.; Shelton, K. W.; Takada, S.; Masamune, S. *J. Chem. Soc., Chem. Commun.* **1971**, 1516.
- (6) Marsden, J. A.; Haley, M. M. in *Metal-Catalyzed Cross-Coupling Reactions, 2nd Ed.*; de Meijere, A.; Diederich, F., Eds.; Wiley-VCH: Weinheim, **2004**, p. 317.
- (7) Recent reviews on various aspects of annulene chemistry, *inter alia*: (a) Hopf, H. *Classics in Hydrocarbon Chemistry*; Wiley-VCH: Weinheim, **2000**, p. 197. (b) Kennedy, R. D.; Lloyd, D.; McNab, H. *J. Chem. Soc., Perkin Trans. 1* **2002**, 1601. (c) Marsella, M. *J. Acc. Chem. Res.* **2002**, *35*, 944. (d) Meier, H. *Synthesis* **2002**, 1213. (e) Marsden, J. A.; Palmer, G. J.; Haley, M. M. *Eur. J. Org. Chem.* **2003**, 2355.
- (8) Balaban, A. T.; Banciu, M.; Ciorba, V. *Annulenes, Benzo-, Hetero-, Homo-Derivatives and their Valence Isomers, Vol. 1-3*, CRC Press: Boca Raton, 1987.
- (9) Miljanic, O. S.; Vollhardt, K. P. C. in *Carbon-Rich Compounds: From Molecules to Materials*; Haley, M. M.; Tykwinski, R. R., Eds.; Wiley-VCH: Weinheim, **2006**, p. 140.
- (10) (a) Perez, D.; Guitian, E. *Chem. Soc. Rev.* **2004**, *33*, 274. (b) Kumar, S. *Liquid Crystals* **2004**, *31*, 1037.

- (11) Hou, X.-L.; Huang, H.; Wong, H. N. C. *Synlett* **2005**, 1073, and references therein.
- (12) Gholami, M.; Tykwinski, R. R. *Chem. Rev.* **2006**, *106*, 4997-5027.
- (13) Herges, R. *Chem. Rev.* **2006**, *106*, 4820-4842.
- (14) Tahara, K.; Tobe, Y. *Chem. Rev.* **2006**, *106*, 5274-5290.
- (15) (a) Willstätter, R.; Waser, E. *Ber.* **1911**, *44*, 3423. (b) Willstätter, R.; Heidelberger, M. *Ber.* **1913**, *46*, 517.
- (16) (a) Hückel, E. *Z. Phys.* **1931**, *70*, 204. (b) Hückel, E. *Z. Phys.* **1931**, *72*, 310. (c) Hückel, E. *Z. Phys.* **1932**, *76*, 628.
- (17) Breslow, R. *Acc. Chem. Res.* **1973**, *6*, 393.
- (18) (a) Fray, G. I.; Saxton, R. G. *The Chemistry of Cyclo-octatetraene and its Derivatives*; Cambridge University Press: New York, 1978. (b) Stevenson, C. D.; Burton, R. D.; Peters, S. J.; Reiter, R. C. *J. Org. Chem.* **1993**, *58*, 5838.
- (19) (a) Stevenson, G. D.; Nebgen, M. A. *J. Am. Chem. Soc.* **1985**, *107*, 5501. (b) Brown, E. C.; Fico, R. M.; Reiter, R. C.; Stevenson, C. D. *J. Org. Chem.* **1998**, *63*, 4444. (c) Stevenson, G. D.; Heinle, L. J.; Davis, J. P.; Reiter, R. C. *J. Am. Chem. Soc.* **2002**, *124*, 2704. (d) Stevenson, C. D.; Gard, M. N.; Reiter, R. C. *J. Org. Chem.* **2003**, *68*, 1464. (e) Peters, S. J.; Reiter, R. C.; Stevenson, C. D. *Org. Lett.* **2003**, *5*, 937. (f) Stevenson, C. D.; Kiesewetter, M. K.; Peters, S. J. *J. Phys. Chem. A* **2004**, *108*, 2278. (g) Nishinaga, T.; Uto, T.; Komatsu, K. *Org. Lett.* **2004**, *6*, 4611. (h) Kiesewetter, M. K.; Reither, R. C.; Stevenson, C. D. *J. Am. Chem. Soc.* **2005**, *127*, 1118. (i) Vogel, E.; Grimme, W.; Korte, S. *Tetrahedron Lett.* **1965**, 3625.
- (20) Sondheimer, F.; Gaoni, Y. *J. Am. Chem. Soc.* **1961**, *83*, 4863.
- (21) (a) Soulen, R. L.; Choi, S. K.; Park, J. D. *J. Fluorine Chem.* **1973**, *3*, 141. (b) Gerson, F.; Huber, W.; Merstetter, P.; Persy, G.; Soulen, R. L.; Spöndlin, C.; Wirz, J. *Helv. Chim. Acta* **1999**, *82*, 1434. (c) Baldrige, K. K.; Siegel, J. S. *J. Am. Chem. Soc.* **2001**, *123*, 1755; Baldrige, K. K.; Siegel, J. S. *J. Am. Chem. Soc.* **2002**, *124*, 5514. (d) Matsuura, A.; Komatsu, K. *J. Am. Chem. Soc.* **2001**, *123*, 1768. (e) Klärner, F.-G. *Angew. Chem. Int. Ed.* **2001**, *40*, 3977 and references therein. (f) Havenith, R. W. A.; Fowler, P. W.; Jenneskens, L. W. *Org. Lett.* **2006**, *8*, 1255.
- (22) Paquette, L. A.; Kesselmeyer, M. A.; Underiner, G. E.; House, S. D.; Rogers, R. D.; Meerholz, K.; Heinze, J. *J. Am. Chem. Soc.* **1992**, *114*, 2644.

(23) (a) Masamune, S.; Seidner, T. *J. Chem. Soc., Chem. Commun.* **1969**, 542. (b) Masamune, S.; Hojo, K.; Bigam, G.; Rabenstein, D. L. *J. Am. Chem. Soc.* **1971**, *93*, 4966. (c) Masamune, S.; Darby, N. *Acc. Chem. Res.* **1972**, *5*, 272.

(24) (a) Haddon, R. C.; Raghavachari, K. *J. Am. Chem. Soc.* **1982**, *104*, 3516. (b) Xie, Y.; Schaefer, H. F.; Liang, G.; Bowen, J. P. *J. Am. Chem. Soc.* **1994**, *116*, 1442. (c) Sulzbach, H. M.; Schleyer, P. v. R.; Jiao, H.; Xie, Y.; Schaefer, H. F. *J. Am. Chem. Soc.* **1995**, *117*, 1369. (d) Schleyer, P. v. R.; Jiao, H.; Sulzbach, H. M.; Schaefer, H. F. *J. Am. Chem. Soc.* **1996**, *118*, 2093. (e) Sulzbach, H. M.; Schaefer, H. F. *J. Am. Chem. Soc.* **1996**, *118*, 3519. (f) King, R. A.; Crawford, T. D.; Stanton, J. F.; Schaefer, H. F. *J. Am. Chem. Soc.* **1999**, *121*, 1078. (g) Castro, C.; Karney, W. L.; McShane, C. M.; Pemberton, R. P. *J. Org. Chem.* **2006**, *71*, 3001.

(25) (a) Vogel, E. *Chem. Soc. Spec. Publ.* **1967**, *21*, 113. (b) Farnell, L.; Kao, J.; Radom, L.; Schaefer, H. F. *J. Am. Chem. Soc.* **1981**, *103*, 2147. (c) Sabljic, A.; Trinajstic, N. *J. Org. Chem.* **1981**, *46*, 3457. (d) Bianchi, R.; Pilati, T.; Simonetta, M. *J. Am. Chem. Soc.* **1981**, *103*, 6426. (e) Scott, L. T.; Kirms, M. A. *J. Am. Chem. Soc.* **1982**, *104*, 3530. (f) Müllen, K.; Meul, T.; Schade, P.; Schmickler, H.; Vogel, E. *J. Am. Chem. Soc.* **1987**, *109*, 4992. (g) Anthony, I. J.; Byrne, L. T.; McCulloch, R. K.; Wege, D. *J. Org. Chem.* **1988**, *53*, 4123.

(26) (a) Sturm, K. D.; Wudl, F.; Lex, J. *J. Org. Chem.* **1991**, *56*, 957. (b) Barrett, D. G.; Liang, G.; McQuade, D. T.; Desper, J. M.; Schladetzky, K. D.; Gellman, S. H. *J. Am. Chem. Soc.* **1994**, *116*, 10525. (c) Rigby, J. H.; Saha, A.; Heeg, M. J. *J. Org. Chem.* **1997**, *62*, 6448. (d) Kuroda, S.; Zuo, S.; Oda, M.; Fukuta, A.; Kajioka, T.; Saito, T.; Furuta, S.; Tsukumo, H.; Sano, K.; Miyatake, R.; Tomoda, S.; Hayakawa, C.; Nozawa, H.; *Bull. Chem. Soc. Jpn.* **2000**, *73*, 1659. (e) Kuroda, S.; Oda, M.; Zuo, S.; Kanayama, K.; Shah, S. I. M.; Furuta, S.; Miyatake, R.; Kyogoku, M. *Tetrahedron Lett.* **2001**, *42*, 6345. (f) Kuroda, S.; Oda, M.; Kanayama, K.; Furuta, S.; Zuo, S.; Thanh, N. C.; Kyogoku, M.; Mouri, M.; Miyatake, R. *Tetrahedron Lett.* **2004**, *45*, 8119.

(27) Jiao, H.; Hommes, N. J. R. v. E.; Schleyer, P. v. R. *Org. Lett.* **2002**, *4*, 2393.

(28) Creary, X.; Miller, K. *J. Org. Chem.* **2003**, *68*, 8683.

(29) (a) Bryant-Friedrich, A. C.; Neidlein, R. *Helv. Chim. Acta* **1997**, *80*, 128. (b) Bryant-Friedrich, A. C.; Neidlein, R. *Helv. Chim. Acta* **1997**, *80*, 1639.

(30) For example: (a) Seiler, R.; Dick, B. *Angew. Chem. Int. Ed.* **2001**, *40*, 4020. (b) Bulo, R. E.; Trion, L.; Ehlers, A. W.; de Kanter, F. J. J.; Schakel, M.; Lutz, M.; Spek, A. L.; Lammertsma, K. *Chem Eur. J.* **2004**, *10*, 5332.

(31) Wiberg, K. B. *Chem. Rev.* **2001**, *101*, 1317.

(32) (a) Oth, J. F. M.; Röttele, H.; Schröder, G. *Tetrahedron Lett.* **1970**, 61. (b) Oth, J. F. M.; Gilles, J.-M.; Schröder, G. *Tetrahedron Lett.* **1970**, 67.

(33) (a) Allinger, N. L.; Sprague, J. T. *J. Am. Chem. Soc.* **1973**, 95, 3893. (b) Loos, D.; Leska, J. *Collect. Czech. Chem. Commun.* **1980**, 45, 187. (c) Hernando, J. M.; Enriquez, F.; Quirante, J. J. *J. Mol. Struct.: THEOCHEM* **1993**, 287, 131. (d) Martin-Santamaria, S.; Lavan, B.; Rzepa, H. S. *J. Chem. Soc., Perkin Trans. 2* **2000**, 1415. (e) Castro, C.; Isborn, C. M.; Karney, W. L.; Mauksch, M.; Schleyer, P. v. R. *Org. Lett.* **2002**, 4, 3431.

(34) Castro, C.; Karney, W. L.; Vu, C. M. H.; Burkhardt, S. E.; Valencia, M. A. *J. Org. Chem.* **2005**, 70, 3602.

(35) Ho, H.; Li, W. *J. Mol. Struct.: THEOCHEM* **2004**, 711, 133.

(36) Gard, M. N.; Reiter, R. C.; Stevenson, C. D. *Org. Lett.* **2004**, 6, 393.

(37) Vogel, E.; Könifshofen, H.; Müllen, K.; Oth, J. F. M. *Angew. Chem., Int. Ed. Engl.* **1974**, 13, 281.

(38) Mugnoli, A.; Simonetta, M. *J. Chem. Soc., Perkin Trans. 2* **1976**, 822.

(39) Scott, L. T.; Kirms, M. A. *J. Am. Chem. Soc.* **1983**, 105, 1372.

(40) Sondheimer, F.; Gaoni, Y. *J. Am. Chem. Soc.* **1960**, 82, 5765.

(41) (a) Oth, J. F. M. *Pure Appl. Chem.* **1971**, 25, 573. (b) Jug, K.; Fasold, E. *J. Am. Chem. Soc.* **1987**, 109, 2263. (c) Baumann, H.; Oth, J. F. M. *Helv. Chim. Acta* **1995**, 78, 679. (d) Choi, C. H.; Kertesz, M. *J. Am. Chem. Soc.* **1997**, 119, 11994. (e) Baumann, H.; Bünzli, J. J. *J. Chem. Soc., Faraday Trans.* **1998**, 94, 2695. (f) Oda, M.; Sakamoto, Y.; Kajioaka, T.; Uchiyama, T.; Miyatake, R.; Kuroda, S. *Angew. Chem. Int. Ed.* **2001**, 40, 2660. (g) Vogel, E.; Engels, H.; Huber, W.; Lex, J.; Müllen, K. *J. Am. Chem. Soc.* **1982**, 104, 3729.

(42) (a) Destro, R.; Pilati, T.; Simonetta, M.; Vogel, E. *J. Am. Chem. Soc.* **1985**, 107, 3185. (b) Moroni, L.; Gellini, C.; Salvi, P. R.; Vogel, E. *J. Phys. Chem. A* **2004**, 108, 8279.

(43) (a) Kiyobayashi, T.; Sakiyama, M.; Sorai, M.; Mitchell, R. H. *J. Org. Chem.* **1997**, 62, 7469. (b) Williams, R. V.; Edwards, W. D.; Vij, A.; Tolbert, R. W.; Mitchell, R. H. *J. Org. Chem.* **1998**, 63, 3125; Mitchell, R. H.; Chen, Y.; Iyer, V. S.; Lau, D. Y. K.; Baldrige, K. K.; Siegel, J. S. *J. Am. Chem. Soc.* **1996**, 118, 2907; Williams, R. V.; Armantrout, J. R.; Twamley, B.; Mitchell, R. H.; Ward, T. R.; Bandyopadhyay, S. *J. Am. Chem. Soc.* **2002**, 124, 13495. (c) Mitchell, R. H.; Williams, R. V.; Mahadevan, R.; Lai,

Y.-H.; Dingle, T. W. *J. Am. Chem. Soc.* **1982**, *104*, 2571. (d) Mitchell, R. H.; Chen, Y.; Khalifa, N.; Zhou, P. *J. Am. Chem. Soc.*, **1998**, *120*, 1785. (e) Mitchell, R. H.; Chaudhary, M.; Dingle, T. W.; Williams, R. V. *J. Am. Chem. Soc.*, **1984**, *106*, 7766; Mitchell, R. H.; Zhang, J. *Tetrahedron Lett.* **1997**, *38*, 6517. (f) Mitchell, R. H.; Jin, X. *Tetrahedron Lett.* **1995**, *36*, 4357. (g) Kimball, D. B.; Haley, M. M.; Mitchell, R. H.; Ward, T. R.; Bandyopadhyay, S.; Williams, R. V.; Armantrout, J. R. *J. Org. Chem.* **2002**, *67*, 8798. (h) Mitchell, R.; Fan, W.; Lau, D. Y. K.; Berg, D. J. *J. Org. Chem.* **2004**, *69*, 549. (i) Laali, K.K.; Bolvig, S.; Raeker T. J.; Mitchell, R. H. *J. Chem. Soc., Perkin Trans. 2* **1996**, 2635; Cerfontain, H.; Koeberg-Telder, A.; Mitchell, R. H.; Khalifa, N.; Tashiro, M. *Recl. Trav. Chim, Pays-Bas*, **1996**, *115*, 293. (j) Lai, Y.-H.; Jiang, J. *J. Org. Chem.* **1997**, *62*, 4412. (k) Cerfontain, H.; Koeberg-Telder, A.; Bakker, B. H.; Mitchell, R. H.; Tashiro, M. *Liebigs Ann. Chem.* **1997**, 873; Murphy, R. S.; Chen, Y.; Ward, T. R.; Mitchell, R. H.; Bohne, C. *Chem. Commun.* **1999**, 2097.

(44) Sondheimer, F.; Gaoni, Y. *J. Am. Chem. Soc.* **1961**, *83*, 4863.

(45) (a) Oth, J. F. M.; Gilles, J.-M. *Tetrahedron Lett.* **1968**, 6259. (b) Johnson, S. M.; Paul, I. C.; King, G. S. D. *J. Chem. Soc. (B)* **1970**, 643.

(46) Wannere, C. S.; Moran, D.; Allinger, N. M.; Hess, B. A.; Schaad, L. J.; Schleyer, P. v. R. *Org. Lett.* **2003**, *5*, 2983.

(47) (a) Stevenson, C. D.; Kurth, T. L. *J. Am. Chem. Soc.* **1999**, *121*, 1623. (b) Kurth, T. L.; Brown, E. C.; Smirnov, A. I.; Reiter, R. C.; Stevenson, C. D. *J. Phys. Chem. A* **1999**, *103*, 8566.

(48) (a) Oth, J. F. M.; Bauman, H.; Gilles, J.-M.; Schroder, G. *J. Am. Chem. Soc.* **1972**, *94*, 3498. (b) Stevenson, G. R.; Reiter, R. C.; Sedgwick, J. B. *J. Am. Chem. Soc.* **1983**, *105*, 6522.

(49) Schröder, G.; Martin, W.; Oth, J. F. M. *Angew. Chem. Int. Ed. Engl.* **1967**, *6*, 870.

(50) Lee, H.; Li, W. *Org. Biomol. Chem.* **2003**, *1*, 2748.

(51) (a) Yoshizawa, K.; Tachibana, M.; Yamabe, T. *Bull. Chem. Soc. Jpn.* **1999**, *72*, 697. (b) Yoshizawa, K.; Kato, T.; Yamabe, T. *J. Phys. Chem.* **1996**, *100*, 5697.

(52) (a) Sondheimer, F.; Wolovsky, R.; Amiel, Y. *J. Am. Chem. Soc.* **1962**, *84*, 274. (b) Longuet-Higgins, H. C.; Salem, L. *Proc. R. Soc. London* **1959**, *251*, 172. (c) Mislow, K. *J. Chem. Phys.* **1952**, *20*, 1489.

(53) Stevenson, C. D.; Kurth, T. L. *J. Am. Chem. Soc.* **2000**, *122*, 722.

- (54) (a) Bregman, J.; Hirshfeld, F. L.; Rabinovich, D.; Schmidt, G. M. J. *Acta Cryst.* **1965**, *19*, 227. (b) Gorter, S.; Rutten-Keulemans, E.; Krever, M.; Romers, C. *Acta Cryst. B* **1995**, *51*, 1036.
- (55) (a) Wannere, C. S.; Sattelmeyer, K. W. Schaefer, H. F.; Schleyer, P. v. R. *Angew. Chem. Int. Ed.* **2004**, *43*, 4200. (b) Wannere, C. S.; Schleyer, P. v. R. *Org. Lett.* **2003**, *5*, 865. (c) Jiao, H.; Schleyer, P. v. R. *Angew. Chem., Int. Ed. Engl.* **1996**, *35*, 2383.
- (56) (a) Shaik, S.; Shurki, A.; Danovich, D.; Hiberty, P. C. *Chem. Rev.* **2001**, *101*, 1501. (b) Jug, K.; Hiberty, P. C.; Shaik, S. *Chem. Rev.* **2001**, *101*, 1477.
- (57) Schulman, J. M.; Disch, R. L. *J. Mol. Struct.: THEOCHEM* **1991**, *234*, 213.
- (58) Ermer, O. *Helv. Chim. Acta* **2005**, *88*, 2262.
- (59) (a) Kurth, T. L.; Brown, E. C.; Hattan, C. M.; Reiter, R. C.; Stevenson, C. D. *J. Phys. Chem. A* **2002**, *106*, 478. (b) Oth, J. F. M.; Woo, E. P.; Sondheimer, F. *J. Am. Chem. Soc.* **1973**, *95*, 7337.
- (60) (a) Oth, J. F. M.; Bunzli, J.; de Zélicourt, Y. *Helv. Chim. Acta* **1974**, *57*, 2276. (b) Oth, J. F. M.; Gilles, J. *J. Phys. Chem. A* **2000**, *104*, 7980.
- (61) Jahn, H. A.; Teller, E. *Proc. R. Soc. London, Ser. A* **1937**, *161*, 220.
- (62) (a) Choi, C. H.; Kertesz, M. *J. Chem. Phys.* **1998**, *108*, 6681. (b) Fincher, C. R.; Chem, C.-E.; Heeger, A. J.; MacDiarmid, A. G. *Phys. Rev. Lett.* **1982**, *48*, 100. (c) Yannoni, C. S.; Clarke, T. C. *Phys. Rev. Lett.* **1983**, *51*, 1191. (d) Kahlert, H.; Leitner, O.; Leising, G. *Synth. Met.* **1987**, *17*, 467. (e) Zhu, Q.; Fisher, J. E. *Solid State Commun.* **1992**, *83*, 179.
- (63) (a) Schleyer, P. v. R.; Jiao, H. *Pure Appl. Chem.* **1996**, *68*, 209. (b) Schleyer, P. v. R.; Maerker, C.; Dransfeld, A.; Jiao, H.; Hommes, N. J. R. v. E. *J. Am. Chem. Soc.* **1996**, *118*, 6317. (c) Chen, Z.; Wannere, C. S.; Corminboeuf, C.; Puchta, R.; Schleyer, P. v. R. *Chem. Rev.* **2005**, *105*, 3842.
- (64) Kato, T.; Yoshizawa, K.; Yamabe, T. *Chem. Phys.* **1999**, *247*, 375.
- (65) Kiran, B.; Nguyen, M. T. *Chem. Phys. Lett.* **2001**, *349*, 307.
- (66) Oth, J. F. M.; de Zélicourt, Y. d. J. *Helv. Chim. Acta* **1999**, *82*, 435.
- (67) (a) Krebs, A. *Angew. Chem.* **1965**, *77*, 966; Krebs, A. *Angew. Chem., Int. Ed. Engl.* **1965**, *4*, 953. (b) Krebs, A.; Byrd, D. *Liebigs Ann. Chem.* **1967**, *707*, 66. (b) Huang, N. Z.; Sondheimer, F. *Acc. Chem. Res.* **1982**, *15*, 96.

(68) (a) Wenthold, P. G.; Lineberger, W. C. *J. Am. Chem. Soc.* **1997**, *119*, 7772. (b) Kato, S.; Lee, H. S.; Gareyev, R.; Wenthold, P. G.; Lineberger, W. C.; DePuy, C. H.; Bierbaum, V. M. *J. Am. Chem. Soc.* **1997**, *119*, 7863. (c) Peters, S. J.; Turk, M. R.; Kiesewetter, M. K.; Stevenson, C. D. *J. Am. Chem. Soc.* **2003**, *125*, 11264. (c) Kiesewetter, M. K.; Reiter, R. C.; Stevenson, C. D. *Org. Lett.* **2005**, *7*, 2623.

(69) Yavari, I.; Norouzi-Arasi, H. *J. Mol. Struct.: THEOCHEM* **2002**, *593*, 199.

(70) (a) Myers, A. G.; Finney, N. S. *J. Am. Chem. Soc.* **1992**, *114*, 10986. (b) Myers, A. G.; Dragovich, P. S. *J. Am. Chem. Soc.* **1993**, *115*, 7021.

(71) (a) Rodríguez, D.; Navarro-Vázquez, A.; Castedo, L.; Domínguez, D.; Saá, C. *J. Am. Chem. Soc.* **2001**, *123*, 9178. (b) Rodríguez, D.; Navarro-Vázquez, A.; Castedo, L.; Domínguez, D.; Saá, C. *Tetrahedron Lett.* **2002**, *43*, 2717. (c) Rodríguez, D.; Castedo, L.; Domínguez, D.; Saá, C. *Synthesis* **2004**, *5*, 761-764. (d) Atienza, C.; Mateo, C.; de Frutos, O.; Echavarren, A. M. *Org. Lett.* **2001**, *3*, 153.

(72) Navarro-Vázquez, A.; Schreiner, P. R. *J. Am. Chem. Soc.* **2005**, *127*, 8150.

(73) (a) Wolovsky, R.; Sondheimer, F. *J. Am. Chem. Soc.* **1962**, *84*, 2844. (b) Wolovsky, R.; Sondheimer, F. *J. Am. Chem. Soc.* **1965**, *87*, 5720. (c) Sondheimer, F.; Wolovsky, R.; Garratt, P. J.; Calder, I. C. *J. Am. Chem. Soc.* **1966**, *88*, 2610.

(74) Jusélius, J.; Sundholm, D. *Phys. Chem. Chem. Phys.* **2001**, *3*, 2433.

(75) Gard, M. N.; Kiesewetter, M. K.; Reiter, R. C.; Stevenson, C. D. *J. Am. Chem. Soc.* **2005**, *127*, 16143.

(76) Nishinaga, T.; Kawamura, T.; Komatsu, K. *J. Org. Chem.* **1997**, *62*, 5354.

(77) Komatsu, K. *Pure Appl. Chem.* **1993**, *65*, 73.

(78) (a) Anthony, J.; Boldi, A. M.; Boudon, C.; Gisselbrecht, J.-P.; Gross, M.; Seiler, P.; Knobler, C. B.; Diederich, F. *Helv. Chim. Acta* **1995**, *78*, 797. (b) Mitzel, F.; Boudon, C.; Gisselbrecht, J.-P.; Gross, M.; Diederich, F.; *Chem. Commun.* **2002**, 2318. (c) Mitzel, F.; Boudon, C.; Gisselbrecht, J.-P.; Seiler, P.; Gross, M.; Diederich, F.; *Helv. Chim. Acta* **2004**, *87*, 1130. (d) Anand, S.; Schlegel, H. B. *Mol. Phys.* **2006**, *104*, 933.

(79) Mayer, J.; Sondheimer, F. *J. Am. Chem. Soc.* **1966**, *88*, 602.

(80) (a) Boydston, A. J.; Haley, M. M. *Org. Lett.* **2001**, *3*, 3599. (b) Boydston, A. J.; Haley, M. M.; Williams, R. V.; Armantrout, J. R. *J. Org. Chem.* **2002**, *67*, 8812.

(81) Higuchi, H.; Asano, K.; Ojima, J.; Yamamoto, K.; Yoshida, T.; Adachi, T.; Yamamoto, G. *J. Chem. Soc., Perkin Trans. 1*, **1994**, 1453.

(82) (a) Weltner, W.; Van Zee, R. J.; *Chem. Rev.* **1989**, *89*, 1713. (b) Maier, J. P. *Chem. Soc. Rev.* **1997**, 21.

(83) (a) Kroto, H. W.; Heath, J. R.; O'Brien, S. C.; Curl, R. F.; Smalley, R. E. *Nature* **1985**, *318*, 162. (b) Kräschmer, W.; Lamb, L. D.; Fostiropoulos, K.; Huffman, D. R. *Nature* **1990**, *347*, 354. (c) Hunter, J.; Fye, J.; Jarrold, M. F. *J. Phys. Chem.* **1993**, *97*, 3460.

(84) (a) Wakabayashi, T.; Kohno, M.; Achiba, Y.; Shiromaru, H.; Momose, T.; Shida, T.; Naemura, K.; Tobe, Y. *J. Chem. Phys.* **1997**, *13*, 4783. (b) Tobe, Y.; Fujii, T.; Matsumoto, H.; Tsumuraya, K.; Noguchi, D.; Nakagawa, N.; Sonoda, M.; Naemura, K.; Achiba, Y.; Wakabayashi, T. *J. Am. Chem. Soc.* **2000**, *122*, 1762. (c) Diederich, F.; Rubib, Y.; Knobler, C. B.; Whetten, R. L.; Schriver, K. E.; Houk, K. N.; Li, Y. *Science* **1989**, *245*, 1088.

(85) Okamura, W. H.; Sondheimer, F. *J. Am. Chem. Soc.* **1967**, *89*, 5991.

(86) (a) Kuwatani, Y.; Watanabe, N.; Ueda, I. *Tetrahedron Lett.* **1994**, *36*, 119. (b) Suzuki, R.; Tsukuda, H.; Watanabe, N.; Kuwatani, Y.; Ueda, I. *Tetrahedron* **1998**, *54*, 2477.

(87) Sworski, T. J. *J. Chem. Phys.* **1948**, *16*, 550.

(88) (a) Rubin, Y.; Knobler, C. B.; Diederich, F. *J. Am. Chem. Soc.* **1990**, *112*, 1607. (b) Rubin, Y.; Knobler, C. B.; Diederich, F. *J. Am. Chem. Soc.* **1990**, *112*, 4966. (c) Diederich, F.; Rubin, Y.; Chapman, O. L.; Goroff, N. S. *Helv. Chim. Acta* **1994**, *77*, 1441.

(89) (a) Nielsen, M. B.; Diederich, F. *The Chemical Record* **2002**, *2*, 189-198. (b) Nielsen, M. B.; Diederich, F. *Chem. Rev.* **2005**, *105*, 1837.

(90) (a) Chauvin, R.; *Tetrahedron Lett.* **1995**, *36*, 397. (b) Godard, C.; Lepetit, C.; Chauvin, R. *Chem. Commun.* **2000**, 1833. (c) Lepetit, C.; Godard, C.; Chauvin, R. *New J. Chem.* **2001**, *25*, 572. (d) Lepetit, C.; Silvi, B.; Chauvin, R. *J. Phys. Chem. A* **2003**, *107*, 464. (e) Lepetit, C.; Peyrou, V.; Chauvin, R. *Phys. Chem. Chem. Phys.* **2004**, *6*, 303.

(91) (a) Jiao, H.; Hommes, N. J. R. v. E.; Schleyer, P. v. R.; de Meijere, A. *J. Org. Chem.* **1996**, *61*, 2826. (b) Maurette, L.; Godard, C.; Frau, S.; Lepetit, C.; Soleilhavoup, M.; Chauvin, R. *Chem. Eur. J.* **2001**, *7*, 1165.

(92) Williams, R. V. *Chem. Rev.* **2001**, *101*, 1185.

(93) (a) Ojima, J.; Ejiri, E.; Kato, T.; Kuroda, S.; Hirooka, S.; Shibutani, M. *Tetrahedron Lett.* **1986**, *27*, 2467. (b) Ojima, J.; Fujita, S.; Masumoto, M.; Ejiri, E.; Kuroda, S.; Nozawa, Y.; Tatemitsu, H. *J. Chem. Soc., Chem. Commun.* **1987**, 534. (c) Higuchi, H.; Yamamoto, H.; Ojima, J.; Iyoda, M.; Yoshida, M.; Yamamoto, G. *J. Chem. Soc. Perkin Trans. 1*, **1993**, 983.

(94) Nakatsuji, S.; Akiyama, S.; Nakagawa, M. *Tetrahedron Lett.* **1976**, 2623.

(95) Mitchell, R. H. *Chem. Rev.* **2001**, *101*, 1301.

(96) Mitchell, R. H.; Iyer, V. S.; Khalifa, N.; Mahadevan, R.; Venugopalan, S.; Weerawarna, S. A.; Zhou, P. *J. Am. Chem. Soc.* **1995**, *117*, 1514 and references therein.

(97) Mitchell, R. H.; Zhou, P. *Tetrahedron Lett.* **1990**, *31*, 5277.

(98) Mitchell, R. H.; Zhou, P. *Tetrahedron Lett.* **1991**, *32*, 6319.

(99) Mitchell, R. H.; Ward, T. R. *Tetrahedron* **2001**, *57*, 3689.

(100) Mitchell, R. H.; Zhou, P.; Venugopalan, S.; Dingle, T. W. *J. Am. Chem. Soc.* **1990**, *112*, 7812.

(101) Mitchell, R. H.; Chen, Y. *Tetrahedron Lett.* **1996**, *37*, 6665.

(102) Mitchell, R. H.; Brkic, Z.; Berg, D. J.; Barclay, T. M. *J. Am. Chem. Soc.* **2002**, *124*, 11983. (c) Mitchell, R. H.; Brkic, Z.; Sauro, V. A.; Berg, D. J. *J. Am. Chem. Soc.* **2003**, *125*, 7581.

(103) Mitchell, R. H. *Eur. J. Org. Chem.* **1999**, 2695.

(104) (a) Mitchell, R. H.; Chen, Y. *Tetrahedron Lett.* **1996**, *37*, 5239. (b) Mitchell, R. H.; Ward, T. R.; Chen, Y.; Wang, Y.; Weerawarna, S. A.; Dibble, P. W.; Marsella, M. J.; Almutairi, A.; Wang, Z.-Q. *J. Am. Chem. Soc.* **2003**, *125*, 2974.

(105) (a) Mitchell, R. H.; Ward, T. R.; Wang, Y.; Dibble, P. W. *J. Am. Chem. Soc.* **1999**, *121*, 2601. (b) Mitchell, R. H.; Bandyopadhyay, S. *Org. Lett.* **2004**, *6*, 1729. (c) Mitchell, R. H.; Bohne, C.; Wang, Y.; Bandyopadhyay, S.; Wozniak, C. B. *J. Org. Chem.* **2006**, *71*, 327.

(106) (a) Liddell, P. A.; Kodis, G.; Andréasson, J.; de la Garza, L.; Bandyopadhyay, S.; Mitchell, R. H.; Moore, T. A.; Moore, A. L.; Gust, D. *J. Am. Chem. Soc.* **2004**, *126*, 4803. (b) Andréasson, J.; Kodis, G.; Terazono, Y.; Liddell, P. A.; Bandyopadhyay, S.; Mitchell, R. H.; Moore, T. A.; Moore, A. L.; Gust, D. *J. Am. Chem. Soc.* **2004**, *126*,

15926. (c) Straight, S. D.; Andréasson, J.; Kodis, G.; Bandyopadhyay, S.; Mitchell, R. H.; Moore, T. A.; Moore, A. L.; Gust, D. *J. Am. Chem. Soc.* **2005**, *127*, 9403.

(107) Iyoda, M.; Kuwatani, Y.; Yamauchi, T.; Oda, M. *J. Chem. Soc., Chem. Commun.* **1988**, 65.

(108) (a) Kuwatani, Y.; Yoshida, T.; Kusaka, A.; Iyoda, M. *Tetrahedron Lett.* **2000**, *41*, 359. (b) Kuwatani, Y.; Yoshida, T.; Hara, K.; Yoshida, M.; Matsuyama, H.; Iyoda, M. *Org. Lett.* **2000**, *2*, 4017.

(109) Kuwatani, Y.; Igarashi, J.; Iyoda, M. *Tetrahedron Lett.* **2004**, *45*, 359.

(110) Haley, M. M.; Wan, W. B. in *Advances in Strained and Interesting Organic Molecules, Volume 8*; Halton, B. Ed.; JAI Press: Stanford, CT, **2000**, p. 1 and references therein.

(111) Wong, H. N. C.; Garratt, P. J.; Sondheimer, F. *J. Am. Chem. Soc.* **1974**, *96*, 5604.

(112) Destro, R.; Pilati, T.; Simonetta, M. *J. Am. Chem. Soc.* **1975**, *97*, 658.

(113) (a) Man, Y.-M.; Mak, T. C. W.; Wong, H. N. C. *J. Org. Chem.* **1990**, *55*, 3214. (b) Müller, M.; Iyer, V. S.; Kübel, C.; Enkelmann, V.; Müllen, K. *Angew. Chem., Int. Ed. Engl.* **1997**, *36*, 1607.

(114) Orita, A.; Hasegawa, D.; Nakano, T.; Otera, J. *Chem. Eur. J.* **2002**, *8*, 2000.

(115) Chaffins, S.; Brettreich, M.; Wudl, F. *Synthesis* **2002**, 1191.

(116) Shimada, S.; Tanaka, M.; Honda, K. *Inorg. Chim. Acta* **1997**, *265*, 1.

(117) Orita, A.; Jiang, L.; Ye, F.; Imai, N.; Akashi, H.; Otera, J. *Acta Cryst.* **2002**, *E58*, m748.

(118) Dosa, P. I.; Whitener, G. D.; Vollhardt, K. P. C.; Bond, A. D.; Teat, S. J. *Org. Lett.* **2002**, *4*, 2075.

(119) (a) Wang, X.-M.; Wang, R.-J.; Mak, T. C. W.; Wong, H. N. C. *J. Am. Chem. Soc.* **1990**, *112*, 7790. (b) Wang, X.-M.; Hou, X.-L.; Zhou, Z.-Y.; Mak, T. C. W.; Wong, H. N. C. *J. Org. Chem.* **1993**, *58*, 7498. (c) Leung, C.-Y.; Mak, T. C. W.; Wong, H. N. C. *J. Chem. Crystallogr.* **1996**, *26*, 227.

(120) (a) Gugel, H.; Meier, H. *Chem. Ber.* **1980**, *113*, 1431. (b) Chan, T.-L.; Huang, N. Z.; Sondheimer, F. *Tetrahedron* **1983**, *39*, 427.

- (121) Chakraborty, M.; Tessier, C. A.; Youngs, W. *J. Org. Chem.* **1999**, *64*, 2947.
- (122) Behr, O. M.; Eglinton, G.; Galbraith, A. R.; Raphael, R. A. *J. Chem. Soc.* **1960**, 3614.
- (123) Campbell, I. D.; Eglinton, G.; Henderson, W.; Raphael, R. A. *Chem. Commun.* **1966**, 87.
- (124) Staab, H. A.; Graf, F. *Tetrahedron Lett.* **1966**, 751.
- (125) Hisaki, I.; Eda, T.; Sonoda, M.; Niino, H.; Sato, T.; Wakabayashi, T.; Tobe, Y. *J. Org. Chem.* **2005**, *70*, 1853.
- (126) Tovar, J. D.; Jux, N.; Jarrosson, T.; Khan, S. I.; Rubin, Y. *J. Org. Chem.* **1997**, *62*, 3432; *ibid.* 5656; *ibid.* **1998**, *63*, 4856.
- (127) Gallagher, M. E.; Anthony, J. E. *Tetrahedron Lett.* **2001**, *42*, 7533.
- (128) Zhou, Q.; Carroll, P. J.; Swager, T. M. *J. Org. Chem.* **1994**, *59*, 1294.
- (129) Bunz, U. H. F.; Enkelmann, V. *Chem. Eur. J.* **1999**, *5*, 263.
- (130) Nishinaga, T.; Nodera, N.; Miyata, Y.; Komatsu, K. *J. Org. Chem.* **2002**, *67*, 6091.
- (131) Ott, S.; Faust, R. *Chem. Commun.* **2004**, 388.
- (132) (a) Cook, M. J.; Heeney, M. J. *Chem. Commun.* **2000**, 969. (b) Cook, M. J.; Heeney, M. J. *Chem. Eur. J.* **2000**, *6*, 3958.
- (133) Garcia-Frutos, E. M.; Fernandez-Lazaro, F.; Maya, E. M.; Vazquez, P.; Torres, T. *J. Org. Chem.* **2000**, *65*, 6841.
- (134) Adams, R. D.; Bunz, U. H. F.; Fu, W.; Nguyen, L. *J. Organomet. Chem.* **1999**, *578*, 91.
- (135) Marsden, J. A.; O'Connor, M. J.; Haley, M. M. *Org. Lett.* **2004**, *6*, 2385.
- (136) Ott, S.; Faust, R. *Synlett* **2004**, 1509.
- (137) Huynh, C.; Linstrumelle, G. *Tetrahedron* **1988**, *44*, 6337.

- (138) Iyoda, M.; Vorasingha, A.; Kuwatani, Y.; Yoshida, M. *Tetrahedron Lett.* **1998**, *39*, 4701.
- (139) Iyoda, M.; Sirinintasak, S.; Nishiyama, Y.; Vorasingha, A.; Sultana, F.; Nakao, K.; Kuwatani, Y.; Matsuyama, H.; Yoshida, M.; Miyake, Y. *Synthesis* **2004**, 1527.
- (140) Li, Y.; Zhang, J.; Wang, W.; Miao, Q.; She, X.; Pan, X. *J. Org. Chem.* **2005**, *70*, 3285.
- (141) Miljanic, O. S.; Vollhardt, K. P. C.; Whitener, G. D. *Synlett* **2003**, 29.
- (142) Barton, J. W.; Shepherd, M. K. *Tetrahedron Lett.* **1984**, *25*, 4967.
- (143) Kehoe, J. M.; Kiley, J. H.; English, J. J.; Johnson, C. A.; Petersen, R. C.; Haley, M. M. *Org. Lett.* **2000**, *2*, 969.
- (144) Sonoda, M.; Sakai, Y.; Yoshimura, T.; Tobe, Y.; Kamada, K. *Chem. Lett.* **2004**, *33*, 972.
- (145) Zhou, Y.; Feng, S. *Solid State Commun.* **2002**, *122*, 307.
- (146) Tobe, Y.; Yoshimura, T.; Inaba, A.; Sakai, Y.; Sonoda, M. unpublished results.
- (147) (a) Eickmeier, C.; Junga, H.; Matzger, A. J.; Scherhag, F.; Shim, M.; Vollhardt, K. P. C. *Angew. Chem., Int. Ed. Engl.* **1997**, *36*, 2103. (b) Matzger, A. J.; Shim, M.; Vollhardt, K. P. C. *Chem. Commun.* **1999**, 1871.
- (148) (a) Furukawa, S.; Uji-i, H.; Tahara, K.; Ichikawa, T.; Sonoda, M.; De Schryver, F. C.; Tobe, Y.; De Feyter, S. *J. Am. Chem. Soc.* **2006**, *128*, 3502. (b) Tahara, K.; Uchino, T.; Ichikawa, T.; Sonoda, M.; Tobe, Y. unpublished results.
- (149) Zhang, D.; Tessier, C. A.; Youngs, W. J. *Chem. Mat.* **1999**, *11*, 3050.
- (150) (a) Ferrara, J. D.; Tessier-Youngs, C.; Youngs, W. J. *J. Am. Chem. Soc.* **1985**, *107*, 6719. (b) Ferrara, J. D.; Tanaka, A. A.; Fierro, C.; Tessier-Youngs, C.; Youngs, W. J. *Organometallics* **1989**, *8*, 2089. (c) Youngs, W. J.; Kinder, J. D.; Bradshaw, J. D.; Tessier, C. A. *Organometallics* **1993**, *12*, 2406.
- (151) Ferrara, J. D.; Tessier-Youngs, C.; Youngs, W. J. *Organometallics* **1987**, *6*, 676.
- (152) Ferrara, J. D.; Tessier-Youngs, C.; Youngs, W. J. *Inorg. Chem.* **1988**, *27*, 2201.

- (153) Ferrara, J. D.; Djebli, A.; Tessier-Youngs, C.; Youngs, W. J. *J. Am. Chem. Soc.* **1988**, *110*, 647.
- (154) Djebli, A.; Ferrara, J. D.; Tessier-Youngs, C.; Youngs, W. J. *Chem. Commun.* **1988**, 548.
- (155) Kinder, J. D.; Tessier, C. A.; Youngs, W. J. *Synlett* **1993**, 149.
- (156) Zhang, W.; Brombosz, S. M.; Mendoza, J. L.; Moore, J. S. *J. Org. Chem.* **2005**, *70*, 10198.
- (157) Staab, H. A.; Bader, R. *Chem. Ber.* **1970**, *103*, 1157.
- (158) Iyoda, M.; Fuchigami, K.; Kusaka, A.; Yoshida, T.; Yoshida, M.; Matsuyama, H.; Kuwatani Y. *Chem. Lett.* **2000**, 860.
- (159) Baldwin, K. P.; Matzger, A. J.; Scheiman, D. A.; Tessier, C. A.; Vollhardt, K. P. C.; Youngs, W. J. *Synlett* **1995**, 1215.
- (160) Baldwin, K. P.; Bradshaw, J. D.; Tessier, C. A.; Youngs, W. J. *Synlett* **1993**, 853.
- (161) Wegner, G. *Z. Naturforsch. B: Chem. Sci.* **1969**, *24*, 824-832; *Makromol. Chem.* **1970**, *134*, 219.
- (162) (a) Marsden, J. A.; Miller, J. J.; Haley, M. M. *Angew. Chem. Int. Ed.* **2004**, *43*, 1694. (b) Marsden, J. A.; Miller, J. J.; Shirtcliff, L. D.; Haley, M. M. *J. Am. Chem. Soc.* **2005**, *127*, 2464.
- (163) (a) Blanchette, H. S.; Brand, S. C.; Naruse, H.; Weakley, T. J. R.; Haley, M. M. *Tetrahedron* **2000**, *56*, 9581.
- (164) (a) Kimball, D. B.; Haley, M. M.; Mitchell, R. H.; Ward T. R. *Org. Lett.* **2001**, *3*, 1709. (b) Hinrichs, H.; Fischer, A. K.; Jones, P. G.; Hopf, H.; Haley, M. M. *Org. Lett.* **2005**, *7*, 3793-3795.
- (165) (a) Laskoski, M.; Steffen, W.; Smith, M. D.; Bunz, U. H. F. *Chem. Commun.* **2001**, 691. (b) Laskoski, M.; Smith, M. D.; Morton, J. G. M.; Bunz, U. H. F. *J. Org. Chem.* **2001**, *66*, 5174. (c) Laskoski, M.; Roidl, G.; Ricks, H. L.; Morton, J. G. M.; Smith, M. D.; Bunz, U. H. F. *J. Organomet. Chem.* **2003**, *673*, 13. (d) Laskoski, M.; Steffen, W.; Morton, J. G. M.; Smith, M. D.; Bunz, U. H. F. *J. Organomet. Chem.* **2003**, *673*, 25.
- (166) Kuwatani, Y.; Ueda, I. *Angew. Chem., Int. Ed. Engl.* **1995**, *34*, 1892.

- (167) Solooki, D.; Bradshaw, J. D.; Tessier, C. A.; Youngs, W. J.; See, R. F.; Churchill, M.; Ferrara, J. D. *J. Organomet. Chem.* **1994**, *470*, 231.
- (168) (a) Haley, M. M.; Bell, M. L.; English, J. J.; Johnson, C. A.; Weakley, T. J. R. *J. Am. Chem. Soc.* **1997**, *119*, 2956. (b) Bell, M. L.; Chiechi, R. C.; Johnson, C. A.; Kimball, D. B.; Matzger, A. J.; Wan, W. B.; Weakley, T. J. R.; Haley, M. M. *Tetrahedron* **2001**, *57*, 3507.
- (169) (a) Haley, M. M.; Brand, S. C.; Pak, J. J. *Angew. Chem. Int. Ed. Engl.* **1997**, *36*, 835. (b) Wan, W. B.; Brand, S. C.; Pak, J. J.; Haley, M. M. *Chem. Eur. J.* **2000**, *6*, 2044.
- (170) Wan, W. B.; Haley, M. M. *J. Org. Chem.* **2001**, *66*, 3893.
- (171) Marsden, J. A.; Haley, M. M. *J. Org. Chem.* **2005**, *70*, 10213.
- (172) Johnson, C. A.; Tahara, K.; Fujita, T.; Haley, M. M.; Tobe, Y. unpublished results.
- (173) Pak, J. J.; Weakley, T. J. R.; Haley, M. M. *J. Am. Chem. Soc.* **1999**, *121*, 8182.
- (174) Sarkar, A.; Pak, J. J.; Rayfield, G. W.; Haley, M. M. *J. Mater. Chem.* **2001**, *11*, 2943.
- (175) Pak, J. J.; Kimball, D. B.; Sarkar, A.; Haley, M. M. unpublished results.
- (176) Nishinaga, T.; Miyata, Y.; Nodera, N.; Komatsu, K. *Tetrahedron* **2004**, *60*, 3375.
- (177) Laskoski, M.; Steffen, W.; Morton, J. G. M.; Smith, M. D.; Bunz, U. H. F. *J. Am. Chem. Soc.* **2002**, *124*, 13814.
- (178) Biliskov, N.; Zimmerman, B.; Baranovic, G. *J. Mol. Struct.* **2003**, *661-662*, 65.
- (179) Boese, R.; Matzger, A. J.; Vollhardt, K. P. C. *J. Am. Chem. Soc.* **1997**, *119*, 2052.
- (180) Dosa, P. I.; Erben, C.; Iyer, V. S.; Vollhardt, K. P. C.; Wasser, I. M. *J. Am. Chem. Soc.* **1999**, *121*, 10430.
- (181) (a) Wan, W. B.; Kimball, D. B.; Haley, M. M. *Tetrahedron Lett* **1998**, *39*, 6795. (b) Wan, W. B.; Chiechi, R. C.; Weakley, T. J. R.; Haley, M. M. *Eur. J. Org. Chem.* **2001**, 3485.

(182) Guo, L.; Bradshaw, J. D.; Tessier, C. A.; Youngs, W. J. *J. Chem. Soc., Chem. Commun.* **1994**, 243.

(183) McQuilkin, R. M.; Garratt, P. J.; Sondheimer, F. *J. Am. Chem. Soc.* **1970**, *92*, 6682.

(184) Haley, M. M.; Bell, M. L.; Brand, S. C.; Kimball, D. B.; Pak, J. J.; Wan, W. B. *Tetrahedron Lett.* **1997**, *38*, 7483.

(185) Baldwin, K. P.; Simons, R. S.; Rose, J.; Zimmerman, P.; Hercules, D. M.; Tessier, C. A.; Youngs, W. J. *J. Chem. Soc., Chem. Commun.* **1994**, 1257.

(186) Nishinaga, T.; Nakayama, H.; Nodera, N.; Komatsu, K. *Tetrahedron Lett.* **1998**, *39*, 7139.

(187) Higuchi, H.; Ojima, J.; Yasunami, M.; Fujimori, K.; Yoshifuji, M. *Tetrahedron Lett.* **1994**, *35*, 1259.

(188) Darky, N.; Cresp, T. N.; Sondheimer, F. *J. Org. Chem.* **1977**, *42*, 1960.

(189) Baxter, P. N. W.; Dali-Youcef, R. *J. Org. Chem.* **2005**, *70*, 4935.

(190) (a) Solooki, D.; Kennedy, V. O.; Tessier, C. A.; Youngs, W. J. *Synlett* **1990**, 427. (b) Solooki, D.; Bradshaw, J. D.; Tessier, C. A.; Youngs, W. J. *Organometallics* **1994**, *13*, 451.

(191) (a) Marsella, M. J.; Reid, R. J. *Macromolecules* **1999**, *32*, 5982. (b) Marsella, M. J.; Kim, I.-T.; Tham, F. *J. Am. Chem. Soc.* **2000**, *122*, 974. (c) Marsella, M. J.; Piao, G.; Tham, F. *Synthesis* **2002**, 1133.

(192) (a) Hara, K.; Hasegawa, M.; Kuwatani, Y.; Enozawa, H.; Iyoda, M. *Chem. Commun.* **2004**, 2042. (b) Iyoda, M.; Hasegawa, M.; Takano, J.; Ogura, E.; Kuwatani, Y. *J. Phys. IV France* **2004**, *114*, 455.

(193) O'Connor, M. J.; Haley, M. M. unpublished work.

(194) Sarkar, A.; Haley, M. M. *Chem. Commun.* **2000**, 1733.

Chapter II

(1) (a) de Meijere, A., Ed.; *Topics in Current Chemistry (Carbon Rich Compounds I)*; Springer: Berlin, 1998; Vol. 196. (b) de Meijere, A., Ed.; *Topics in Current Chemistry*

(Carbon Rich Compounds II); Springer: Berlin, 1999; Vol. 201. (c) Diederich, F.; Stang, P. J.; Tykwinski, R. R., Eds.; *Acetylene Chemistry: Chemistry, Biology, and Material Science*; Wiley-VCH: Weinheim, 2005. (d) Haley, M. M.; Tykwinski, R. R., Eds.; *Carbon-Rich Compounds: From Molecules to Materials*; Wiley-VCH: Weinheim, 2006.

(2) Reviews, inter alia: (a) *Organic Light Emitting Devices: Synthesis, Properties and Applications*; Müllen, K.; Scherf, U., Eds.; Wiley-VCH: Weinheim, 2006. (b) Chen, J.; Reed, M. A.; Dirk, S. M.; Price, D. W.; Rawlett, A. M.; Tour, J. M.; Grubisha, D. S.; Bennett, D. W. In *NATO Science Series II: Mathematics, Physics, Chemistry (Molecular Electronics: Bio-Sensors and Bio-Computers)*; Plenum: New York, 2003; Vol. 96, pp 59-195. (c) Domerco, B.; Hreha, R. D.; Zhang, Y.-D.; Haldi, A.; Barlow, S.; Marder, S. R.; Kippelen, B. *J. Poly. Sci. Part B: Poly. Phys.* **2003**, *41*, 2726-2732. (d) Shirota, Y. *J. Mater. Chem.* **2000**, *10*, 1-25. (e) Schwab, P. F. H.; Levin, M. D.; Michl, J. *Chem. Rev.* **1999**, *99*, 1863-1933. (f) *Electronic Materials: The Oligomer Approach*; Müllen, K.; Wegner, G. Eds.; Wiley-VCH: Weinheim, 1998. (g) *Nonlinear Optics of Organic Molecules and Polymers*; Nalwa, H. S.; Miyata, S., Eds.; CRC Press: Boca Raton, 1997.

(3) Recent examples, inter alia: (a) Kang, H.; Evrenenko, G.; Dutta, P.; Clays, K.; Song, K.; Marks, T. J. *J. Am. Chem. Soc.* **2006**, *128*, 6194-6205. (b) Knox, J. E.; Halls, M. D.; Hratchian, H. P.; Schlegel, H. B. *Phys. Chem. Chem. Phys.* **2006**, *8*, 1371-1377. (c) Shukla, V. K.; Kumar, S.; Deva, D. *Synth. Met.* **2006**, *156*, 387-391. (d) Seminario, J. M. *Nature Mater.* **2005**, *4*, 111-113. (e) Hughes, G.; Bryce, M. R. *J. Mater. Chem.* **2005**, *15*, 94-107. (f) Van der Auweraer, M.; De Schryver, F. C. *Nature Mater.* **2004**, *3*, 507-508. (g) Special Issue on 'Organic Electronics', *Chem. Mater.* **2004**, *16*, 4381-4846. (g) Simpson, C. D.; Wu, J.; Watson, M. D.; Müllen, K. *J. Mater. Chem.* **2004**, *14*, 494-504.

(4) (a) Marsden, J. A.; Miller, J. J.; Shirtcliff, L. D.; Haley, M. M. *J. Am. Chem. Soc.* **2005**, *127*, 2464-2476. See also: (b) Marsden, J. A.; Haley, M. M. *Angew. Chem. Int. Ed.* **2004**, *43*, 1694-1697. (c) Miller, J. J.; Marsden, J. A.; Haley, M. M. *Synlett* **2004**, 165-168.

(5) (a) Bunz, U. H. F.; Rubin, Y.; Tobe, Y. *Chem. Soc. Rev.* **1999**, 107-119. (b) Haley, M. M.; Wan, W. B. In *Advances in Strained and Interesting Organic Molecules*; Halton, B., Ed.; JAI Press: Greenwich, 2000; Vol. 8, pp 1-41. (c) Watson, M. D.; Fechtenkötter, A.; Müllen, K. *Chem Rev.* **2001**, *101*, 1267-1300. (d) Nielsen, M. B.; Diederich, F. In *Modern Arene Chemistry*; Astruc, D., Ed.; Wiley-VCH: Weinheim, 2002; pp 196-216.

(6) Inter alia: (a) Zhao, Y.; Slepko, A. D.; Akoto, C. O.; McDonald, R.; Hegmann, F. A.; Tykwinski, R. R. *Chem. Eur. J.* **2005**, *11*, 321-329. (b) Bunz, U. H. F. *Adv. Polym. Sci.* **2005**, *177*, 1-52. (c) Fasina, T. M.; Collings, J. C.; Lydon, D. P.; Albesa-Jove, D.; Batsanov, A. S.; Howard, J. A. K.; Nguyen, P.; Bruce, M.; Scott, A. J.; Clegg, W.; Watt, S. W.; Viney, C.; Marder, T. B. *J. Mater. Chem.* **2004**, *14*, 2395-2404. (d) Boydston, A. J.; Yin, Y.; Pagenkopf, B. L. *J. Am. Chem. Soc.* **2004**, *126*, 3724-3725. (e) Gonzalo-

Rodriguez, J.; Esquivias, J.; Lafuente, A.; Diaz, C. *J. Org. Chem.* **2003**, *68*, 8120-8128. (f) Bunz, U. H. F. *Chem Rev.* **2000**, *100*, 1605-1644. (g) Tykwinski, R. R.; Gubler, U.; Martin, R. E.; Diederich, F.; Bosshard, C.; Günter, P. *J. Phys. Chem. B* **1998**, *102*, 4451-4465. (h) Tykwinski, R. R.; Schreiber, M.; Carlón, R. P.; Diederich, F.; Gramlich, V. *Helv. Chim. Acta* **1996**, *79*, 2249-2280.

(7) (a) Slepko, A.; Marsden, J. A.; Miller, J. J.; Shirtcliff, L. D.; Haley, M. M.; Kamada, K.; Tykwinski, R. R.; Hegmann, F. A. in *Nonlinear Optical Transmission and Multiphoton Processes in Organics III*; Proc. SPIE **2005**, *5934*, 29-34. (b) Zhang, X.-B.; Feng, J.-K.; Ren, A.-M.; Sun, C.-C. *Opt. Mater.* **2006**, in press. (c) Slepko, A.; Hegmann, F. A.; Tykwinski, R. R.; Kamada, K.; Ohta, K.; Marsden, J. A.; Spitler, E. L.; Miller, J. J.; Haley, M. M. *Opt. Lett.* **2006**, *31*, 3315-3317.

(8) (a) Bazan, G. C.; Bartholomew, G. P. *J. Am. Chem. Soc.* **2002**, *124*, 5183-5196. (b) Bazan, G. C.; Bartholomew, G. P. *Synthesis* **2002**, 1245-1255. (c) Nguyen, P.; Lesley, G.; Marder, T. B. *Chem. Mater.* **1997**, *9*, 406-408. (d) Meier, H.; Mühling, B.; Kolshorn, H. *Eur. J. Org. Chem.* **2004**, 1033-1042. (e) Meier, H.; Gerold, J.; Kolshorn, H.; Mühling, B. *Chem. Eur. J.* **2004**, *10*, 360-370.

(9) (a) Wilson, J. N.; Bunz, U. H. F. *J. Am. Chem. Soc.* **2005**, *127*, 4124-4125. (b) Zuccherro, A. J.; Wilson, J. N.; Bunz, U. H. F. *J. Am. Chem. Soc.* **2006**, *128*, 11872-11881. (c) Wilson, J. N.; Josowicz, M.; Wang, Y.Q.; Bunz, U. H. F. *Chem. Commun.* **2003**, 2962-2963.

(10) (a) Huang, J.-H.; Wen, W.-H.; Sun, Y.-Y.; Chou, P.-T.; Fang, J.-M. *J. Org. Chem.* **2005**, *70*, 5827-5832. (b) Yamaguchi, Y.; Kobayashi, S.; Wakamiya, T.; Matsubara, Y.; Yoshida, Z. *Angew. Chem. Int. Ed.* **2005**, *44*, 7040-7044.

(11) (a) Marsden, J. A.; Palmer, G. J.; Haley, M. M. *Eur. J. Org. Chem.* **2003**, 2355-2369. (b) Jones, C. S.; O'Connor, M. J.; Haley, M. M. In *Acetylene Chemistry: Chemistry, Biology, and Material Science*; Diederich, F.; Stang, P. J.; Tykwinski, R. R., Eds.; Wiley-VCH: Weinheim, **2005**; pp 303-385. (c) Spitler, E. L.; Johnson, C. A.; Haley, M. M. *Chem. Rev.* **2006**, *106*, 5344-5386.

(12) (a) Marsden, J. A.; Haley, M. M. in *Metal Catalyzed Cross-Coupling Reactions (2nd Ed)*; de Meijere, A.; Diederich, F., Eds.; Wiley-VCH: Weinheim, 2004, pp 317-394. (b) Sonogashira, K. in *Metal-Catalyzed Cross-coupling Reactions*; Diederich, F.; Stang, P.J., Eds.; Wiley-VCH: Weinheim, 1998, pp 203-230.

(13) (a) Haley, M. M.; Bell, M. L.; English, J. J.; Johnson, C. A.; Weakley, T. J. R. *J. Am. Chem. Soc.* **1997**, *119*, 2956-2957. (b) Bell, M. L.; Chiechi, R. C.; Johnson, C. A.; Kimball, D. B.; Wan, W. B.; Weakley, T. J. R.; Haley, M. M. *Tetrahedron* **2001**, *57*, 3507-3520.

(14) Gaussian 98, Revision A.6, Frisch, M. J.; Trucks, G. W.; Schlegel, H. B.; Scuseria, G. E.; Robb, M. A.; Cheeseman, J. R.; Zakrzewski, V. G.; Montgomery, Jr., J. A.; Stratmann, R. E.; Burant, J. C.; Dapprich, S.; Millam, J. M.; Daniels, A. D.; Kudin, K. N.; Strain, M. C.; Farkas, O.; Tomasi, J.; Barone, V.; Cossi, M.; Cammi, R.; Mennucci, B.; Pomelli, C.; Adamo, C.; Clifford, S.; Ochterski, J.; Petersson, G. A.; Ayala, P. Y.; Cui, Q.; Morokuma, K.; Malick, D. K.; Rabuck, A. D.; Raghavachari, K.; Foresman, J. B.; Cioslowski, J.; Ortiz, J. V.; Stefanov, B. B.; Liu, G.; Liashenko, A.; Piskorz, P.; Komaromi, I.; Gomperts, R.; Martin, R. L.; Fox, D. J.; Keith, T.; Al-Laham, M. A.; Peng, C. Y.; Nanayakkara, A.; Gonzalez, C.; Challacombe, M.; Gill, P. M. W.; Johnson, B.; Chen, W.; Wong, M. W.; Andres, J. L.; Gonzalez, C.; Head-Gordon, M.; Replogle, E. S.; Pople, J. A. Gaussian, Inc., Pittsburgh, PA, 1998.

(15) Becke, A. D. *J. Chem. Phys.* **1993**, *98*, 5648-5652.

(16) (a) Nguyen, P.; Todd, S.; Van den Biggelaar, D.; Taylor, N. J.; Marder, T.B.; Wittman, F.; Friend, R. H. *Synlett* **1994**, 299-301. (b) Tolulope, M. F.; Collings, J. C.; Burke, J. M.; Batsanov, A. S.; Ward, R. M.; Albesa-Jove, D.; Porres, L.; Beeby, A.; Howard, J. A. K.; Scott, A. J.; Clegg, W.; Watt, S. W.; Viney, C.; Marder, T. B. *J. Mater. Chem.* **2005**, *15*, 690-697.

(17) For similar conventions, see Spitler, E. L.; McClintock, S. P.; Haley, M. M. *J. Org. Chem.* **2007**, *72*, 6692-6699.

(18) (a) Pak, J. J.; Weakley, T. J. R.; Haley, M. M. *J. Am. Chem. Soc.* **1999**, *121*, 8182-8192. (b) Sarkar, A.; Pak, J. J.; Rayfield, G. W.; Haley, M. M. *J. Mater. Chem.* **2001**, *11*, 2943-2945.

(19) (a) Seo, J.; Kim, S.; Park, S. Y. *J. Am. Chem. Soc.* **2004**, *126*, 11154-11155. (b) Yam, V. W.-W.; Wong, K. M.-C.; Zhu, N. *J. Am. Chem. Soc.* **2002**, *124*, 6506-6507. (c) Hong, J. W.; Woo, H. Y.; Liu, B.; Bazan, G. C. *J. Am. Chem. Soc.* **2005**, *127*, 7435-7443. (d) Spange, S.; Prause, S.; Vilsmeier, E.; Thiel, W. R. *J. Phys. Chem.* **2005**, *109*, 7280-7289. (e) Gawinecki, R.; Trzebiatowska, K. *Polish J. Chem.* **2001**, *75*, 231-239.

(20) (a) Rogers, D. W.; Matsunaga, N.; Zavitsas, A. A.; McLafferty, F. J.; Liebman, J. F. *Org. Lett.* **2003**, *5*, 2373-2375.

(21) Drushel, H. V.; Sommers, A. L.; Cox, R. C. *Anal. Chem.* **1963**, *35*, 2166-2172.

(22) (a) Tolbert, L. M.; Nesselroth, S. M.; Netzel, T. L.; Raya, N.; Stapleton, M. *J. Phys. Chem.* **1992**, *96*, 4492-4496. (b) Englman, R.; Jortner, *J. Mol. Phys.* **1970**, *18*, 145-154. (c) Caspar, J. V.; Meyer, T. J. *J. Phys. Chem.* **1983**, *87*, 952-957.

(23) Gerhardt, W. W.; Zuccherro, A. J.; Wilson, J. N.; South, C. R.; Bunz, U. H. F.; Weck, M. *Chem. Commun.* **2006**, *20*, 2141-2143.

(24) (a) Rogers, D. W.; Matsunaga, N.; Zavitsas, A. A.; McLafferty, F. J.; Liebman, J. F. *Org. Lett.* **2003**, *5*, 2373-2375. (b) Rogers, D. W.; Matsunaga, N.; Zavitsas, A. A.; McLafferty, F. J.; Liebman, J. F. *J. Org. Chem.* **2004**, *69*, 7143-7417. (c) Jarowski, P. D.; Wodrich, M. D.; Wannere, C. S.; Schleyer, P. v. R.; Houk, K. N. *J. Am. Chem. Soc.* **2004**, *126*, 15036-15037.

(25) Hauck, M.; Schonhaber, J.; Zuccherro, A. J.; Hardcastle, K. I.; Muller, T. J. J.; Bunz, U. H. F. *J. Org. Chem.* **2007**, *72*, 6714-6725.

(26) Bosch, E.; Schultheiss, N. *Crystal Growth & Design* **2003**, *3*, 263-266.

(27) (a) Suslick, K. S.; Rakow, N. A.; Sen, A. *Tetrahedron* **2004**, *60*, 11133-11138. (b) Albert, K. J.; Lewis, N. S.; Schauer, C. L.; Sotzing, G. A.; Stitzel, S. E.; Vaid, T. P.; Walt, D. R. *Chem. Rev.* **2000**, *100*, 2595-2626. (c) Wiksur, S. L.; Ait-Haddou, H.; Lavigne, J. J.; Anslyn, E. V. *Acc. Chem. Res.* **2001**, *34*, 963-972.

(28) Spitler, E. L.; Monson, J. M.; Haley, M. M., in preparation.

(29) Miljanic, O. S.; Vollhardt, K. P. C.; Whitener, G. D. *Synlett* **2003**, 29-32.

(30) Goldfinger, M. B.; Crawford, K. B.; Swager, T. M. *J. Am. Chem. Soc.* **1997**, *119*, 4578-4593.

(31) Tovar, J. D.; Swager, T. M. *J. Organomet. Chem.* **2002**, *653*, 215-222.

Chapter III

(1) (a) de Meijere, A., Ed.; *Topics in Current Chemistry (Carbon Rich Compounds I)*; Springer: Berlin, 1998; Vol. 196. (b) de Meijere, A., Ed.; *Topics in Current Chemistry (Carbon Rich Compounds II)*; Springer: Berlin, 1999; Vol. 201. (c) Diederich, F.; Stang, P. J.; Tykwinski, R. R., Eds.; *Acetylene Chemistry: Chemistry, Biology, and Material Science*; Wiley-VCH: Weinheim, 2005. (d) Haley, M. M.; Tykwinski, R. R., Eds.; *Carbon-Rich Compounds: From Molecules to Materials*; Wiley-VCH: Weinheim, 2006.

(2) Reviews, inter alia: (a) *Organic Light Emitting Devices: Synthesis, Properties and Applications*; Müllen, K.; Scherf, U., Eds.; Wiley-VCH: Weinheim, 2006. (b) Chen, J.; Reed, M. A.; Dirk, S. M.; Price, D. W.; Rawlett, A. M.; Tour, J. M.; Grubisha, D. S.; Bennett, D. W. In *NATO Science Series II: Mathematics, Physics, Chemistry (Molecular Electronics: Bio-Sensors and Bio-Computers)*; Plenum: New York, 2003; Vol. 96, pp 59-195. (c) Domerco, B.; Hreha, R. D.; Zhang, Y.-D.; Haldi, A.; Barlow, S.; Marder, S. R.; Kippelen, B. *J. Poly. Sci. Part B: Poly. Phys.* **2003**, *41*, 2726-2732. (d) Shirota, Y. J.

Mater. Chem. **2000**, *10*, 1-25. (e) Schwab, P. F. H.; Levin, M. D.; Michl, J. *Chem. Rev.* **1999**, *99*, 1863-1933. (f) *Electronic Materials: The Oligomer Approach*; Müllen, K.; Wegner, G. Eds.; Wiley-VCH: Weinheim, 1998. (g) *Nonlinear Optics of Organic Molecules and Polymers*; Nalwa, H. S.; Miyata, S., Eds.; CRC Press: Boca Raton, 1997.

(3) Recent examples, inter alia: (a) Kang, H.; Evrenenko, G.; Dutta, P.; Clays, K.; Song, K.; Marks, T. J. *J. Am. Chem. Soc.* **2006**, *128*, 6194-6205. (b) Knox, J. E.; Halls, M. D.; Hratchian, H. P.; Schlegel, H. B. *Phys. Chem. Chem. Phys.* **2006**, *8*, 1371-1377. (c) Shukla, V. K.; Kumar, S.; Deva, D. *Synth. Met.* **2006**, *156*, 387-391. (d) Seminario, J. M. *Nature Mater.* **2005**, *4*, 111-113. (b) Hughes, G.; Bryce, M. R. *J. Mater. Chem.* **2005**, *15*, 94-107. (e) Van der Auweraer, M.; De Schryver, F. C. *Nature Mater.* **2004**, *3*, 507-508. (f) Special Issue on 'Organic Electronics', *Chem. Mater.* **2004**, *16*, 4381-4846. (g) Simpson, C. D.; Wu, J.; Watson, M. D.; Müllen, K. *J. Mater. Chem.* **2004**, *14*, 494-504.

(4) (a) Marsden, J. A.; Miller, J. J.; Shirtcliff, L. D.; Haley, M. M. *J. Am. Chem. Soc.* **2005**, *127*, 2464-2476. See also: (b) Marsden, J. A.; Haley, M. M. *Angew. Chem. Int. Ed.* **2004**, *43*, 1694-1697. (c) Miller, J. J.; Marsden, J. A.; Haley, M. M. *Synlett* **2004**, 165-168. (d) Spitler, E. L.; Shirtcliff, L. D.; Haley, M. M. *J. Org. Chem.* **2007**, *72*, 86-96. (e) Samori, S.; Tojo, S.; Fujitsuka, M.; Spitler, E. L.; Haley, M. M.; Majima, T. *J. Org. Chem.* **2007**, *72*, 2785-2793.

(5) (a) Bunz, U. H. F.; Rubin, Y.; Tobe, Y. *Chem. Soc. Rev.* **1999**, 107-119. (b) Haley, M. M.; Wan, W. B. In *Advances in Strained and Interesting Organic Molecules*; Halton, B., Ed.; JAI Press: Greenwich, 2000; Vol. 8, pp 1-41. (c) Watson, M. D.; Fechtenkötter, A.; Müllen, K. *Chem Rev.* **2001**, *101*, 1267-1300. (d) Nielsen, M. B.; Diederich, F. In *Modern Arene Chemistry*; Astruc, D., Ed.; Wiley-VCH: Weinheim, 2002; pp 196-216. (e) Baxter, P. N. W.; Dali-Youcef, R. *J. Org. Chem.* **2005**, *70*, 4935-4953.

(6) Inter alia: (a) Zhao, Y.; Slepko, A. D.; Akoto, C. O.; McDonald, R.; Hegmann, F. A.; Tykwinski, R. R. *Chem. Eur. J.* **2005**, *11*, 321-329. (b) Bunz, U. H. F. *Adv. Polym. Sci.* **2005**, *177*, 1-52. (c) Fasina, T. M.; Collings, J. C.; Lydon, D. P.; Albesa-Jove, D.; Batsanov, A. S.; Howard, J. A. K.; Nguyen, P.; Bruce, M.; Scott, A. J.; Clegg, W.; Watt, S. W.; Viney, C.; Marder, T. B. *J. Mater. Chem.* **2004**, *14*, 2395-2404. (d) Boydston, A. J.; Yin, Y.; Pagenkopf, B. L. *J. Am. Chem. Soc.* **2004**, *126*, 3724-3725. (e) Gonzalo-Rodriguez, J.; Esquivias, J.; Lafuente, A.; Diaz, C. *J. Org. Chem.* **2003**, *68*, 8120-8128. (f) Bunz, U. H. F. *Chem Rev.* **2000**, *100*, 1605-1644. (g) Tykwinski, R. R.; Gubler, U.; Martin, R. E.; Diederich, F.; Bosshard, C.; Günter, P. *J. Phys. Chem. B* **1998**, *102*, 4451-4465. (h) Tykwinski, R. R.; Schreiber, M.; Carlón, R. P.; Diederich, F.; Gramlich, V. *Helv. Chim. Acta* **1996**, *79*, 2249-2280. (i) Tahara, K.; Furukawa, S.; Uji-i, H.; Uchino, T.; Ichikawa, T.; Zhang, J.; Mamdouh, W.; Sonoda, M.; De Schryver, F. C.; De Feyter, S.; Tobe, Y. *J. Am. Chem. Soc.* **2006**, *128*, 16613-16625.

(7) (a) Slepko, A.; Marsden, J. A.; Miller, J. J.; Shirtcliff, L. D.; Haley, M. M.; Kamada, K.; Tykwinski, R. R.; Hegmann, F. A. in *Nonlinear Optical Transmission and Multiphoton Processes in Organics III*; *Proc. SPIE* **2005**, 5934, 29-34. (b) Zhang, X.-B.; Feng, J.-K.; Ren, A.-M.; Sun, C.-C. *Opt. Mater.* **2007**, 29, 955-962. (c) Slepko, A.; Hegmann, F. A.; Tykwinski, R. R.; Kamada, K.; Ohta, K.; Marsden, J. A.; Spitler, E. L.; Miller, J. J.; Haley, M. M. *Opt. Lett.* **2006**, 31, 3315-3317.

(8) (a) Bazan, G. C.; Bartholomew, G. P. *J. Am. Chem. Soc.* **2002**, 124, 5183-5196. (b) Bazan, G. C.; Bartholomew, G. P. *Synthesis* **2002**, 1245-1255. (c) Nguyen, P.; Lesley, G.; Marder, T. B. *Chem. Mater.* **1997**, 9, 406-408. (d) Meier, H.; Mühling, B.; Kolshorn, H. *Eur. J. Org. Chem.* **2004**, 1033-1042. (e) Meier, H.; Gerold, J.; Kolshorn, H.; Mühling, B. *Chem. Eur. J.* **2004**, 10, 360-370. (f) Zimmerman, B.; Baranovic, G.; Stefanic, Z.; Rozman, M. *J. Mol. Struct.* **2006**, 794, 115-124. (g) Wakabayashi, S.; Kato, Y.; Mochizuki, K.; Suzuki, R.; Matsumoto, M.; Sugihara, Y.; Shimizu, M. *J. Org. Chem.* **2007**, 72, 744-749.

(9) (a) Wilson, J. N.; Bunz, U. H. F. *J. Am. Chem. Soc.* **2005**, 127, 4124-4125. (b) Zuccheri, A. J.; Wilson, J. N.; Bunz, U. H. F. *J. Am. Chem. Soc.* **2006**, 128, 11872-11881. (c) Wilson, J. N.; Josowicz, M.; Wang, Y.Q.; Bunz, U. H. F. *Chem. Commun.* **2003**, 2962-2963.

(10) (a) Johnson, C. A.; Haley, M. M.; Rather, E.; Han, F.; Weakley, T. J. R. *Organometallics* **2005**, 24, 1161-1172. (b) Johnson, C. A.; Baker, B. A.; Berryman, O. B.; Zakharov, L. N.; O'Connor, M. J.; Haley, M. M. *J. Organomet. Chem.* **2006**, 691, 413-421. (c) Marsden, J. A.; Miller, J. J.; Haley, M. M. *Angew. Chem. Int. Ed.* **2004**, 43, 1694-1697. (d) Tobe, Y.; Kishi, J.; Ohki, I.; Sonoda, M. *J. Org. Chem.* **2003**, 68, 3330-3332.

(11) Calculated from the steady-state spectra using the techniques described in: Drushel, H. V.; Sommers, A. L.; Cox, R. C. *Anal. Chem.* **1963**, 35, 2166-2172.

(12) (a) Anstead, G. M.; Katzenellenbogen, J. A. *J. Phys. Chem.* **1988**, 92, 6249-6258. (b) Lackowicz, J. R. *Principles of Fluorescence Spectroscopy*; Plenum: New York, 1983.

(13) (a) Tolbert, L. M.; Nesselroth, S. M.; Netzel, T. L.; Raya, N.; Stapleton, M. J. *Phys. Chem.* **1992**, 96, 4492-4496. (b) Englman, R.; Jortner, J. *J. Mol. Phys.* **1970**, 18, 145-154. (c) Caspar, J. V.; Meyer, T. J. *J. Phys. Chem.* **1983**, 87, 952-957.

(14) Gaussian 03, Revision B.04. Frisch, M. J.; Trucks, G. W.; Schlegel, H. B.; Scuseria, G. E.; Robb, M. A.; Cheeseman, J. R.; Montgomery, Jr., J. A.; Vreven, T.; Kudin, K. N.; Burant, J. C.; Millam, J. M.; Iyengar, S. S.; Tomasi, J.; Barone, V.; Mennucci, B.; Cossi, M.; Scalmani, G.; Rega, N.; Petersson, G. A.; Nakatsuji, H.; Hada, M.; Ehara, M.; Toyota, K.; Fukuda, R.; Hasegawa, J.; Ishida, M.; Nakajima, T.; Honda,

Y.; Kitao, O.; Nakai, H.; Klene, M.; Li, X.; Knox, J. E.; Hratchian, H. P.; Cross, J. B.; Adamo, C.; Jaramillo, J.; Gomperts, R.; Stratmann, R. E.; Yazyev, O.; Austin, A. J.; Cammi, R.; Pomelli, C.; Ochterski, J. W.; Ayala, P. Y.; Morokuma, K.; Voth, G. A.; Salvador, P.; Dannenberg, J. J.; Zakrzewski, V. G.; Dapprich, S.; Daniels, A. D.; Strain, M. C.; Farkas, O.; Malick, D. K.; Rabuck, A. D.; Raghavachari, K.; Foresman, J. B.; Ortiz, J. V.; Cui, Q.; Baboul, A. G.; Clifford, S.; Cioslowski, J.; Stefanov, B. B.; Liu, G.; Liashenko, A.; Piskorz, P.; Komaromi, I.; Martin, R. L.; Fox, D. J.; Keith, T.; Al-Laham, M. A.; Peng, C. Y.; Nanayakkara, A.; Challacombe, M.; Gill, P. M. W.; Johnson, B.; Chen, W.; Wong, M. W.; Gonzalez, C.; Pople, J. A.; Gaussian, Inc., Pittsburgh PA, 2003.

(15) (a) Becke, A. D. *J. Chem. Phys.* **1993**, *98*, 5648-5652. (b) Lee, C.; Yang, W.; Parr, R. G. *Phys. Rev. B* **1988**, *37*, 785-789.

(16) Huang, J.-H.; Wen, W.-H.; Sun, Y.-Y.; Chou, P.-T.; Fang, J.-M. *J. Org. Chem.* **2005**, *70*, 5827-5832.

Chapter IV

(1) (a) Miller, J. J.; Marsden, J. A.; Haley, M. M. *Synlett* **2004**, 165-168. (b) Marsden, J. A.; Miller, J. J.; Shirtcliff, L. D.; Haley, M. M. *J. Am. Chem. Soc.* **2005**, *127*, 2464-2476. (c) Spitler, E. L.; Shirtcliff, L. D.; Haley, M. M. *J. Org. Chem.* **2007**, *72*, 86-96. (d) Samori, S.; Tojo, S.; Fujitsuka, M.; Spitler, E. L.; Haley, M. M.; Majima, T. *J. Org. Chem.* **2007**, *72*, 2785-2793.

(2) (a) de Meijere, A., Ed.; *Topics in Current Chemistry (Carbon Rich Compounds I)*; Springer: Berlin, 1998; Vol. 196. (b) de Meijere, A., Ed.; *Topics in Current Chemistry (Carbon Rich Compounds II)*; Springer: Berlin, 1999; Vol. 201. (c) Diederich, F.; Stang, P. J.; Tykwinski, R. R., Eds.; *Acetylene Chemistry: Chemistry, Biology, and Material Science*; Wiley-VCH: Weinheim, 2005. (d) Haley, M. M.; Tykwinski, R. R., Eds.; *Carbon-Rich Compounds: From Molecules to Materials*; Wiley-VCH: Weinheim, 2006.

(3) Reviews, *inter alia*: (a) *Functional Organic Materials*; Müller, T. J. J.; Bunz, U. H. F., Eds.; Wiley-VCH: Weinheim, 2007. (b) *Organic Light Emitting Devices: Synthesis, Properties and Applications*; Mullen, K.; Scherf, U., Eds.; Wiley-VCH: Weinheim, 2006. (c) Chen, J.; Reed, M. A.; Dirk, S. M.; Price, D. W.; Rawlett, A. M.; Tour, J. M.; Grubisha, D. S.; Bennett, D. W. In *NATO Science Series II: Mathematics, Physics, Chemistry (Molecular Electronics: Bio-Sensors and Bio-Computers)*; Plenum: New York, 2003; Vol. 96, pp 59-195. (d) Shirota, Y. *J. Mater. Chem.* **2000**, *10*, 1-25. (e) Schwab, P. F. H.; Levin, M. D.; Michl, J. *Chem. Rev.* **1999**, *99*, 1863-1933. (f) *Electronic Materials: The Oligomer Approach*; Müllen, K.; Wegner, G. Eds.; Wiley-VCH: Weinheim, 1998. (g) *Nonlinear Optics of Organic Molecules and Polymers*; Nalwa, H. S.; Miyata, S., Eds.; CRC Press: Boca Raton, 1997.

(4) Recent examples, *inter alia*: (a) Kang, H.; Evrenenko, G.; Dutta, P.; Clays, K.; Song, K.; Marks, T. J. *J. Am. Chem. Soc.* **2006**, *128*, 6194-6205. (b) Knox, J. E.; Halls, M. D.; Hratchian, H. P.; Schlegel, H. B. *Phys. Chem. Chem. Phys.* **2006**, *8*, 1371-1377. (c) Shukla, V. K.; Kumar, S.; Deva, D. *Synth. Met.* **2006**, *156*, 387-391. (d) Seminario, J. M. *Nature Mater.* **2005**, *4*, 111-113. (e) Hughes, G.; Bryce, M. R. *J. Mater. Chem.* **2005**, *15*, 94-107. (f) Van der Auweraer, M.; De Schryver, F. C. *Nature Mater.* **2004**, *3*, 507-508. (g) Special Issue on 'Organic Electronics', *Chem. Mater.* **2004**, *16*, 4381-4846. (h) Simpson, C. D.; Wu, J.; Watson, M. D.; Müllen, K. *J. Mater. Chem.* **2004**, *14*, 494-504.

(5) *Inter alia*: (a) Zhao, Y.; Slepko, A. D.; Akoto, C. O.; McDonald, R.; Hegmann, F. A.; Tykwinski, R. R. *Chem. Eur. J.* **2005**, *11*, 321-329. (b) Bunz, U. H. F. *Adv. Polym. Sci.* **2005**, *177*, 1-52. (c) Fasina, T. M.; Collings, J. C.; Lydon, D. P.; Albesa-Jove, D.; Batsanov, A. S.; Howard, J. A. K.; Nguyen, P.; Bruce, M.; Scott, A. J.; Clegg, W.; Watt, S. W.; Viney, C.; Marder, T. B. *J. Mater. Chem.* **2004**, *14*, 2395-2404. (d) Boydston, A. J.; Yin, Y.; Pagenkopf, B. L. *J. Am. Chem. Soc.* **2004**, *126*, 3724-3725. (e) Gonzalo-Rodriguez, J.; Esquivias, J.; Lafuente, A.; Diaz, C. *J. Org. Chem.* **2003**, *68*, 8120-8128. (f) Nielsen, M. B.; Diederich, F. In *Modern Arene Chemistry*; Astruc, D., Ed.; Wiley-VCH: Weinheim, 2002; pp 196-216. (g) Watson, M. D.; Fechtenkötter, A.; Müllen, K. *Chem. Rev.* **2001**, *101*, 1267-1300. (h) Tykwinski, R. R.; Gubler, U.; Martin, R. E.; Diederich, F.; Bosshard, C.; Günter, P. *J. Phys. Chem. B* **1998**, *102*, 4451-4465.

(6) (a) Slepko, A.; Marsden, J. A.; Miller, J. J.; Shirtcliff, L. D.; Haley, M. M.; Kamada, K.; Tykwinski, R. R.; Hegmann, F. A. in *Nonlinear Optical Transmission and Multiphoton Processes in Organics III*; Proc. SPIE **2005**, *5934*, 29-34. (b) Slepko, A.; Hegmann, F. A.; Tykwinski, R. R.; Kamada, K.; Ohta, K.; Marsden, J. A.; Spitler, E. L.; Miller, J. J.; Haley, M. M. *Opt. Lett.* **2006**, *31*, 3315-3317. (c) Zhang, X.-B.; Feng, J.-K.; Ren, A.-M.; Sun, C.-C. *Opt. Mater.* **2007**, *29*, 955-962. (d) See also: Kang, H.; Zhu, P.; Yang, Y.; Facchetti, A.; Marks, T. J. *J. Am. Chem. Soc.* **2004**, *126*, 15974-15975.

(7) (a) Wilson, J. N.; Bunz, U. H. F. *J. Am. Chem. Soc.* **2005**, *127*, 4124-4125. (b) Zuccherro, A. J.; Wilson, J. N.; Bunz, U. H. F. *J. Am. Chem. Soc.* **2006**, *128*, 11872-11881. (c) McGrier, P. L.; Solntsev, K. M.; Schönhaber, J.; Brombosz, S. M.; Tolbert, L. M.; Bunz, U. H. F. *Chem. Commun.* **2007**, 2127-2129.

(8) (a) Nguyen, P.; Todd, S.; Van den Biggelaar, D.; Taylor, N. J.; Marder, T. B.; Wittman, F.; Friend, R. H. *Synlett* **1994**, 299-301. (b) Tolulope, M. F.; Collings, J. C.; Burke, J. M.; Batsanov, A. S.; Ward, R. M.; Albesa-Jove, D.; Porres, L.; Beeby, A.; Howard, J. A. K.; Scott, A. J.; Clegg, W.; Watt, S. W.; Viney, C.; Marder, T. B. *J. Mater. Chem.* **2005**, *15*, 690-697.

(9) *Inter alia*: (a) Marsden, J. A.; Haley, M. M. *J. Org. Chem.* **2005**, *70*, 10213-10226. (b) Miller, J. J.; Marsden, J. A.; Haley, M. M. *Angew. Chem. Int. Ed.* **2004**, *43*, 1694-1697. (c) Marsden, J. A.; Palmer, G. J.; Haley, M. M. *Eur. J. Org. Chem.* **2003**, 2355-2369. (d) Haley, M. M. *Synlett* **1998**, 557-565.

(10) (a) Marsden, J. A.; Haley, M. M. in *Metal Catalyzed Cross-Coupling Reactions (2nd Ed)*; de Meijere, A.; Diederich, F., Eds.; Wiley-VCH: Weinheim, 2004, pp 317-394. (b) Sonogashira, K. in *Metal-Catalyzed Cross-coupling Reactions*; Diederich, F.; Stang, P.J., Eds.; Wiley-VCH: Weinheim, 1998, pp 203-230.

(11) (a) Haley, M. M.; Bell, M. L.; English, J. J.; Johnson, C. A.; Weakley, T. J. R. *J. Am. Chem. Soc.* **1997**, *119*, 2956-2957. (b) Bell, M. L.; Chiechi, R. C.; Johnson, C. A.; Kimball, D. B.; Wan, W. B.; Weakley, T. J. R.; Haley, M. M. *Tetrahedron* **2001**, *57*, 3507-3520.

(12) Brooke, G. M. *J. Fluorine Chem.* **1997**, *86*, 1-76.

(13) (a) Pak, J. J.; Weakley, T. J. R.; Haley, M. M. *J. Am. Chem. Soc.* **1999**, *121*, 8182-8192. (b) Sarkar, A.; Pak, J. J.; Rayfield, G. W.; Haley, M. M. *J. Mater. Chem.* **2001**, *11*, 2943-2945.

(14) (a) Boldi, A. M.; Anthony, J.; Gramlich, V.; Knobler, C. B.; Boudon, C.; Gisselbrecht, J. P.; Gross, M.; Diederich, F. *Helv. Chim. Acta* **1995**, *78*, 779-796. (b) Tykwinski, R. R.; Zhao, Y. *Synlett* **2002**, 1939-1953. (c) Burri, E.; Diederich, F.; Nielsen, M. B. *Helv. Chim. Acta* **2001**, *84*, 2169-2182.

(15) Moonen, N. N. P.; Diederich, F. *Org. Biomol. Chem.* **2004**, *2*, 2263-2266.

(16) Meier, H.; Mühling, B.; Kolshorn, H. *Eur. J. Org. Chem.* **2004**, 1033-1042.

(17) (a) Thompson, A. L.; Ahn, T-S.; Thomas, K. R. J.; Thayumanavan, S.; Martinez, T. J.; Bardeen, C. J. *J. Am. Chem. Soc.* **2005**, *127*, 16348-16349. (b) Lee, S.; Thomas, K. R. J.; Thayumanavan, S.; Bardeen, C. J. *J. Phys. Chem. A* **2005**, *109*, 9767-9774.

(18) (a) Seo, J.; Kim, S.; Park, S. Y. *J. Am. Chem. Soc.* **2004**, *126*, 11154-11155. (b) Yam, V. W.-W.; Wong, K. M.-C.; Zhu, N. *J. Am. Chem. Soc.* **2002**, *124*, 6506-6507. (c) Hong, J. W.; Woo, H. Y.; Liu, B.; Bazan, G. C. *J. Am. Chem. Soc.* **2005**, *127*, 7435-7443. (d) Spange, S.; Prause, S.; Vilsmeier, E.; Thiel, W. R. *J. Phys. Chem.* **2005**, *109*, 7280-7289. (e) Gawinecki, R.; Trzebiatowska, K. *Polish J. Chem.* **2001**, *75*, 231-239. (f) Anstead, G. M.; Katzenellenbogen, J. A. *J. Phys. Chem.* **1988**, *92*, 6249-6258. (g) Lackowicz, J. R. *Principles of Fluorescence Spectroscopy*; Plenum: New York, 1983. (h) Drushel, H. V.; Sommers, A. L.; Cox, R. C. *Anal. Chem.* **1963**, *35*, 2166-2172.

(19) (a) Tolbert, L. M.; Nesselroth, S. M.; Netzel, T. L.; Raya, N.; Stapleton, M. *J. Phys. Chem.* **1992**, *96*, 4492-4496. (b) Englman, R.; Jortner, *J. Molec. Phys.* **1970**, *18*, 145-154. (c) Caspar, J. V.; Meyer, T. J. *J. Phys. Chem.* **1983**, *87*, 952-957.

(20) Baldwin, K. P.; Matzger, A. J.; Scheiman, D. A.; Tessier, C. A.; Vollhardt, K. P. C.; Youngs, W. J. *Synlett* **1995**, 1215-1218.

(21) Bangerter, B. W.; Chan, S. I. *J. Am Chem. Soc.* **1969**, *91*, 3910-3921.

(22) For example: (a) Vaganova, E.; Yitzchaik, S.; Shapiro, L.; Sigalov, M.; Khodorkovsky, V. *Adv. Mater.* **2006**, *12*, 1669-1671. (b) Yeh, S-J.; Chen, H-Y.; Wu, M-F.; Chan, L-H.; Chiang, C-L.; Chen, C-T.; Lee, J-H. *Org. Electron.* **2006**, *7*, 137-143 and references therein.

(23) (a) Sheats, J. R. *J. Mater. Res.* **2004**, *19*, 1974-1989. (b) Dhananabalan, A.; Dos Santos Jr., D. S.; Mendonca, C. R.; Misoguti, L.; Balogh, D. T.; Giacometti, G. A.; Zillio, S. C.; Oliveira Jr., O. N. *Langmuir* **1999**, *15*, 4560-4564. (c) Michl, J. in *Photochromism-Molecules and Systems*; Durr, H.; Bouas-Laurent, H., Eds.; Elsevier: Amsterdam, 1990, pp. 919-930.

(24) (a) Gaab, K. M.; Thompson, A. L.; Xu, J.; Martinez, T. J.; Bardeen, C. J. *J. Am. Chem. Soc.* **2003**, *125*, 9288-9289. (b) Thompson, A. L.; Gaab, K. M.; Xu, J.; Bardeen, C. L.; Martinez, T. J. *J. Phys. Chem. A* **2004**, *108*, 671-682.

(25) (a) Roberts, J. C.; Pincock, J. A. *J. Org. Chem.* **2006**, *71*, 1480-1492. (b) Zimmerman, H. E. *J. Am. Chem. Soc.* **1995**, *117*, 8988-8991. (c) Lewis, F. D.; Yang, J.-S. *J. Am. Chem. Soc.* **1997**, *119*, 3834-3835. (d) Yamaguchi, Y.; Kobayashi, S.; Wakamiya, T.; Matsubara, Y.; Yoshida, Z. *Angew. Chem. Int. Ed.* **2005**, *44*, 7040-7044.

Chapter V

(1) (a) Spitler, E. L.; Johnson, C. A.; Haley, M. M. *Chem. Rev.* **2006**, *106*, 5344-5386; (b) Pak, J. J.; Weakley, T. J. R. *J. Am. Chem. Soc.* **1999**, *121*, 8182-8192; (c) Sarkar, A.; Pak, J. J.; Rayfield, G. W.; Haley, M. M. *J. Mater. Chem.* **2001**, *11*, 2943-2945

(2) (a) Spitler, E. L.; McClintock, S. P.; Haley, M. M. *J. Org. Chem.* **2007**, *72*, 6692-6699; (b) Marsden, J. A.; Miller, J. J.; Shirtcliff, L. D.; Haley, M. M. *J. Am. Chem. Soc.* **2005**, *127*, 2464-2476.

(3) (a) Spitler, E. L.; Shirtcliff, L. D.; Haley, M. M. *J. Org. Chem.* **2007**, *72*, 86-96; (b) Samori, S.; Tojo, S.; Fujitsuka, M.; Spitler, E. L.; Haley, M. M.; Majima, T. *J. Org. Chem.* **2007**, *72*, 2785-2793; (c) Slepko, A.; Hegmann, F. A.; Tykwinski, R. R.; Kamada, K.; Ohta, K.; Marsden, J. A.; Spitler, E. L.; Miller, J. J.; Haley, M. M. *Opt. Lett.* **2006**, *31*, 3315-3317; (d) Anand, S.; Varnavski, O.; Marsden, J. A.; Haley, M. M.; Schlegel, H. B.; Goodson, T. *J. Phys. Chem. A* **2006**, *110*, 1305-1318; (e) Sarkar, A.; Guda, R.; Haley, M. M.; Goodson, T. *J. Am. Chem. Soc.* **2006**, *128*, 13972-13973.

(4) (a) Johnson, C. A.; Lu, Y.; Haley, M. M. *Org. Lett.* **2007**, *9*, 3725-3728; (b) Tahara, K.; Johnson, C. A.; Fujita, T.; Sonoda, M.; DeSchryver, F. C.; DeFeyer, S.;

Haley, M. M.; Tobe, Y. *Langmuir* **2007**, *23*, 10190-10197; (c) Shin, Y.; Fryxell, G. E.; Johnson, C. A.; Haley, M. M. *Chem. Mater.* **2007**, ASAP Article.

(5) Marsden, J. A.; Haley, M. M. *J. Org. Chem.* **2005**, *70*, 10213-10226.

(6) (a) Meier, H.; Mühling, B.; Kolshorn, H. *Eur. J. Org. Chem.* **2004**, 1033-1042; (b) Moonen, N. N. P.; Diederich, F. *Org. Biomol. Chem.* **2004**, *2*, 2263-2266 and references contained therein.

(7) (a) Frassinetti, C.; Ghelli, S.; Gans, P.; Sabatini, A.; Moruzzi, M. S.; Vacca, A. *Anal. Biochem.* **1995**, *231*, 374-382; (b) Frassinetti, C.; Alderighi, L.; Gans, P.; Sabatini, A.; Vacca, A.; Ghelli, S. *Anal. Bioanal. Chem.* **2003**, *376*, 1041-1052; (c) Vacca, A.; Nativi, C.; Cacciarini, M.; Pergoli, R.; Roelens, S. *J. Am. Chem. Soc.* **2004**, *126*, 16456-16465.

Appendix A

(1) (a) de Meijere, A., Ed.; *Topics in Current Chemistry (Carbon Rich Compounds I)*; Springer: Berlin, 1998; Vol. 196. (b) de Meijere, A., Ed.; *Topics in Current Chemistry (Carbon Rich Compounds II)*; Springer: Berlin, 1999; Vol. 201. (c) Diederich, F.; Stang, P. J.; Tykwinski, R. R., Eds.; *Acetylene Chemistry: Chemistry, Biology, and Material Science*; Wiley-VCH: Weinheim, 2005. (d) Haley, M. M.; Tykwinski, R. R., Eds.; *Carbon-Rich Compounds: From Molecules to Materials*; Wiley-VCH: Weinheim, 2006.

(2) Reviews, inter alia: (a) *Organic Light Emitting Devices: Synthesis, Properties and Applications*; Müllen, K.; Scherf, U., Eds.; Wiley-VCH: Weinheim, 2006. (b) Chen, J.; Reed, M. A.; Dirk, S. M.; Price, D. W.; Rawlett, A. M.; Tour, J. M.; Grubisha, D. S.; Bennett, D. W. In *NATO Science Series II: Mathematics, Physics, Chemistry (Molecular Electronics: Bio-Sensors and Bio-Computers)*; Plenum: New York, 2003; Vol. 96, pp 59-195. (c) Domerco, B.; Hreha, R. D.; Zhang, Y.-D.; Haldi, A.; Barlow, S.; Marder, S. R.; Kippelen, B. *J. Poly. Sci. Part B: Poly. Phys.* **2003**, *41*, 2726-2732. (d) Shirota, Y. *J. Mater. Chem.* **2000**, *10*, 1-25. (e) Schwab, P. F. H.; Levin, M. D.; Michl, J. *Chem. Rev.* **1999**, *99*, 1863-1933. (f) *Electronic Materials: The Oligomer Approach*; Müllen, K.; Wegner, G. Eds.; Wiley-VCH: Weinheim, 1998. (g) *Nonlinear Optics of Organic Molecules and Polymers*; Nalwa, H. S.; Miyata, S., Eds.; CRC Press: Boca Raton, 1997.

(3) Recent examples, inter alia: (a) Kang, H.; Evrenenko, G.; Dutta, P.; Clays, K.; Song, K.; Marks, T. J. *J. Am. Chem. Soc.* **2006**, *128*, 6194-6205. (b) Knox, J. E.; Halls, M. D.; Hratchian, H. P.; Schlegel, H. B. *Phys. Chem. Chem. Phys.* **2006**, *8*, 1371-1377. (c) Shukla, V. K.; Kumar, S.; Deva, D. *Synth. Met.* **2006**, *156*, 387-391. (d) Seminario, J. M. *Nature Mater.* **2005**, *4*, 111-113. (e) Hughes, G.; Bryce, M. R. *J. Mater. Chem.* **2005**, *15*, 94-107. (f) Van der Auweraer, M.; De Schryver, F. C. *Nature Mater.* **2004**, *3*, 507-

508. (f) Special Issue on 'Organic Electronics,' *Chem. Mater.* **2004**, *16*, 4381-4846. (g) Simpson, C. D.; Wu, J.; Watson, M. D.; Müllen, K. *J. Mater. Chem.* **2004**, *14*, 494-504.

(4) (a) Marsden, J. A.; Miller, J. J.; Shirtcliff, L. D.; Haley, M. M. *J. Am. Chem. Soc.* **2005**, *127*, 2464-2476. See also: (b) Marsden, J. A.; Haley, M. M. *Angew. Chem. Int. Ed.* **2004**, *43*, 1694-1697. (c) Miller, J. J.; Marsden, J. A.; Haley, M. M. *Synlett* **2004**, 165-168. (d) Spitler, E. L.; Shirtcliff, L. D.; Haley, M. M. *J. Org. Chem.* **2007**, *72*, 86-96. (e) Samori, S.; Tojo, S.; Fujitsuka, M.; Spitler, E. L.; Haley, M. M.; Majima, T. *J. Org. Chem.* **2007**, *72*, 2785-2793. (f) Marsden, J. A.; Haley, M. M. *J. Org. Chem.* **2005**, *70*, 10213-10226. (g) Spitler, E. L.; McClintock, S. P.; Haley, M. M. *J. Org. Chem.* **2007**, *72*, 6692-6699. (h) Tahara, K.; Johnson, C. A., II; Fujita, T.; Sonoda, M.; De Schryver, F. C.; De Feyter, S.; Haley, M. M.; Tobe, Y. *Langmuir* **2007**, ASAP Article.

(5) (a) Bunz, U. H. F.; Rubin, Y.; Tobe, Y. *Chem. Soc. Rev.* **1999**, 107-119. (b) Haley, M. M.; Wan, W. B. In *Advances in Strained and Interesting Organic Molecules*; Halton, B., Ed.; JAI Press: Greenwich, 2000; Vol. 8, pp 1-41. (c) Watson, M. D.; Fechtenkötter, A.; Müllen, K. *Chem Rev.* **2001**, *101*, 1267-1300. (d) Nielsen, M. B.; Diederich, F. In *Modern Arene Chemistry*; Astruc, D., Ed.; Wiley-VCH: Weinheim, 2002; pp 196-216.

(6) Inter alia: (a) Zhao, Y.; Slepko, A. D.; Akoto, C. O.; McDonald, R.; Hegmann, F. A.; Tykwinski, R. R. *Chem. Eur. J.* **2005**, *11*, 321-329. (b) Bunz, U. H. F. *Adv. Polym. Sci.* **2005**, *177*, 1-52. (c) Fasina, T. M.; Collings, J. C.; Lydon, D. P.; Albesa-Jove, D.; Batsanov, A. S.; Howard, J. A. K.; Nguyen, P.; Bruce, M.; Scott, A. J.; Clegg, W.; Watt, S. W.; Viney, C.; Marder, T. B. *J. Mater. Chem.* **2004**, *14*, 2395-2404. (d) Boydston, A. J.; Yin, Y.; Pagenkopf, B. L. *J. Am. Chem. Soc.* **2004**, *126*, 3724-3725. (e) Gonzalo-Rodriguez, J.; Esquivias, J.; Lafuente, A.; Diaz, C. *J. Org. Chem.* **2003**, *68*, 8120-8128. (f) Bunz, U. H. F. *Chem Rev.* **2000**, *100*, 1605-1644. (g) Tykwinski, R. R.; Gubler, U.; Martin, R. E.; Diederich, F.; Bosshard, C.; Günter, P. *J. Phys. Chem. B* **1998**, *102*, 4451-4465. (h) Tykwinski, R. R.; Schreiber, M.; Carlón, R. P.; Diederich, F.; Gramlich, V. *Helv. Chim. Acta* **1996**, *79*, 2249-2280. (i) Tahara, K.; Furukawa, S.; Uji-i, H.; Uchino, T.; Ichikawa, T.; Zhang, J.; Mamdouh, W.; Sonoda, M.; De Schryver, F. C.; De Feyter, S.; Tobe, Y. *J. Am. Chem. Soc.* **2006**, *128*, 16613-16625.

(7) (a) Slepko, A.; Marsden, J. A.; Miller, J. J.; Shirtcliff, L. D.; Haley, M. M.; Kamada, K.; Tykwinski, R. R.; Hegmann, F. A. in *Nonlinear Optical Transmission and Multiphoton Processes in Organics III*; *Proc. SPIE* **2005**, *5934*, 29-34. (b) Zhang, X.-B.; Feng, J.-K.; Ren, A.-M.; Sun, C.-C. *Opt. Mater.* **2007**, *29*, 955-962. (c) Slepko, A.; Hegmann, F. A.; Tykwinski, R. R.; Kamada, K.; Ohta, K.; Marsden, J. A.; Spitler, E. L.; Miller, J. J.; Haley, M. M. *Opt. Lett.* **2006**, *31*, 3315-3317.

(8) (a) Bazan, G. C.; Bartholomew, G. P. *J. Am. Chem. Soc.* **2002**, *124*, 5183-5196. (b) Bazan, G. C.; Bartholomew, G. P. *Synthesis* **2002**, 1245-1255. (c) Nguyen, P.; Lesley, G.; Marder, T. B. *Chem. Mater.* **1997**, *9*, 406-408. (d) Meier, H.; Mühlhng, B.; Kolshorn,

H. *Eur. J. Org. Chem.* **2004**, 1033-1042. (e) Meier, H.; Gerold, J.; Kolshorn, H.; Mühling, B. *Chem. Eur. J.* **2004**, *10*, 360-370. (f) Zimmerman, B.; Baranovic, G.; Stefanic, Z.; Rozman, M. *J. Mol. Struct.* **2006**, *794*, 115-124. (g) Wakabayashi, S.; Kato, Y.; Mochizuki, K.; Suzuki, R.; Matsumoto, M.; Sugihara, Y.; Shimizu, M. *J. Org. Chem.* **2007**, *72*, 744-749.

9 (a) Wilson, J. N.; Bunz, U. H. F. *J. Am. Chem. Soc.* **2005**, *127*, 4124-4125. (b) Zuccherro, A. J.; Wilson, J. N.; Bunz, U. H. F. *J. Am. Chem. Soc.* **2006**, *128*, 11872-11881. (c) Wilson, J. N.; Josowicz, M.; Wang, Y.Q.; Bunz, U. H. F. *Chem. Commun.* **2003**, 2962-2963. (d) Zen, A.; Bilge, A.; Galbrecht, F.; Alle, R.; Meerholz, K.; Grenzer, J.; Neher, D.; Scherf, U.; Farrell, T. *J. Am. Chem. Soc.* **2006**, *128*, 3914-3915. (e) Kang, H.; Evmenenko, G.; Dutta, P.; Clays, K.; Song, K.; Marks, T. J. *J. Am. Chem. Soc.* **2006**, *128*, 6194-6205. (f) Hu, K.; Zhu, P. W.; Yu, Y.; Facchetti, A.; Marks, T. J. *J. Am. Chem. Soc.* **2004**, *126*, 15974-15975. (g) Sorensen, J. K.; Vestergaard, M.; Kadziola, A.; K.; Nielsen, M. B. *Org. Lett.* **2006**, *8*, 1173-1176.

(10) Pak, J. J.; Weakley, T. J. R.; Haley, M. M. *J. Am. Chem. Soc.* **1999**, *121*, 8182-8192.

(11) (a) Suslick, K. S.; Rakow, N. A.; Sen, A. *Tetrahedron* **2004**, *60*, 11133-11138. (b) Albert, K. J.; Lewis, N. S.; Schauer, C. L.; Sotzing, G. A.; Stitzel, S. E.; Vaid, T. P.; Walt, D. R. *Chem. Rev.* **2000**, *100*, 2595- 2626. (c) Wiksur, S. L.; Ait-Haddou, H.; Lavigne, J. J.; Anslyn, E. V. *Acc. Chem. Res.* **2001**, *34*, 963-972. (d) Huang, J.-H.; Wen, W.-H.; Sun, Y.-Y.; Chou, P.-T.; Fang, J.-M. *J. Org. Chem.* **2005**, *70*, 5827-5832.

(12) Calculated from steady-state spectra using methods described in: Drushel, H. V.; Sommers, A. L.; Cox, R. C. *Anal. Chem.* **1963**, *35*, 2166-2172.